

**Investigation of combustion and performance
characteristics of CAI combustion engine with positive and
negative valve overlap**

A thesis submitted for the degree of Doctor of Philosophy

By

Changho Yang

School of Engineering and Design
Brunel University
United Kingdom

July 2008

Brunel University
School of Engineering and Design
United Kingdom

Changho Yang

**Investigation of combustion and performance characteristics of CAI
combustion engine with positive and negative valve overlap**

July 2008

Abstract

In the first part of studies, Controlled Auto-Ignition (CAI) combustion was investigated in a Ricardo E6 single cylinder, four stroke gasoline engine. CAI combustion is achieved by employing positive valve overlap configuration in combination with various compression ratios and intake air temperature strategies. The CAI operational region is limited by engine load due to knock and partial burned boundaries. The combustion characteristics and emissions are studied in order to understand the major advantages and drawbacks of CAI combustion with positive valve overlap.

The enlargement of the CAI operational region is obtained by boosting intake air and external EGR. The lean-boosted operation elevators the range of CAI combustion to the higher load region, and the use of external EGR allows the engine to operation with CAI combustion in the mid range of region between boosted and N/A CAI operational range. The results are analyzed and combustion characteristics, performance and emissions are investigated.

A Ricardo Hydra single cylinder, four stroke optical gasoline engine with optical access is then experimented to investigate CAI combustion through negative valve overlap configuration and an intake heater. The effects of direct fuel injection timings spark timings and air/fuel ratio are studied by means of simultaneous in-cylinder heat release study and direct visualization, chemiluminescence techniques which uses full, OH radical and CHO species. Both heat release analysis and chemiluminescence results have identified the pressure of minor combustion during the NVO period. Both the charge cooling and local air/fuel ratio effects are also investigated by varying the quantity of direct air injection.

Acknowledgements

First and foremost, I would like to express my greatest respect, admiration and gratitude to Professor Hua Zhao for his interest, guidance and support throughout the course of my PhD, allowing me to study in his esteemed Centre for Advanced Powertrain and Fuels Research group.

I am also grateful to Dr Xi Jiang, who has given academic advice and provided guidance throughout my time at Brunel.

I express my appreciation to Chief Technicians Bob Webb and John Langdon for their continual assistance, Technicians Clive Barrett, Ken Anstiss for their advice and technical support. I also would like to thank Paul and Les in the stores, giving sincere advice, technical and substantial support, and above all friendship.

I would also like to take this opportunity to thank my contemporaries and good friends, Kiranjeev Gill, Dr. Navin Kalian, Dr. Mario Martins, Dr. Kayiu Mann, Dr. Ben Leach and my successor, Manida Tongroon for so many things. I also wish to thank Reza Herfatmanesh and Alvaro Rodriguez and Lyn Mcwilliam with whom it's been a pleasure to work in the same research group.

Finally, I would like to thank my wife, Youngok Lee and daughter, Eunseo Yang for listening and lending support throughout this project. I am also extremely grateful to thank my mother, Sunduck Son and parents in law, Taewon Lee and Hyunjoo Jin for their mental and substantial support and sacrifices.

Nomenclature

General Abbreviations

AFR	Air/Fuel Ratio
AI	Auto-Ignition
ATAC	Active Thermo-Atmospheric Combustion
ATDC	Active Thermo Atmosphere Combustion
ATDC	After Top Dead Centre
BDC	Bottom Dead Centre
BMEP	Brake Mean Effective Pressure
BSCO	Brake Specific Carbon Monoxide
BSFC	Brake Specific Fuel Consumption
BSHC	Brake Specific Hydro-Carbons
BSNO	Brake Specific Nitrogen Oxides
BTDC	Before Top Dead Centre
CA	Crank Angle
CAI	Controlled Auto-Ignition
CARB	Californian Air Resource Board
CAAA	California Air Act Amendments
CR	Compression Ratio
deg	degree
DI	Direct Injection
ECU	Electronic Control Unit
EGR	Exhaust Gas Re-circulation
EV	Electric Vehicle
EVC	Exhaust Valve Closing
EVO	Exhaust Valve Opening
FID	Flame ionized detector
GDI	Gasoline Direct Injection
HCCI	Homogeneous Charge Compression Ignition
HRR	Heat Release Rate
HSDI	High Speed Direct Injection

IC	Internal Combustion
IMEP	Indicated Mean Effective Pressure
ISCO	Indicated Specific Carbon Monoxide
ISFC	Indicated Specific Fuel Consumption
ISHC	Indicated Specific Hydro-carbons
ISNO	Indicated Specific Nitrogen Oxides
IVC	Intake Valve Closing
IVO	Intake Valve Opening
LEV	Low Emission Vehicle
LII	Laser induced incandescence
LIF	Laser induced fluorescence
LIPF	Laser induced pre-dissociative fluorescence
MBT	Minimum Spark Advance for Best Torque
MFB	Mass Fraction Burn
NDIR	Nondispersive infrared gas analyser
NO _x	Nitrogen Oxides
NVO	Negative Valve Overlap
PC	Personal Computer
PFI	Port Fuel Injection
PLIF	Planar laser induced fluorescence
PM	Particulate Matter
PMEP	Pumping Mean Effective Pressure
ppm	Parts per Million
PRF	Primary Reference Fuel
RON	Research Octane Number
rpm	Revolutions per Minute
SA-CAI	Spark Assisted Controlled Auto-Ignition
SI	Spark Ignition
SOI	Start of Injection
SULEV	Super Low Emissions Vehicle
TDC	Top Dead Centre
uHC	Unburned Hydrocarbons
VVA	Variable Valve Actuation

WOT	Wide Open Throttle
ZEV	Zero Emission Vehicle

Symbols

a	Crank radius
c	Specific heat
C_i	Concentration of species
C_p	Specific heat at constant pressure
C_v	Specific heat at constant volume
CV	Calorific Value
m	Mass
\dot{m}	Mass flow rate
M_x	Molecular weight (where x is chemical species)
N	Crankshaft rotational speed
n_R	Number of crank revolutions
P	Power
ppm	Parts per million
Q	Cumulative heat release
q	Heating value
Q_λ	Absorption efficiency
R	Gas constant/Connecting rod length/Crank radius
T	Temperature
U	Internal energy
V_c	Clearance volume
V_d	Displacement volume
V	Volume
V_{cg}	Volume concentration
W	Work
W_c	Work per cycle
γ	Ratio of specific heat

η_c	Combustion efficiency
η_f	Fuel conversion efficiency
η_h	Heat exchanger efficiency
λ , Lambda	Relative air/fuel ratio
μm	Micrometer
ρ	Density
ϕ	Fuel/Air equivalence ratio

Chemical symbols

C_2	Carbon
CH	Methyl-dyne radical
CHO	
CH ₂ O	Formaldehyde
CH ₄	Methane
C ₃ H ₈	Propane
C _a H _b O _c	Generic fuel type
CO	Carbon monoxide
CO ₂	Carbon dioxide
H	Hydrogen atom
HC	Hydro Carbon
NO	Nitric oxide
NO ₂	Nitrogen dioxide
NO _x	Nitrogen oxides
O	Oxygen atom
O ₃	Ozone
OH	Hydroxyl radical

Contents

CHAPTER 1 – INTRODUCTION	14
1.1 INTRODUCTION.....	14
1.2 OBJECTIVES.....	16
1.3 OUTLINE OF THESIS	17
CHAPTER 2 LITERATURE REVIEW	20
2.1 INTRODUCTION.....	20
2.2 GASOLINE ENGINE EMISSIONS	21
2.2.1 World Emissions standards.....	21
2.2.2 Unburnt hydrocarbon	23
2.2.3 Carbon-monoxide.....	24
2.2.4 Nitrogen Oxides	25
2.3 CURRENT AUTOMOTIVE ENGINES AND TECHNOLOGIES.....	26
2.4 CONTROLLED AUTO-IGNITION (CAI)	27
2.4.1 Introduction.....	27
2.4.2 Historical background	28
2.4.3 Principle and combustion characteristics of CAI engines.....	30
2.4.3.1 Heat release rate.....	31
2.4.3.2 CAI operating region	32
2.4.3.3 IMEP and Cycle to cycle variation	35
2.4.3.4 Engine output emissions	36
2.4.3.5 Combustion control.....	37
2.4.4 Challenges facing CAI combustion	38
2.4.5 Applications of CAI combustion	41
2.5 OPTICAL TECHNIQUES	42
2.5.1 Introduction.....	42
2.5.2 Direct Visualization	44
2.5.3 Chemiluminescence	46

CHAPTER 3 – EXPERIMENT FACILITIES AND DATA ANALYSIS.....	52
3.1 INTRODUCTION.....	52
3.2 EXPERIMENTAL SETUP AND TEST FACILITIES	53
3.2.1 General description	53
3.2.2 Test procedure.....	54
3.2.3 Engine Control and Operation	54
3.2.3.1 Dynamometer.....	54
3.2.3.2 Variable compression ratio	54
3.2.3.3 Variable Valve Timing Camshaft	55
3.2.3.4 Air Intake System	55
3.2.3.5 Exhaust (EGR recirculation) system.....	56
3.2.3.6 Fuel Supply and Injection System	57
3.2.3.7 Spark ignition system and Shaft Encoder	57
3.3 EXPERIMENTAL MEASUREMENT AND DATA ANALYSIS	58
3.3.1 In-Cylinder Gas Pressure Measurement.....	58
3.3.2 Data acquisition system	59
3.3.3 Exhaust Measurement	59
3.3.3.1 CO, CO ₂ , O ₂ , and Air/Fuel Ratio measurement	60
3.3.3.2 NO _x Measurements	62
3.3.3.3 Unburned Hydrocarbon Measurement.....	63
3.3.3.4 Calculation of Specific Emissions	63
3.3.4 Fuel and Air mass flow rate Measurement	65
3.3.5 Temperature Measurement.....	66
3.4 DATA PROCESSING AND ANALYSIS	66
3.4.1 Engine Load and combustion.....	66
3.4.1.1 Indicated Mean Effect Pressure	66
3.4.1.2 Coefficient of Variation	67
3.4.1.3 Knocking Combustion Analysis	68
3.4.1.4 Combustion Efficiency	68
3.4.1.5 Exhaust Heat Recovery through a Heat Exchanger	69
3.4.2 Fuel Conversion Efficiency	70
3.4.3 Calculations of Trapped residuals and Mixture temperature	70
3.4.4 Heat Release Analysis.....	72
3.5 SUMMARY	73

CHAPTER 4 INVESTIGATION OF CAI COMBUSTION WITH POSITIVE VALVE OVERLAP	75
4.1 INTRODUCTION.....	75
4.2 POSITIVE VALVE OVERLAP AND TEST METHODOLOGY.....	76
4.3 ENGINE OPERATION AND TEST PROCEDURE.....	78
4.3.1 Cold Start Procedure	78
4.3.2 Test procedure.....	78
4.4 INVESTIGATION OF CAI COMBUSTION BY VARIABLE COMPRESSION RATIO AND INTAKE TEMPERATURE	81
4.4.1 Introduction.....	81
4.4.2 CAI operating and load range	82
4.4.3 Fuel consumption and Engine output Emissions	84
4.4.4 Combustion characteristics	89
4.4.4.1 Combustion stability	89
4.4.4.2 Combustion efficiency	90
4.4.4.3 Combustion timing.....	91
4.4.4.4 Heat exchanger efficiency.....	93
4.4.4.5 Exhaust temperature and EGR.....	95
4.4.5 Summary	98
4.5 ENLARGEMENT OF CAI OPERATING RANGE BY INTAKE AIR BOOSTING AND EXTERNAL EGR	99
4.5.1 Introduction.....	99
4.5.2 Enlargement of CAI operating range	100
4.5.3 Fuel consumption and Engine output emissions.....	102
4.5.4 Combustion characteristics	108
4.5.4.1 Combustion stability	108
4.5.4.2 Combustion efficiency	109
4.5.4.3 Heat exchanger efficiency.....	110
4.5.4.4 Exhaust temperature and EGR Concentration	111
4.5.5 Summary	113
4.6 SUMMARY	114

**CHAPTER 5 IN-CYLINDER STUDIES OF CAI COMBUSTION WITH
NEGATIVE VALVE OVERLAP..... 116**

5.1. INTRODUCTION.....	116
5.2 EXPERIMENTAL FACILITIES	118
5.2.1 Ricardo Hydra Research Engine	118
5.2.2 Optical Parts of the Engine	119
5.2.3 Pressure transducer and Positioning System.....	120
5.2.4 Air-Assisted Fuel Injection System	121
5.2.5 Ignition System	122
5.2.6 Temperature Measurements and Emissions.....	122
5.2.7 Data acquisition system	123
5.2.8 High Speed Camera and Intensifier	123
5.3 EXPERIMENTAL PREPARATIONS AND PROCEDURE.....	124
5.3.1 Experimental Setup	124
5.3.2 Test procedure.....	126
5.4 IN-CYLINDER STUDIES OF CAI COMBUSTION WITH NVO.....	127
5.4.1 Effect of injection timing	127
5.4.1.1 Introduction.....	127
5.4.1.2 Engine performance	127
5.4.1.3 Combustion Characteristics	128
5.4.1.4 Fuel Consumption and Emissions.....	131
5.4.1.5 Simultaneous In-cylinder Heat release and Chemiluminescence Measurements	133
5.4.1.5.1 Introduction	133
5.4.1.5.2 Full chemiluminescence of direct visualization	133
5.4.1.5.3 OH Chemiluminescence	146
5.4.1.5.4 CHO Chemiluminescence	153
5.4.2 Effect of Spark Timing.....	162
5.4.2.1 Introduction.....	162
5.4.2.2 Engine performance	162
5.4.2.3 Combustion Characteristics	164
5.4.2.4 Fuel consumption and emissions	165
5.4.2.5 Simultaneous In-cylinder studies and Full Chemiluminescence	167
5.4.3 Effect of Air-Fuel Ratio at Lambda 1 and 1.2	175
5.4.3.1 Introduction.....	175
5.4.3.2 Engine performance at lambda 1.2	175
5.4.3.3 Combustion characteristics at lambda 1.2.....	176

5.4.3.4 Fuel consumption and emissions at lambda 1.2.....	178
5.4.3.5 Simultaneous in-cylinder studies and chemiluminescence	180
5.4.3.5.1 Introduction	180
5.4.3.5.2 Simultaneous In-cylinder studies at lambda 1 and 1.2	181
5.4.3.5.3 Full chemiluminescence	191
5.4.3.5.4 OH chemiluminescence	201
5.4.3.5.5 CHO chemiluminescence	206
5.4.4 Effect of air injection on low temperature combustion.....	211
5.4.4.1 Combustion characteristics and performance	211
5.4.4.2 Simultaneous in-cylinder studies and full chemiluminescence	215
5.5 SUMMARY	233

CHAPTER 6 – SUMMARY AND CONCLUSIONS..... 235

6.1 INTRODUCTION.....	235
6.2 CAI OPERATION WITH POSITIVE VALVE OVERLAP	236
6.3 ENLARGEMENT OF CAI OPERATIONAL RANGE	237
6.4 IN-CYLINDER STUDIES OF CAI COMBUSTION WITH NEGATIVE VALVE OVERLAP	238
6.5 RECOMMENDATIONS FOR FUTURE WORK.....	240

REFERENCES..... 241

APPENDIX

Chapter 1

Introduction

Chapter 1 – Introduction

1.1 Introduction

Since the four-stroke 'OTTO' cycle was developed in 1897 by Nikolaus August Otto, this has led to the introduction of the internal combustion (IC) engine. This introduction has provided the means of a power plant used throughout the world and for many applications including that of the automobile. Although research and development on the IC engine have improved performance and efficiency over the years, world wide emissions legislation and the reduction in fossil fuel resources have motivated IC engine manufacturers to provide more advanced technologies, producing cleaner and more efficient power plants. Alternative technologies such as fuel cells and electric vehicles that have been introduced in the market come with associated problems. These include high cost, changes required to the fuelling infrastructure and lack of development to support these technologies.

Research and development of the IC engines for automotive applications have over the decades introduced various technologies including catalysts and intelligent engine management systems that have contributed to the achievement of lower emissions and fuel consumption yet maintaining or even improving output performance. Other innovative developments include variable valve actuation (VVA), direct fuel injection, and cylinder activation. The future of IC engines will incorporate these technologies to provide considerably cleaner and better fuel economy than the current IC engines. Furthermore alternative combustion technology are also being investigated and in particular Controlled Auto-Ignition (CAI) also known as Homogeneous Charge Compression Ignition (HCCI). Over the past few decades, CAI has been increasingly researched and developed as it shows potential to reduce fuel consumption and NO_x emissions that meet the most stringent of legislation now and in the future. The technology of CAI is attractive as there is no need for huge modifications to the existing hardware of IC engines and with the low NO_x emissions, De-NO_x after treatment systems required for future engines to meet legislation can be avoided.

CAI is achieved by the control of in-cylinder conditions such as temperature and pressure whilst under lean-burn combustion and open throttle. The lean-burn combustion with its lower peak temperatures contributes to the low NO_x emissions, while the open throttle reduces pumping losses and increases thermal efficiency. In order to initiate CAI combustion, extra thermal energy is required which could be obtained from either an external heater with exhaust gas recirculation (EGR) and/or exhaust gas trapping. External heating is required to heat the charge entering the combustion chamber and thus allowing auto-ignition whilst the exhaust gases being introduced back into the combustion chamber either by EGR or exhaust gas trapping via valve overlapping dilutes the charge to control the heat release rate. Due to the high level of thermal energy occupied in the combustion chamber, combustion operation is limited in the engine load range by knock, partial burn and misfire regions.

For the purpose of this thesis, several control strategies are combined and investigated to achieve stable CAI combustion with emphasis to enlarge the CAI operating region. These include:

1. Exhaust gas recirculation
 - a. Externally
 - b. Positive valve overlapping
 - c. Negative valve overlapping
2. Compression ratio
3. Intake charge heating
4. Intake charge boosting
5. Combustion phasing

The recirculation or trapping (via the valves) of exhaust gases is in itself unable to retain the heat required for auto-ignition and thus it is necessary to utilise higher compression ratios and intake charge heating. Although it is common to use negative valve overlap to trap exhaust gases and initiate CAI combustion, this thesis will also investigate positive valve overlap. Air boosting is also used to improve the CAI operating region. Results for intake air boosting and the addition of exhaust gas in the cylinder shows impressive improvement to the CAI operating region.

However, the level of boosting pressure compromises the efficiency of the engine. Combustion phasing is also researched and discussed in this thesis. The effect of combustion phasing has been used to improve the lower load range as well as the combustion characteristics.

To further analyse and understand the effects of recycled or trapped exhaust gases, combustion characteristics, and the combustion sequence, direct visualization with in-cylinder pressure measurements are used. Chemiluminescence images of chemical species during combustion are studied to monitor the chemical reaction and combustion characteristics, along with in-cylinder properties when running CAI combustion.

1.2 Objectives

This study is undertaken on two research engines; a Ricardo E6 single cylinder engine and a Ricardo hydra single cylinder optical engine. Initial investigations performed on the Ricardo E6 engine concentrates on the characteristics of CAI combustion with an attempt to enlarge the operational range using positive valve overlapping, variable compression ratio and intake charge heating. Further investigations using the Ricardo hydra optical engine operating in CAI with negative valve overlapping is researched with chemiluminescence imaging and heat release analysis. The main objectives of this thesis are to:

1. Investigate CAI combustion by using positive valve overlap strategy in combination with variable compression ratio and intake charge heating
2. Enlarge the CAI operational region by using intake air boosting, external EGR and positive valve overlap strategy
3. Investigate the effects on auto-ignition and combustion characteristics of direct fuel injection; spark assisted ignition, air-fuel ratio and direct air injection by means of in-cylinder optical diagnosis.

1.3 Outline of thesis

Following this introduction, chapter 2 presents a review of the literature relating to the investigation as well as historical and current background of CAI gasoline engine and optical techniques. The current and future emission legislation is studied in order to motivate research and development of internal combustion engine. The background of CAI combustion is detailed with combustion characteristics and performance. In addition emissions are compared to SI engines. Finally, an optical technique is introduced in order to investigate simultaneous in-cylinder studies and chemiluminescence approaches.

Following this introduction, chapter 2 presents a review of the literature relating to the investigation of CAI gasoline engines and optical techniques as well as historical and current background. The current and future emission legislation is also reviewed and discusses the motivation for research and development of the internal combustion engine. Details of combustion characteristics and performance from past researchers when operating CAI combustion is discussed and their emissions are compared to that of present spark ignition (SI) engines. Finally, an optical technique is introduced in order to investigate simultaneous in-cylinder studies and chemiluminescence approaches.

The Ricardo E6 has the ability to vary its compression ratio, valve timings and intake charge heating. In addition, it has been set-up to accept boosted air from a site main compressor which is connected to the air intake. Chapter 3 details the experimental test facility, set up and data analysis method of the Ricardo E6 single cylinder engine. Instrumentation, measurement equipments and the data acquisition system is also detailed along with the formulas and calculations required for analysis.

Chapter 4 presents the investigation of CAI combustion by positive valve overlap. CAI operational range is investigated at variable engine speeds and air-fuel ratios at various compression ratios and intake charge temperatures. Air boosting into the intake (upto 1bar) in conjunction with external EGR are used to study the affect of variable EGR rate on the CAI operational range.

Chapter 5 details the experimental facilities, set-up and data analysis on the Ricardo hydra optical engine. Simultaneous in-cylinder pressure measurements and chemiluminescence images are obtained and analysed to better understand the underlying physical and chemical processes during auto-ignition combustion. The following four different strategies are performed to study in detail these effects:

1. Direct fuel injection timings
2. Spark timings
3. Air-fuel ratio
4. Direct air injection

The effect of direct fuel injection resulted in a mini combustion in the negative valve overlap (NVO) period which is in turn seen to affect the main combustion. Air injection is then investigated to study its influence on the mini and main combustion.

Conclusions on the investigation of CAI combustion and optical chemiluminescence analysis are summarised in chapter 6. Recommendations for additional work and suggestions are also given for future research and development into CAI combustion.

Chapter 2

Literature review

Chapter 2 Literature review

2.1 Introduction

Powertrain developments in recent days concentrate on lowering fossil fuel consumption and attempt to tackle the environmental issues rather than its performance achievements since the lack of fossil fuel energy resources and global environmental concerns such as the greenhouse effect, ozone layer depletion and weather disaster. Vehicles with internal combustion engines are considered as one of the major sources of environment damage because of their damaging emissions such as Carbon Dioxide (CO₂), Oxides of Nitrogen (NO_x), and Unburned Hydrocarbon (HC). Under the Kyoto Protocol [1], the UK has committed to a reduction of 12% in the CO₂ emissions by 2010.

Over the past several years and across the world, many different approaches have been researched and focused for the reduction of fossil fuel consumption and lower emissions out of the vehicles. However, there are many concerns when considering these technologies and having them implemented to the commercial and mass production market. Concerns of which include changes to the fuelling infrastructure, safety and costs of these technologies. Electric battery cars have in recent times been introduced to the passenger cars market as Hybrid type of vehicles; they still have critical weaknesses such as high costs to buy and maintain, lack of substantial infrastructures and recycling concerns. Alternative and renewable fuels have also been researched and can be a solution so that they support the preservation of fossil fuel resources and often create a less pollutant environment.

Sufficient research has carried out on internal combustion engines in order to develop and implement new combustion techniques such as Homogeneous Charge Compression Ignition (HCCI) or Controlled Auto-Ignition (CAI) to satisfy the environmental challenges facing IC engines. This study investigates the benefits and effect of CAI combustion such as lower fuel consumption and emissions, especially NO_x emissions. As one of investigations by Brunel University in conjunction with FORD in 2002, it has been proved that CAI combustion is effective of NO_x reduction of 90% improvement and 30% of brake specific fuel consumption (bsfc) improvement at low load and 18.6 % improvement of whole cycle on Ford Mondeo

through the NEDC (European New Emission Drive Cycle) [2]. This chapter describes the study of CAI combustion since introduced by Onishi and Naguchi in 1979[3] [4].

2.2 Gasoline Engine Emissions

2.2.1 World Emissions standards

The major pollutants released from burning fossil fuel in internal combustion gasoline engines are carbon monoxide (CO), oxides of nitrogen (NO_x) and unburnt hydrocarbons (uHC). Those pollutants are indispensable products to investigate gasoline engine technology due to the absence of practical energy resource alternatives in automotive industry, but also raise serious concerns with regard to their environmental impact at the same time.

Over the last 30 years, dramatic reduction and improvement of those emissions have been achieved through the development of exhaust gas after-treatment technologies such as the catalytic converters. The stricter band of legislation related to emission of these pollutants has enforced in the united States (USA), Japan and Europe countries (EU) and has lead to the large achievement of technology. Table 2.1 shows the legislation levels of emission from passenger cars for European Union and the California Air Resources Board (CARB) [5] [6].

EU emission legislation was introduced in the 1970s, restricting CO, uHC, NO_x, PM. The emission reduction has been planned as 6 steps, EURO IV adopted from 1st of January 2006 and EURO V from 2008. Table 2.1 shows the trend and significant reduction of emissions limits that are required in every steps and EURO V in 2008 and additionally proposed EURO VI in 2014. EU emission legislations demand that all vehicles manufactured after stated years must meet the permitted emission levels based on specific basis and over a standard cycle, intended to be representative of a typical drive cycle.

Euro Standard	Year	Engine type	CO (g/km)	HC/NMOG (g/km)	NOx (g/km)	HC+NOx (g/km)	PM (g/km)
Euro III	2001	SI	2.3	0.2	0.15	-	-
		CI	0.64	-	0.5	0.56	0.05
Euro IV	2005	SI	1.00	0.1	0.08	-	-
		CI	0.5	-	0.25	0.3	0.025
Euro V	2008	SI	-	0.05	0.08	-	0.0025
		CI	-	0.05	0.08	-	0.0025
CARB (LEV II)	2004-10		2	0.033	0.04	-	-
TLEV			-	-	-	-	-
LEV			4.2	0.056	0.07	-	0.01
ULEV			2.1	0.034	0.07	-	0.01
SULEV			1	0.006	0.02	-	-

Table 2.1 Current and future EU and CARB legislating emissions levels for passenger cars

The US standards consist of 2 sets: Tier 1 and Tier 2 defined for light-vehicles in the Clean Air Act Amendments (CAAA) founded in 1990. Tier 1 was proposed in 1991 and completely implemented in 1997. Tier 2 was adopted in 1996, phased-in beginning of 2004. The CARB has specified additional standards to Tier 2 regulations. The current CARB has following categories: Tier 1, Transitional Low Emission Vehicles (TLEV), Low Emission Vehicles (LEV), Ultra Low Emission Vehicles (ULEV), Super Ultra Low Emission Vehicles (SULEV) and Zero Emission Vehicles (ZEV).

The US CARB legislation is shown to be significantly different from EU standards in that it is based on a “Fleet-averaged” emission strategy, where the automotive manufacturers must meet the average emissions levels from the total sales of products range within the prescribed limits. It is not applicable directly to compare EU standard to US EPA (Environmental Protection Agency) standard due to the differences in the test drive cycle and measurement methods. Johnson [7] pointed out, through the normalization of the EU and US standards, that the level of unburnt hydrocarbon by US and EURO IV, V standards are roughly similar but US LEV II permits approximately half amount of NOx emissions. This means that recent technology of IC engines is going to be seriously limited in terms of NOx emissions

until adequate exhaust gas aftertreatment systems are developed, in spite of development of High Speed Direct Injection (HSDI) for diesel engines and Gasoline Direct Injection (GDI).

In addition to emission standards, CO₂ emissions are also limited by government policy in the UK and many European countries in order to reduce global climate change. This takes the form of heavy taxation of fuel, advantages on Road Fund Duty/road tax for small capacity vehicles and recently introduction of “company car tax” that imposes heavy penalties for operation of vehicles with high CO₂ emissions. A number of European car manufacturers have reached voluntary agreement with that their fleet average CO₂ emissions from current 160 g/km to 120 g/km by the year 2012, equivalent to a 25% reduction.

2.2.2 Unburnt hydrocarbon

Unburnt Hydrocarbons (uHC) or appropriately organic emissions from uHC are the consequence of incomplete combustion of the hydrocarbon fuel. Typical levels of unburnt hydrocarbon emission in the exhaust gas of SI combustion engine under normal operation are in the range 1000 to 3000 ppm [8]. HC emission goes up rapidly when the mixture AFR becomes substantially richer than stoichiometric. When combustion quality deteriorates, e.g., with very lean mixture, HC emissions could rise rapidly by incomplete combustion or misfire. Such a feature leads higher HC levels in CAI combustion than in SI combustion. There are several mechanisms that contribute to total HC emissions in which this section describes sufficient fundamental mechanisms that are likely to be important.

The mechanisms of HC emissions formation in SI engines have been proposed. Four possibilities are outlined below where the fuel-air mixture is premixed.

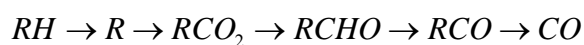
1. Flame quenching at the combustion walls
2. The filling of crevice volumes with unburnt mixture
3. Absorption of fuel vapor into oil layers on the cylinder wall
4. Incomplete combustion

When the flame approaches to the chamber wall, a quench layer containing unburned and partially burned air-fuel mixture is left at the wall due to its cooler temperature. Within the combustion chamber geometry, there exist other volumes such as crevices in the combustion chamber, threads around the spark plug, the head gasket crevice and intake and exhaust valve heads. Those volumes where the flame is unable to penetrate are the major source of unburned HC. Those volumes trap the unburned HC pushed by the rising in-cylinder pressure during the compression stroke. The presence of lubricating oil in the fuel or the walls in the chamber is also known to increase HC levels in the exhaust gas since it is burned with fuel. Lastly, incomplete combustion in the engine's operating cycles increases HC levels since partially burning and misfiring combustion occur.

One of the major factors in determining Spark Ignition (SI) engine emissions is the Air Fuel Ratio (AFR). SI engines are normally operated close to stoichiometric or slightly richer to get smooth and reliable operation. When AFR gets richer, HC emission levels increases rapidly. Lean mixtures could be used to produce lower HC emissions until combustion quality deteriorates. In general, Three-way catalyst technology is one of the best solutions to decrease HC emission.

2.2.3 Carbon-monoxide

Carbon Monoxide (CO) is one of the major emissions from internal combustion engines. This species are controlled primarily by the Air-Fuel ratio. CO formation is one of the principal chemical reaction steps in the hydrocarbon combustion mechanism, which may be summarized by:



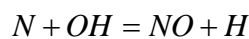
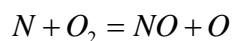
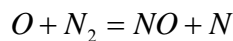
Where R stands for the hydrocarbon radical. This formation occurs in the combustion process and then oxidized to CO² at a slower rate. CO concentrations in the exhaust are increased steadily in condition of fuel-rich mixture and vary little with leaner mixture conditions.

Although many questions remain about the detail of the CO oxidation mechanisms, the practical approach to exhaust emissions could be determined by AFR. The

achievement of control within the engine has come from improving mixture uniformity and leaning out the intake mixture. In multi-cylinder engines, CO concentrations are increased rapidly as the inlet mixture becomes richer than stoichiometric and cylinder-to-cylinder variations are important. Additionally CO emissions during engine warm-up are much higher than emissions in the fully warmed/hot conditions. The reduction of CO emissions beyond that achieved in the engine is possible with exhaust after-treatment systems. Oxidation of CO in the exhaust system without exhaust after-treatment system does not occur to any significant degree.

2.2.4 Nitrogen Oxides

Nitric oxide (NO) and Nitrogen dioxide (NO₂) are considered as NO_x emissions. Nitric oxide is the predominant oxide of nitrogen produced in the engine cylinder. The mechanism of NO formation generally occurs in the combustion of a near stoichiometric air-fuel mixture. The principal reactions are:



The burned gas temperature distribution and pressure in the cylinder during the combustion and expansion processes impact upon the NO formation process. The most important engine variables for NO_x emissions are the air-fuel ratio, the burned gas fraction of the in-cylinder unburned mixture, and spark timing.

NO emissions peak at slightly leaner than stoichiometric AFR. As the mixture is leaned out, increasing oxygen concentration increases the gas temperature. In richer mixtures, substantial NO decomposition occurs at the maximum in-cylinder pressure. In leaner mixture, NO concentration freeze and little NO decomposition occurred. The burned residual gas from previous cycle is recycled to the intake for NO_x emissions control. Increasing burned gas fraction reduces NO emissions levels since the burned gases act as a diluent in the unburned mixture. Substantial reductions of NO concentrations are achieved with about 15~25 percent EGR.

Spark timing significantly affects NO emission levels. Advanced spark timing advances combustion in the cycle and increases in-cylinder pressure and in turn leads to higher peak burned gas temperature and thus higher NO formation rates occur.

2.3 Current automotive engines and technologies

The ultimate emission legislations have forced manufacturers to develop more and more efficient engines with ultra-low pollutant emissions. Although practical zero emission vehicles (ZEVs) with acceptable performance have been introduced in the market, there are still a number of technical obstacles to the application of fuel-cell technologies. Manufacturers have been faced with developing new fuel-cell technologies, altering infrastructure, the engineering optimization, etc. Therefore, fuel-cell technology is not the best solution to implement into the market in the short and medium terms.

Various models of hybrid vehicles using internal combustion engine and battery cells have also been introduced in the market (such as the Toyota Prius and the Honda Insight). However, these vehicles have limited market penetration as they have disadvantages of higher cost due to added complexity in control system and drawback of fuel consumption due to extra weight of batteries with an electric motor.

While hybrid vehicles may satisfy the market in the short term whilst leading the way to a true ZEV, substantial improvements in emissions and fuel consumption are currently being achieved in traditional SI and CI diesel engine technology. The 3-way catalytic converter in SI gasoline engine reduces engine-output emissions of CO, uHC and NO_x by over 90%. However, a close to stoichiometric operation is required in SI engine so that the catalyst can operate efficiently [9]. This precise near-stoichiometric mixture formation is beyond the traditional carburetor engines and so has been rapidly replaced by electronically controlled fuel injection systems with a lambda sensor and closed loop control. This electronically controlled engine at the continuous stoichiometric operation prevents a lean AFR engine operation at part load, resulting in small but significant increase in overall fuel consumption.

Stratified Charge Gasoline Direct Injection (GDI) engines have been introduced to allow lean combustion with electronically controlled engine by load control and independent airflow. This lean combustion, however, prevents the effective use of traditional exhaust after-treatments in terms of NO_x reduction. Although deNO_x catalysts have been introduced into the market, they are currently expensive and require the development of infrastructure. In addition, the emissions legislation beyond EU V and US Tier 2 demands levels of Particulate Matter (PM) as well, which can be achieved only by a PM filters within the exhaust

As an alternative combustion technology, Homogeneous Charge Compression Ignition (HCCI) or Controlled Auto-Ignition (CAI) combustion has been introduced that offer ultra low NO_x emissions and virtually no smoke emissions. It has the potential to offer not only to meet current and future emissions legislations, but also no need for the extra expense and complexity of exhaust gas after-treatment systems.

2.4 Controlled Auto-ignition (CAI)

2.4.1 Introduction

Over the last 30 years, the IC engines from vehicles have been dramatically improved to reduce the levels of NO_x, CO and VOC emissions by the use of exhaust gas after-treatment systems, such as the catalytic converter. Even though IC engines have been developed to improve the fuel consumption and lower emissions, for example with direct injection system, Variable Valve actuation system, etc, drawbacks with IC engines are still constrained by costs and requirements of more advanced technology. Over the decades, alternative combustion technology, well known as Homogeneous Charge Compression Ignition (HCCI) or Controlled Auto-Ignition (CAI) combustion, has been seriously considered as the next generation technology since it has the potential to achieve negligible NO_x emissions and improved fuel consumption when operating at lean conditions. This combustion mode with significant potential benefits also faces its own challenges, such as higher HC emission levels, limit of operating region and difficulty in controlling the combustion phasing.

2.4.2 Historical background

The pioneers of Controlled Auto-Ignition (CAI combustion) can be considered to be Onishi [3] and Noguchi [4] in 1979, who investigated an alternative combustion process within a 2-stroke engine which was at the time named “Active Thermo-Atmospheric Combustion (ATAC)”. However, the theoretical origin of HCCI/CAI combustion is considered to be due to the Russian scientist Nikolai Semenov and his colleagues in the 1930s. Semenov established his own chemical and chain theory of ignition and exploited a chemical-kinetics controlled combustion process for IC engines. His theory was based on challenges to the limited physical process of SI and CI engines. He developed an engine utilizing a lean air/fuel mixture in order to limit heat release rates to more uniform levels. His design consisted of a separate pre-chamber in which was designed for a partially burned mixture and high temperature discharge. A rich mixture is mixed up with a partially burned mixture in the main chamber and initiate homogeneous combustion in lean condition of active chemical species and high temperature gas.

Following Onishi and Noguchi’s work which demonstrated the significant potential to improve fuel consumption and emissions by CAI, Honda carried out further research and development, leading to the introduction of the first production CAI automotive engine, the 2-stroke ARC 250 motorbike engine [10]. This was different from conventional gasoline engine combustion in that ATAC occurs spontaneously at many points in the combustion chamber and sometimes leads to erratic combustion. Their research showed that the presence or absence of an electric spark has no effect on the combustion pattern. No conventional flame front propagation was seen in their experiments; rather combustion occurred, irregularly and spontaneously in the chamber. They showed also the different feature of uniform mixture with air and fuel from conventional Diesel combustion without any exhaust smoke. They demonstrated that ATAC requires few conditions so that the quantity of mixtures and air/fuel ratio be uniform from cycle to cycle, and cyclic regularity of the scavenging directivity and velocity for the residual gases, and suitable temperature in the combustion chamber. It could be achieved with a lean mixture at the part-throttle operation.

After introducing the potential of such a combustion process in terms of reduction of fuel consumption and emissions, the first investigation and application to a 4-stroke engine was carried out by Najt and Foster in 1983 [11]. They achieved heat release control in CAI combustion using highly diluted intake charge by intake heating. However, their approach was limited by the engine load range and drawbacks of intake heating, such as extra energy source of the intake heating method.

The later achievements of CAI was introduced by Thring in 1989 [12], the first investigation on the effects of Exhaust Gas Recirculation (EGR) with heat release characteristics and operating regions by air-fuel ratio (particularly very lean condition) at limited engine operation load. It was investigated that CAI requires high EGR rates (13~33%) to control heat release rates and high intake temperature, is limited by operation on low engine speed and load. He also found that it offers relatively good fuel consumption under the right conditions (isfc: 180~200g/kwh) and in comparison to Diesel engine at idle and light load, also improved specific power output.

The first four-cylinder gasoline engine in CAI combustion was shown by Stockinger, et al in 1992 [13], operating at limited engine speed and load range by means of higher compression ratio and the pre-heating intake heater. Different types of fuels has also been investigated to achieve CAI combustion, research using Primary reference fuels (PRFs) has shown that auto-ignition is significantly influenced by fuel composition, molecular size and structure [14], giving great potential for CAI combustion with various fuels.

Olsson, et al [15], in the late 1990s, demonstrated auto-ignition on the largest capacity engine; a 12- litre six cylinder diesel engine, but running on a mixture of isooctane and heptane through closed loop control. They achieved auto-ignition combustion over a large speed and load range by a combination of fuel blend, turbocharging, high compression ratio and intake air heating. In 1999, Christensen, et al [16] showed the flexibility of different fuels on CAI that any type of liquid fuel can be used in CAI engine and low NO_x emissions. Experiment condition was based on a combination of variable compression ratio and intake heating temperature, resulting in that inlet temperature range could be determined by compression ratio

and lower compression ratio leads to lower heat release rate, in-cylinder pressure and combustion efficiency.

It has become apparent that the major challenge for auto-ignition control is employing sufficient thermal energy into the chamber. Since the use of inlet air heating is faced with difficulties on a production engine in the short term, researchers have turned their attention into the exhaust gas recirculation (EGR) approach, thus using the ready thermal energy from exhaust gas. As mentioned earlier, Thring introduced external EGR on a SWRI Labeco CLR engine to accomplish CAI combustion. However, external EGR approach showed inherent problems in that it causes cycle to cycle variation and heat losses through the external device. In addition, it is very difficult to regulate the quantity of EGR into the chamber.

One of the most significant progresses in CAI is the use of residual gas trapping by negative valve overlap [17-20], during which burned gas after main combustion is trapped within the cylinder through the early closure of the exhaust valves coupled with delayed opening of the intake valves in a 4-stroke gasoline engine [17]. The CAI operation was achieved over a range of speed and load. With the variable valve actuation systems, it is possible to achieve much greater potential of CAI as demonstrated by Law [20]. Another effective approach to use hot burned gases is by internal EGR through positive valve overlap, during which the exhaust gas is re-breathed back into the chamber.

As researched intensively over the last few years, the residual gas trapping appears the best solution for achieving CAI combustion in a production gasoline engine, in the short to medium term. It does not require any massive modification of the engine architectures and associated high expenses.

2.4.3 Principle and combustion characteristics of CAI engines

The CAI combustion operation has the same mixture preparation process as the conventional SI combustion operation, i.e., the air and fuel mixture is formed in the intake system or in the cylinder with direct injection. The premixed mixture is compressed by the compression stroke and combustion is initiated by auto-ignition in

a similar way to the conventional CI engine. The initiation of auto-ignition requires increasing the charge temperature at the beginning of the compression stroke above that of conventional SI combustion, which can be achieved by an intake heater or hot EGR. Heated intake charge results in a higher gas temperature and the faster chemical reaction through the compression stroke, leading to homogeneous combustion initiation. Even though the main heat release requires the high temperature condition in value of 1050-1100K for gasoline and less than 800K for diesel, low temperature oxidation reactions also occurs with many hydrocarbon components. This low temperature heat release is influenced not only by the chemical kinetics of the fuel and the dilution strategy, but also by the temperature and pressure history that the mixture undergoes through the compression stroke.

CAI is characterized by relatively fast and high peak heat release rate and shorter combustion duration than conventional SI combustion. Onishi, et al. [3] showed the maximum heat release rate to be increased up to 30 % over conventional combustion, Lada, et al. [21] showed that combustion duration can be shorter up to 30% using a ceramic cylinder head than the conventional aluminium type. They also found that it promotes more advanced ignition and better combustion efficiency by lower heat transfer characteristics of the ceramic material. The rapid combustion and high peak heat release rate encountered by CAI due to the simultaneous mixture combustion must be controlled by using a lean air-fuel mixture and/or charge dilution to prevent engine damage and emissions control.

2.4.3.1 Heat release rate

The heat release characteristics of the CAI combustion are shown in Figure 2.1 [22], in comparison to SI combustion. The horizontal axis represents the fraction of total mixture mass (m_c) and the vertical axis represents the specific heating value of the in-cylinder charge. The cumulative heat release (Q) is calculated by a mass (m) and heating value (q) of mixture.

In case of SI combustion showing significant flame propagation, a thin layer in between burned area and unburned area of the cylinder charge is a hot reaction zone (δ_m) that the full charge mixture is combusted in. The sum of heat released by a

mass of this heating zone (dm) and the heating value per unit mass of air and fuel mixture is the cumulative heat release (Q) where N is the number of reaction zones in SI engine. Thus, the entire heating value of mixture is released during the limited duration, in the reaction zone.

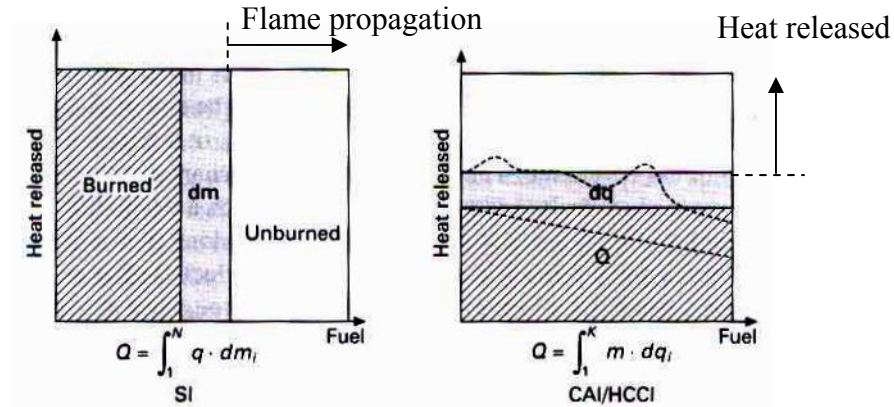


Figure 2.1 Heat Release Characteristics of SI and CAI combustion

In an idealized CAI combustion, combustions take place almost simultaneously in all parts of the charge in CAI combustion. The cumulative heat release is therefore the total heating value of intermediate reactants (dq) and the complete mixture (m) in the cylinder where K is the total number of heat release reactions. Thus, heat release takes place uniformly across the entire charge. However, the mixture composition and temperature distribution in a real engine is not homogeneous, hence heat release process will not be completely uniform throughout the mixture. Furthermore, the less diluted mixture and high temperature region exists and take place heat release, resulting in a non-uniform heat release trend shown the dashed line area.

2.4.3.2 CAI operating region

The CAI operating range is one of the major challenges for research into CAI combustion, compared to conventional SI and CI engines. Since Onishi and Noguchi [3,4] demonstrated the ATAC engine at low loads over the full speed range of a two-stroke gasoline engine (1000~4500rpm), the limit of CAI region in a four-stroke engine was confirmed in a single cylinder engine by Thring [12] in 1989. He carried out a brief investigation into the effects of engine speed on CAI combustion by increasing intake temperatures. However, he did not attempt CAI at engine speeds higher than 2000 rpm since Ferguson [23] reported that engine speed does not have

any measurable effects on CAI combustion duration, unlike the case of SI combustion. He pointed out that the mixture composition, temperature and pressure should be altered to ensure properly phased combustion. This theory was supported by the modelling work by Najt and Foster [11]. They showed that as engine speed is increased, the initial charge temperature should be also increased to compensate for the reduced time available for combustion to complete and reactions leading to auto ignition.

Li, et al. [24] described the CAI operating range by engine speed versus load map in 2001. They showed an operating range at engine speed from 1000 rpm up to 3500 rpm and load range from 0.5 bar to 4 bar bmep as shown in figure 2.2.

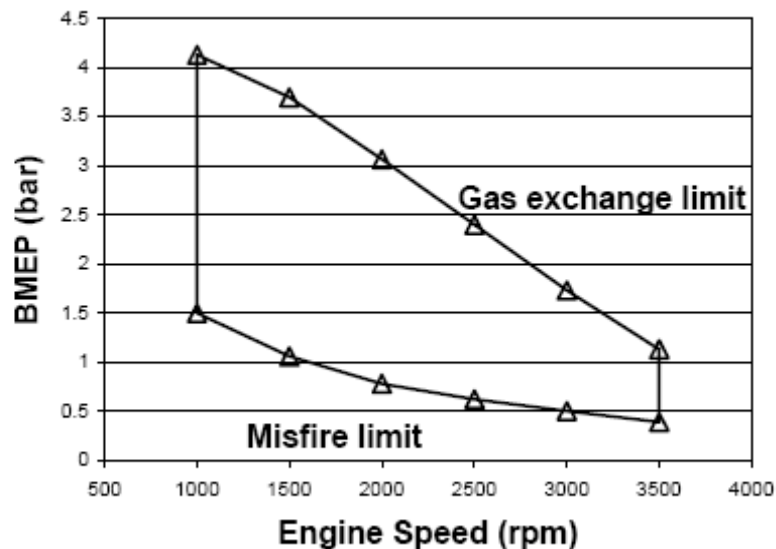


Figure 2.2 Operating range of CAI combustion [24]

They identified two main limits for CAI operating region - the gas exchange limit at the high engine load, the misfire limit at lower engine load. The gas exchange limit is caused by lower valve lift and shorter valve duration of camshafts in terms of NVO (Negative Valve Overlap) strategy, which restricts intake air flow. The misfire limit is caused by the low exhaust gas temperature, which is too low to initiate CAI combustion.

A comprehensive CAI operating region was introduced for a range of AFR and EGR rates by Oakley, A. [25] in 2001 in a single cylinder research engine. CAI operation

was achieved by an intake heater increasing to 320 °C and external EGR trapping method. Figure 2.3 shows a boundary region for CAI operation. The vertical axis represents the overall AFR of the charge in the exhaust pipe and the horizontal axis represents the total percent of trapped EGR in the cylinder. As his map introduced the limits of CAI operating region, knock and partial burnt region were clearly presented and challenged to enlarge them in this study.

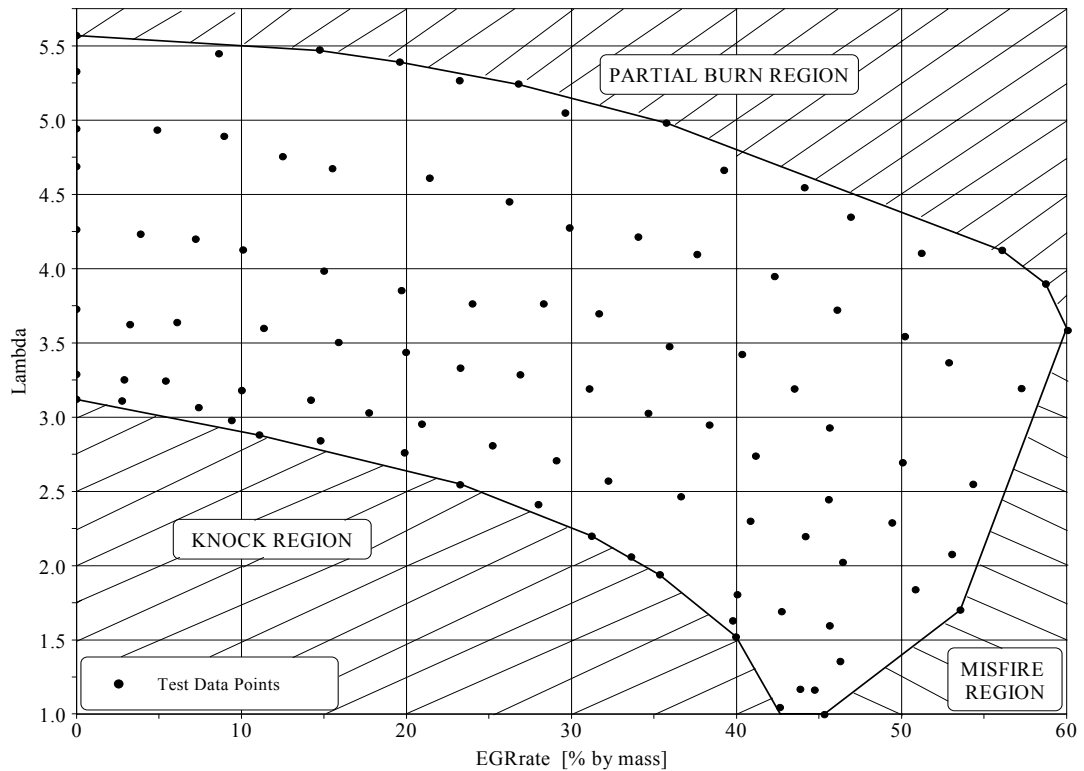


Figure 2.3 Boundary regions for CAI operation, unleaded gasoline [25]

The operating region is limited by three boundaries:

1. Knock region
2. Partial burn region
3. Misfiring region

The knock boundaries are defined as the AFR is getting richer and lower EGR rate. The richest AFR (lambda 3.15) is achieved when there is no EGR trapped and the maximum EGR at this knock region is brought closer lambda 1 with 43% EGR. This knock region is the most challenging part to enlarge the CAI operating region since it is the potential area to achieve the highest engine loads in CAI.

The partial burn boundaries are limited by excessively reduced fuelling rate. The reduced fuelling, leaner condition leads the lower combustion temperature since the fuel oxidation cannot occur completely. This results in high concentration of partially unburned combustion components in the exhaust gas.

The last boundary defines the misfire region at higher EGR rate and richer AFR. The CO² and H₂O content of the intake charge is significantly increased, resulting in the ignition timing retarded and eventually causes the combustion failure in a small proportion of cycles. The border area between knock and misfire region is interesting since the highest imep of 3.8 bar is achieved. The imep is linearly decreased with AFR as the fuelling is reduced at constant air flow rate.

2.4.3.3 IMEP and Cycle to cycle variation

The imep is a crucial indicator of IC engines performance characterizing the engine load range, especially for CAI operation due to the limited load range. Higher engine loads in CAI are achieved by increasing fuelling rate, resulting in lower lambda value. The highest loads are achieved at lower EGR rates due to the EGR dilution effect. The lowest imep achievable in CAI depends on various conditions such as acceptable levels of uHC and CO emissions, specific fuel consumption and cyclic variation. A typical imep map in CAI operating region is clearly defined by Oakley, A. [25], shown in figure 2.4.

Cycle to cycle variations has been shown to correlate with engine torque variations, directly affecting vehicle drivability [8]. These arise as a result of changes in mixture composition and temperature and the charge formation process. In addition, cylinder to cylinder variations occur in multi-cylinder engines caused by non-uniformed air/fuel mixture distributions in the cylinder and temperature gradients within the physical engine geometry, resulting in differential heat transfer. Therefore, it is crucial that the cyclic variations should be minimized in the design phase for smooth engine operation and optimized performance in terms of emissions and efficiency.

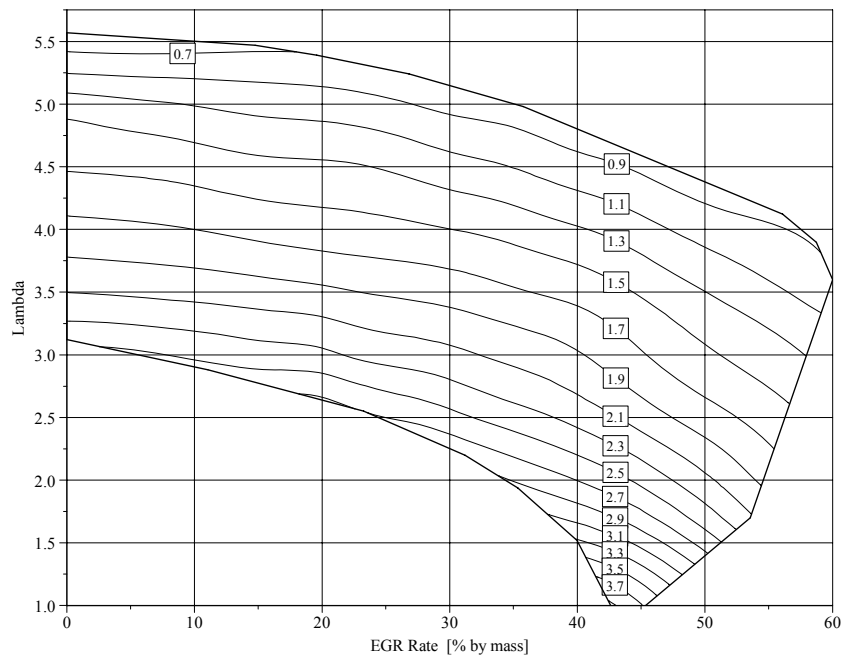


Figure 2.4 Net IMEP (bar) for standard gasoline fuel [25]

Most researchers working on CAI combustion cyclic variation have focused on the variation in the maximum cylinder pressure amongst successful cycles. As a result, the cyclic variation on CAI is shown to be lower and smoother than SI combustion. However, it has been pointed out that low cyclic variations on CAI by the maximum pressure unnecessarily lead to low cyclic variations in torque output. A statistical method of the cyclic variation is known as the coefficient of variation (COV) and the coefficient of variation in IMEP (COV_{imep}) is commonly used to quantify the variation between cycles.

2.4.3.4 Engine output emissions

One of the major potential benefits of CAI combustion is reductions in NO_x emissions in the region of 90-98% maybe possible. The reduction of NO_x emissions is caused by the lower temperature of the combustion reaction zones, compared to the relatively high temperatures encountered with SI and CI combustion. However, this lower temperature can also lead to higher CO and uHC emissions in four-stroke gasoline engine [26]. These emissions are normally associated with incomplete combustion, low temperature and cyclic variation.

Onishi, et al. [3] reported ways to prevent higher CO and uHC emissions. They used a two way catalyst to reduce CO and uHC emissions to the low level of 50 ppm and

0.03% respectively. Although NO_x emissions were slightly increased at higher load, they found this did not affect the catalyst operation. Lavy, et al. [17] showed a comparison between CAI and SI pre-catalyst emission characteristics on a Honda 250cc ARC engine. They showed that both HC and NO_x emissions were decreased by up to 35 % at 2500 rpm and 1.75 bar imep load.

Aoyama, et al. [27] also compared CAI, CI and GDI operation, showing a large NO_x reduction of 80-99% on a volumetric basis with CAI. While NO_x emissions are generally decreased by leaner AFR in CAI, HC emissions tended to rise with increasing air dilution as shown by Noguchi, et al. [4].

Christensen, et al. [16] showed the results of emissions in their study of various fuels including isooctane, ethanol, and natural gas. All fuels generally resulted in the highest levels of NO_x emissions occurring at higher loads and at higher intake temperatures. HC levels are shown more than two times of levels from SI combustion and CO levels approach reasonable levels at loads of all the tested fuels. They pointed out that EGR is extremely effective to reduce NO_x emissions at higher fuelling rate for isooctane and ethanol, but not natural gas. It was concluded that higher air dilution reduces NO_x emissions, but engine loads are reduced since the best efficiency requires maximum air flow. However, it is well established that EGR rates can be increased to optimize combustion and reduce NO_x emissions. EGR tends to decrease HC emissions with minimal effect on CO emissions.

Oakley, et al. [25] introduced the trend of specific exhaust gas emissions in the map of CAI operating range, described in the previous section. They plotted emissions in conjunction with air dilution in the achievable AFR and EGR dilution in trapped EGR rate in CAI combustion.

2.4.3.5 Combustion control

Combustion within CAI is extremely difficult to control since CAI combustion is governed by chemical kinetics which initiate spontaneously depending on temperature, pressure and mixture composition. However, a number of researches have been introduced to control CAI combustion auto-ignition timing by typically

ignition timing, heat release, spark timing and injection timing by gasoline direct injection (GDI). In addition, Christensen et al [92] exposed several potential parameters such as compression ratio, inlet temperature and pressure, fuel type, AFR, EGR rates, engine speed and coolant temperature.

Oakley [25] also presented well CAI combustion characteristics in CAI operating range. Combustion is monitored as the crank angles at 10, 50, and 90% of the charge mass burned. The 10 % of mass of fraction burned is considered as the start of combustion and the 10-90% of it is considered as the combustion duration. He also found that EGR rates higher than 40% significantly retards ignition timing when A/F ratio is reduced. However, EGR rates less than 40% is generally very small effect on ignition timing.

CAI combustion is commonly achieved nowadays through negative valve overlap (NVO) with variable camshaft timing (VCT) systems, which allows combustion control much further by determining quantity of residual gas, effective compression ratio. Furthermore, GDI system also allows much intensive injection timing control for CAI combustion timing.

2.4.4 Challenges facing CAI combustion

CAI combustion has been achieved by using many different methods over the last few decades. Much of the work performed in this area has focused on achieving improved fuel economy and lower pollutant emissions, mainly NO_x emissions. However, several obstacles exist which must be overcome for successful commercial application to occur, the most important of which is effective combustion control. This can be achieved by controlling the temperature, pressure and composition of the in-cylinder mixture generally through controlling a combination of the following parameters [22]:

- EGR or residual rate
- Air-fuel ratio
- Compression ratio
- Inlet mixture temperature

- Inlet manifold pressure
- Fuel properties or fuel blends
- Injection/spark timing
- Coolant temperature

It is very difficult to trap the larger quantities of hot internal residuals required to achieve CAI combustion using conventional SI engine camshafts which feature positive valve overlap. Hence, intake air heating has been investigated in conjunction with variable compression ratios to achieve CAI, the impact of which has been studied by several groups. Thring [12] heated up the intake air at a compression ratio of 8:1 and achieved CAI combustion at a range of different EGR rates and air-fuel ratios. Aroonsrisopon, et al [28] investigated a range of intake temperatures from 300K to 400K on a single cylinder engine with different fuels. Sjoberg and DEC [29] studied the effects of intake temperature on CAI combustion phasing. Christensen, et al [16] found that the required preheated charge temperature can be reduced with increased compression ratio. With a compression ratio of 22.5:1, they obtained CAI combustion without heating the intake air. Aoyama, et al. [27] achieved CAI combustion at CR 17.6:1, intake temperature of 300K and boosting air pressure of 1.28 bar.

Since negative valve overlap (NVO) is a strategy widely employed to achieve CAI combustion through trapping hot residual from exhaust gases, variable valve actuation technology has been developed for the fast and direct control of combustion phasing by varying the effective compression ratio and/or the quantity of hot exhaust gases trapped in the cylinder. Recently, one of most promising developments in the control of combustion phasing has been through direct injection technology which allows alteration of the local fuel concentration and variation of injection timing. Several studies have shown that early injection timing provides more time for fuel to vaporize and mix with air to achieve homogeneous charge [30 - 32]. Urushihara, et al. [30] found that the direct injection helps to expand the CAI region without any further increase in NO_x emissions by direct injection into the hot residual gas for reforming it.

One of other major challenges facing the commercial application of CAI combustion is the limited operating boundary compared to SI combustion. As a consequence of CAI combustion by hot residual gas trapped and the diluted mixture, CAI operation is limited in two limiting regions where knock occurs at high load and partial burn or misfire at low load.

The limiting knock region at high load can be extended by boosting of the intake air combined with a leaner mixture, as shown by Christensen, et al. [33]. Although thermal efficiency was reduced due to higher heat transfer, higher load boundary of CAI combustion was dramatically enlarged by using a reduced compression ratio (17:1) and higher boost pressure (2 bar). Christensen et al. [34] also investigated HCCI by supercharging a single cylinder engine with variable compression ratio and with a pilot fuel injection of iso-octane and with cooled EGR, which resulted in the extension of the higher load boundary. Olsson, et al. [35] discussed the effects of cooled EGR on HCCI combustion using a turbocharged multi-cylinder engine and found that the presence of external EGR introduces a pressure drop and negatively affects the performance of the turbocharger. Yab, et al. [36, 37] studied the effects of boosting on a gasoline engine with residual gas trapping. They found that there is a limit of boosting pressure without intake heating and with a certain amount of trapped residual due to the limit of heating effect. They also discussed that higher EGR rates with higher boost pressure can reduce NO_x emissions further, but higher fuel consumption and CO emissions occur due to the increased pumping losses and lower combustion efficiency. Wilhelmsson, et al. [38] showed an operational strategy for HCCI in a heavy duty, turbocharged, dual fuel port injected engine. They stated that the lower exhaust temperature, a natural consequence of CAI, tends to limit the maximum boosting pressure by pumping losses. This means that the boosting strategy for CAI has limitations and generally aims to apply as little boost as possible while ensuring NO_x emissions are satisfactory.

The lower load limit at the partial and misfire boundary can be improved by spark assisted ignition. Kalian, et al. [39] showed recently that spark ignition assists CAI/HCCI combustion at lower load operations by providing more favourable in-cylinder conditions for auto-ignition to occur. Spark assisted CAI also allows lower compression ratio or lower intake temperature to be used throughout the wider CAI

operating range as shown by Hyvonen, et al. [40]. Some studies [41 - 43] have found that spark assistance strategies in CAI show potential in the transition between internal EGR operated CAI and SI operation since spark assistance strategies allows mode transfer with thermally activated HCCI operation by high compression ratio and fast thermal management. More recently, Urushihara, et al. [44] extended the spark assisted CAI concept to the hybrid concept with SI and CAI combustion by igniting a stratified charge near the spark plug so that the pressure rise from the SI combustion causes the diluted, premixed mixture to auto ignition.

Furthermore, some other techniques have been studied to enlarge the low and high load regions of CAI operation. Milovanovic, et al. [45] demonstrated that both the low and high load regions of CAI operation can be extended by regulating coolant water temperature. They extended the upper limit by up to 14% through decreasing coolant temperature and extended the lower limit by up to 28% by increasing coolant temperature. They also found that reducing coolant temperature increases uHC and NO_x emissions since the lower cylinder wall temperature suppresses fuel oxidation. Aroonsrisopon, et al. [46] demonstrated that stratified charge shows potential for more stable CAI combustion at the lean low-load limit by using a port fuel injector (PFI) for premixed charge and a direct injector (DI) for stratified charge. Another novel approach to enlarge the operating region is discussed by Osbourne, et al. [42] who showed that CAI/HCCI boundary region can be increased by the prospect of two-stroke/four-stroke switching engines. Two-stroke operation is useful in the high load region and offers exceptional torque at low engine speeds while four-stroke operation is beneficial for low/mid load ranges and low/medium engine speeds.

2.4.5 Applications of CAI combustion

Although CAI combustion has achieved dramatic improvements in terms of the reduction in fuel consumption and pollutant emissions, the attainable operating range of CAI is evidently limited compared to SI and CI combustion. This is due to the air and/or EGR dilution required coupled with the reduced quantity of fuel, thus limiting the maximum engine output compared to conventional combustion engines.

Consequently, it is unlikely that CAI combustion alone will be employed in commercial, mass production applications. The most promising application is a CAI/SI hybrid operation implemented in a four-stroke gasoline engine to cover the complete load and speed range of the engine. CAI operation would be employed at the low to mid load range while high load and even very low load range could be operated in SI mode. This hybrid-type operation has been proven to show improvements in emissions and fuel consumption at part-load associated with CAI combustion, while maintaining the full load engine performance associated with SI combustion.

Recent studies have investigated the transition between CAI and SI modes, optimizing control parameter settings. Koopmas et al. [47] demonstrated the successful transition mode between CAI to SI combustion on a single cylinder camless engine. They found a smooth transition between modes by tuning for the first few cycles after a mode change, although they encountered challenges in switching from SI to CAI mode. Milovanovic et al. [48] demonstrated that the 'mixed mode' CAI-SI engine is achievable with two different VVT systems, such as a cam profile switching and phasing device (CPS-P) or a fully variable electro-hydraulic (Pro AVT) system. They pointed out that the transition mode requires the valve train and engine management system to provide seamless operations while keeping all relevant engine and combustion parameters within an acceptable range. The VVT system has to be as flexible as possible and a fully variable electro-hydraulic Pro AVT system was introduced since a new ECU was required for the synchronization of the valve profile switching and throttles response.

2.5 Optical techniques

2.5.1 Introduction

Various optical techniques have been developed over time to provide visualization of the mixture formation and combustion process in internal combustion engines. Typical combustion related properties can be obtained by the use of laser diagnostics, for example, in-cylinder temperature, flow velocity, fuel droplet size, evaporation characteristics, and chemical species distribution/concentration.

Many combustion properties can be measured by means of physical measurement proving equipment such as thermocouples and gas chromatographs. Optical techniques, however, are superior in several aspects compared to physical measurements, for example they are largely non-intrusive in that the equipment is not directly affected by chemical or physical properties. Additionally, the laser techniques can be used to investigate spatial and temporal resolution, for example with the well known laser induced incandescence (LII) technique, something not possible by physical methods. Typical pulse duration of lasers used in combustion research is around 10ns, which allows study of the chemical reactions occurring via the chemical species present, typically CH, OH, NO or formaldehyde by the laser induced fluorescence (LIF) technique. This technique allows imaging of particular chemical species by the use of appropriate filters with known wavelengths coinciding with those of the particular chemical species under investigation.

However, the application of optical techniques also has distinct drawbacks in the implementation of these laser based techniques, amongst which is the limited optical access and measurement area available in IC engines. These techniques are not easy to operate and maintain for some applications. Since significant modifications are required to allow optical access, a trade-off between achieving realistic engine operation and providing a high level of access must be made.

In general, quartz or fused silica is commonly used for the optical window materials, with more expensive sapphire also frequently used due to its benefits of high wear resistance and transparency ranging from the UV to the infra-red region. For optical access a steel spacer is commonly equipped with windows, fitting between the cylinder head and block. This steel spacer causes some geometry drawbacks in order to determine the compression ratio compared to the standard geometry. The piston crown window is probably the most commonly used design for in-cylinder visualization and frequently used with laser diagnostic techniques. Optical access through this piston crown window can be achieved via a 45 ° mirror fitted in the middle of a piston extension. With this piston crown window, it is important to introduce an oil-free environment to prevent any contamination, for example by dry piston rings. This technique is known to have some drawbacks such as a large

crevice volume and limited load capacity. However, it can be improved by the combination with an optical spacer.

These optical techniques are very useful to investigate the various aspects of IC engines, especially in combination with other experimental techniques, such as quantitative data acquisition.

2.5.2 Direct Visualization

Visualization of engine combustion was first carried out by direct recording of luminous combustion. Traditionally, photographic films were the only means of imaging and the limited shutter speeds meant only one image was captured from one cycle, which means that a sequence of images were captured over many different cycles. However, photoelectric devices have been introduced allowing much faster image acquisition so that hundreds of images can be continuously captured from the same engine cycle.

Since the optical windows available in the 1920s were limited in strength, Glyde [49] mounted six button-like windows in a line traversing the cylinder head of a SI engine to view the flames through a slit in a revolving disk above the cylinder head. His design was improved to provide sufficient spatial resolution to plot flame position with such windows over the cylinder head by Marvin and Best [50].

The first successful implementation of a quartz window was introduced by Withrow and Rassweiler [51] in 1936 in an L-head engine whom, with a high speed cine film camera, obtained up to 30 pictures during a single combustion event. They found the initiation of combustion for the first time that appeared with a flame kernel at the spark plug, followed by growth of the kernel into a wrinkled flame front. They also developed a method of calculating a mass fraction burned profile from the cylinder pressure data associated with their combustion video [52].

Weak luminosity of the flame at leaner or diluted conditions with SI combustion was found by Nakanishi [53], who investigated the effect of charge dilution with high speed photography. He introduced a specially designed high speed camera to record

the weak blue flames of diluted mixtures since a high-speed film camera was only suited to the rich mixture combustion, shown as bright yellow luminance.

The intensified camera was introduced to record direct images of the weak luminance of the initial flame kernel by Bates [54] in 1989. He employed two intensified CCD (ICCD) video cameras with a sapphire liner and transparent piston so that one pair of images was recorded at a preset crank angle in each engine cycle. The intensifier gain was adjusted in order to prevent the ICCD cameras from overexposing by the strong radiation from the main combustion. Because flame propagation is extremely sensitive to density changes, Schlieren/Shadowgraph techniques were introduced for studies of flame initiation and development and have been used extensively in auto-ignition and knock studies. Ask et al. [55] employed a Schlieren system to study the flame kernel development, the axisymmetric Schlieren image was achieved by a circular aperture and a circular cut off aperture. Miller [56] reported photographic studies of knock by using a high-speed Schlieren system and found that auto-ignition of the end gas is not essential to the creation of a detonation wave. More high-speed Schlieren photographic studies on knocking combustion have been carried out by many researchers, recently by Smith, et al. [57] in the Sandia and Konig and Sheppard [58] in a two-stroke SI engine.

The first two-dimensional Mie scattering technique with a laser sheet was applied to study the flame structure in SI engines by Baritaud and Green [59] and Zur Loye et al. [60]. They employed an intensified solid state camera and the 2nd harmonic of a pulsed Nd:YAG laser as the illumination source due to its high power and relatively low cost. Although they experienced serious window fouling, evidence of increasing flame front wrinkles was obtained with peninsulas and pockets of unburned mixture in the burned gas region.

High-speed continuous recording of flame front structures was carried in a transparent square piston SI engine by Ziegler et al. [61] in 1988. They synchronized the laser, camera and digitized the film images using a CCD camera. The flame front was determined by a threshold in the image processing software where the light intensity changes from the un-burnt gases to the burnt gases. They determined Radii

of curvature, wrinkling factors and turbulent burning velocities at different engine speeds and crank angles.

Three-dimensional visualization was employed with four spatially separated laser sheets by Mantzaras et al. [62] in 1988. The four laser beams were the 2nd and 3rd harmonic beams of an Nd:YAG laser, along with the first stroke and first anti-stroke from an hydrogen Raman cell pumped at the 2nd harmonic. They found that the islands of un-burnt gases in 2-D images were through ‘fingers’ of un-burnt mixture on the different planes within the combustion chamber. Hicks et al. [63] also employed a similar setup to characterize the flame structure and turbulence scales in a two stroke SI engine in 1994. They found that islands of un-burnt gases behind the flame front were associated with encirclement by large-scale combustion structures rather than partial-burn or total quenching due to flame stretch.

2.5.3 Chemiluminescence

Chemiluminescence imaging allows a lot of information to be obtained by analyzing the natural flame emission by chemical species produced in the combustion process. Each radical species emits a specific spectral profile. Emission and absorption of combustion species are characterized by band spectra in the visible and UV regions. Table 2.2 shows prominent spectral peaks of intermediates and products of combustion in the visible and UV regions. Imaging through appropriate filters of a particular spectral wavelength shows the presence of the chemical species produced by the associated combustion reaction.

CH (nm)	OH (nm)	CH ₂ O (nm)	CO ₂ (μm)	H ₂ O (μm)	C ₂ (nm)
314	281-283	368		1.13-1.87	470-474
387-389	302-309	384	2.69-2.77	2.66-2.74	516
431		395	4.25-4.3	3.17	558-563
		412-457		6.27	

Table 2.2 Strong emission peaks of major combustion species in IC engine [74]

In the 1930s, a spectroscopic study was performed on both normal combustion and knocking combustion by Withrow and Rassweiler [64, 65]. They showed that the flame front under normal conditions showed the band spectra of CH, C₂ and OH, while the spectrum of knocking combustion showed a strong continuum in the red. They also found that the band of C₂ and CH were weaker from the knocking combustion zone.

Spectroscopic studies of the auto-ignition process were performed by the absorption spectra of end gases by Withrow and Rassweiler [66, 67]. They found that formaldehyde appeared prior to the arrival of flame and was more intense under knocking conditions. Their work was confirmed by Downs et al [68] in 1953 who showed that excited formaldehyde was the source of the cool flame radiation.

Noguchi et al. [4] introduced spectroscopic research with a new 3rd generation of IC engine to investigate the initiation and development of this new combustion process in 1979. They found that the emissions from radicals of OH, CH, C₂ and Hydrogen were detected separately while the emissions from CHO, HO₂ and Oxygen radicals were obtained together. This means that CHO, HO₂ and O radicals were detected first, followed by CH, C₂ and H radicals, with OH radical at the end in their new combustion, what would now be termed CAI combustion.

Shoji et al. [69,70] performed spectroscopic research to investigate pre-flame reactions in a SI engine in 1994 and 1996. They showed that formaldehyde was detected by emission at 395.2 nm and the OH radical was measured simultaneously by absorption from a xenon lamp at 306.4 nm. They concluded that those species are produced at the same time in the end gas region and formaldehyde appears prior to OH radicals.

Eckbreth [71] presented their findings that these emissions are the dominant source of luminosity in premixed combustion in 1996. The strong chemical species were introduced as for example, CH at 430 nm, OH at 308 nm, and C₂ at 516 nm. They were detected by spectral filtering of the collected signal in case of no severe overlap of wavelength.

Dec and Espey [72] used this chemiluminescence technique when investigating the auto-ignition process on an HD diesel engine under a variety of operating conditions. They presented their findings that the main contributors to the chemiluminescence signal were formaldehyde (CH₂O) and CH, well known spectra from ‘cool flames’ by spectrally resolved detection of chemiluminescence.

Optical studies in HCCI combustion using both CH and OH imaging was also performed by Hultqvist et al. [73]. They found that the integrated intensity of the chemiluminescence correlates with the rate of heat release in HCCI engine.

2.5.3.1 OH radical

The OH radical is one of the major chemical intermediates of combustion. Since OH radical is produced during the combustion process and detected in the high temperature region, OH radical is used as a good indicator of flame front and hot burned region not only in SI combustion at stoichiometric but also in CAI combustion at highly diluted AFR. Due to the very low peak temperature in CAI combustion by the highly diluted characteristics, the quantity of OH radical excited can be relatively small compared to SI or CI combustion.

The first PLIF measurement of OH radicals was carried out in a single cylinder two stroke SI engine by Felton et al. [75] in 1988. Although they found that the resolution of their imaging system was not sufficient to match the quality and precision, the OH LIF signal was detected by using a band pass filter of 313±5 nm and a Nd:YAG pumped dye laser operating 284.26 nm. The greater level of fluorescence of OH radicals was imaged through a transparent cylinder head by Schipperijn et al. [76]. Similar results were performed in a single cylinder four-stroke SI gasoline engine by Tanaka and Tabata [77] in 1994. They performed an investigation into the OH distribution in both the flame front and burned gas zone. OH concentration could be increased by intensifying combustion with increasing swirl, when the level of uHC emission in the exhaust was a minimum.

The PLIF measurements of OH radicals discussed were limited to qualitative images by severe quenching. Serpenguzel et al. [78] reported that the LIF signal during combustion was 15 times lower than in an atmospheric flame due to the rapid

increase in quenching at high pressure. To overcome the difficulty of severe quenching, Andresen et al. [79] proposed Laser induced pre-dissociative fluorescence (LIPF) for the measurement of OH radicals. They showed that the LIPF line of OH improves the lack of quenching and the fluorescence, 2-3 times higher spectral brightness than in normal LIF measurement.

The measurement of OH radicals requires a powerful excitation source. Excitation and detection of this radical can be improved by detecting the signal at 308 nm, rather than 280 nm.

2.5.3.2 Formaldehyde (CH₂O)

Formaldehyde (CH₂O) or CH radical is well known as an intermediate species, appearing during combusting hydrocarbon fuel. Since the CH₂O molecule appears through low temperature oxidation in the early stage of the combustion process, it is considered to be an indicator of the first stage of combustion and a marker for zones with low temperature reactions in cool flames. For CAI combustion, it is frequently mentioned as the beginning of the auto-ignition process of hydrocarbons.

Rassweiler and Withrow [65] first found that Formaldehyde appears in engines prior to knocking combustion. A number of studies have been performed, showing that it is formed at the first stage of the auto-ignition process and associated with the weak blue light emission of cool flames. Formaldehyde is consumed very rapidly in the second stage of the auto-ignition process, the relatively high temperature phase of the auto-ignition process as shown by Benson [80]. PLIF measurements of formaldehyde distribution were performed in a two-stroke engine in 1994 by Bauerle et al. [81]. They achieved this by using a band pass filter (400-4500 nm) in front of an ICCD camera and a tunable dye laser, exciting at 353.2 nm.

LIF of formaldehyde measurements was achieved with the 3rd harmonic of an Nd:YAG laser by Brackmann [82] and Metz et al. [83]. In the low temperature reaction, a number of other aldehydes and ketones are formed with formaldehyde. However, these intermediates are at much lower concentrations than formaldehyde and no any effects on the measurement results. Since PLIF measurements of

formaldehyde in CAI combustion were performed to characterize the combustion by Graf et al. [84] in 2001, several other researchers have performed similar [85, 86, 87].

Since formaldehyde is assumed to reflect the fuel distribution before the main combustion process, it can also be used as a marker of zones where fuel is present under some conditions. This shows the investigation of fuel mixing timings for different injection timings as shown by Richter [88].

2.6 Summary

This chapter has described the background, current and future emission legislations of IC Gasoline engines. Since the CAI/HCCI engine has shown very promising future potential, it has been subject to intensive research and development over the last decade.

The principles, benefits and drawbacks of CAI/HCCI combustion in Gasoline engines have been highlighted. CAI combustion has shown to have the ultra low NO_x emissions and low fuel consumption but higher uHC and sometimes higher CO emissions and limited operating range. The CAI combustion process has been studied and the effects of different parameters discussed. Finally, optical diagnostic techniques to study CAI combustion have also been examined and techniques used in this investigation described.

Chapter 3

Experiment Facilities and Data Analysis

Chapter 3 – Experiment Facilities and Data Analysis

3.1 Introduction

This chapter describes the experimental facilities and the data analysis methodology used for researching CAI combustion in the Ricardo E6 research engine. The key features of the Ricardo E6 engine facility are variable compression ratio, variable cam timing, an intake air heater and an air boost system. The investigation of CAI operating range is performed by using variable compression ratio and intake air heating method, followed by enlargement of operating range of CAI combustion with intake air boosting and external EGR rate management.

Part of the experimental facilities is the data acquisition system (DAQ) for in-cylinder pressure and heat release analysis. Its setup is described and the appropriate formulas for heat release, combustion and engine performance are presented.

3.2 Experimental setup and Test Facilities

3.2.1 General description

The Ricardo E6/T variable compression engine (Figure 3.1), supplied by Ricardo, was used to obtain the results of CAI combustion with positive valve overlap in this thesis. It is a single-cylinder, poppet valve, four-stroke type, and has a bore of 76.2mm and a stroke of 111.1mm respectively. Although the normal speed range is 1000-3000 rev/min, the current work was limited to speeds of 2000 rev/min due to safety reasons. The compression ratio could be varied from 4.5:1 to 20:1.

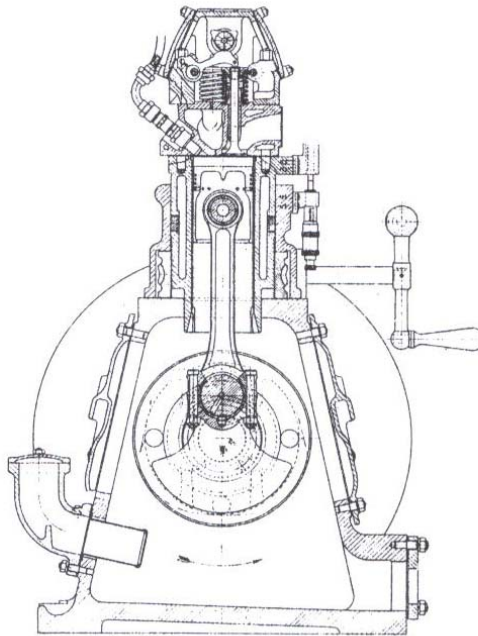


Figure 3.1 Ricardo E6 single-cylinder research engine

The lubricating system is the wet sump type and the oil is delivered from the crank case of the engine directly to the crankshaft by a pump sitting in front of the engine and controlled by a relief valve. The oil is heated up in the crank case by an electrical heater of 0.5 KW for cold start and cooled down by a heat exchanger. The coolant is circulated around the engine by a centrifugal pump driven by an electrical motor. The water temperature was controlled by an electric controller and the magnetic gate valve was controlled by the controller.

3.2.2 Test procedure

In order to allow CAI combustion to take place, it was crucial to warm up the engine and test devices. The test started from heating up the inlet charged air to provide higher thermal energy for CAI combustion. The inlet temperature was fixed while the engine speed and lambda values were varied. The CR (Compression Ratio) was varied depending on the inlet temperature variation. The injection duration was varied by the injection controller to achieve the desired lambda value. The engine speed was varied by the swinging field dynamometer. The engine was operated with WOT (Wide Open Throttle) and spark was left on throughout the experiments, this has found to stabilize combustion particularly in the partial burnt region.

3.2.3 Engine Control and Operation

3.2.3.1 Dynamometer

The engine was coupled to a Laurence Scott 'NS' type Swinging Field AC Dynamometer. The dynamometer could be used for motoring, measuring power output and running constant engine speed. It is supplied with a 3-phase, 440 volts, and mains power supply. The speed of the dynamometer was achieved by a separated oil-cooled regulator controlled by a hand wheel. Speed measurement was undertaken using the clock output of the crankshaft encoder; this was checked against a wall-mounted manual speed meter.

3.2.3.2 Variable compression ratio

The engine has a cast-iron cylinder with a hardened high-phosphorus cast-iron liner inside. Variable compression ratio mechanism has a worm teeth arrangement and is used to vary the compression ratio. The compression ratio was varied by rotating a worm gear which could raise or lower the cylinder. A calibrated micrometer is attached to the cylinder, mounted on the side of the engine, this allows a calibration graph to convert measured value to a compression ratio. Varying compression ratio on Ricardo E6 engine was one of main strategies to enlarge the CAI operating range. Three different compression ratios were used; 12:1, 14:1 and 16:1.

3.2.3.3 Variable Valve Timing Camshaft

A new cam shaft was designed and implemented in order to change the cam-phase manually (Figure 3.2). The camshaft has an 8mm valve lift, 224°CA inlet valve duration and 229 °CA exhaust valve duration. There is a 69 CA deg positive valve overlap, Exhaust Valve Closing time of 59 CA deg ATDC Intake stroke and Inlet Valve Opening time of 10 CA deg BTDC of Intake-stroke, as shown in Figure 3.2.

The engineering drawing can be found in Appendix A.



	Inlet valve	Exhaust Valve
Opening	10 BTDC	190 BTDC
Closing	216 ATDC	59 ATDC

Figure3.2 Variable cam shaft

3.2.3.4 Air Intake System

Test was carried out at naturally aspirated and boosted air intake conditions. NA (Naturally Aspirated) condition was undertaken to evaluate the operation of CAI with different strategies such as varied compression ratio and varied intake air temperature. Boosted air intake test was used to significantly enlarge operating range of CAI combustion.

During the NA operation, air flows through the intake filter from atmosphere and passes through an intake heater of 3KW (Secomak Lt. Model 632). The heater is closed-loop controlled by a sophisticated PDI (Proportional and Integral and Differential) controller. A thermocouple mounted in front of the intake port delivered feedback to the controller. The maximum capable temperature by the heater is up to 400 °C at its exit and the varied test temperatures were from 120 °C to 220 °C. The temperature could be controlled to within ± 1 °C under steady state operation. The throttle was set at WOT (Wide Open Throttle) for the CAI operation.

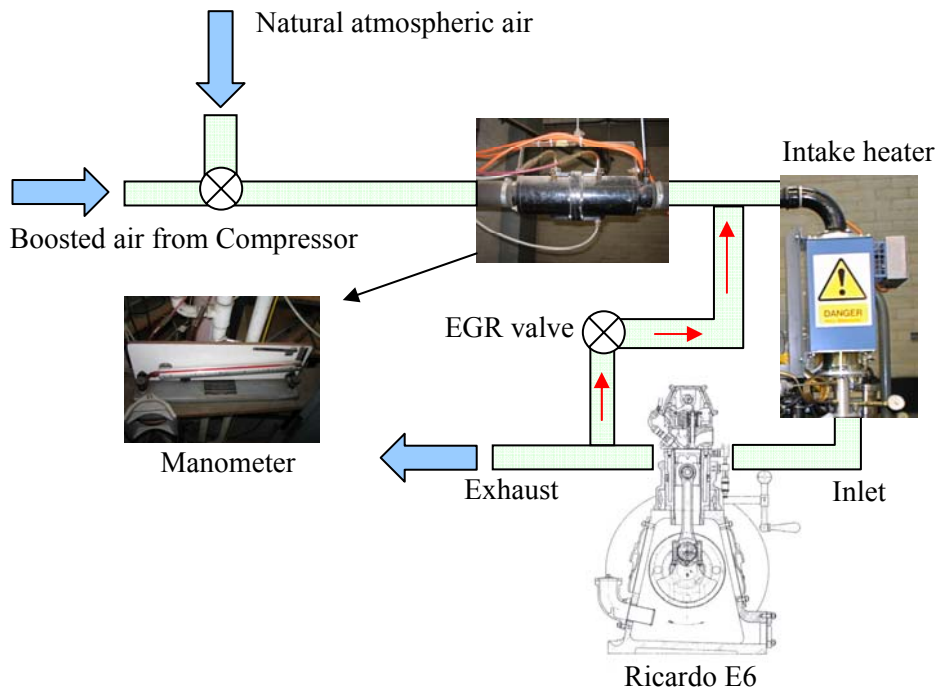


Figure 3.3 Schematic diagram of the experimental setup

Boosted air is obtained by a main compressor, capable of providing 5 bar gauge pressure. The steel intake pipe system contains two gate valves to manage the air pressure. The boosted engine tests were carried out from 0.5 bar to 1 bar gauge with a reservoir to damp out the pressure variation. Figure 3.3 illustrates a schematic of the experimental setup of the Ricardo E6 engine. As shown in the figure, air path is determined by a three way valve mounted at entry to the intake pipe. When the boosting is required, the air pressure is fully controlled by two gate valves mounted upstream in the main pipe line connected to the main compressor.

3.2.3.5 Exhaust (EGR recirculation) system

The exhaust system was divided into two different streams, the main exhaust and EGR recirculation pipe. The exhaust gas composition and the lambda value are measured from the main exhaust stream. A gate valve is installed in the main exhaust pipe to increase the exhaust backpressure. The amount of EGR is varied by altering the exhaust backpressure in conjunction with the EGR valve in the EGR pipe line, as shown in Figure 3.3. Exhaust gas passes through the EGR pipe and mixes with air before the intake heater, allowing a homogeneous mixture at a known temperature to be inducted into the cylinder.

3.2.3.6 Fuel Supply and Injection System

A single Bosch fuel injector is installed in the intake port. Fuel is provided by an underground main fuel tank and pressurized by a production type fuel pump at 2.5 bar gauge pressure. A pressure regulator is used to maintain a constant fuel line pressure. The fuel flow rate is measured in a burette mounted on the wall of 100 ml capacity.

The injector is controlled via a control box, reading a triggering signal from the shaft encoder on the crank shaft. It was calibrated to measure the actual flow rate from the burette. The flow rate was determined by the oscillated pulse-width of the injector, which has a maximum duration of 12.5 ms. The injection was timed at compression TDC when the intake valves were closed so that fuel evaporation could take place before the induction process.

3.2.3.7 Spark ignition system and Shaft Encoder

A modern coil ignition system is fitted to replace the original magneto type ignition system on the engine. The range of spark timing is from 79 °CA BTDC to 45°CA ATDC compression with accuracy of 0.1 °CA.

The spark ignition timing is controlled by the ignition control box ‘Dial-a-Time’ unit, manufactured by Lucas Engineering Ltd. This unit drives a contact open in the ‘low tension’ circuit of the coil when the trigger signal arrives. The collapse of current in the coil induces a high voltage in the ‘high tension’ side of the coil, forcing a spark to jump the gap between the electrodes in the spark plug, and initiate combustion.

The control unit takes two different signals from the crankshaft encoder on the engine. One of them is a ‘trigger’ signal generated once every crankshaft revolution. The second signal is known as a ‘clock’ signal that have 360 TTL pulses per crankshaft revolution. They are used to set the fuel injection and to trigger the computer DAQ system for in-cylinder pressure measurements.

3.3 Experimental Measurement and Data analysis

3.3.1 In-Cylinder Gas Pressure Measurement

In-cylinder pressure is a crucial parameter for engine research since the majority of engine operating characteristics can be quantified by its measurements. The in-cylinder pressure data are used for heat release analysis, such as instantaneous burning rate, mass fraction burnt and they can also be used for performance analysis such as engine load, cycle-by-cycle variation.

Instantaneous in-cylinder pressure measurements are crucial to the analysis of combustion characteristics and to determine whether SI or CAI combustion is occurring. In addition, they have been used to identify knocking combustion and misfiring regions, from which the CAI operating boundary is determined.

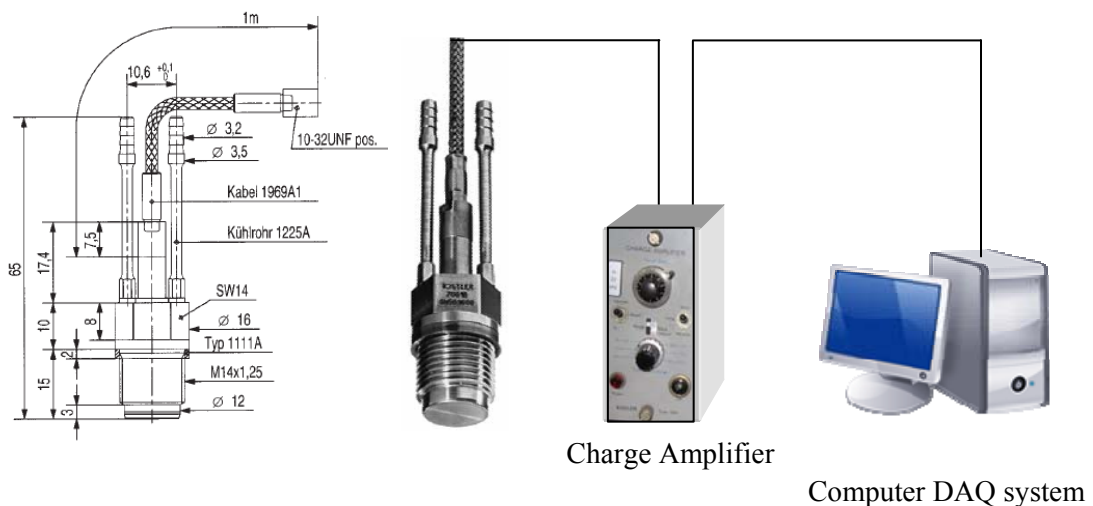


Figure 3.4 Schematic of Kistler 7061B piezoelectric transducer and DAQ system setup

A water cooled piezoelectric pressure transducer (Kistler type 7061B) is installed in the engine head on the opposite side of the spark plug. The charge output generated on the pressure transducer is supplied to the charge amplifier (Kistler type 5001) via a high impedance shield cable due to the minimal level of signal output. The transducer output is converted to voltage and then amplified by the charge amplifier. The pressure transducer was calibrated with an oil filled ‘dead weight’ testing machine, a known pressure was applied to the testing machine and adjusted so that it corresponds to 10 bar/V, over a range of 10 V (100 bar) by setting the calibration

factor in the charge amplifier to the one supplied by the manufacturer and adjusting the gain factor. The measurement range of the pressure transducer is capable of gauge pressure of 0-100 bar. Water cooled transducer benefits from minimized 'thermal shock', in which an incorrect pressure measurement may result due to high exhaust gas temperature heat during the exhaust stroke.

3.3.2 Data acquisition system

As mentioned in the previous section, a number of data calculations can be performed on in-cylinder pressure. The computer DAQ (Data Acquisition System) consists of two parts; a physical hardware system and data processing software. A personal computer (PC) was used to store the data and perform the calculations. The DAQ card is a National Instrument™ type PCIMIO 16-1, designed for a PC computer. There are three inputs to the DAQ cards; the charge amplifier output from the in-cylinder pressure transducer, the clock signal and the trigger signals from the shaft encoder. The clock and trigger signals to the DAQ system are required so that the in-cylinder pressure output can be sampled at every crank angle (1 °CA) and its phasing relative to the 4-stroke cycle can be established.

Labview™ software is used in conjunction with the DAQ card for the real-time data acquisition and data analysis. The program used for the experiment work with this thesis was written by John Williams, a former research student at Brunel University for the data acquisition of in-cylinder pressure data. The program performs an array of functions such as heat release analysis, IMEP, COVimep calculation and knocking combustion analysis. All related calculations are presented in the next section.

3.3.3 Exhaust Measurement

Three exhaust gas measurement devices were used throughout this study: Horiba Mexa 554JE Emission analyzer, Rotork Analysis Automation Model 440 NOx analyzer and Model 520 HC analyzer. They provide the emissions measurements as volumetric concentration in PPM (Parts per Million) or percentage which are converted to specific mass emission (g/KWh) as to be shown in the next section.

3.3.3.1 CO, CO₂, O₂, and Air/Fuel Ratio measurement

Concentrations of CO, CO₂, O₂, and air/fuel ratio in the exhaust gas are measured by a Horiba Mexa 554JE gas analyzer, which is a typical type used by the UK ministry of Transport (MOT) for regulatory tests of privately owned Light Goods Vehicles (LGV) and motorcycles. The exhaust gas is picked up in the middle of the exhaust gas pipe and delivered via a silicon rubber sample line, a water trap and a combined concentrate and particulate removal filter. It is calibrated by the calibration gases in the calibration bottle with 3.48% Carbon Monoxide, 1975 ppm Hydrocarbons (HC), 14.04% Carbon Dioxide, and 21.22% Oxygen by Horiba Instrument Ltd before each experiment. It measures values of CO, CO₂, O₂, HC and calculated exhaust A/F (Air Fuel Ratio) or Lambda.

Cooled exhaust gas from the exhaust pipe is drawn into the Horiba gas analyzer by an integral vacuum pump and the gas is divided by into an infrared absorption cell and a galvanic cell. A nondispersive infrared (NDIR) absorption cell measures CO and CO₂ and a galvanic cell measures the oxygen content of exhaust gas to determine the air/fuel ratio. NDIR absorption cell also measures the concentration of unburned hydrocarbons in the exhaust gas. However it is not accurate since a variety of hydrocarbon species with a wide spectra of absorption are normally present. Therefore, the flame ionized detector (FID) technique was used for the determining of unburned hydrocarbon concentration by a Signal Ambitech 520 HC analyzer, detailed later in this section.

The analyzer is a nondispersive type, no dispersing element (prism or grating) since NDIR instrument performs with no diffraction light and measurements are taken in present of total absorption over a given wavelength. The amount of radiation absorbed by species is given by Beer's law,

$$a_{\lambda} = 1 - \exp(-C_i Q_{\lambda} L) \quad \text{Equation 3.1}$$

Where, C_i is the concentration of species i , Q_{λ} is the absorption efficiency, L is the optical path length.

The main components of a nondispersive infrared gas analyzer (NDIR) are shown in Figure 3.5. The infrared light sources are prepared by heated filaments and emit back radiation over a broad band of wave length. The detector cells are filled with the measured gas in order to absorb the radiation in the absorption band of the gas. The detector cells are divided by a diaphragm that moves between two plates of a capacitor. Each detector cells are pressurized by energy absorption.

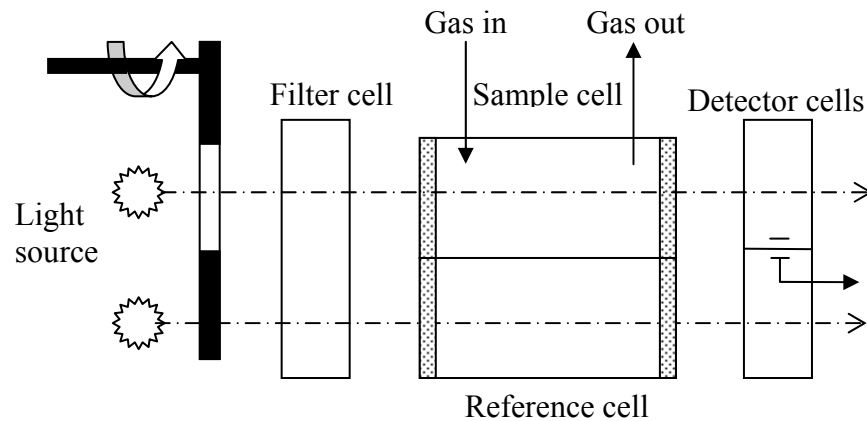


Figure 3.5 NDIR Analysers with Differential Detectors

Two beams pass through the sample cell, containing the gas to be analyzed and reference cell, filled with a non-absorbing gas (nitrogen). The detector cell absorbs different radiation because the attenuation in the sample cell causes deflected diaphragm in proportion to the difference in the rates of energy absorption. The deflection is calibrated to read in units of concentration. For example, CO₂ and CO have a strong absorbance at 4.2 μm and 4.6 μm respectively. The filter cell is placed between the infrared sources and the sample and reference cells so that it eliminates the overlap between the absorption bands of CO and CO₂.

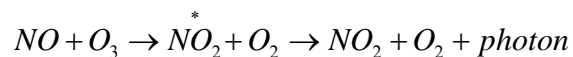
The galvanic cell is used in the determination of air/fuel ratio from the oxygen content of the exhaust gas. It contains a gold plated PTFE diaphragm that serves as a cathode and a silver plated anode. These components are placed in the electrolyte of potassium chloride gel and have a potential placed across the electrodes. The electrochemical reduction occurs when the oxygen spreads through the membrane and the current flows proportional due to the partial pressure of the oxygen in the sample. The current is calibrated to the reading value of the oxygen content.

Although the galvanic cell responds to the other gas components such as CO₂, its sensitivity to the other gases is low enough not to affect the results in practice.

3.3.3.2 NO_x Measurements

A 'Rotork automation analysis series 420' Chemiluminescent NO_x analyzer was employed to quantify exhaust NO_x concentration. The sample gas from the exhaust pipe is drawn into the analyzer by a vacuum pump, -30Hg in the analyzer and heated up in the sample line in order to prevent water condensation. 1890ppm Nitric Oxide, total NO_x 1910ppm and Zero grade air are used for the span gas and operation.

Nitrogen dioxide (NO₂) is excited and emits the light electrically and the amount of the light is measured by this chemiluminescence analyzer to determine the NO_x concentration in the exhaust gas. The IC engine produces typically both nitric oxide (NO) and nitrogen oxide (NO₂), the sample is catalytically converted to NO. Zero grade gas is passed through an electrical discharge to convert some of oxygen to ozone (O₃). These NO and O₃ in the sample gas are introduced into the reaction chamber in order to take place the reaction combining them to an excited NO₂ and O₂. The activated NO₂ returns to the normal state either by emission of a photon or by collision with another molecule. The reaction taking place in the chamber is shown below



A small amount of light emitted is proportional to the concentration of NO and NO₂ (NO_x) combined in the exhaust gas and is collected and measured by a photomultiplier before amplification. The low pressure is maintained in the reaction chamber so that it prevents excessive molecular collisions and promotes light emission. In addition, it restricts the strong deactivating effects of carbon dioxide and water vapor on nitrogen dioxide.

The analyzer was maintained and calibrated just before the experiments by the Signal Ambitech Ltd to ensure accurate measurement. 1910ppm total NO_x span gas was used for the calibration and zero grade air for the zero grade Nitrogen to calibrate

before every experiment. Zero grade air is used for ozone production in the analyzer during the operation.

3.3.3.3 Unburned Hydrocarbon Measurement

As mentioned before the flame ionized detector (FID) technique was used to determine the unburned hydrocarbon concentration by a Rotork analysis automation series 520 HC analyzer. The sample gas is pumped into the analyzer and through the heated line to prevent the condensation of water vapor in the sample gas.

FID technique relies on the detection of electrons and positive ions, which are formed when hydrocarbons are burned. The combustion in the analyzer takes place in the presence of an electric field and current is generated and measured accurately, which is proportional to the number of carbon atoms present. The limitation of this FID technique exists due to its inability to differentiate between the concentrations of individual hydrocarbon species.

The sample gas is drawn into the analyzer and mixed with FID fuel and stoichiometric quantity of pure air in the chamber with an electrode system. The combustion is occurring by the mixture in the diffusion flame, which resides in an electric field. The generated current flow is amplified and scaled for the reading of concentration by an internal galvanometer. Hydrogen helium is a usual fuel burned in a non-ionizing flame to ensure a correct measurement. High purity air is also usual to prevent the effect of any hydrocarbon or other species to impair the results.

The gas analyzer unit requires three gas bottles for normal operation. These are 41.3 % hydrogen/helium for the fuel, zero grade air and 517.6ppm propane for the span gas. The calibration and maintenance was also performed before the experiments.

3.3.3.4 Calculation of Specific Emissions

All the raw emissions data were initially observed as volume concentration (ppm, %) and the quantity of any specifies is dependent on the total exhaust flow rate. There are a few methods to convert volume concentration of exhaust gas to mass flow rate, which allows comparison of the engine effectiveness in reducing exhaust emissions

at the same load. Volume concentration (V_{cg}) in the exhaust gas of proportion are measured as parts per million (ppm), or as percentage by volume (%vol).

$$V_{cg} = V_{ppmg} \div 10^6 = V_{\%g} \div 100 \quad \text{Equation 3.2}$$

The Indicated Specific exhaust gas flow rate, is given by

$$IsX (g / kWh) = (1 + AFR) \times isfc \times V_{cg} \times \left(\frac{M_X}{M_{air}} \right) \quad \text{Equation 3.3}$$

Where, X is species of exhaust gas (NO, HC, CO), AFR is Air Fuel Ratio, and M_X is Molecular weights of exhaust gas.

The Molecular weight of carbon monoxide is $M_{CO} = 28.0101g / mole$. In the measurement of hydrocarbons, either by an NDIR (Non-Dispersive Infrared) device or an FID (Flame Ionization Detector), measurements are normally quoted as ppm methane, or ppm hexane. However, Propane gas ($M_{C_3H_8} = 44.06g / mole$) was used as a span gas of the analyzer and hence the molecular weight of propane gas was used. The same process for nitrogen oxide emissions was undertaken and $M_{NO} = 30.00614 (g/mole)$. Total molecular weight of exhaust gas (M_{EX}) was presumed as the same as molecular weight of air ($M_{air} = 29g / mole$).

3.3.4 Fuel and Air mass flow rate Measurement

The unleaded 95 RON gasoline fuel was supplied from the university main fuel tank and pressurized by a production type 2.5 bar fuel pump. The fuel flow rate was measured by a 100cc burette mounted on the wall of a test bay and the fuel quantity was volumetrically measured and calibrated for the injector. The injection time/duration was monitored on the oscilloscope as pulse width and calculated later with measured volume.

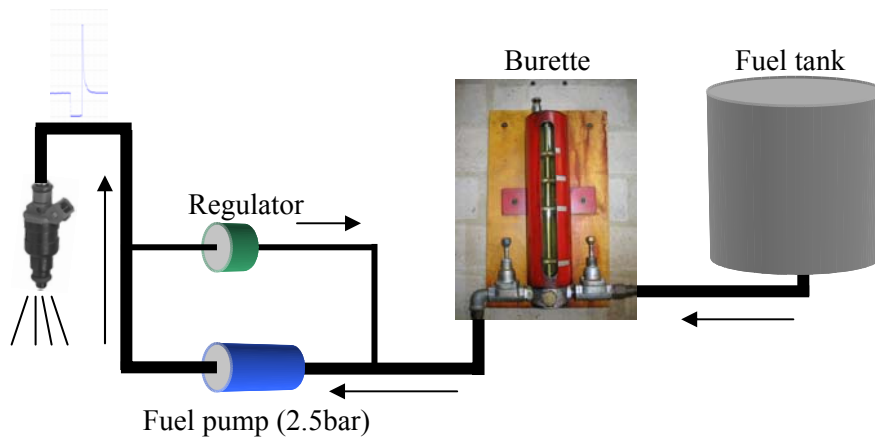


Figure 3.6 Schematic of Gasoline Fuel Flow

This fuel flow rate was converted to Indicated Specific Fuel consumption (I_{sfc}), which is a more useful parameter of how efficiently the engine consumes the fuel to produce work.

$$I_{sfc}(g / kW \cdot h) = \frac{\dot{m}_f}{P(KW)} \quad \text{Equation 3.4}$$

Where \dot{m}_f is the mass flow rate of fuel and P (kW) is Power output.

Power out was initially calculated out of the Indicated Mean Effective Power, which was stated in section 3.4.1.1.

$$P(kW) = \frac{imep(kPa) \times V_d(dm^3) \times N(rev/min)}{n_R \times 10^3} \quad \text{Equation 3.5}$$

Where, $V_d(dm^3)$ = engine swept volume, n_R = the number of crank revolutions for each power stroke per cylinder

A manometer was installed in the middle of intake pipe line and measured the air flow rate and converted to the mass of air as shown in Figure 3.3. A pressure gauge was mounted just after the intake heater to ensure the pressure while it was boosted.

The manometer is a differential pressure (Orifice plate) measurement type and consists of a measurement part and a reading meter part, which are connected by hoses with a dyed blend of paraffin of S.G 0.787. Measurements are based on volumetric unit on a manometer reading value and then converted to the mass unit by using a calibration factor of paraffin, which are provided by Ricardo & Co by Airflow Developments Ltd. The pictures and technical information of a manometer can be found in Appendix B.

3.3.5 Temperature Measurement

Standard RS K type thermocouples were installed to measure temperature. Thermocouples generate a small voltage as output and it is converted to the calibrated temperature on the display. They are all installed very carefully to ensure that the location is in the middle of pipe and does not have any contact with the wall which leads to errors in reading.

Water and oil temperature is controlled and measured by thermocouples placed in a water and oil supply pipes. An intake air temperature thermocouple is located in just below the intake heater in order to measure the temperature properly without any heat loss. A thermocouple, very close to the exhaust port, is used to measure the exhaust temperature and also used to infer the in-cylinder temperature at exhaust valve closing time. All thermocouple readings were displayed on the digital displays.

3.4 Data Processing and Analysis

3.4.1 Engine Load and combustion

3.4.1.1 Indicated Mean Effect Pressure

The Indicated Mean Effect Pressure (IMEP) is the best indication of engine load in a single-cylinder research engine. It is crucial to know how the cylinder pressure

behaves in partnership with cylinder volume as determined by the engine geometry. It presents the specific work done on the piston over the four stroke cycle and is numerically determined by the ratio of the area enclosed by the pressure curve, shown in Figure 3.7, and the cylinder displacement volume.

$$IMEP = \frac{1}{V_d} \oint P dV \quad \text{Equation 3.6}$$

IMEP calculation should be done as the net IMEP, which presents work delivered for entire 4-stroke cycle rather than Gross IMEP, which is work over the compression and expansion strokes only. Consequently, pumping work per cycle is considered as an engine operating loss and is calculated by subtracting the Gross IMEP from net IMEP.

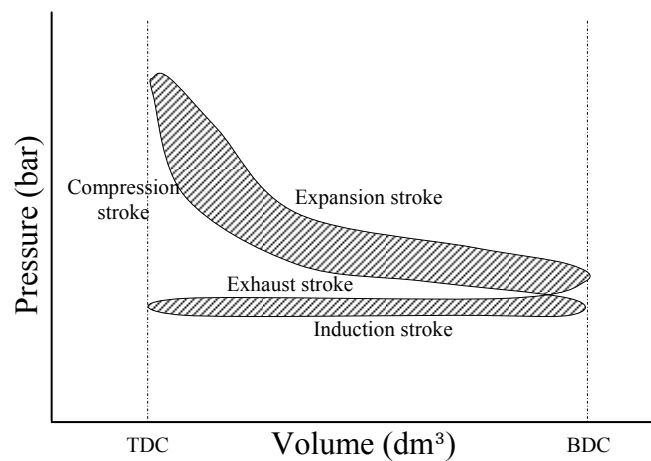


Figure 3.7 Example of a P-V diagram for a 4-stroke cycle engine

3.4.1.2 Coefficient of Variation

The coefficient of Variation of indicated mean effective pressure (COV_{imep}) is a good indicator for defining the cyclic variability for the combustion engine. It is defined as

$$COV_{imep} = \frac{\sigma_{imep}}{imep} \times 100(\%) \quad \text{Equation 3.7}$$

The imep value is calculated out of total complete cycles which are 100 cycles in this study, and σ_{imep} is the standard deviation in Imep. A maximum value of 10 % is normally defined as acceptable for vehicle drivability in this study.

3.4.1.3 Knocking Combustion Analysis

One of the major objectives to fulfill the experiment work on this Ricardo E6 engine was to enlarge the operating range of CAI combustion. To enlarge the operating range, the ‘Knock’ combustion which is experienced for high load operating region has to be correctly defined. A Labview™ program was used to calculate and determine the rate of pressure rise noise and hence the occurrence of knocking combustion during engine testing.

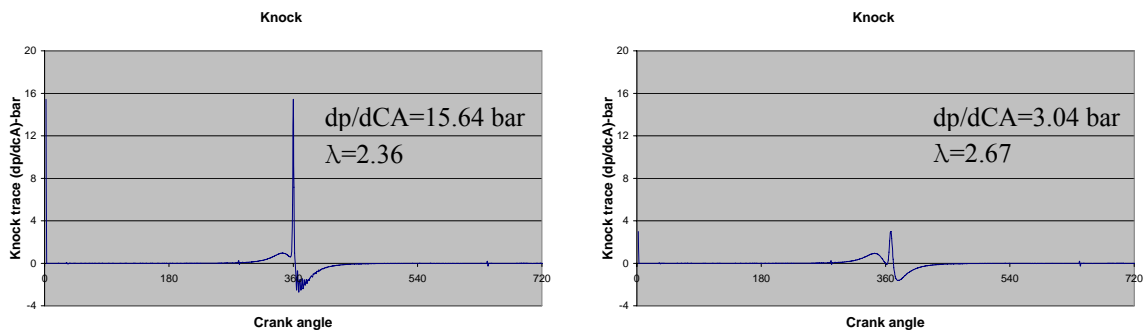


Figure 3.8 Knock trace (dp/dCA), CR16:1, 1500 rev/minute, 120°C intake air temperature, Wide Open Throttle.

Although many methods of defining knocking boundary for CAI combustion have been proposed, the occurrence of knocking combustion was defined by the rate of pressure rise. Excessive rate of pressure rise leads to not only noise problem and but also structural damage. The maximum rate of pressure rise was defined as 10bar/CA and monitored more precisely with COVimep to make a decision for CAI operating range boundary. Figure 3.8 shows the examples of knocking and normal combustion at high and low load conditions respectively. This high rate of pressure rise of dp/dCA=15.64bar was therefore precluded from the experiment data.

3.4.1.4 Combustion Efficiency

It is useful to calculate the combustion efficiency for CAI combustion as it is sometimes experiences incomplete combustion.

Combustion Efficiency can be calculated as follows

$$\eta_c(\%) = \left[1 - \frac{(\dot{m}_{CO} \times CV_{CO}) + (\dot{m}_{HC} \times CV_{HC})}{\dot{m}_{fuel} \times CV_{fuel}} \right] \times 100 \quad \text{Equation 3.8}$$

Where \dot{m} is mass flow rate (g/h), CV is the heating (Calorific) value (MJ/Kg).

A number of chemical products are produced and obtained in the exhaust gas of an internal combustion engine. However, they are specified as incomplete combustion products (e.g., CO, H₂, unburned hydrocarbon, soot) and complete combustion products (CO₂ and H₂O). The concentrations of incomplete species (CO, H₂, unburned hydrocarbon, particulates) are required to calculate the combustion efficiency. The composition of the unburned HC is not particularly known but CV_{HC} is comparable the same as CV_{fuel} (i.e., the unleaded 95 RON gasoline 44MJ/Kg). The heating value of CO is known as 10.1 MJ/Kg. Mass flow rate of these combustible products in the exhaust gas was converted from volume concentration by the gas analyzer to g/h unit, which is stated in the following section.

3.4.1.5 Exhaust Heat Recovery through a Heat Exchanger

The experiment facilities of the Ricardo E6 engine include three heat exchangers providing external heat capabilities which heat up water, oil, and intake air. However, heat exchangers for water and oil were set by a constant status in order not to have any interruption out of effects of them.

An intake air heat exchanger is a crucial device to manage the intake air temperature as CAI combustion can be operated. Hence it is important that intake temperature needs to be determined as reasonable level by a heat exchanger efficiency with measured exhaust gas temperature simultaneously.

$$\eta_h = \frac{T_h - T_i}{T_e - T_i} \times 100 \quad \text{Equation 3.9}$$

The engine is considered as an open system with an intake heater which exchanges heat and work with the surrounding environment at atmosphere. The heat exchanger efficiency of the engine confirms what the minimum exhaust temperature should be. For obtained experimental data, the efficiency is considered as given heat exchanger efficiency of 80%.

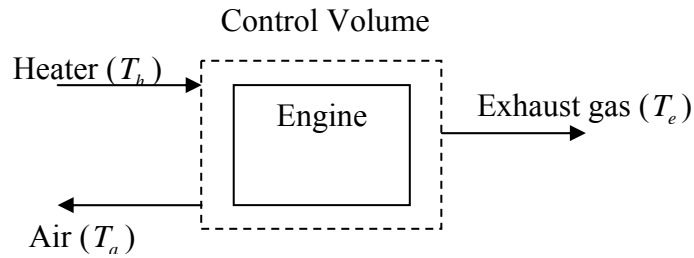


Figure 3.9 control volume surrounding engine

The exhaust temperature was monitored simultaneously and the CAI combustion operating boundary was confirmed by the heat exchanger efficiency with acceptable intake temperature.

3.4.2 Fuel Conversion Efficiency

There are a couple of different ways to describe the engine efficiency. However, fuel conversion Efficiency is preferred in terms of fuel consumption as it presents more precise quantity and clear definitions.

$$\eta_f(\%) = \frac{W_c}{\dot{m}_f \times CV} \times 100 = \frac{imep \times V_d \times N}{n_R \times 10^3 \times \dot{m}_f \times CV} \times 100 \quad \text{Equation 3.10}$$

Where, W_c is the work per cycle, \dot{m}_f is the mass of fuel inducted per cycle, CV is Calorific Value (Unleaded 95 RON gasoline fuel=44MJ/kg), V_d represents Swept Volume (dm^3).

3.4.3 Calculations of Trapped residuals and Mixture temperature

The amount of trapped residuals is one of the crucial parameters and they directly affect autoignition and CAI combustion performances. The steady flow energy equation is implemented to calculate and analyze it since internal energy of a mixture

is equal to the sum energy of each component mixing. Steady flow energy equation is shown here.

$$U_{mixture} = U_{air} + U_{residual} + U_{fuel} \quad \text{Equation 3.11}$$

The equation is converted to the calculation for the mass of residual as below.

$$m_R C_{p_R} T_R + m_a C_{p_a} T_a + m_f C_{p_f} T_f = (m_R + m_a + m_f) C_{p_{mix}} T_{mix} = \frac{P_{evc} V_{evc}}{R} C_{p_{mix}} \quad \text{Equation 3.12}$$

Where sub-character ‘R’ represents the trapped residual gas, ‘a’ represents air, and ‘f’ represents fuel.

The cylinder volume is calculated at EVC and based on the engine geometry. The temperature of residual gas is assumed as temperature of the burnt gas temperature at EVC, measured at the exhaust manifold by a thermocouple. The temperature of air and fuel is assumed as the same mass of air and fuel and is measured simultaneously. The properties of every component are referred from “internal combustion engine fundamental” by John B. Heywood [5] where, $C_{p_{mix}} = 1.06$, $C_{p_f} = 1.7$ (vapor), $C_{p_a} = 1.016$, $C_{p_R} = 1.4$, $R = 0.287$ [KJ/KgK].

The mass of residual is calculated from Equation 3.12 as

$$m_R = \frac{1}{C_{p_R} T_R} \left[\frac{P_{evc} V_{evc}}{R} C_{p_{mix}} - m_a C_{p_a} T_a - m_f C_{p_f} T_f \right] \quad \text{Equation 3.13}$$

The in-cylinder mixture temperature is calculated also from ideal gas law from Equation 3.12, as shown below.

$$T_{mix} = \frac{1}{(m_R + m_a + m_f)} \times \frac{P_{evc} V_{evc}}{R} \quad \text{Equation 3.14}$$

Consequently, it could be calculated and analyzed as a trapped residual to total in-cylinder charge.

$$\text{Trapped Residual} = \frac{m_R}{m_R + m_a + m_f} \times 100 \quad \text{Equation 3.15}$$

3.4.4 Heat Release Analysis

Heat release analysis is a very useful method to characterize combustion events of both SI, and CI engines. As shown in Figure 3.10, the significant difference and features of SI and CAI combustion in terms of combustion phase, speed and peak rate.

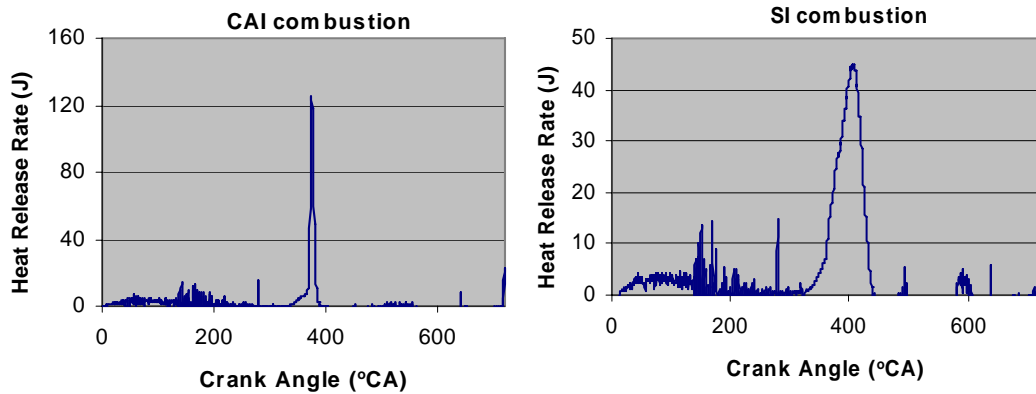


Figure 3.10 Heat release rate of CAI and SI combustion

The first law of thermodynamics is implemented to all the cylinder contents, which means the cylinder is considered as a closed system for the combustion event. In order to implement the equation, the combustion chamber is considered as a single zone, where no temperature gradients exist and the reactants and products are completely mixed. The reactants and products are also assumed to have the same properties.

$$\delta Q_{hr} = dU + \delta W + \delta Q_{ht} \quad \text{Equation 3.16}$$

Where δQ_{hr} is the heat released in the combustion chamber during combustion, dU is the internal energy raised, δW is the work done on the piston by the considered system and δQ_{ht} is the heat exchange occurring within the combustion chamber wall. Each of the terms is:

$$\delta W = p dV \quad \text{Equation 3.17}$$

$$dU = mc_v dT \quad \text{Equation 3.18}$$

The ideal gas law states the equation:

$$m dT = \frac{1}{R} [p dV + V dp] \quad \text{Equation 3.19}$$

The net heat release rate is now presented as an angle incremental basis.

$$\frac{dQ_{net}}{d\theta} = \left(\frac{dQ_{hr}}{d\theta} \right) - \left(\frac{dQ_{ht}}{d\theta} \right) = \left(\frac{\gamma}{\gamma-1} p \frac{dV}{d\theta} \right) + \left(\frac{1}{\gamma-1} V \frac{dp}{d\theta} \right) \quad \text{Equation 3.20}$$

Where γ (the ratio of specific heats) = $\frac{c_p}{c_v}$ and θ is the crank angle.

The heat release rate is obtained from the measured pressure trace and calculated with cylinder volume with respect to crank angle and with the estimated average ratio of specific heats value. A cumulative heat release could be calculated from the heat release rate and presented using Burned mass fraction (MFB). This quantifies ignition timing, combustion duration, defined as the 10-90% MFB CA respectively.

3.5 Summary

The experimental facilities and setup employed on Ricardo E6 research engine have been described to investigate CAI combustion with positive valve overlap. The engine is capable of operating CAI combustion by variable compression ratio, an intake heater, intake air boosting system, and external EGR device. The DAQ system is introduced to deal with the data and physical measurements. A detailed description of the data processing and analysis is presented.

Chapter 4

Investigation of CAI combustion with Positive Valve Overlap

Chapter 4 Investigation of CAI combustion with Positive Valve Overlap

4.1 Introduction

This chapter describes the study of CAI (Controlled Auto-Ignition) combustion and enlargement of its operating range on a Ricardo E6 research engine respectively. CAI combustion is achieved by positive valve overlap, intake air heating and variable compression ratio. The operating range of CAI combustion is investigated and then enlarged by intake air boosting and external EGR trapping method.

For each valve overlap setting, the intake air charge temperature and compression ratio are varied to determine the operational range of CAI combustion, defined by the knock and the partial burned limits. In addition, the relative air and fuel ratio is varied during each experiment.

Due to the limited operating range of CAI, intake air boosting is employed to shift the knock boundary to a much higher load. External EGR is also implemented to cover the gap between the operating ranges of non-boosting and lean-boosted CAI combustion.

4.2 Positive valve overlap and Test methodology

Although the negative valve overlap is one of the well known strategies to achieve CAI combustion, positive valve overlap can also be used to achieve CAI combustion in combination with heating intake air charge heating. The positive valve overlap strategy obtains the burned gas by recalculating internally the exhaust gas back into the chamber, offering the thermal energy to the CAI combustion. The negative valve overlap traps the burned residual gas in the chamber within the overlap period. The positive valve overlap is not the appropriate strategy by itself to achieve CAI combustion except when combined with extra strategies. Therefore, compression ratio was varied in order to provide the adequate intake temperature ranges for CAI combustion.

The valve lift was 8mm and exhaust valve timing was 190 CA deg ATDC of opening, 419 CA deg ATDC of closing and intake valve timing was 350 CA deg BTDC of opening, 574 CA deg ATDC of closing which means 69 CA deg positive valve overlap duration. Table 4.1 shows this positive valve overlap strategy.

Valve Timing	Intake	350 CA deg ATDC	574 CA deg ATDC
	Exhaust	190 CA deg ATDC	419 CA deg ATDC
Intake heater	120~220 °C		
Engine speed	1000~2000 rpm		
Oil temperature	55 °C		
Coolant temperature	80 °C		
CR	12:1, 14:1, 16:1		

Table 4.1 Positive valve overlap strategy and engine operation condition

The results of initial tests on CAI combustion show that every variable affects combustion timing. The combustion phasing is allowed to vary over the dilution ranges of CAI combustion. Over-advanced combustion timing results in accelerating heat release rate, knocking combustion and high NO_x emission with high in-cylinder temperature. In-cylinder temperature was calculated by measurements of in-cylinder pressure, volume and mass of fuel, air and residual. On the other hand, if it is over-

retarded, the heat release rate is slowed down and incomplete combustion can occur. Intake temperature range depends on compression ratio at CR 12:1~16:1. CAI combustion is achieved at intake temperature range of 120 deg C~140 deg C at CR 14:1 at 150 deg C~180 deg C and at CR 16:1 at 190 deg C~220 deg C, shown in Table 4.2.

	Intake temperature(°C)											
									190	200	210	220
CR 12:1												
CR 14:1				150	160	170	180					
CR 16:1	120	130	140									
0.5 bar Boost with EGR							180					
0.5 bar Boost without EGR							180					
1 bar Boost with EGR							180					
1 bar Boost without EGR									200			

Table 4.2 Combination of testing parameters

Since boosting air introduces higher air density into the chamber and provides leaner mixture but higher fuelling rate, This higher fuelling rate significantly improves the knocking limit of CA While applying the boosted air into the engine, fuelling rate is increased dramatically overall at much leaner mixture condition due to the higher air density. Since the operating region with air boosting is located at much higher load range than no boosting region, external EGR is applied to the intake to fill in the gap of the operating range. While the external EGR is applied, boosting pressure has to be increased to maintain the inlet pressure as introduced EGR drops down the inlet pressure. An exhaust gate valve is closed gradually to increase the exhaust pressure to force the exhaust gas back into the intake.

4.3 Engine Operation and Test Procedure

4.3.1 Cold Start Procedure

CAI combustion using gasoline fuel by variable compression ratio and intake temperature is limited by knocking combustion at the richest condition and partial burnt combustion at the leanest condition. To achieve adequate intake charge and coolant temperature and oil temperatures, warm-up procedure is required before CAI combustion can take place.

There are two methods to warm up the engine sufficiently. The engine can be motored with a water and oil heater on. When all temperatures reach the required level, the fuel pump is switched on at required lean A/F ratio ($\lambda = 2-4.5$). CAI combustion occurs gradually and becomes stable, and combustion efficiency increases reaching steady state. Alternatively, the engine starts in SI mode with the water and oil heater on, but the intake heater is kept off. Heat transfer from the combustion chamber ensures that the coolant temperature is heated during steady conditions. When the engine operates at a steady condition, the intake heater is switched on. This leads to a decrease in air density and a richer A/F ratio. Injection duration is shortened to compensate for this richer condition. As the intake temperature approaches the required level depending on compression ratio, CAI combustion starts to occur in some cycles and eventually takes over stable combustion. All tests were carried out with spark discharge, which was found to have little effect during most of the CAI operation regions and could help stabilize combustion near the partial burn limits.

4.3.2 Test procedure

Testing commences when the engine and ancillaries are fully warmed up and stable operating condition are achieved. Firstly, all of the gas analyzers are checked to ensure that they are fully warmed up and operating properly. Secondly, all of the unused devices are checked to ensure that they are isolated or closed such as the EGR gate valve and the air boost gate valve. Compression ratio and engine speed are fixed while the engine is running at the required intake temperature. Injection duration is adjusted so that the engine is operating under the richest A/F ratio

condition and knocking combustion. Knocking combustion is monitored on Labview® Data acquisition system, combustion is reported as ‘knocking’ by the dp/dCA values, which has a 10 bar/CA intensity threshold. Once combustion is established, fuelling is reduced slightly in order to avoid critical knocking combustion and physical engine damage. This operating condition is the starting point of the test, shown at point A in Figure 4.1.

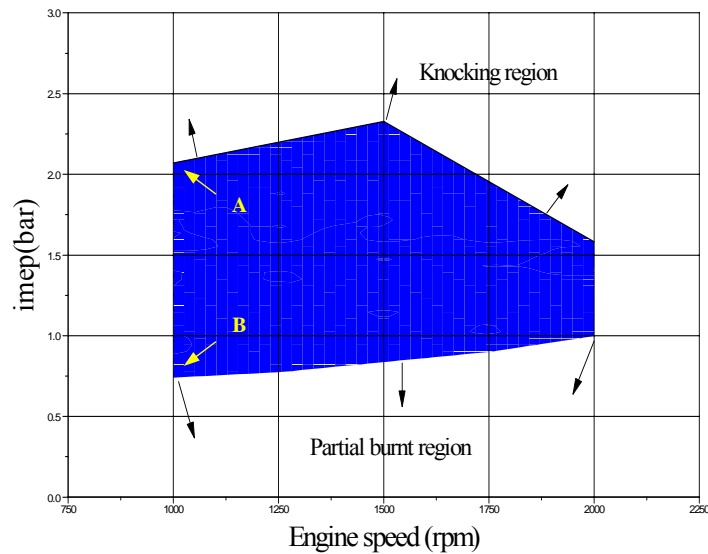


Figure 4.1 CAI operating range with variable CR and Intake temperature

The engine and measurement systems are left to stabilize for a few minutes. A/F ratio and exhaust CO_2 , O_2 , and CO are taken from the Horiba 540J gas analyzer and recorded onto a Microsoft Office Excel spreadsheet of the computer. NO_x and unburned HC are similarly taken from Rotork Analysis Automation® NO_x and HC analyzers respectively. The spreadsheet contains equations and calculations described in Chapter 3. The DAQ system captures 100 consecutive in-cylinder pressure cycles, and the data is saved to the hard drive for post-processing. After a test point is obtained with all data, injection duration is reduced gradually to the leaner condition. The leanest A/F ratio is found by monitoring the partial burnt area, which was determined by CoV (Coefficient of variation) of IMEP less than 10 %. The leanest test point is shown at point B in Figure 4.1.

The engine speed is adjusted manually by a dynamometer speed control handle to the next engine speed. The engine is tested in the engine speed range from 1000 rpm to 2000 rpm. The engine is stopped and the compression ratio is changed manually to

the next required set-up and the engine is tested again with a different range of intake temperature.

When the engine is operating with boosted air, the boosting pressure regulator is opened to supply the compressed air, while the engine is still connected with naturally aspirated air intake. Then three-way valve in the intake is switched to the compressed air intake. It is important during the procedure to monitor the pressure gauge on the intake port of engine and ensure that there is no mechanical damage of engine. The fuelling rate is increased to meet the highest load range which is the knock region, monitoring COV_{mep} at the same time. Once the highest load point is captured, all data points are captured subsequently by reducing the fuelling rate until the lowest load point meets the partial burned boundary.

During engine operation with boosted air, the external EGR gate valve is opened to allow exhaust gas recycled into the intake path, followed by increasing boosting pressure due to the reduction of air intake pressure. At the same time, the exhaust pressure is adjusted by the backpressure valve in the exhaust to ensure that it is higher than the intake pressure. All test points are measured in the same manner as in previous tests.

4.4 Investigation of CAI combustion by variable compression ratio and intake temperature

4.4.1 Introduction

Several different methods have been introduced to achieve CAI combustion as stated in Chapter 2. The most practical method to initiate and control CAI combustion for gasoline engines is using burned gas recycling to provide the desired thermal energy, which allows the fuel to auto-ignite, and to provide dilution control for the subsequent heat release rate. However, intake air heating is an alternative method to provide the thermal inertia into the chamber for CAI combustion. Positive valve overlap is employed to breathe back the burned gas into the cylinder for CAI combustion. Intake charge air is heated up by an intake heater in order to provide additional thermal energy. As discussed in previously, the intake charge heater was employed to mimic an heat exchanger that has the capability to recoup some of the exhaust heat. Therefore, the maximum intake temperature had been determined by the exhaust gas temperature and the effectiveness of the heat exchanger, as illustrated in section 4.4.4.3 and 4.4.4.4.

CAI combustion and emissions characteristics are not only dependent on the composition of the charge, but also on its pressure and temperature histories. Therefore, the effects of intake temperature and compression ratio, which determine the temperature and pressure histories, are documented in this chapter

The measured values are obtained during the tests using the DAQ system for the pressure histories and knocking combustion detection. Gas analyzers are used to measure emissions and Air/Fuel ratio. In fact, one of the objectives of these tests is to define the two dimensional region of intake temperature and the air/fuel ratio in which CAI combustion can be attained. The results also presented NO_x, CO₂ and HC emission results. All tests were undertaken by the detailed procedures, warming up the engine up to the desired engine temperature, 80°C and oil temperature 55°C. Emission analyzers were also warmed up to operate appropriately.

4.4.2 CAI operating and load range

The CAI operating region with positive valve overlap, intake air heating and compression ratio is determined by operating limits of high and low load boundaries. The operating limits are defined by combustion stability and engine knock.

The high load range of the CAI operating region is limited by knocking combustion. The knock is determined by the maximum averaged rate of in-cylinder pressure rise monitored on the data acquisition system. Reduced mass of trapped residual may also lead to misfire at the high load boundary. However, no miss firing was detected at high load operations in this study since intake charge temperature was sufficient hot to initiate and sustain CAI combustion.

Although knock occurs when the intake charge air temperature is increased in SI engines, the temperature initiates CAI combustion in this test. Therefore, the limits of higher load and knock occurrence are reached by increasing the fuel quantity to the richest A/F ratio at the same engine speed.

Figure 4.2 shows the CAI operating range with IMEP iso-lines in the map of lambda versus compression ratio. It is obvious that the engine output in the CAI operating range is determined by the relative air/fuel ratio since the richer mixture leads to the higher engine output. In general, the range of CAI operation is shifted towards lower charge temperature and leaner mixture as the compression ratio is increased from 12:1 to 16:1 (Figure 4.2a to 4.2c). The maximum load is achieved up to 2.5 bar IMEP at the lowest compression ratio of 12 and the lower tested intake temperature condition (Figure 4.2a and 4.2b). Although it was expected to occur at the highest compression ratio where the compression temperature is higher, the minimum load limit of about 0.5 bar IMEP is obtained at the compression ratio 14:1 (Figure 4.2c). At the compression ratio of 16, there were more cycle to cycle variations in the in-cylinder pressure due to lower intake charge temperature.

Previously, this partial burn and ultra-lean conditions investigated by Thring [12] was found at 0 bar BMEP. However, since the engine he used was a single cylinder research type, having an unquantified FMEP. From the motoring engine tests, it was found that the FMEP of the current engine is - 0.11bar. Therefore, the current results

indicate that CAI combustion could be sustained even under the deceleration/fast idle conditions giving the right intake charge temperature, air/fuel ratio, and compression ratio.

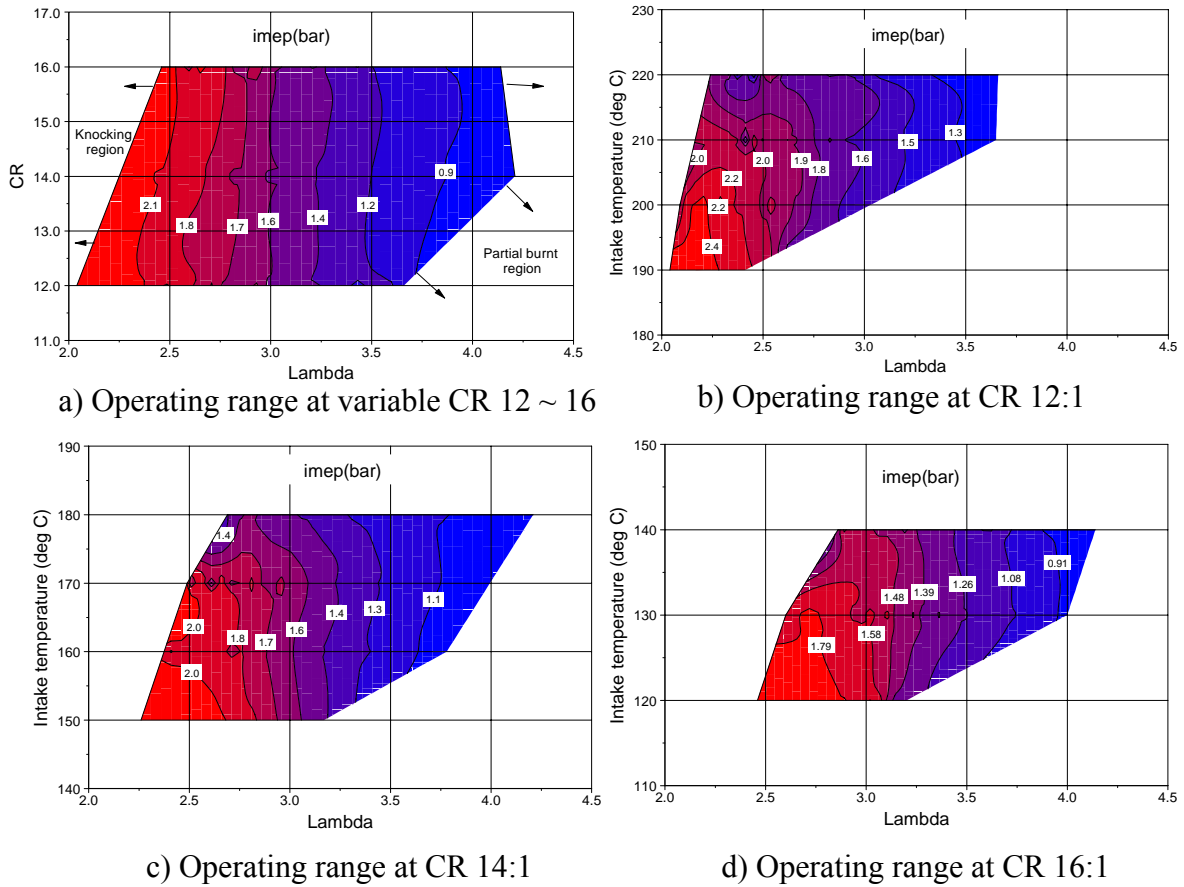


Figure 4.2 CAI operating range with IMEP by variable CR and intake temperature

Although the operating knock boundary is enlarged a little by reducing compression ratio at higher intake temperature, it is not a massive improvement of the engine load range. It shows even the reduction of load range in the partial burned region since combustion efficiency is decreased by the higher compression ratio, detailed in section 4.4.4.

The higher load limit can be enlarged by boosting the intake air pressure. The boosted intake pressure applies much higher air density, allowing more fuelling rate and more powerful load range. The control of the operating region between naturally aspirated and boosted operation is managed by using the external EGR trapping method, detailed section 4.5.

4.4.3 Fuel consumption and Engine output Emissions

The typical best value of specific fuel consumption of a SI engine is known as about 270 g/KWh [8]. As shown in Figure 4.3, specific fuel consumption in CAI combustion is generally lower than in SI combustion. However, it is a little higher at the partial burned area due to lower combustion efficiency in this region.

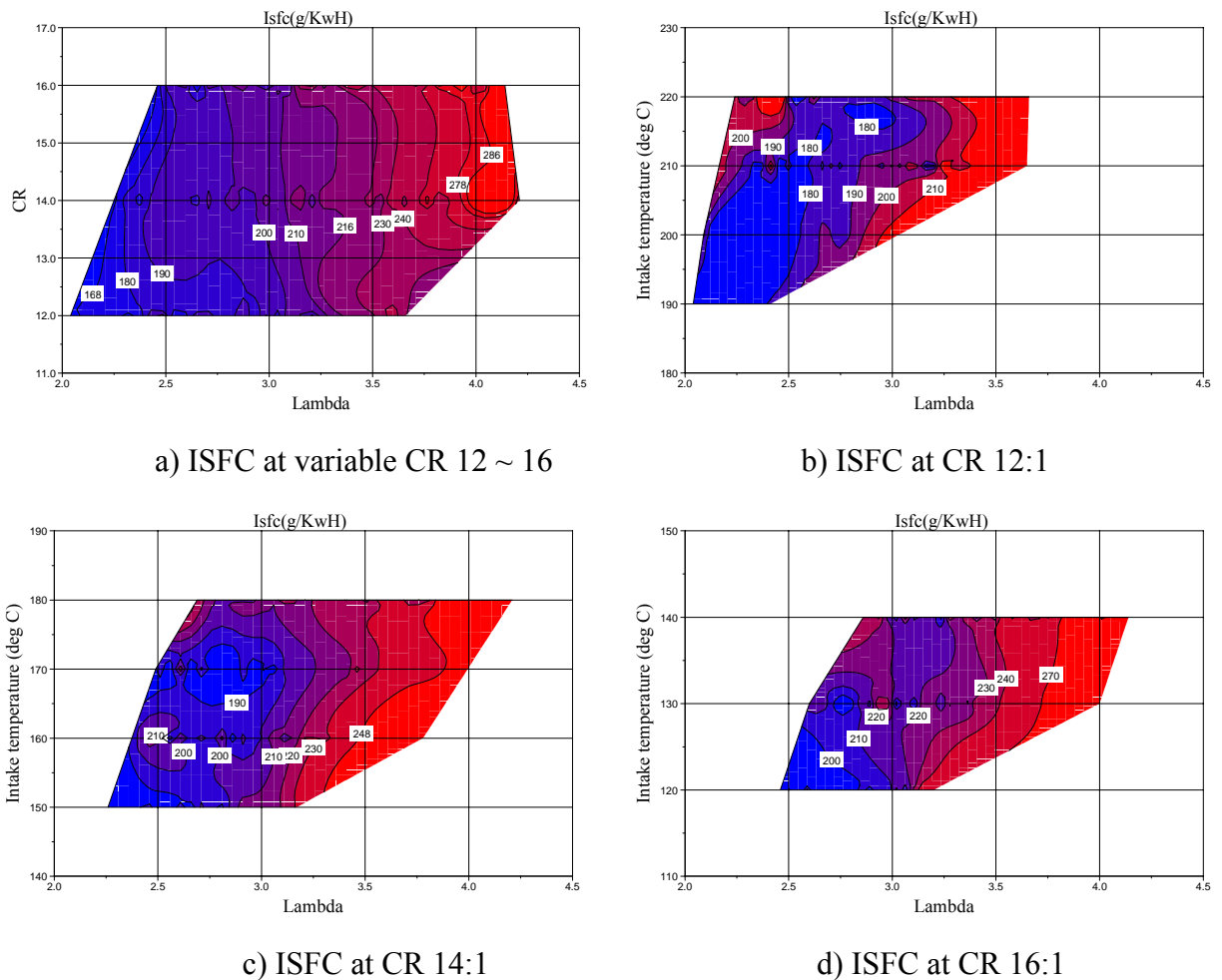


Figure 4.3 ISFC with IMEP by variable CR and intake temperature

As lower compression ratio and higher intake temperature determines the higher load range of CAI operation, ISFC obviously is a strong function of AFR and IMEP and tends to have lower values at the higher load range. Compared to a SI engine, ISFC of CAI combustion is shown generally lower, but slightly higher or even similar level at very low load range at the highest compression ratio range. It means that CAI by variable compression ratio and heating intake air seems to have the ability to achieve the lower ISFC in CAI combustion, not more than CR 16:1 in terms of the reduction of ISFC, shown in Figure 4.4.

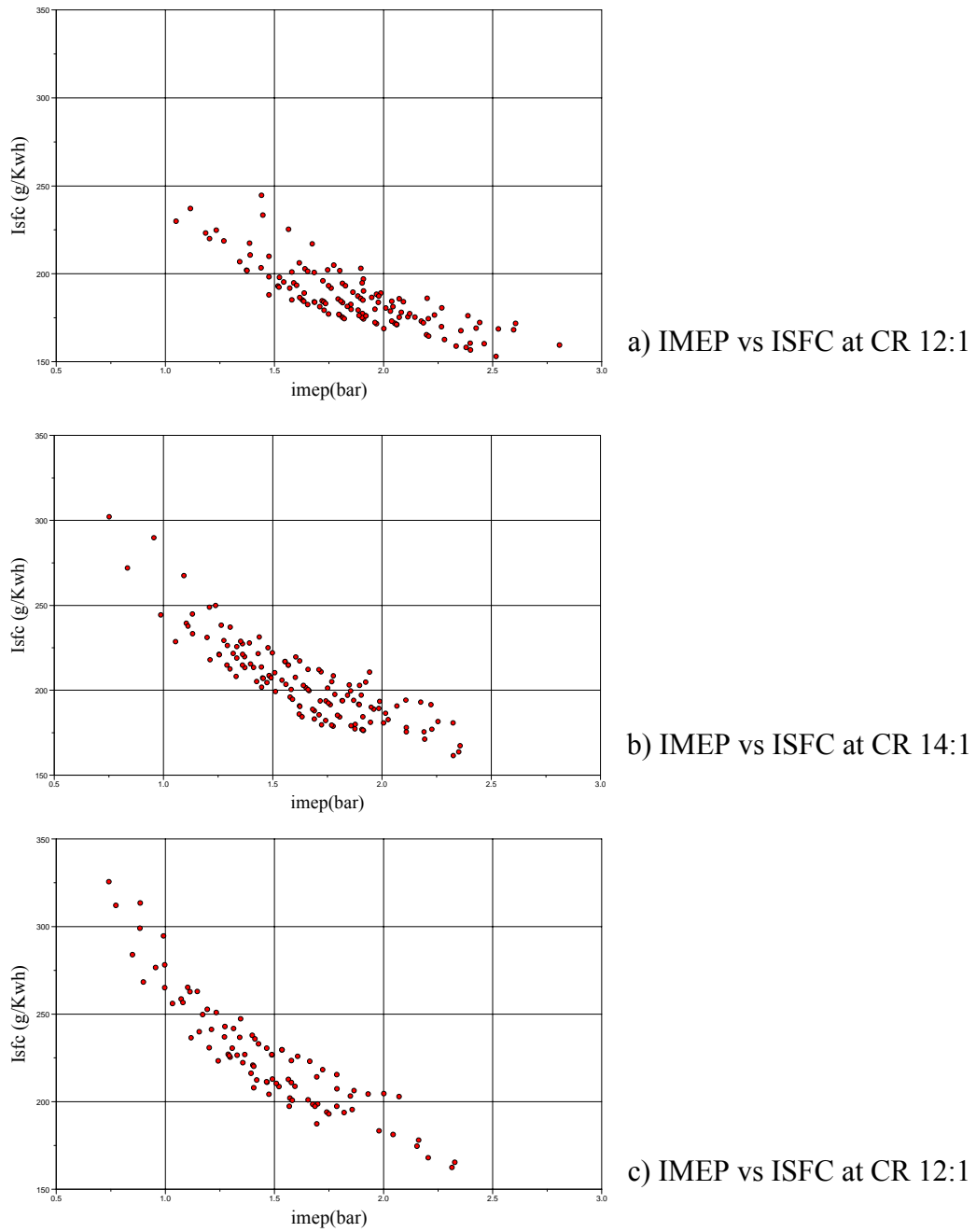
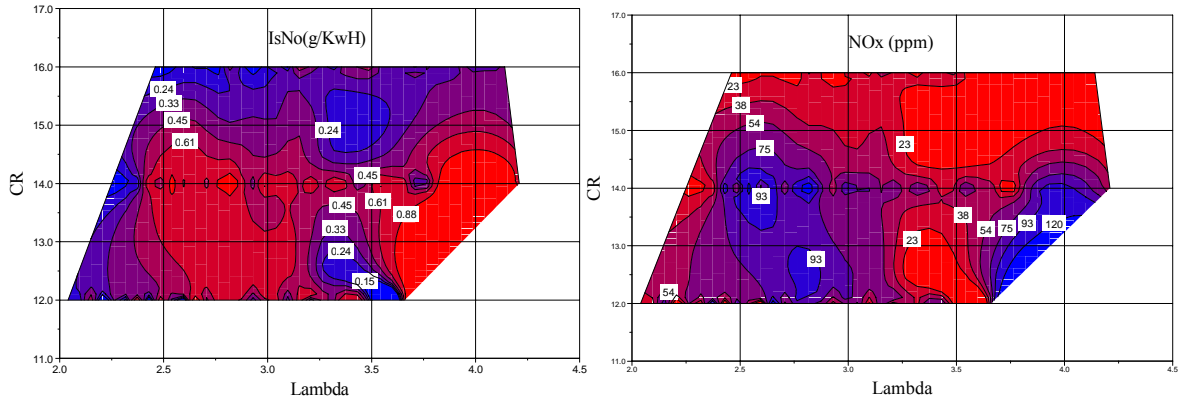
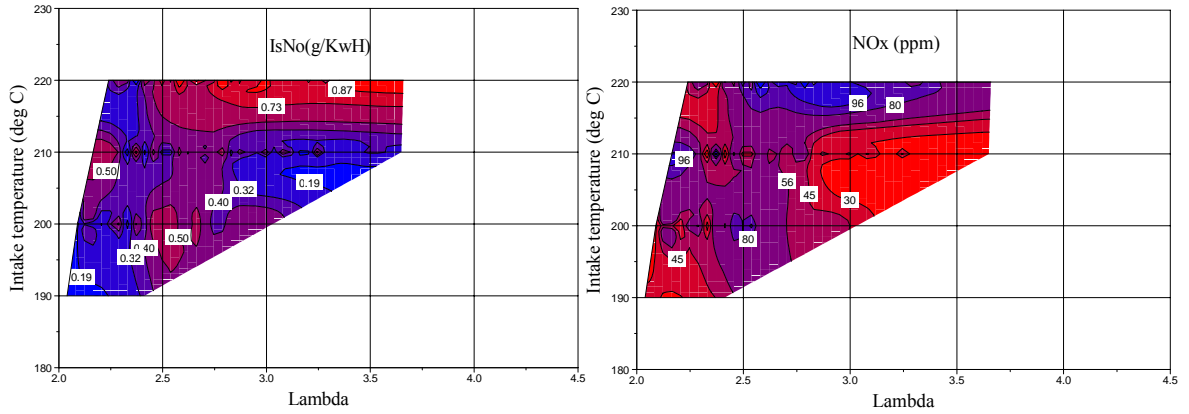


Figure 4.4 IMEP versus ISFC at variable compression ratio

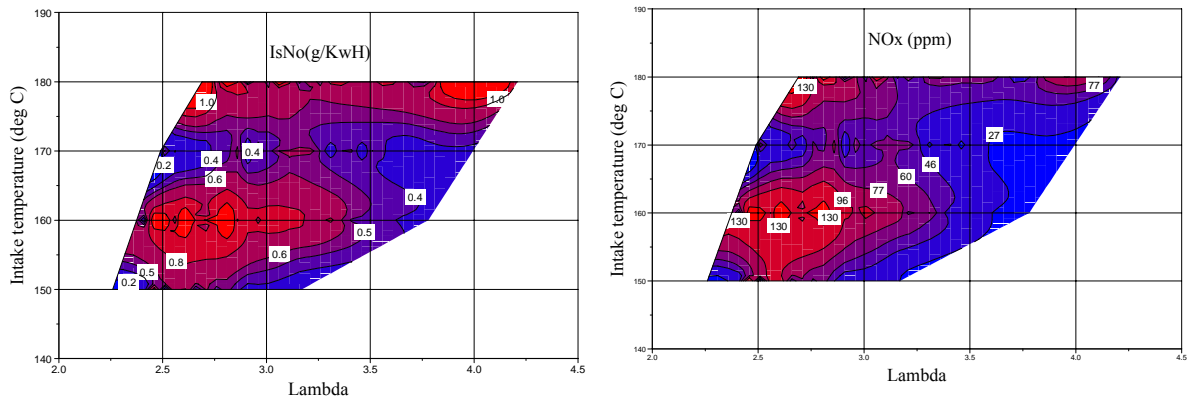
It is known that reduction of NO_x emission is one of the major advantages of CAI combustion. The result in Figure 4.5 shows that CAI combustion leads to massive reduction in NO_x emissions compared with SI combustion. For example, the typical NO_x emission in SI combustion is shown about 2500 ppm or 11 g/KWh at lambda 1.1, 1600 rpm and $\eta_v = 50\%$ [8], while the NO_x emission is typically one order of magnitude less.



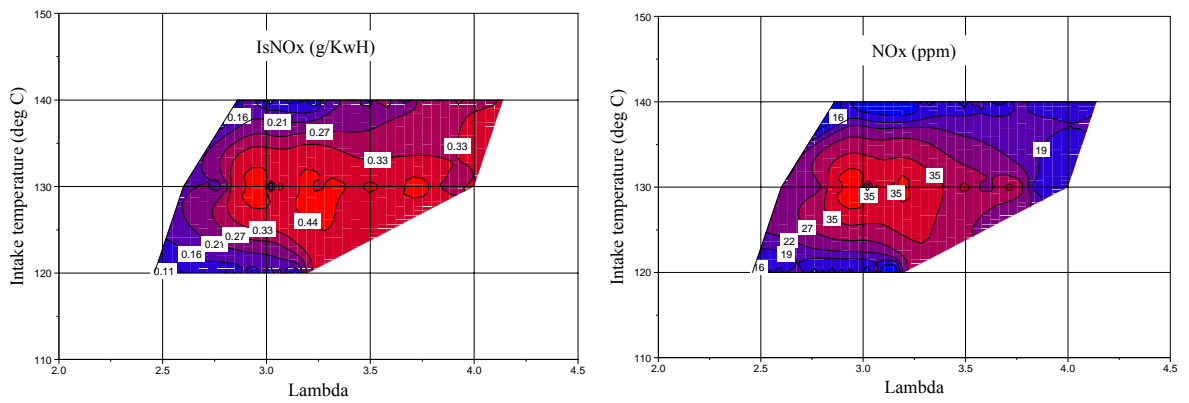
a) ISNOx and Absolute NOx at variable CR 12 ~ 16



b) ISNOx and Absolute NOx at CR 12:1



c) ISNOx and at Absolute NOx CR 14:1



d) ISNOx and Absolute NOx at CR 16:1

Figure 4.5 ISNOx and Absolute NOx at variable compression ratio

There is not a clear trend of NO_x emission in the CAI operating range. The maximum of NO_x emission, 0.88 g/KWh appears at the partial burned region, CR 12:1, due to very low load operation resulting from the extremely poor combustion efficiency at the high lambda region. The minimum NO_x emission of 0.11 g/KWh is shown at the knock boundary region, CR 16:1 at a higher heat release rate and combustion temperature unexpectedly. Again this is because the specific NO_x emission is normalized by the engine load. At this condition, the absolute NO_x emission is 16 ppm. This experimental work shows that CAI combustion operation leads to an average of 96% reduction in NO_x emission compared to SI combustion. More description of the relations with heat release and combustion temperature is detailed in section 4.4.4.

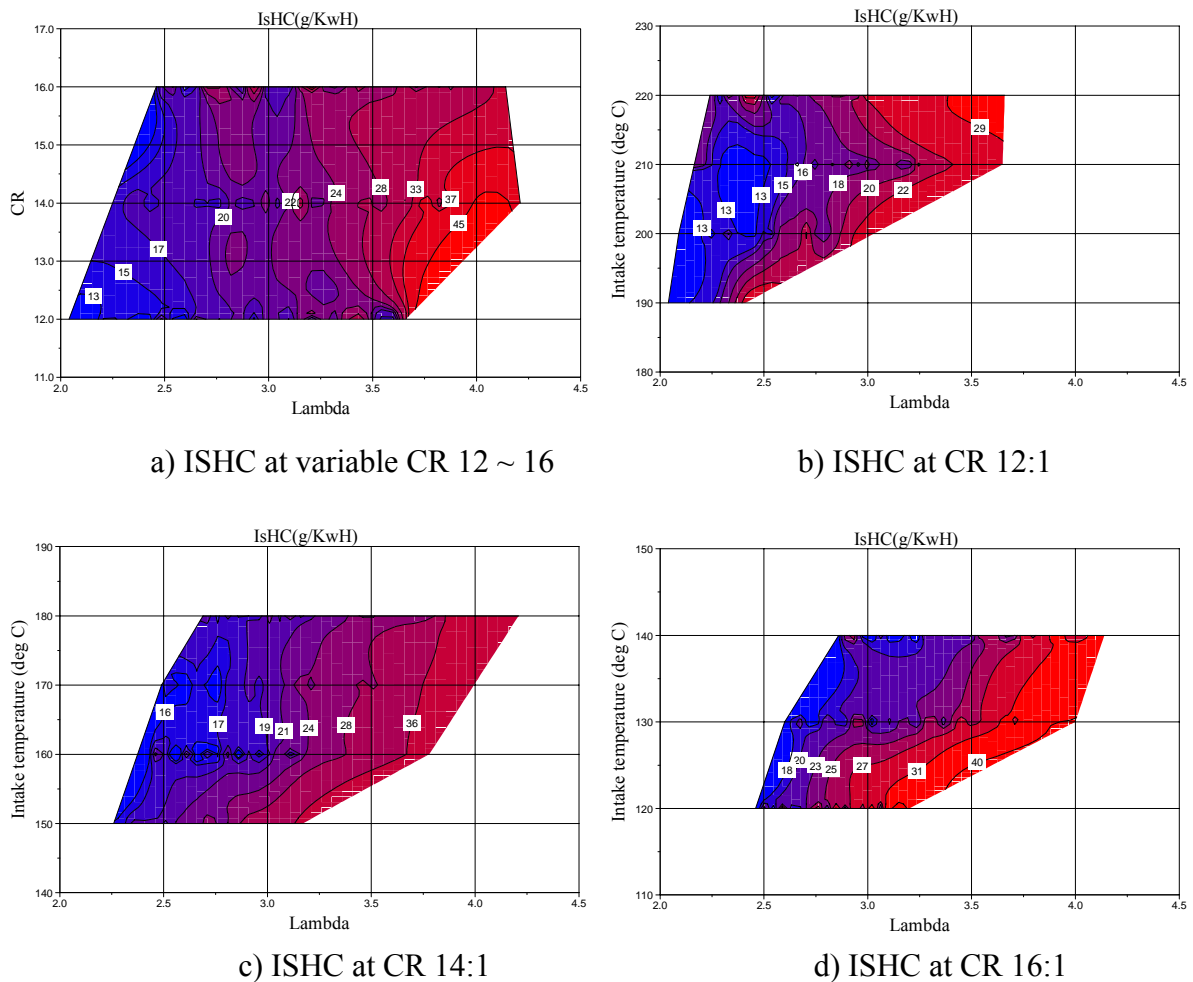


Figure 4.6 ISHC with IMEP by variable CR and intake temperature

Figure 4.6 shows the uHC emission output in the CAI operating range. In general, the levels of uHC in CAI are higher over the entire operating range than in SI combustion at approximately 5g/KWh. These emissions are increased as lambda is increased at leaner and lower engine loads region. This trend is caused by lower heat release rate and combustion temperature at lower engine loads since there is not enough time for the air-fuel mixture to be oxidized completely at lower temperature, which leads to lower oxidation rate and incomplete combustion of some fuel/air mixtures during expansion and exhaust strokes.

The highest level of uHC is about 45g/KWh and obtained at the lowest engine load area, CR 16:1 and lower intake temperature. The lowest level of uHC is about 13 g/KWh and obtained at a higher engine load area, CR 12:1 and higher intake temperature. This is one of crucial disadvantages in CAI combustion, but can be overcome by 3-way catalyst technology.

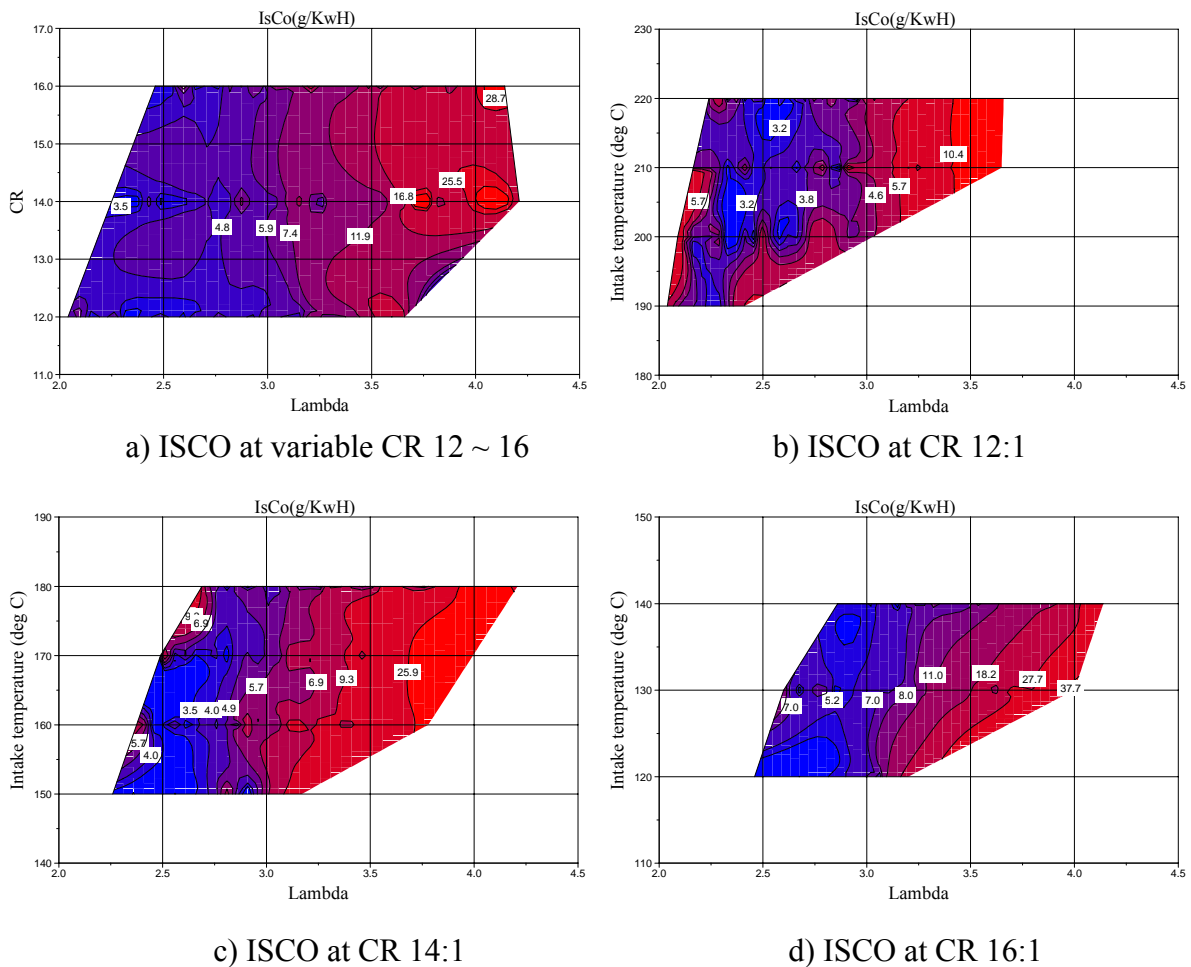


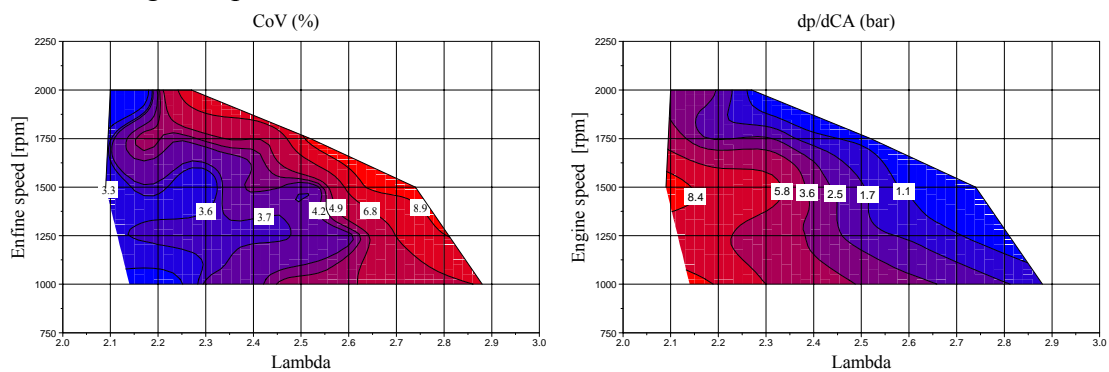
Figure 4.7 ISCO with IMEP by variable CR and intake temperature

The trend of CO emissions in CAI operating range is very similar to the levels of uHC, higher emissions at the low engine load region, shown in Figure 4.7. The highest level of CO emission is about 37 g/KWh and the lowest level of CO is 3.2 g/KWh, comparable CO emissions in SI operation is approximately 20g/KWh. In general, total CO emission is relatively lower than in SI operation, but at lower engine loads. Apparently, higher CR (16:1) and lower intake temperature provide more CO emissions than lower CR (12:1) in CAI operation.

4.4.4 Combustion characteristics

4.4.4.1 Combustion stability

The Coefficient of Variation with dilution is presented in Figure 4.8a. Combustion stability is clearly affected by increasing air dilution. The limit of drivability is at 10 % CoV, mostly this limit occurs at the partial burn area and leanest A/F ratio condition. Test results shown in figure 4.8a, are captured at compression ratio 12:1, intake charge temperature 200 °C.



a) Coefficient of Variation

b) Rate of in-cylinder pressure rise

Figure 4.8 Combustion variability at CR 12:1, Intake temperature 200 °C

The in-cylinder pressure data is post processed to determine the maximum rate of pressure during the CAI combustion. Figure 4.8b shows the results of rate of in-cylinder pressure rise. The rate of pressure rise indicates the values of pressure rise rate whether combustion causes engine knock. As shown in Figure 4.7b, the rate of pressure rise increases with load as the relative air/fuel ratio is decreased. The maximum rate of pressure rise is limited by 10% KOF at filtered pressure threshold of 1 bar and it occurs at about $\lambda=2.1$ at the experimental conditions for Figure 4.8.

4.4.4.2 Combustion efficiency

Conventional SI gasoline engines have combustion efficiency in the range of 95~98 % with stoichiometric mixture [14]. In the present investigation, combustion efficiencies of CAI combustion at leaner conditions are presented in Figure 4.9.

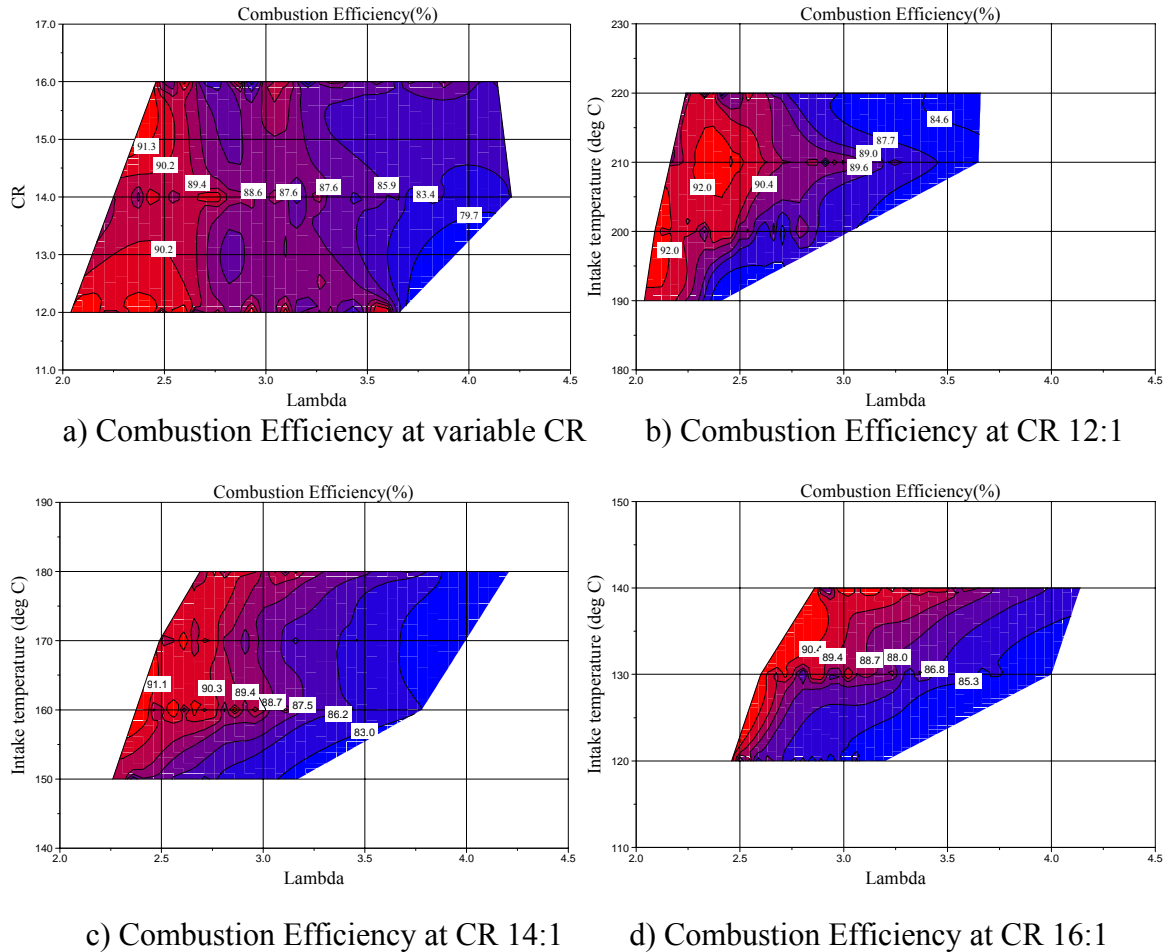
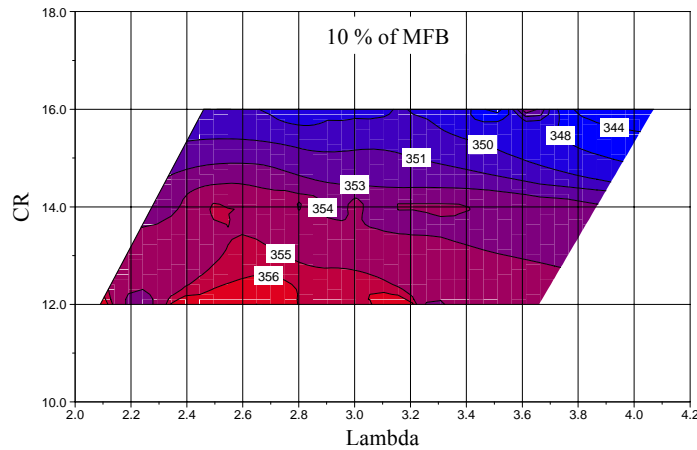


Figure 4.9 Combustion Efficiency at Variable CR and Intake Charge Temperature

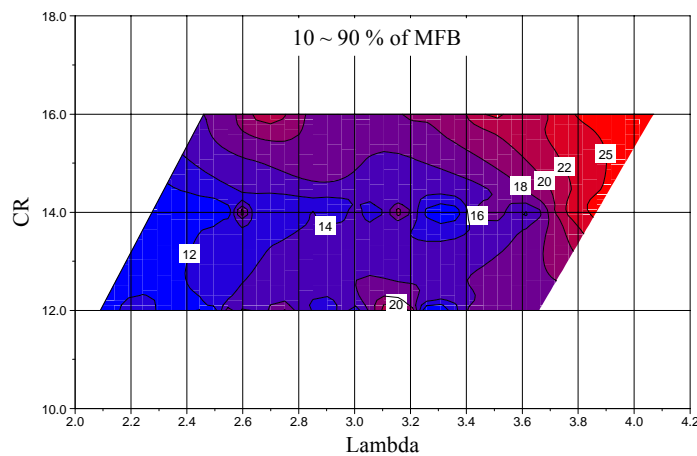
The trend of combustion efficiency with variable compression ratio and intake charge temperature is shown at very lean conditions, lambda 2.2 ~ 4.2 and shows lower efficiency with leaner A/F ratio. In the previous section, it has shown that richer A/F ratio conditions leads to more stable combustion quality than leaner condition and produces less incomplete combustion products in the exhaust gas (e.g., CO, H₂, unburned hydrocarbon, soot). The maximum combustion efficiency occurs apparently at the richest A/F ratio condition and maximum IMEP. However, this maximum combustion efficiency (92%) obtained on CAI combustion is lower than the conventional SI gasoline engine operating stoichiometric mixture.

4.4.4.3 Combustion timing

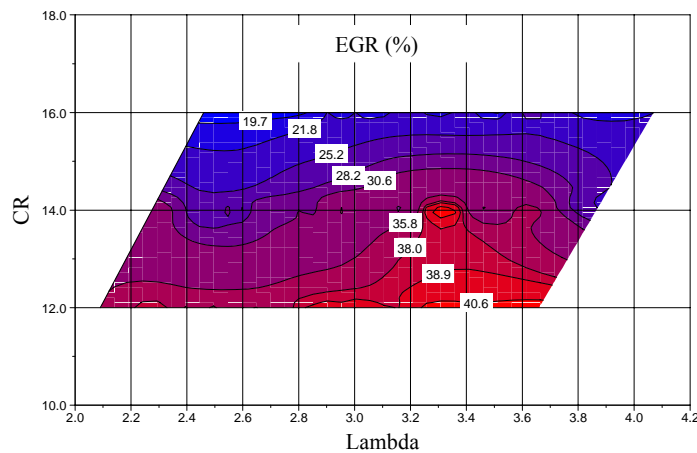
In order to describe combustion characteristics, mass fraction burn (MFB) rate is calculated as 10, 50 and 90 % of the charge mass burn. Combustion duration is considered from 10 % to 90 % of MFB and a start of combustion is considered as 10 % of MFB. Figure 4.10 shows the results of combustion characteristics with MFB, compression ratio, lambda and EGR rate at engine speed of 1500 rpm.



a) Start of combustion (10% burn crank angle), (deg CA, TDC=360)



b) Combustion duration (10%-90% burn crank angle), (deg CA, TDC=360)



a) EGR rate with compression ratio and lambda

Figure 4.10 CAI combustion characteristics by variable compression ratio

A start of combustion is normally preferred to occur near TDC so that more complete combustion is anticipated. However, start of CAI combustion in this study appears further advanced than TDC by positive valve overlap strategy compared to NVO strategy since lower EGR was trapped at higher compression ratio, shown in Figure 4.10c. Higher compression ratio leads to more advanced combustion phasing, but not much effect by air/fuel ratio. The most advanced start of combustion occurs at 344 deg CA with highest compression ratio of 16 and leanest condition of lambda 4.1, shown in Figure 4.10a.

The fastest combustion appears for about 12 crank angles at richer region and lower compression ratio of 12. However, leaner condition results in longer combustion duration from lambda 3.4 to 4.1, but no significant effect from compression ratio, shown in Figure 4.10b.

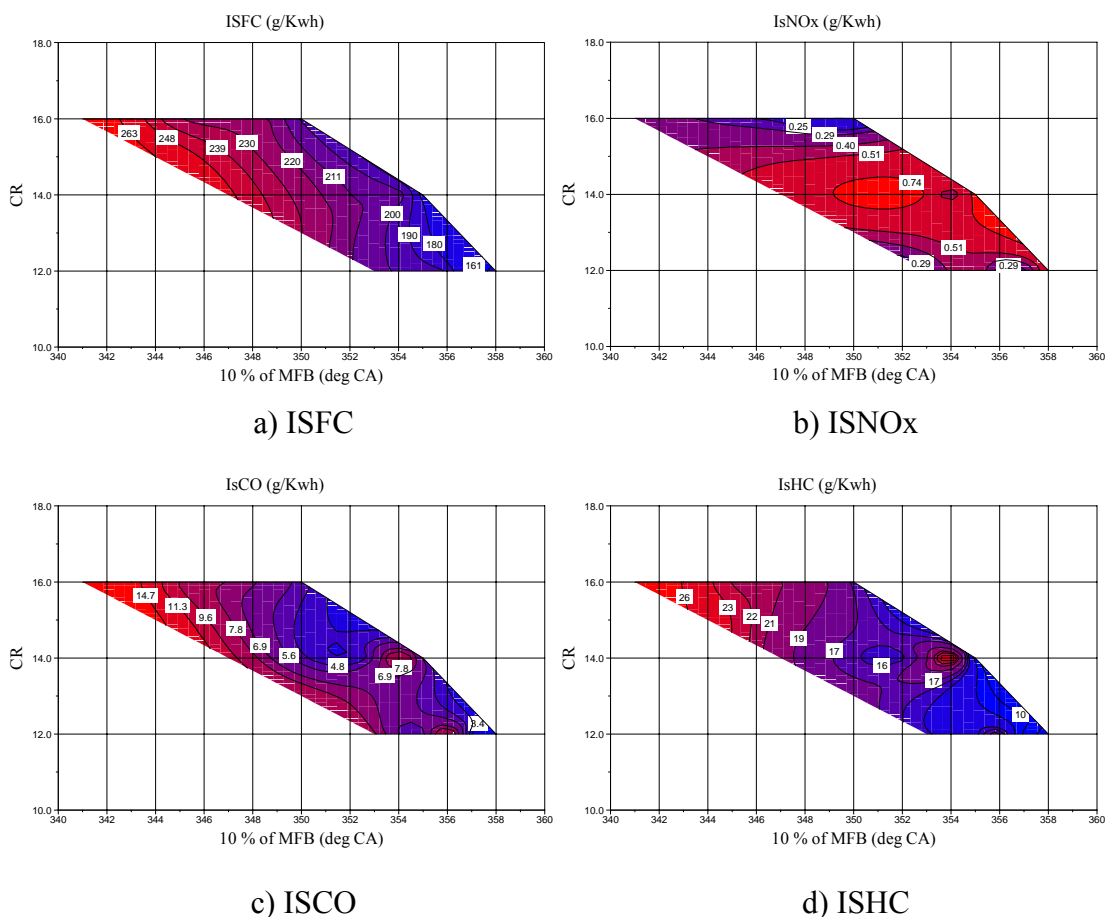


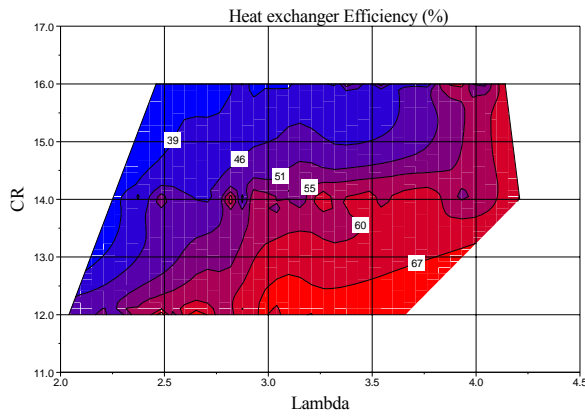
Figure 4.11 Indicated specific values at map of SOI vs CR

Figure 4.11 shows the results of indicated specific values with the start of combustion. The start of combustion near TDC leads to lower indicated specific fuel consumption, CO and HC emissions since more complete combustion is achieved by a start of combustion near TDC. However, compression ratio did not affect the results of those values. The lowest fuel consumption is achieved 161 g/Kwh at a start of combustion at 358 deg CA. In the same condition, the lowest ISCO and ISHC are achieved 3.4 g/Kwh and 10 g/Kwh respectively, shown in Figure 4.11a, 4.11c and 4.11d.

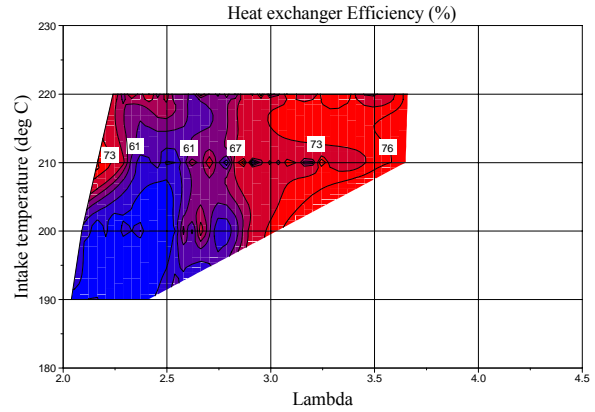
However, the start of combustion is not strong function with ISNO_x. Higher compression ratio results in low level of NO_x emission since less EGR trapped and leading to lower in-cylinder temperature. Although the level of NO_x emission appears extremely low in the entire zone, the lowest ISNO_x is achieved 0.25 g/Kwh at compression ratio of 16 and at the start of combustion of 348 and 350 deg CA, shown in Figure 4.11b.

4.4.4.4 Heat exchanger efficiency

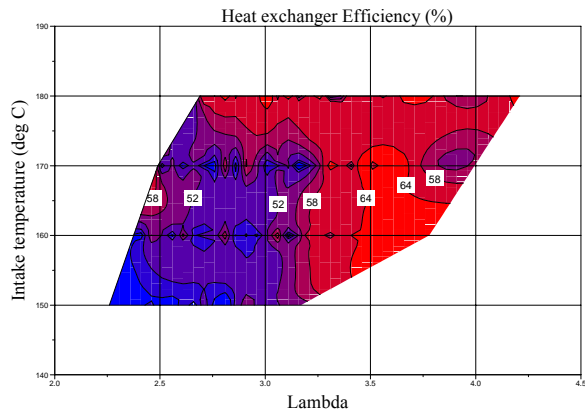
Due to the needs of an external heating device for CAI combustion, it is important to monitor actual heating availability of an heating source. Ideally, the thermal energy from the exhaust should be utilized through an heat exchanger, where the intake air is heated up by the hot exhaust gas. In order to determine the feasible intake temperature during the CAI operation, the exhaust temperature is monitored throughout each experiment and used to determine the heat exchanger efficiency required to obtain the intake charge temperature. The details of calculation are described in Chapter 3, section 3.4.1. A maximum heat exchanger efficiency of 80% is used to determine the maximum intake charge temperature that can be obtained under each operating condition. This occurs particularly in the partial burned region where the exhaust temperature is very low in the extremely lean condition. Figure 4.12 shows the results of the heat exchange efficiency required for each operating conditions.



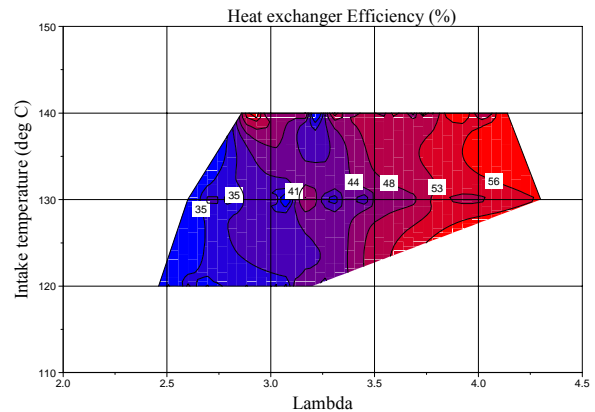
a) Heat exchange Efficiency at variable CR



b) Heat exchange Efficiency at CR 12:1



c) Heat exchange Efficiency at CR 14:1



d) Heat exchange Efficiency at CR 16:1

Figure 4.12 Heat exchange efficiency at Variable CR and Intake Charge Temperature

It is noted that the entire CAI operating range reported in this study can be achieved through intake air heating by a heat exchanger with a maximum efficiency of 80%. Thus, the employment of a heat exchanger can be considered as a feasible means to achieve CAI combustion in a gasoline engine. However, a more effective heat exchanger and/or addition heating will be required at the very low load region to achieve CAI combustion at compression ratio 12:1. Another problem to use an intake heater is the installation of an intake heater onto the production engine, requires new design or modification for the space. Furthermore, management of transient thermal response of the intake air will need to be considered.

4.4.4.5 Exhaust temperature and EGR

The exhaust temperature is monitored intensively during CAI operation, shown in Figure 4.13 in order to calculate the heat exchanger efficiency and also to investigate its effect.

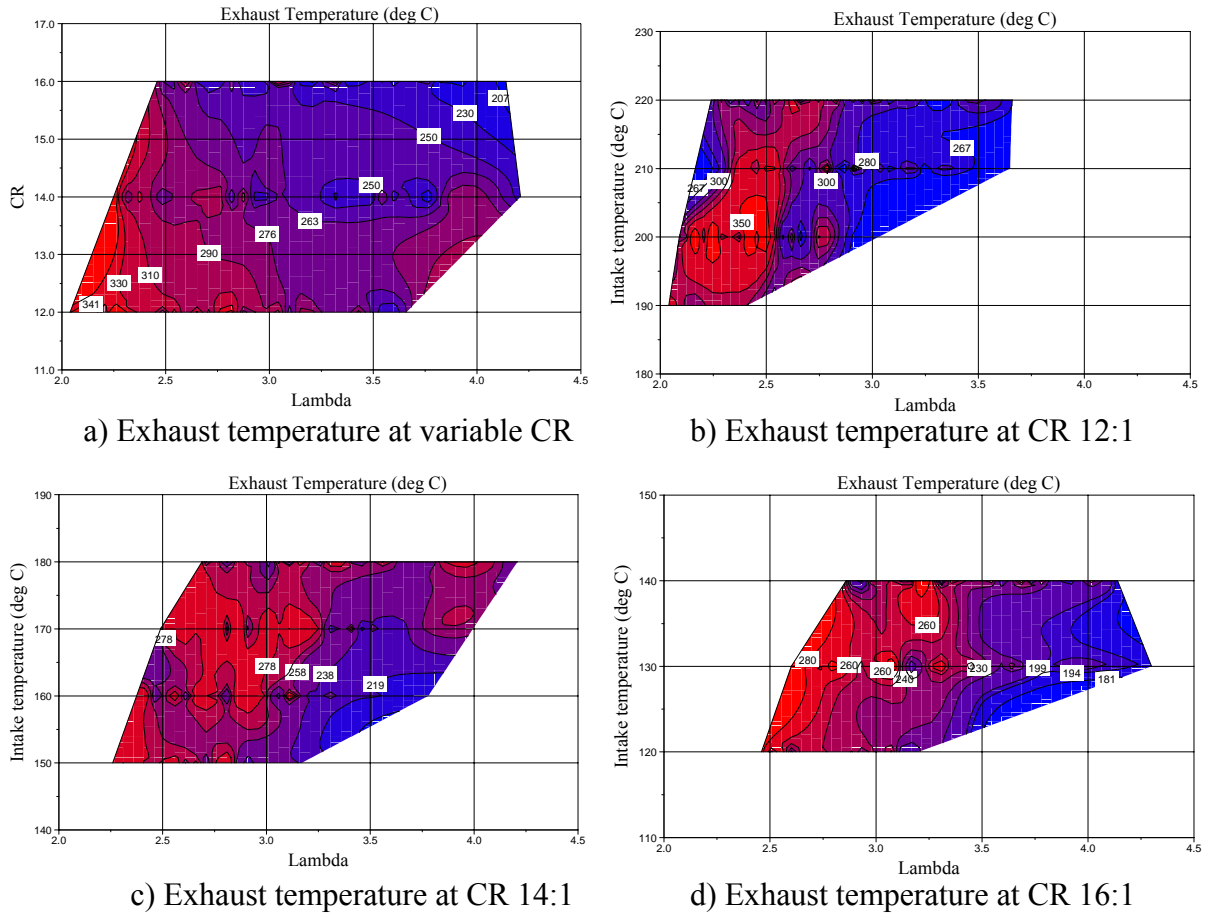
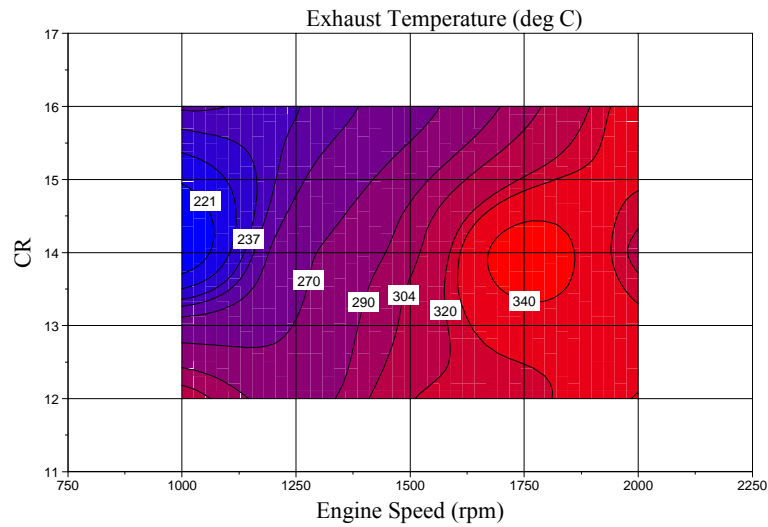
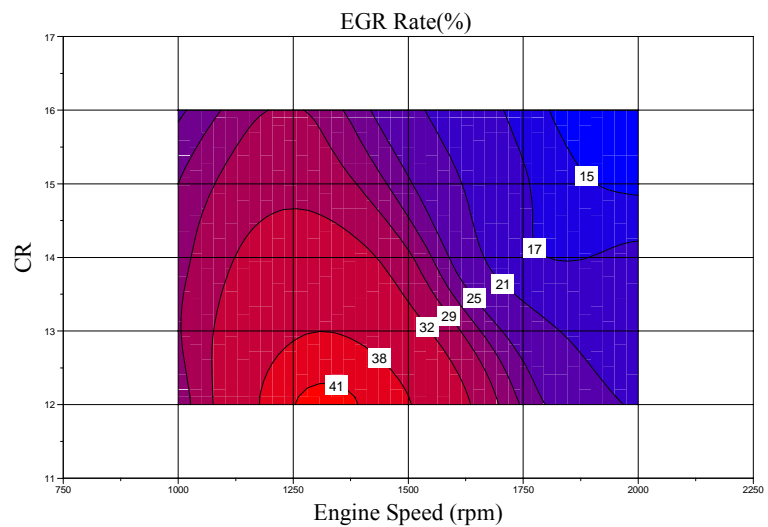


Figure 4.13 Exhaust temperatures at Variable CR and Intake Charge Temperature

The highest exhaust temperature is measured at the lowest compression ratio (CR 12:1) and higher intake temperature (190 ~220 °C). The lowest temperature is measured at higher compression ratio due to higher expansion ration and lower intake temperature (120 ~140 °C). Due to reduced heat release, the exhaust temperature is dropped down at leaner conditions and low loads.



a) Exhaust temperature at Variable CR vs. Engine Speed (rpm)

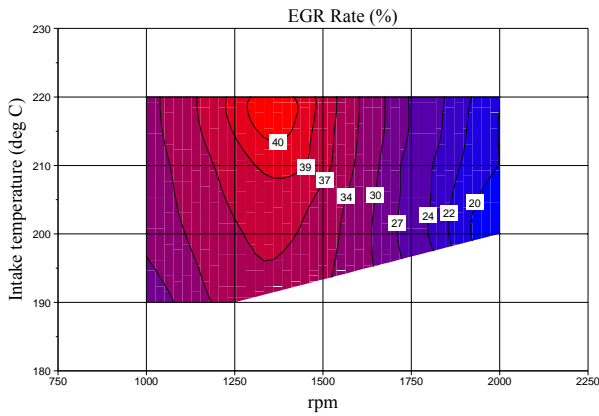


b) EGR Rate (%) at Variable CR vs. Engine Speed (rpm)

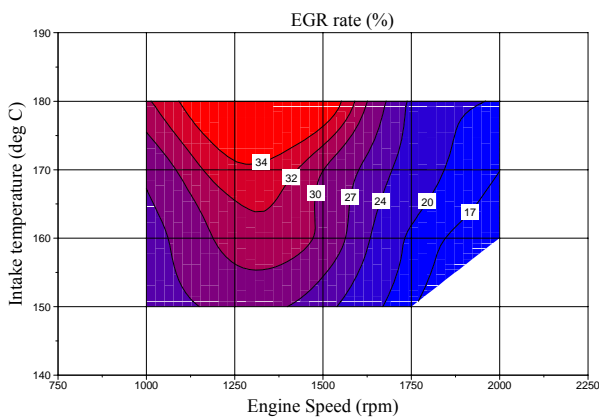
Figure 4.14 Exhaust temperature and EGR Rate at Variable CR vs. Engine Speed

Figure 4.14 shows the comprehensive results of the exhaust temperature and internal EGR in CAI combustion by using variable compression ratio and intake temperature. It is noted that the engine speed is one of the major parameters to determine the quantity of EGR. The highest amount of EGR occurs at around 1300rpm and reduces at lower engine speed. The amount of internal EGR reduces at the higher engine speed due to the higher exhaust temperature and shorter time available for rebreathing to take place. Figure 4.15 shows the results of EGR rate at variable intake temperature versus engine speed. Maximum EGR occurs at highest intake temperature and intermediate speed, where the high intake temperature compensates for the dilution effect of EGR to achieve stable autoignition and combustion. On the

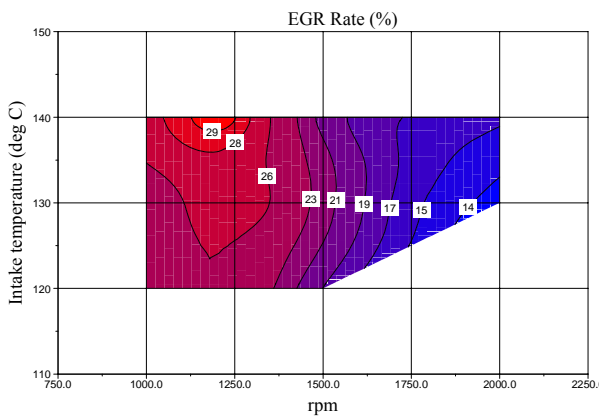
other hand, the increased heat loss at lower engine speed could be responsible for the reduced level of EGR observed experimentally.



a) EGR Rate (%) at CR 12:1



b) EGR Rate (%) at CR 14:1



c) EGR Rate (%) at CR 16:1

Figure 4.15 EGR Rates at Variable intake temperature vs. Engine Speed

4.4.5 Summary

The operating range of CAI combustion is investigated by using positive valve overlap strategy, in combination with variable compression ratios and intake charge temperature. The higher intake temperature allows the lower compression ratio to be used to achieve successful CAI combustion. Due to insufficient heating from the internally recycled exhaust gas, an intake heater is implemented to supply additional thermal energy for CAI combustion.

The CAI operating range is presented as the map of lambda versus compression ratio or intake temperature. The engine performance is shown in the operating map, as a function of the fuelling rate and internal EGR. One of the major advantages to introduce CAI combustion is the lower levels of NO_x emission in extremely lean mixture conditions due to lower in-cylinder temperature. The levels of CO emission are shown to be lower than that in SI combustion. On the other hand, higher level of uHC is shown over the operating range but it can be overcome by the 3-way catalyst technology.

The EGR rates over the operation range are studied in conjunction with the exhaust temperature and engine speed variation. The quantity of EGR strongly depends on the exhaust temperature. More EGR dilutes the air-fuel mixture and leads to the lower exhaust temperature. The engine speed has a dominant effect on the EGR rate. The EGR rate decreases with engine speed as the EGR temperature increases and shorter time for exhaust gas rebreathing to take place.

4.5 Enlargement of CAI operating range by intake air boosting and external EGR

4.5.1 Introduction

In the previous section, CAI combustion and its operating range by using positive valve overlap strategy with variable compression ratio and intake temperature are discussed. The results show not only the characteristics of CAI, but also the limit of the operating region, mainly limited by knocking at high load and partial burned combustion at low load. As one of the major drawbacks of CAI combustion, the limited operating range can be overcome to the knock region by boosting intake air pressure. The enlargement of operating range is achieved on the same Ricardo E6 research engine, but only at compression ratio 12:1 and a range of intake temperatures limited by the maximum heat exchanger efficiency.

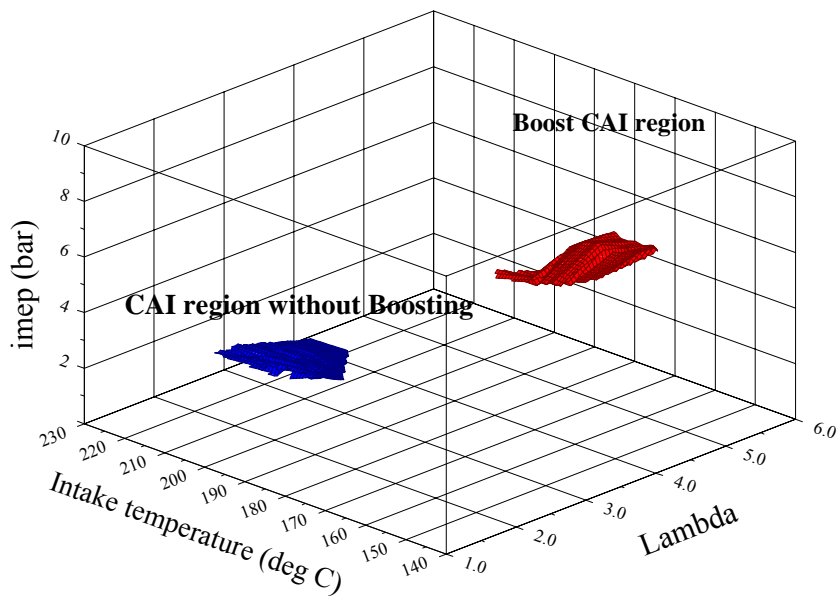
The experiments were performed first by 1 bar air boosting pressure at variable intake temperature, showing massive improvement of CAI operation limit in terms of engine performance. Thereafter, 0.5 bar air boosting pressure was employed to obtain the middle region in the CAI operation between the 1 bar boosting and naturally aspirated operation.

Positive valve overlap strategy leads to lower EGR compared to the negative valve overlap strategy. The external EGR trapping path was therefore introduced to increase the quantity of EGR and CAI operation range, particularly in the mid region. The study was performed under two different boosting pressures (0.5 and 1 bar) with external EGR.

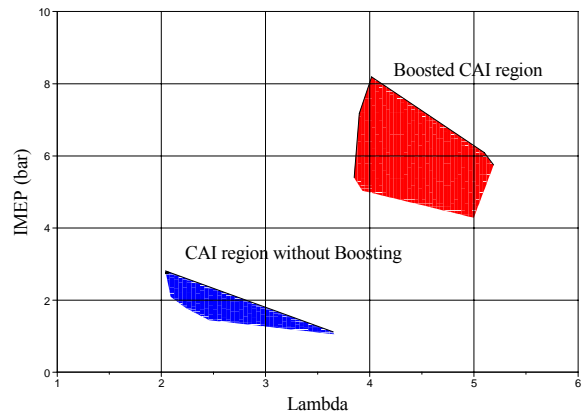
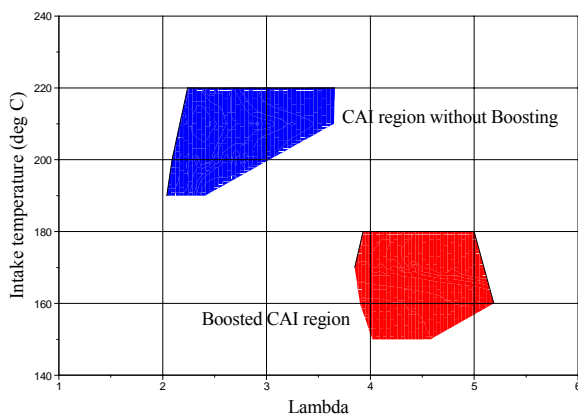
The investigation included the analysis of combustion characteristics and the measurements of exhaust emissions. The CAI operating regions and the results of CAI combustion are shown together with those of naturally aspirated condition, for every each boosting pressure and EGR.

4.5.2 Enlargement of CAI operating range

The enlargement of CAI operating range to the knock boundary by boosting intake air pressure (1 bar) was performed at compression ratio (12:1) and intake temperature (150 ~ 180 °C). Figure 4.16 shows the results of boosting intake air pressure on CAI with lower EGR by positive valve overlap. It is obvious that the boosted intake air provides much higher engine load up to IMEP 8 bar. It also allows a much lower intake temperature at the same compression ratio compared to the naturally aspirated CAI combustion.



a) Comparison of CAI operating range in boosting air and NA at CR 12



b) Intake temperature range with boosted CAI

c) Load performance with boosted CAI

Figure 4.16 Enlargement of CAI operating range by 1 bar boosting air pressure at CR 12:1

The boosted air pressure with higher air density leads to a higher fuelling rate to achieve CAI combustion. The increased in-cylinder pressure leads to a higher engine load performance at much leaner air-fuel mixture condition (λ 3.8 ~ 5.2). The results show significant improvements of the CAI operating range compared to the knock boundary region of NA CAI combustion. The highest engine load is apparently obtained up to IMEP 8 bar at the richer AFR condition (λ 4) but lower intake temperature. The lowest engine load is obtained at λ 5, limited by the partial burned combustion.

In order to achieve CAI combustion between the highly boosted region and NA region, a lower boosting pressure (0.5 bar) was then tested at only intake temperature 180 °C without EGR. Thereafter, external EGR was introduced to both boosting conditions. The EGR gate valve was opened to allow exhaust gas to be recycled into the intake externally. The exhaust gate valve was partially closed to increase the exhaust back pressure to be higher than the intake boosted air pressure. When boost pressure was 0.5bar and 1.0bar, the exhaust pressure was regulated to about 0.7 bar and 1 bar respectively.

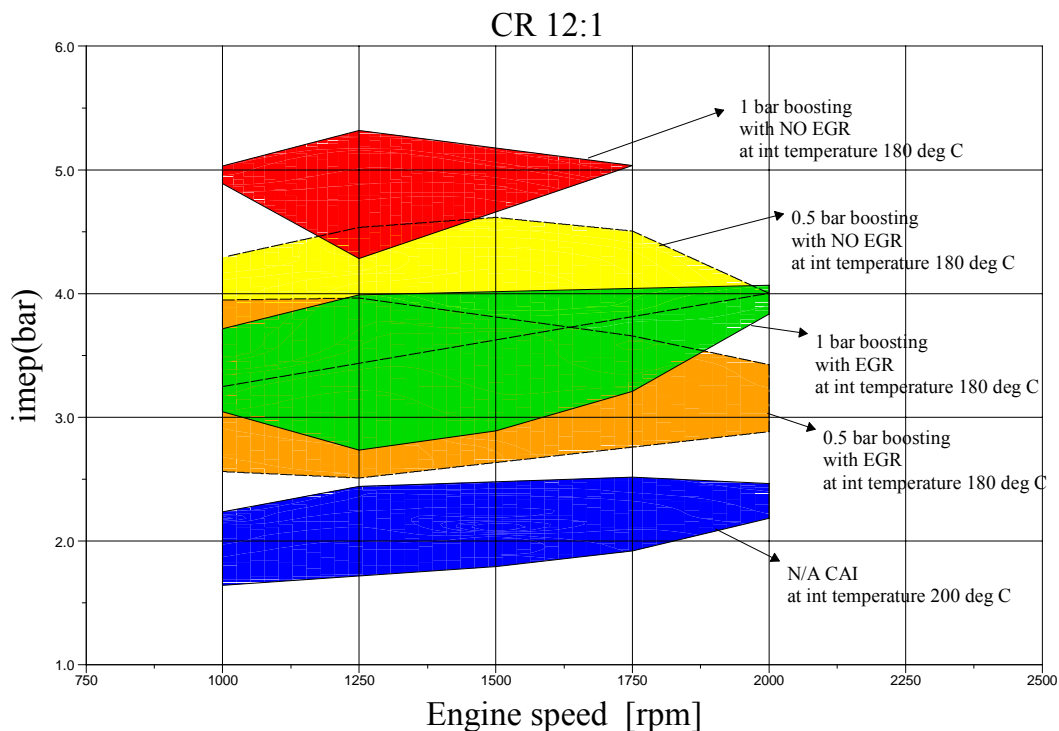


Figure 4.17 Enlargement of CAI operating range by boosting air pressure at CR 12:1

Figure 4.17 shows the comparison of CAI operating range at 180 °C for the following conditions; 0.5 bar boosting with and without external EGR, 1 bar boosting with and without external EGR. The 0.5 bar boosting resulted in the mid range operation between 1 bar boosting and N/A CAI region, as expected.

Additional EGR by an external path increases the EGR rate in the charge and lowers engine loads as shown Figure 4.16. The details of external EGR are described in Section 4.5.5.

4.5.3 Fuel consumption and Engine output emissions

Fuel conversion efficiency

One major advantage in CAI combustion is lower fuel consumption. As shown in Figure 4.18, the naturally aspirated CAI is achieved at fuel conversion efficiency from 42 % up to about 53 % at compression ratio 12:1, intake temperature 180 °C and by using unleaded commercial gasoline fuel. The fuel conversion efficiency of N/A CAI is increased at higher engine loads due to higher combustion efficiency.

The 1 bar boosting pressure provides better fuel conversion efficiency than NA CAI in either cases of with or without external EGR. The CAI combustion are achieved at fuel conversion efficiency from 55 % up to 59 % at 1 bar boosting pressure without external EGR and 40 % to 42 % by 1 bar with external EGR. The fuel conversion efficiency at 1 bar boosting without external EGR is strongly affected by the engine loads when the load is below IMEP 4.6 bar. Above this mid region, it is a stronger function of both engine speed and internal EGR. The 1 bar boosting operation with external EGR shows more complicated trends of fuel conversion efficiency and it is affected by both the operating loads and total EGR.

The best fuel conversion efficiency in the entire CAI operating range is obtained by 0.5 boosting pressure without EGR from about 55 % up to 71 %. The CAI operation by 0.5 bar boosting and external EGR is achieved at also better fuel conversion efficiency at about 54 % to 63 % compared to 1 bar boosting pressure. Since the introduction of external EGR was achieved at higher exhaust back pressure, the

pumping losses increased and hence higher fuel consumption was measured under such conditions.

In this study, 0.5 bar boosting pressure is the best option in terms of fuel consumption, compared to the 1 bar boosting pressure and naturally aspirated CAI. The results of 0.5 bar boosting pressure show the similar results to 1 bar boosting pressure. The highest efficiency is obtained at higher speed and higher load conditions.

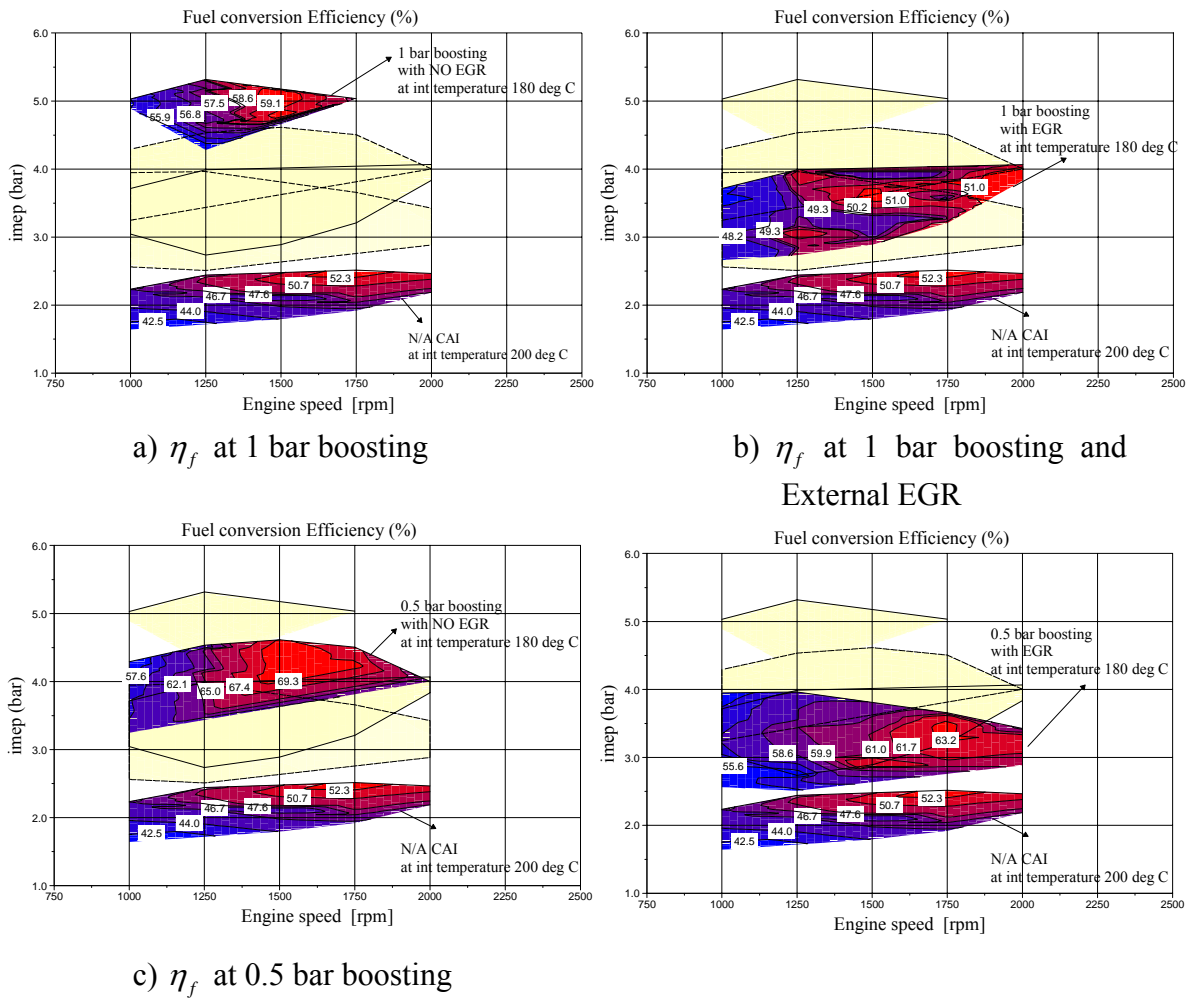


Figure 4.18 Fuel Conversion Efficiency (η_f) in the enlarged CAI operating region

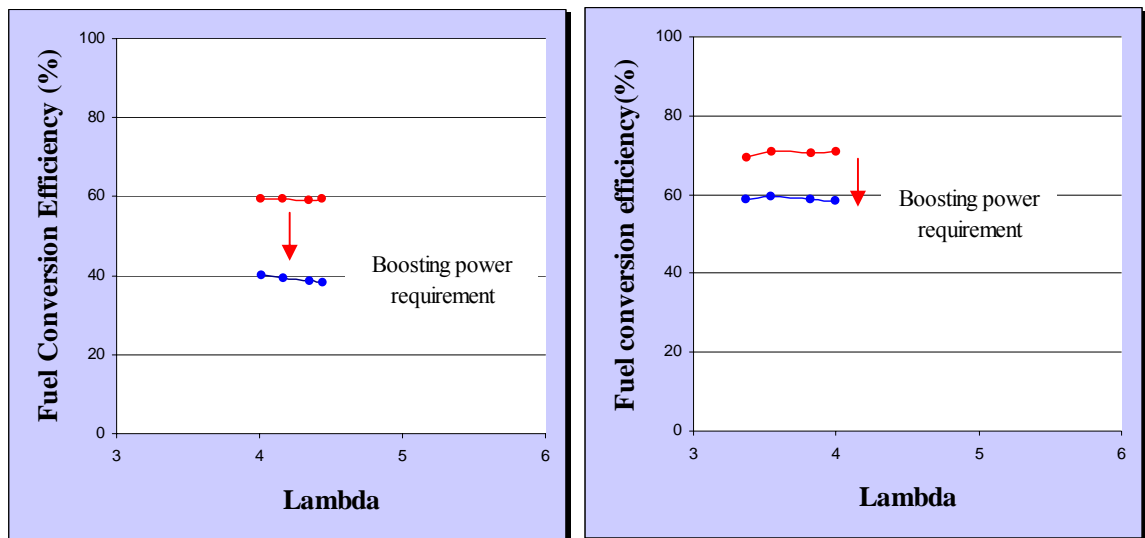
However, the above analysis does not take into account of the additional energy required to provide the compressed air. In the following analysis, two scenarios will be considered for the source of compressed air and associated energy requirement, from which the overall fuel conversion efficiency will be evaluated.

Boosting pressure (bar)	Air density (Kg/m ³)	Mass of air (g/sec)	Volumetric Efficiency (%)	Compressor efficiency (%)	Power requirement of supercharger (KW)
0.5 bar boosted	1.16	5.77	78.5	60	0.46
1 bar boosted	1.54	8.35	85	60	1.067

Table 4.3 Power requirement of supercharging system at $C_p = 1.016$ (kJ/KgK), Intake temperature = 180°C, Engine speed = 1500rpm, CR=12

As an additional device to increase air density and volume, power requirement of supercharging system is calculated. Table 4.3 shows the results of calculated volumetric efficiency and power requirement and measured mass of air while engine speed is considered constant at 1500 rpm.

Figure 4.19 shows reduction of fuel conversion efficiency by subtracting the power requirement of boosting device. More fuelling rate is required to boost intake air as an additional equipment on the engine, leading to higher specific fuel consumption or lower fuel conversion efficiency. 1 bar and 0.5 boosting pressures require about 20 % and 10 % of reduction in fuel conversion efficiency respectively.



a) η_f at 1 bar boosting pressure

b) η_f at 0.5 bar boosting pressure

Figure 4.19 Reduction of Fuel Conversion Efficiency (η_f) by power requirement of boosting equipment at 1500 rpm, CR 12, Intake temperature 180°C

NOx emissions

The reduction of NOx emissions in CAI operation by boosting intake charge is achieved spectacularly compared to not only SI combustion but also to the naturally aspirated CAI operation, shown in Figure 4.21. As presented in sec 4.5.2, the regions of CAI operation by boosting air intake occurs at much leaner condition and hence lower in-cylinder temperature than NA CAI operations, thus even lower NOx emissions.

In addition, it is noted that NOx emission increases with load in the presence of EGR (Figure 4.20b and 4.20d), due to reduced amount of EGR. However, in the case of boosting without external EGR (Figure 4.20a and 4.20c) the effect of engine speed seems more dominant. Furthermore, at the same load conditions, the presence of EGR (Figure 4.27b and 4.27d) leads to lower NOx emission at leaner operation. However, the use of EGR was achieved at the expense of higher boosting pressure and backpressure, hence increased fuel consumption.

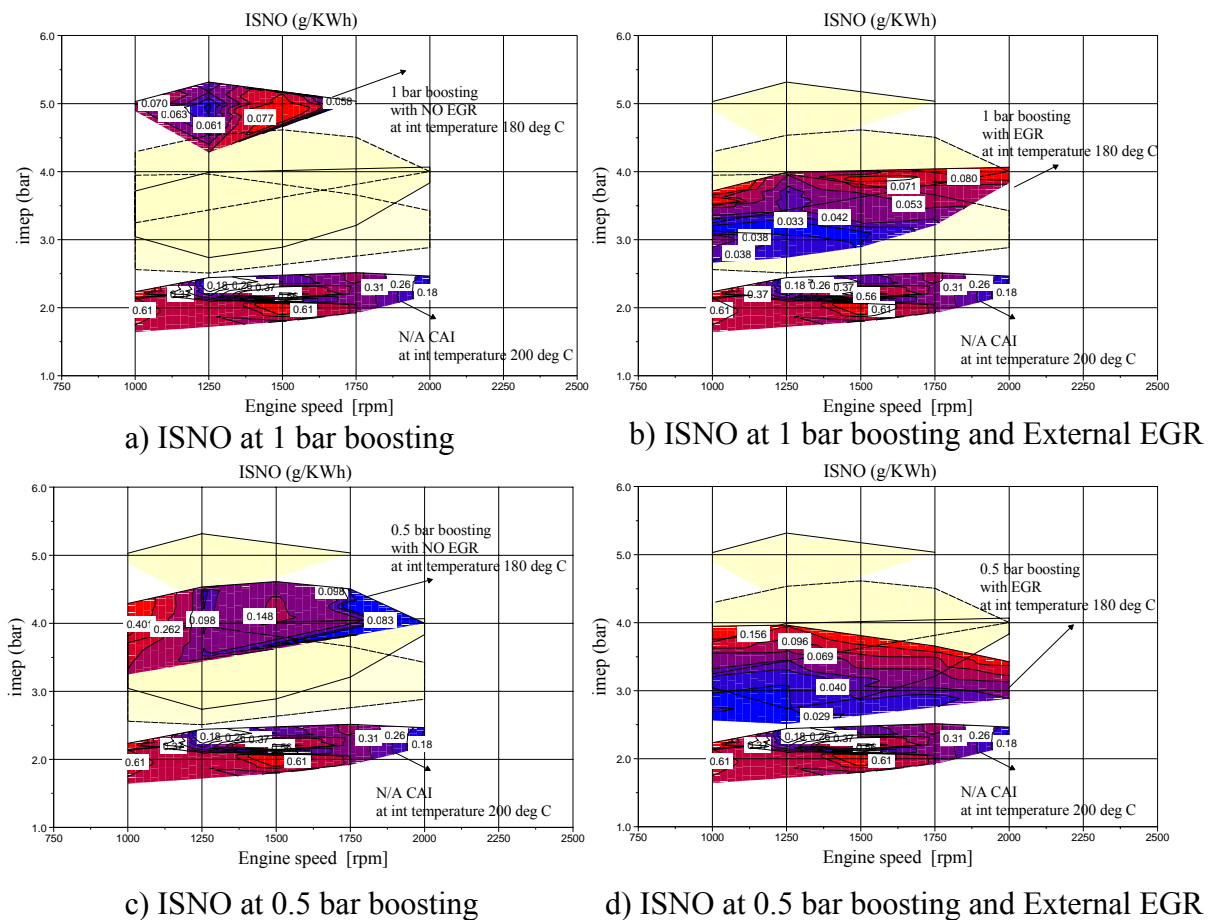


Figure 4.20 ISNO in the enlarged CAI operating region

Unburned hydrocarbon and CO emissions

As shown previously, the levels of uHC in CAI operation are higher than SI combustion. However, Figure 4.21 shows that in general uHC emissions are reduced at elevated intake pressures. With EGR, uHCs are principally affected by the engine load. As the load increases and EGR reduces, uHCs are reduced due to higher combustion temperature and more complete oxidation. In the case of lean boosting operations, the uHC emissions are mostly dependent on the engine speed. As the speed increases, less internal EGR is present and higher combustion temperature appears, causing more complete combustion and oxidation of uHCs. The highest level of uHC emissions is obtained at about 25 g/KWh at 0.5 bar boosting pressure and engine speed of 1000rpm, shown in Figure 4.21c. The lowest level of uHC emissions is shown to be about 5.8 g/KWh at 1 bar boosting pressure and external EGR, shown Figure 4.21b.

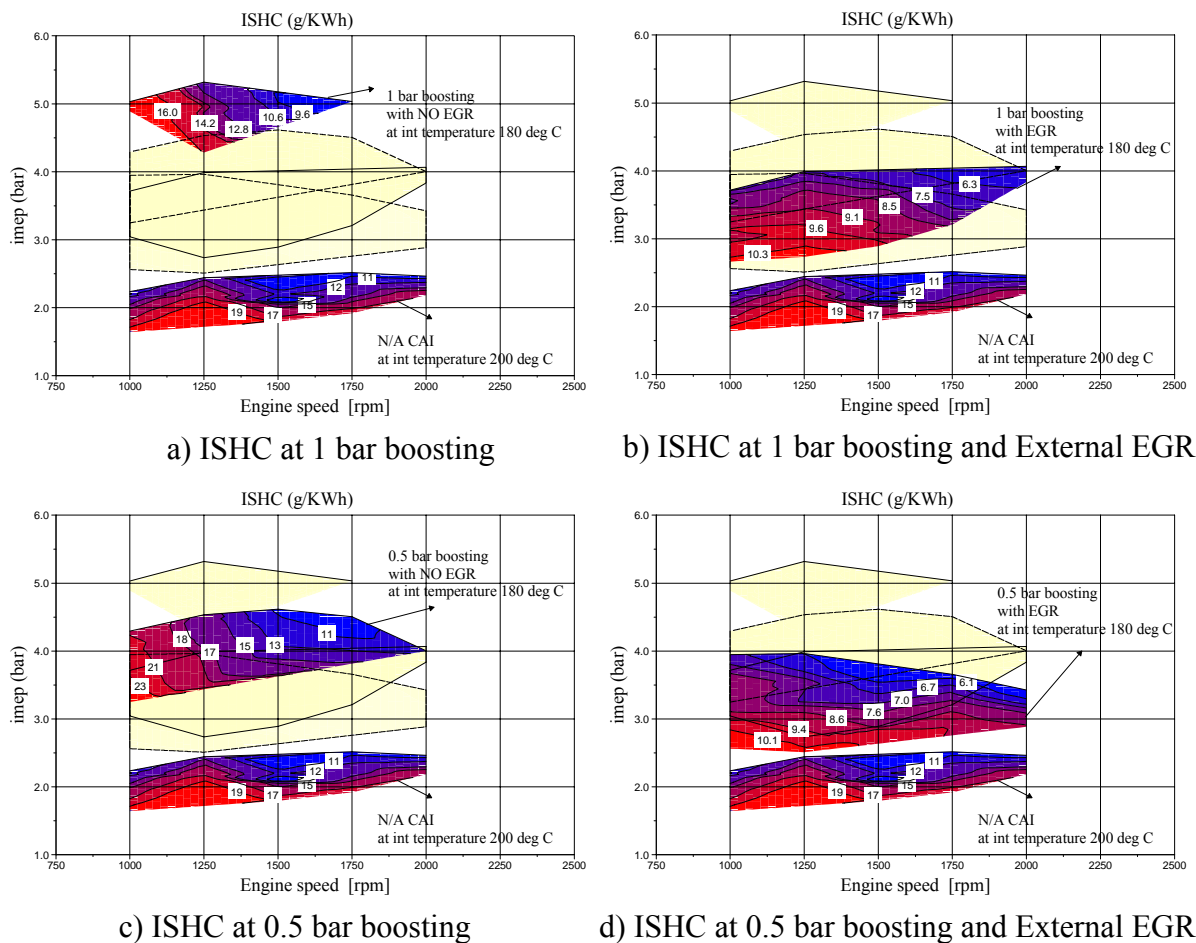


Figure 4.21 ISHC in the enlarged CAI operating region

The levels of CO emissions in boosted CAI region is shown in Figure 4.22. The results show slightly higher levels than the naturally aspirated CAI region, but still less than SI combustion, stated in Chapter 2. The trends of CO emissions are strongly in dependant on the engine loads and fuelling rates over the entire operating range of CAI. However, the boosting pressure without external EGR shows that the CO emissions are affected by engine speed as well as due to the lower quantity of trapped residual. As a result, the levels of CO emissions in the boosted CAI operating range are lower than SI combustion with the enormous enlargement of the CAI operating region.

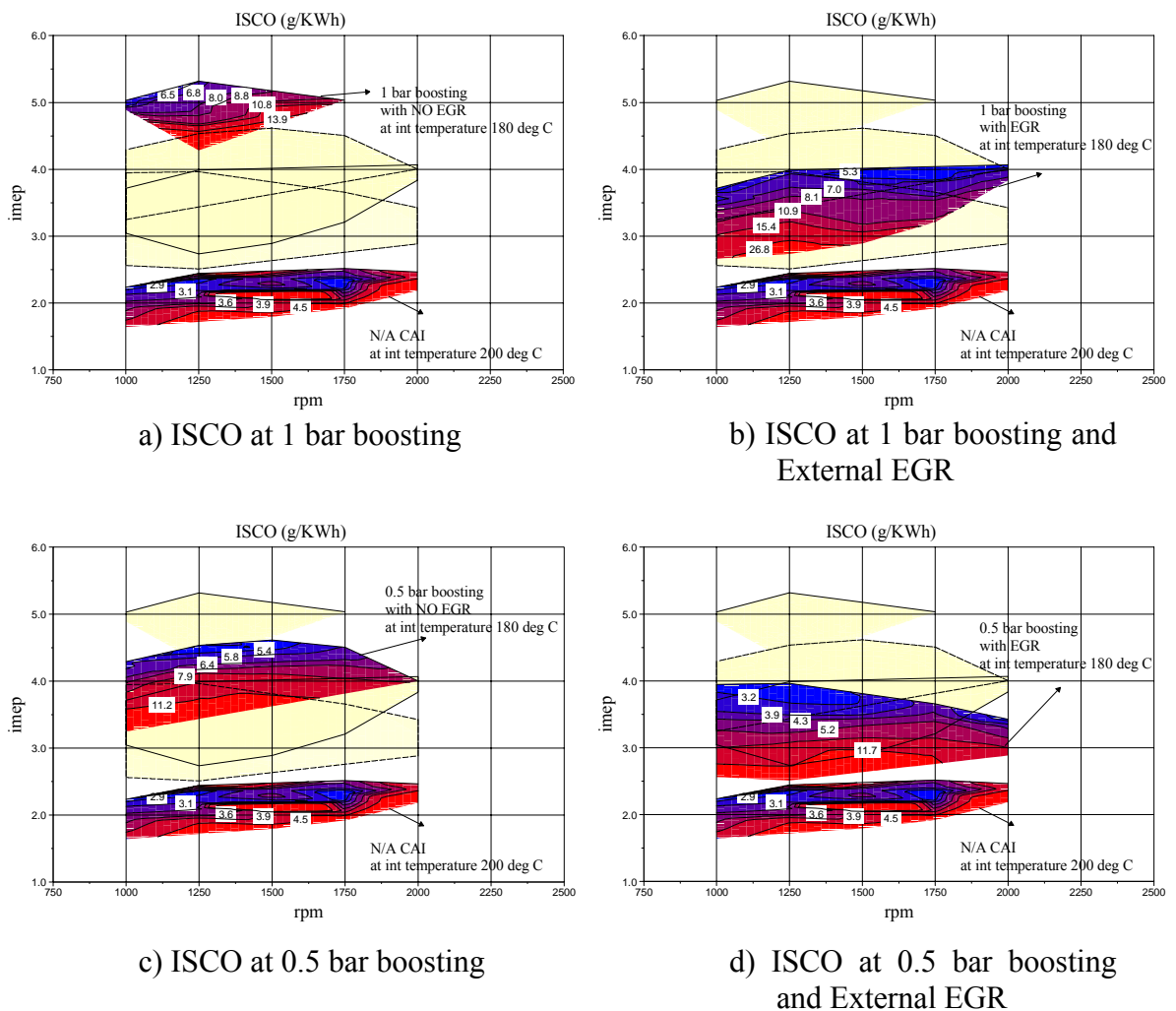


Figure 4.22 ISCO in the enlarged CAI operating region

The results of enlarging the CAI operating range is very promising in order to overcome one of major drawbacks of CAI combustion, by boosting intake charge from 0.5 bar to 1 bar pressure and external EGR respectively. For the commercial application, this study shows the potential of CAI operation from the lower loads to

the higher loads, additionally remarkable reduction of NO_x and CO emissions. Due to the stricter regulation of the CO₂ emissions, it can be an alternative for the internal combustion engines, as a hybrid application with SI mode in the automotive industry. The uHC emissions are definitely one disadvantage in CAI combustion, as shown in the results in this chapter. However, the after treatment catalyst technology of the internal combustion engine has been developed over several decades and can solve these problems.

4.5.4 Combustion characteristics

4.5.4.1 Combustion stability

Combustion variability and rate of in-cylinder pressure rise are analyzed during the boosted engine operations. Figure 4.23 shows the results obtained at CR 12:1 and possible intake charge temperature, 150 ~180 °C where stable CAI combustion could be achieved. As shown, higher combustion variation during CAI combustion occurs at leaner A/F ratio condition and higher engine speed. The rate of in-cylinder pressure rise tends not to be related to the engine speed, but it is a strong function of the A/F ratio. The region of boosted CAI operation is determined by the limits of maximum COV 10% at high speed and low loads which leads to partial burn combustion and maximum dp/dt of 10 bar/CA at the rich and high load operations which leads to knock.

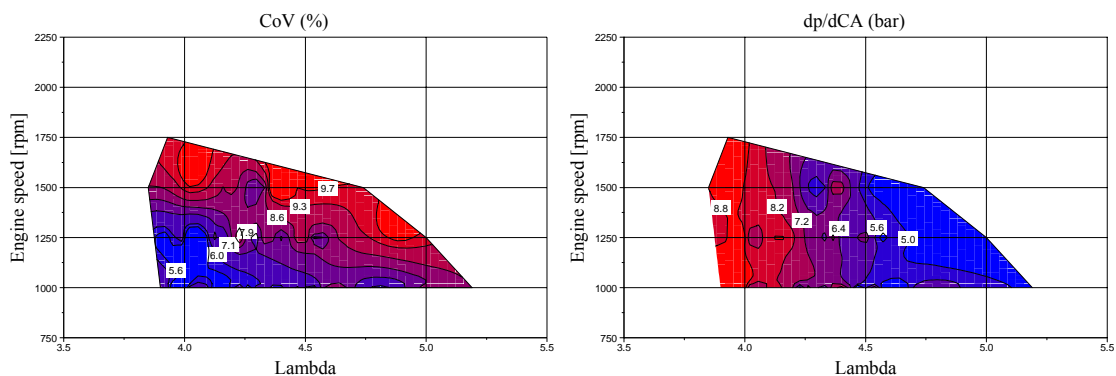


Figure 4.23 Combustion variability and stability of CAI by boosting intake charge 1 bar pressure at variable intake temperature

4.5.4.2 Combustion efficiency

The combustion efficiency in boosted CAI operating range is presented in Figure 4.24. In general, the combustion efficiency is lower than SI combustion since CAI combustion takes place at extremely lean mixture condition and at lower combustion temperature. For both 0.5 bar and 1.0 bar boosting operations, the best combustion efficiency is obtained with external EGR varying between 91% at low load to about 95 % at high load and high speed operations. On the other hand, the boosted operation without external EGR achieves slightly lower combustion efficiency than natural aspirated CAI because the CAI operation with boost is performed with lower quantity of internal EGR at both 0.5 bar and 1 bar boosting pressure.

The combustion efficiency is apparently very in dependant on the engine loads and lambda. Higher combustion efficiency is achieved at higher loads and with relatively richer mixture. However, the engine speed affects the combustion efficiency at very high loads by boosting pressure 1 bar without external EGR, shown in Figure 4.25 a).

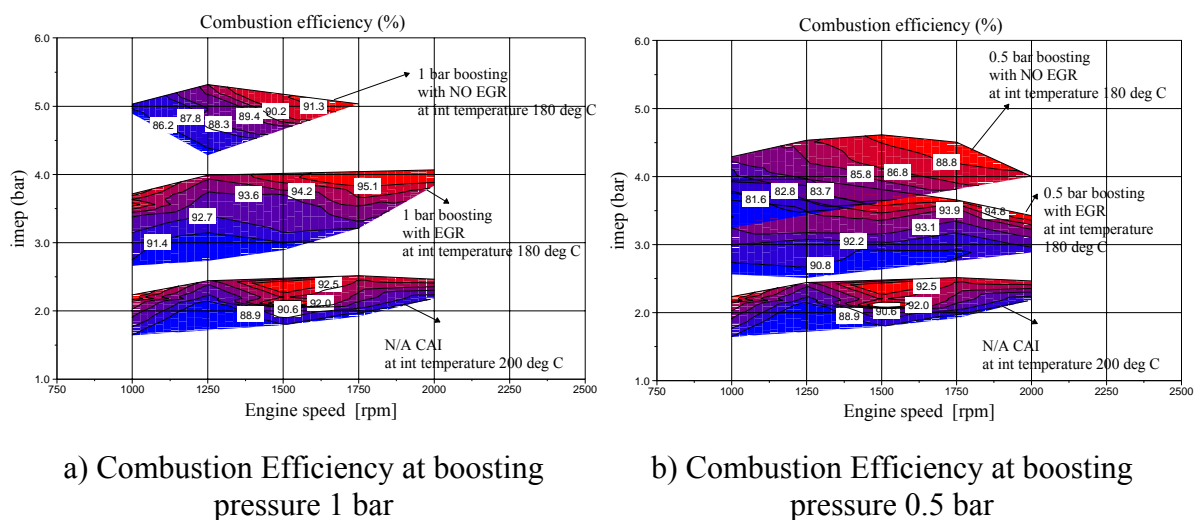


Figure 4.24 Combustion Efficiency in boosted CAI

4.5.4.3 Heat exchanger efficiency

The intake heater is employed to provide the thermal energy since high boosting pressure reduces the thermal efficiency that decrease the in-cylinder temperature. In practice, the intake heating is preferably achieved through an exhaust gas heat exchanger. The amount of heating that can be obtained will be determined by the exhaust gas temperature, flow rate, and the heat exchanger efficiency. Figure 4.25 shows the results of calculated heat exchanger efficiency required to raise the intake charge temperature for stable CAI combustion.

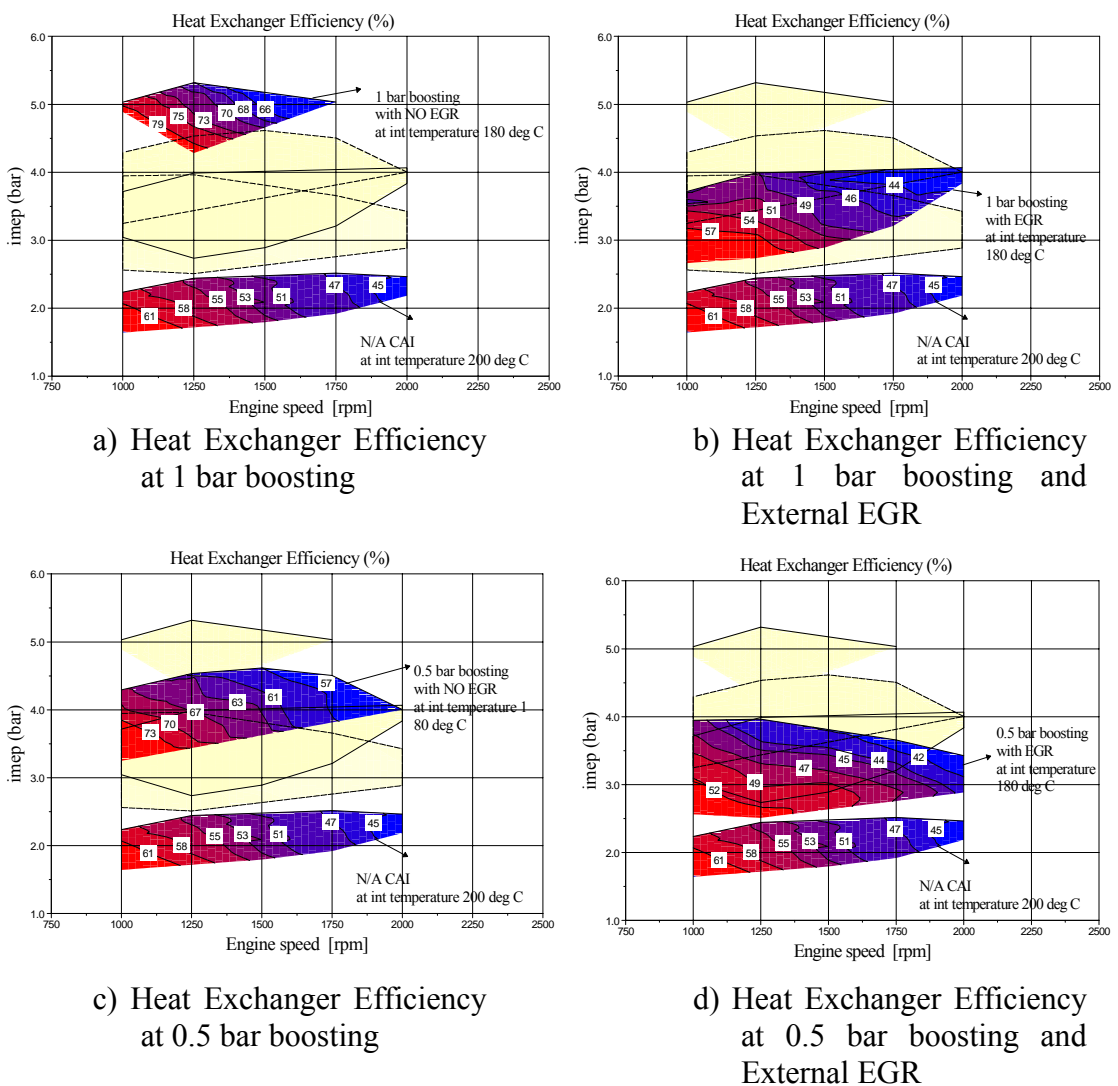


Figure 4.25 Heat Exchanger Efficiency in the enlarged CAI operating region

In general, there is sufficient thermal energy to raise the intake charge temperature for the engine to operate with CAI combustion assuming a maximum heat exchanger efficiency of 80%. It shows that higher efficiency is required at lower engine speed and load conditions where higher intake charge temperature is required to achieve CAI combustion operations. It is also noted that the boosting without external EGR requires higher heat exchanger efficiency (Figure 4.25a and c) and the higher boost pressure. In contrast, the combined external EGR and boost tends to lower the heating requirement than the NA operation as hot external EGR is used.

4.5.4.4 Exhaust temperature and EGR Concentration

Exhaust temperature is monitored throughout each experiment not only to calculate the required heat exchanger efficiency, but also to analyze the combustion characteristics since it affects directly the in-cylinder temperature and combustion quality.

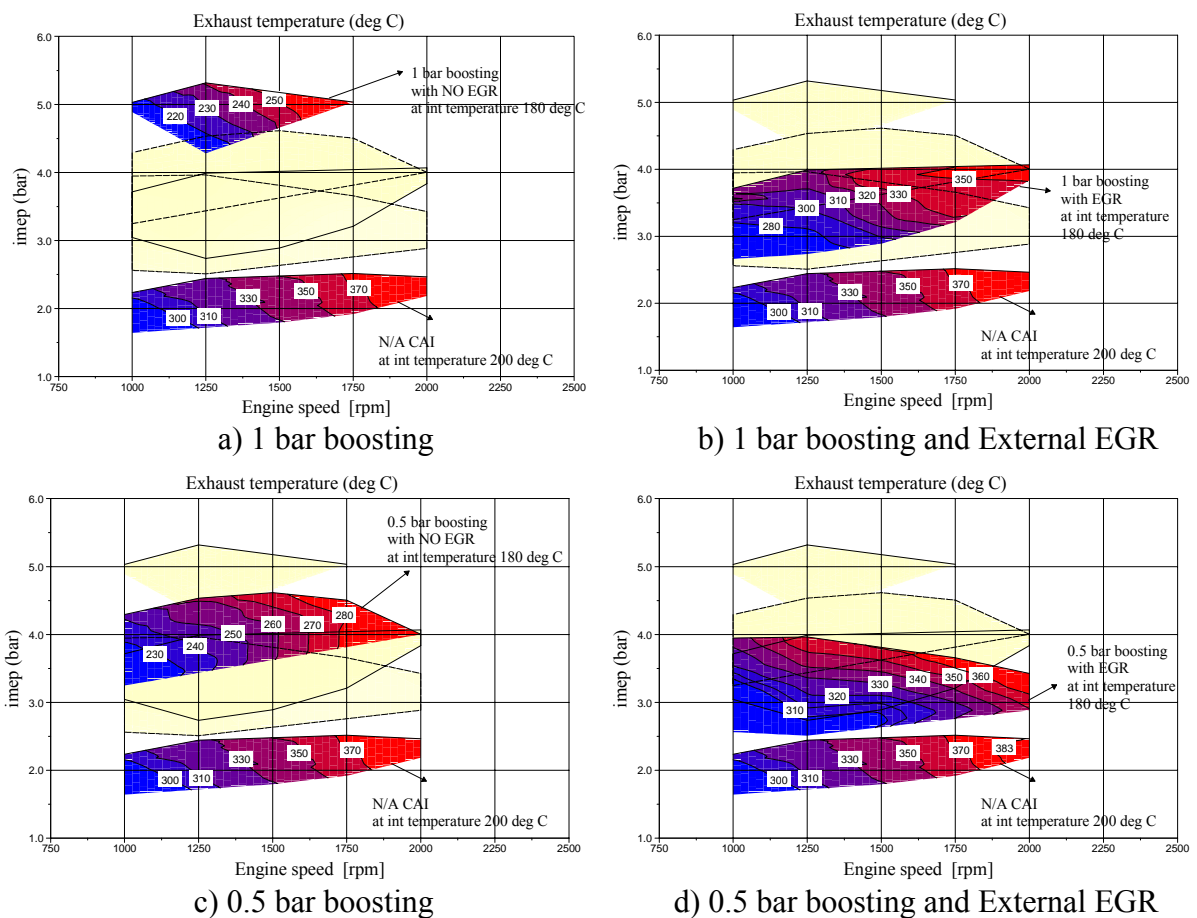


Figure 4.26 Exhaust Temperature in the enlarged CAI operating region

Figure 4.26 shows the results of exhaust temperature on the map of engine speeds versus loads IMEP. In general, the exhaust temperature is increased with the load and engine speed as more fuel is burned and there is less time for heat loss. The exhaust temperature decreases with boosting pressure as the mixture becomes leaner. As a result, higher heat exchanger efficiencies are required at boosted conditions to achieve CAI combustion as shown in Figure 4.25. The lowest exhaust temperature is shown at about 210 °C at lambda 4.2 and engine speed 1000 rpm at boosting 1 bar pressure without external EGR. The highest exhaust temperature is obtained at about 375 °C at lambda 3.5 and engine speed 2000 rpm at boosting 0.5 bar pressure and with external EGR.

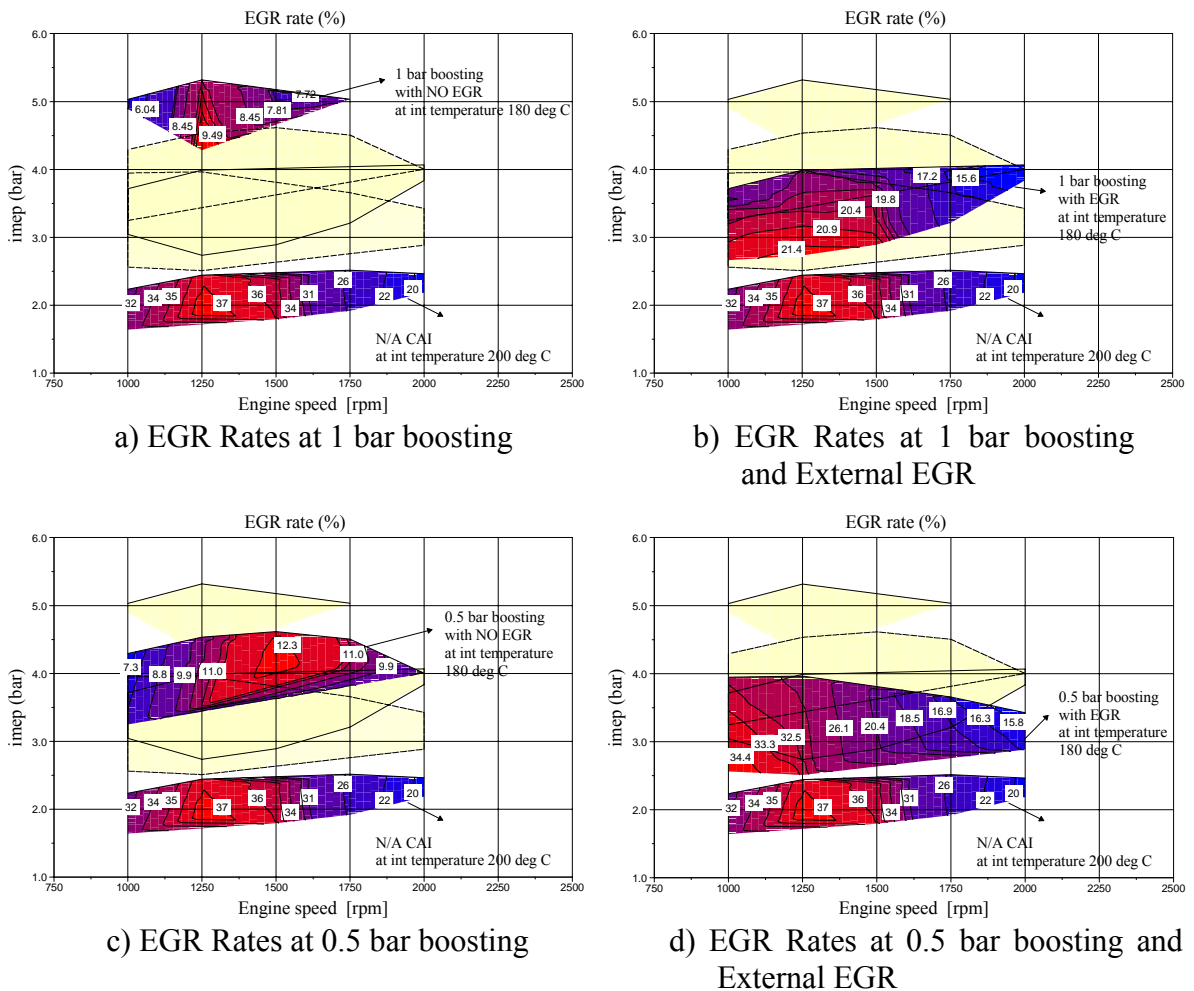


Figure 4.27 EGR distributions in the enlarged CAI operating region

The results of total in-cylinder EGR concentration in boosted CAI operating range are shown in Figure 4.27. Naturally aspirated CAI combustion in Positive valve overlap shows EGR rate of 18 ~ 37 %. Although the boosting inlet charge strategy enlarged the operating region, higher boosting pressure traps less internal EGR gases due to the reduced exhaust backflow during positive valve overlap period and hence would require higher efficiency heat exchanger to compensate for the lower exhaust temperature and leaner mixture. The maximum EGR rate is obtained in the middle range of engine speeds since higher engine speed increases heat losses and reduces the overlap period for backflow to take place. The maximum EGR rate in the boosted CAI operating region is performed at about 35 % at engine speed 1000 rpm and lambda 2.6 at a boosting pressure of 0.5 bar and external EGR. The minimum EGR rate is obtained at about 5 % at a boosting pressure of 1 bar and no external EGR at engine speed 1000 rpm and lambda 4.2.

4.5.5 Summary

The enlargement of CAI operating range is achieved by boosting inlet charge with an intake heater and external EGR. Firstly, this study shows the potential of enlargement in CAI by boosting pressure 1 bar at variable intake temperature. Thereafter, the effect of boosting pressures, 0.5 and 1 bar is performed at an intake temperature of 180 °C. One of the major benefits in CAI combustion is the lower level of NO_x emissions along with all the combustion characteristics described. Due to the lower level of internal EGR by boosting pressure in CAI, external EGR is implemented to provide the thermal energy and dilution effect.

The maximum load limit of CAI operating region is increased to 8 bar IMEP (Figure 4.16a) with almost negligible NO_x and very low CO emissions, but slightly higher HC emissions which can be overcome by catalyst technology. It is found that the boosting inlet charge is not always beneficial to achieve the CAI combustion due to heat loss and has to compromise the level of boosting pressure. External EGR is introduced to compensate for the disadvantage of the boosting strategy for the better combustion efficiency

4.6 Summary

This chapter presents the investigation of CAI combustion with positive valve overlap strategy at variable compression ratios and intake temperatures. CAI combustion is used as a potential alternative to SI combustion since it provides extremely lower level of NO_x emissions and better fuel consumption. However, it is also found that CAI suffers from the limitation of knock, partial burned and misfiring regions. This study describes the boundaries of knock and partial burned combustion, determined by the fuelling rate from the extremely lean to rich conditions. The results show that CAI combustion can be obtained with positive valve overlap at compression ratios between 12 to 16 and the intake temperature in the range of 120 ~ 220 °C. It is also found that higher intake temperature allows lower compression ratio to be used to achieve stable CAI combustion.

The enlargement of CAI operating range is achieved by boosting inlet pressure at 0.5 and 1 bar. The combustion characteristics and emissions under boosted CAI operations are presented. The knock limit of CAI region is increased to 8 bar IMEP at 1 bar boost pressure with extremely low NO_x emissions and low CO emissions but slightly higher HC emissions. However, boosting leads to worsening combustion efficiency and thermal efficiency. The combination of external EGR and boosting produces the best combustion efficiency and the lowest exhaust emission.

Chapter 5

In-cylinder Studies of CAI Combustion with Negative Valve Overlap

Chapter 5 In-cylinder Studies of CAI Combustion with Negative Valve Overlap

5.1. Introduction

After the operating region of CAI with positive valve overlap is studied in the previous chapter, CAI with negative valve overlap and autoignition reactions are investigated. This chapter presents the investigation of simultaneous in-cylinder heat release and chemiluminescence analyses of CAI combustion with negative valve overlap on a Ricardo Hydra single cylinder engine with optical access. An air-assisted injection system provided by Orbital Pty is used together with a specially fabricated cylinder head, detailed in section 5.2.4. The effects of injection and spark timings on CAI have been studied through the detection of full chemiluminescence, OH and CHO radicals by a high speed intensified video camera. In addition, CAI heat release and combustion characteristics of stoichiometric and lean-burn mixtures are compared and studied by simultaneous in-cylinder heat release studies and chemiluminescence images.

Direct fuel injection strategy is implemented at exhaust valve closing timings, negative valve overlap and intake valve opening timings, and intake valve closing timings. The effect of injection timings is investigated [91] in the following three categories.

1. Early injection timing; Injection timings at exhaust valve closing timing is used for the purpose of reforming the air/fuel charge or even initiating minor combustion by injecting into the hot residual gas, leading to improvement in ignitability.
2. Mid injection timing; Injection during negative valve overlap period and intake valve opening timing provides a more homogeneous mixture and improved volumetric efficiency.
3. Late injection timing; Injection during the intake valve opening duration and intake valve closing timing can produce a stratified charge mixture to controlling ignition timing.

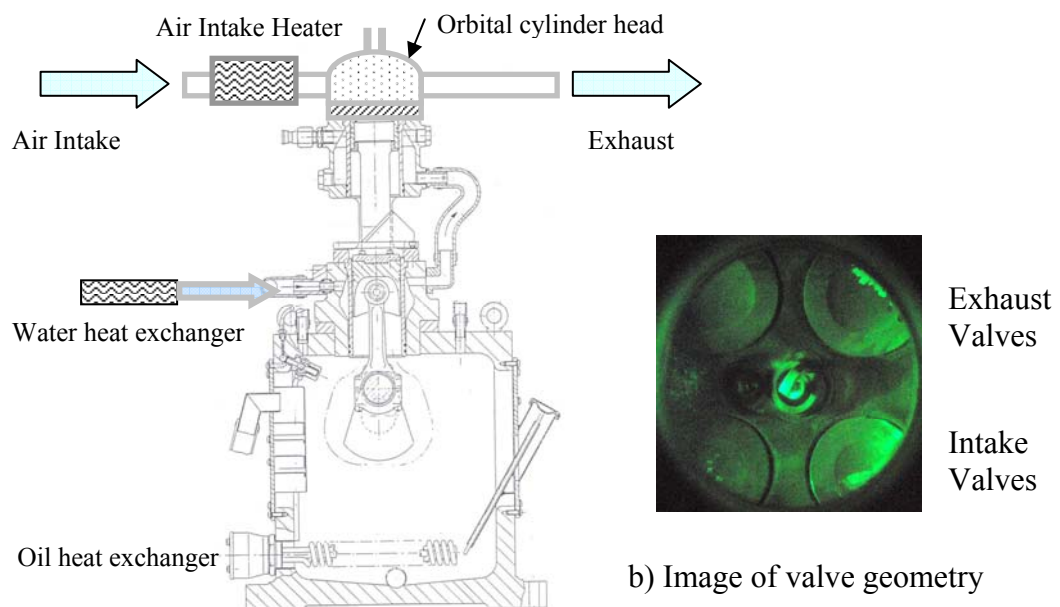
At early injection timing, the effects of spark timings are also investigated. OH and CHO radical are simultaneously captured with in-cylinder pressure, temperature and heat release rate so that more precise study of CAI combustion within the same cycles is performed, whilst the previous studies involved images from different cycles and the results could be affected by the cyclic variations.

It was also found that a small quantity of thermal energy is released in the recompression stroke from minor combustion by injecting the fuel into the hot residual gas with excess oxygen. Therefore, the effect of different quantities of air in the injected mixture is investigated at early injection timings and the results are presented with full chemiluminescence images.

5.2 Experimental Facilities

5.2.1 Ricardo Hydra Research Engine

A Ricardo Hydra single cylinder research engine, mounted on dedicated single cylinder engine test bed and linked to a 4-quadrant DC motor, was used for this investigation as shown in Figure 5.1. The engine has a swept volume of 450 CC, 9:1 Compression ratio, bore of 80.26 mm, and stroke of 88.9 mm respectively. The cylinder head is a prototype single cylinder direct injection type, supplied by Orbital Engine Corporation Ltd. The geometry of the valves is shown in Figure 5.1 b), with two exhaust valves and two intake valves.



a) Ricardo Hydra research engine

Figure 5.1 Ricardo Hydra research engine

The engine is naturally aspirated through the intake air being heated up to 175 °C by a 3 KW air heater installed in the intake pipe. The lubrication of the entire engine consists of two sections which are split into the upper piston and cylinder head section and the “lower piston section”. An oil pump at the bottom of cylinder block provides oil lubrication for the “lower piston section” and cylinder head section. The oil is heated up by passing through a heat exchanger and controlled by a Spirax Sparco sensor situated in a pocket within the left hand side of the coolant tank. The coolant water is also heated up by passing through a 3KW water heater.

5.2.2 Optical Parts of the Engine

The engine is designed in order to visualize the combustion in the chamber through a sandwich plate. The sandwich plate is located in between the cylinder head and block and has been designed so that it provides side access from four directions mainly for laser illumination. In this section, optical design features of the engine such as optical access with a high speed camera and intensifier are detailed. Figure 5.2 shows the optical access of the engine and the high speed imaging system and in-cylinder pressure acquisition system.

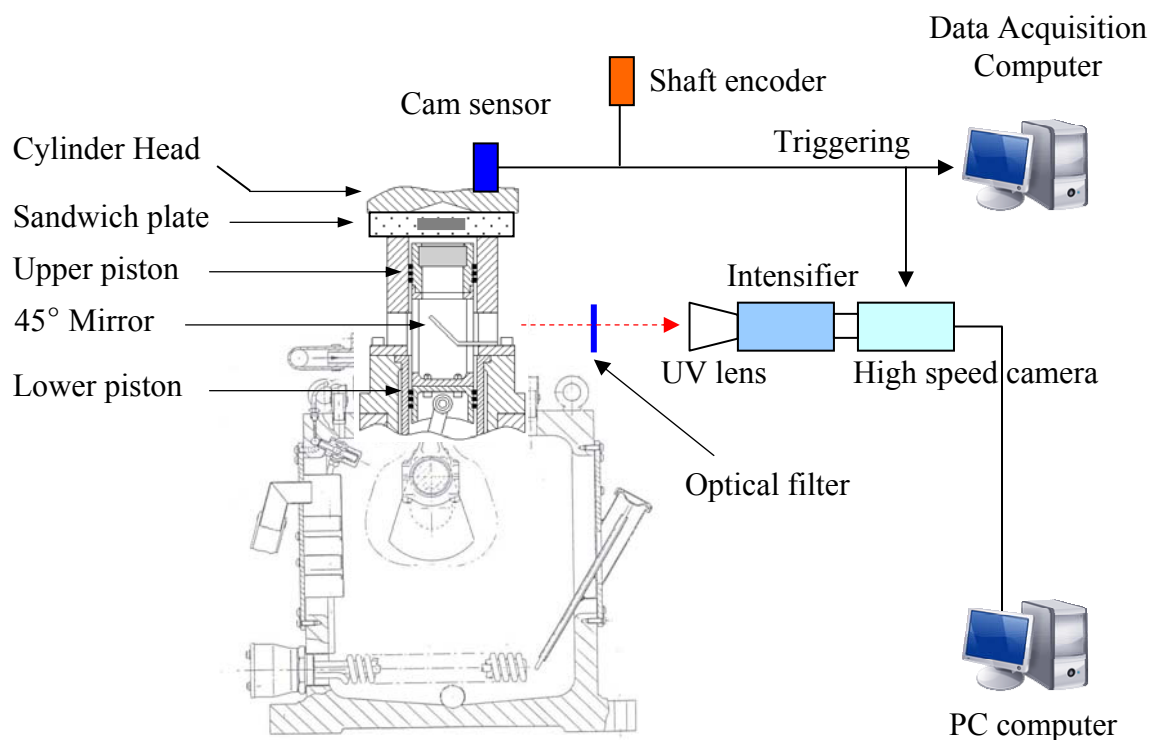


Figure 5.2 Schematic diagram of Optical features on Ricardo Hydra engine

The engine allows optical access through the piston window to the combustion chamber by the specially designed extended piston and cylinder block. The extended upper piston is installed on the top of lower piston. A 45° mirror is fitted in the middle of the extended piston and reflects the combustion images to the camera.

It is necessary for the extended piston, piston rings, and cylinder walls to have adequate lubrication and avoid contamination of the piston window. Therefore, the production type steel piston rings are replaced by 1 compression ring and 2 wider

carbon graphite rings (Lecarbon grade 5890). The carbon graphite rings provided sufficient lubrication with the cylinder liner which is further enhanced by lubricating grease applied to the top compression ring after each decommissioning of the engine.

The upper piston has a window, which is fitted on top of the piston and secured by gaskets and spacers and reduces any problems with leakage and fragility.

5.2.3 Pressure transducer and Positioning System

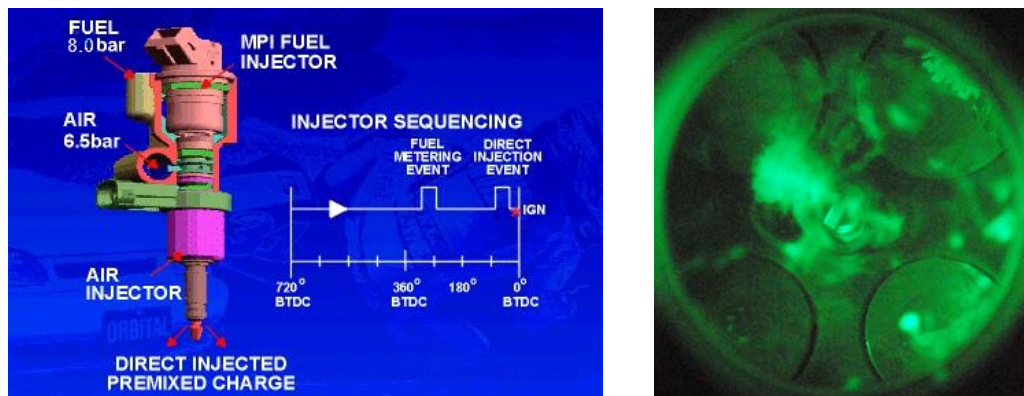
A Kistler type 6055, piezo electric pressure transducer is fitted in the combustion chamber to measure cylinder pressure. Measurement range is 0-100 gauge bar and sensitivity of - 6 PC/bar. This pressure transducer is connected to a charge amplifier (Kistler type 501) via a high impedance cable. The charge amplifier converts the electric charge generated by the transducer into an amplified voltage. The pressure data is recorded by the PC-based acquisition system as described in section 3.3.2.

A shaft encoder is fitted to one end of the crankshaft and provides angular position data. This shaft encoder generates a reference signal with a pulse every engine revolution and a clock signal pulse for every crank angle degree of rotation.

The crankshaft encoder generates a reference signal every engine revolution, whereas the 4 stroke cycle has 2 revolutions every cycle. Thus two reference signals per cycle occur and hence no indication of each engine revolution is given. A Hall Effect sensor mounted on top of the cylinder head and sensing from the camshaft, provides one signal for every two engine revolutions. The two mentioned signals are passed through an “And” logic gate which results in one pulse being outputted for each engine cycle. This pulse reference signal is sent to the data acquisition system, Labview USB interface and triggers the high speed camera in order to simultaneously record the pressure trace and video for the exact same cycle.

5.2.4 Air-Assisted Fuel Injection System

The air-assisted injector was supplied by Orbital Engine Corporation Ltd and is a direct injection spray guided system for stratified charge SI engines. The injector sits in the middle of the cylinder head and injects not only the fuel metered by the Multi-Point Injection (MPI) injector but also a quantity of compressed air. Figure 5.3 shows a typical injection sequence and a schematic of injection signal pulse, and actual spray image.



a) Schematic of Injector by Orbital Engine Corporation Ltd

b) Spray image of Injector

Figure 5.3 Orbital Air-assisted Injector with Typical Injection Sequence

The injection system supplies the fuel and air from a cylinder of compressed air, a regulator on the cylinder controls the pressure since a conventional fuel pump is not sufficient to supply the fuel due to the corrosive and degrading effects of fuel dopants. The fuel is supplied from an accumulator where a compressed nitrogen cylinder pressurizes the fuel and transfers it to the injector.

Two delay units, built specially for this injection system by Brunel University, control each air and fuel injector and send the signals to a timer unit. The timer unit allows control of the pulse width of each injection signal. The fuel and air pressures are regulated at 8 and 6.5 bar gauge respectively.

5.2.5 Ignition System

A Lucas 'Dial-a-Time' receives the reference and clock signal from the "And" logic gate unit and sends out the output signal to the ignition system with the desired ignition timing (Dwell). Figure 5.4 shows a schematic diagram of the spark ignition system.

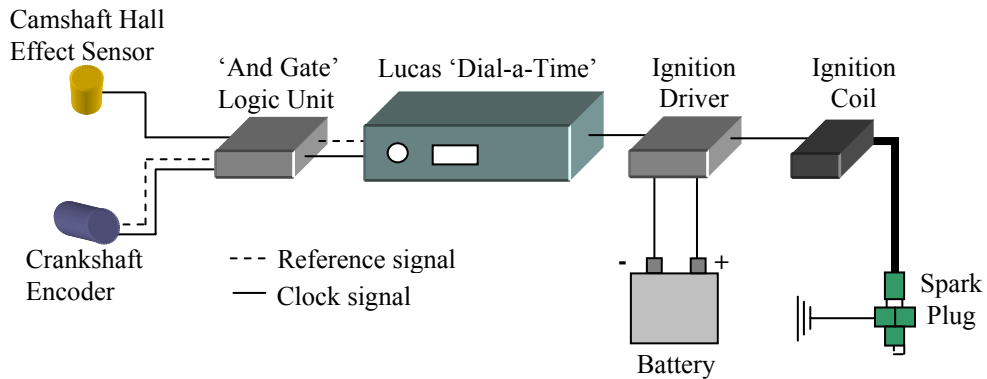


Figure 5.4 Schematic Diagram of Spark Ignition System

The crankshaft encoder is set to provide the reference signal at 80° CA BTDC on the compression stroke in order to allow spark timing to be advanced from TDC. The ignition driver unit amplifies the signal from the "Dial-a-Time" unit and the output is connected to the ignition coil. The range of ignition timing available is from 79° CA BTDC to 45° CA ATDC in 0.5° increments.

5.2.6 Temperature Measurements and Emissions

Thermocouples are mounted in the air inlet and exhaust pipes, and on the coolant heat exchanger. Values are displayed and monitored on the thermo-meters simultaneously. Emissions were measured not only to calculate in-cylinder temperature but also to characterize CAI exhaust emissions. A Rotork Analysis Automation Series NO_x and HC analyzer and Horiba Mexa 554JE analyzer were used for emissions measurements, as detailed in section 3.2.

A UEGO wide band fast response heated lambda sensor is installed in the exhaust pipe and is capable of measurement from lambda 0 ~ 9.99 and oxygen concentration 0 ~ 25 % vol. The lambda sensor is connected to a Horiba Mexa-110 AFR analyzer unit, which displays the lambda readings.

5.2.7 Data acquisition system

During the experiments, measurements were taken to determine the combustion characteristics such as engine load, in-cylinder pressure, camshaft position, intake and exhaust temperature, and so on. The majority of measurements and data analysis are considered in the same manner as with the Ricardo E6 engine.

In-cylinder measurement by a pressure transducer was captured by a Labview data acquisition system on the PC in the same manner as the Ricardo E6 engine as mentioned in the previous section. Heat release rate is calculated from this pressure trace and in-cylinder temperature is also calculated by measured exhaust temperature and molecular weight of emissions species. Cylinder pressure measurements and high speed camera were triggered by a reference signal and recorded simultaneously so that the exact same cycle has been captured to allow precise analysis due to the cycle to cycle variation, shown in Figure 5.2.

5.2.8 High Speed Camera and Intensifier

A NAC Memrecam fx 6000 high speed colour video camera was used to obtain high resolution video (512 x 248 pixels, 10000 fp/sec) of CAI combustion. The camera and the data acquisition system were triggered by the same reference signal to simultaneously record high speed images and cylinder pressure data of 100 cycles. With 4 GB on-board memory, about 15 cycles of combustion sequence at engine speed 1600 rpm could be recorded and stored by the camera. The final selected videos were saved to a PC computer and converted to a common playing video format, "avi", to be edited and analyzed in "Image pro" video software.

Due to the low intensity of autoignition and premixed combustion, a DRS Hadland Model ILS3-11 high speed image intensifier was lens-coupled to the high speed camera. The setup of intensifier was 10-50 microseconds exposure time and 55% of gain or 40% of Automatic Brightness Control.

5.3 Experimental Preparations and Procedure

5.3.1 Experimental Setup

The visualisation of CAI combustion was performed using the single cylinder optical engine with the lens-coupled intensified high speed camera. Negative valve overlap was used for trapping the residual gases internally and an intake heater heated the intake air to provide the thermal energy and the rest of engine specs and test settings are shown in Table 5.1.

Valve Timing	Intake	440 CA deg ATDC	560 CA deg ATDC
	Exhaust	190 CA deg ATDC	280 CA deg ATDC
Intake heater	175 °C		
Engine speed	1600 rpm		
Oil temperature	55 °C		
Coolant temperature	100 °C		

Table 5.1 Engine setup on the Ricardo optical engine

The investigation of injection strategies to achieve CAI combustion was carried out at 1600 rpm. Figure 5.5 shows the injection strategy used to achieve CAI combustion with and without spark assistance.

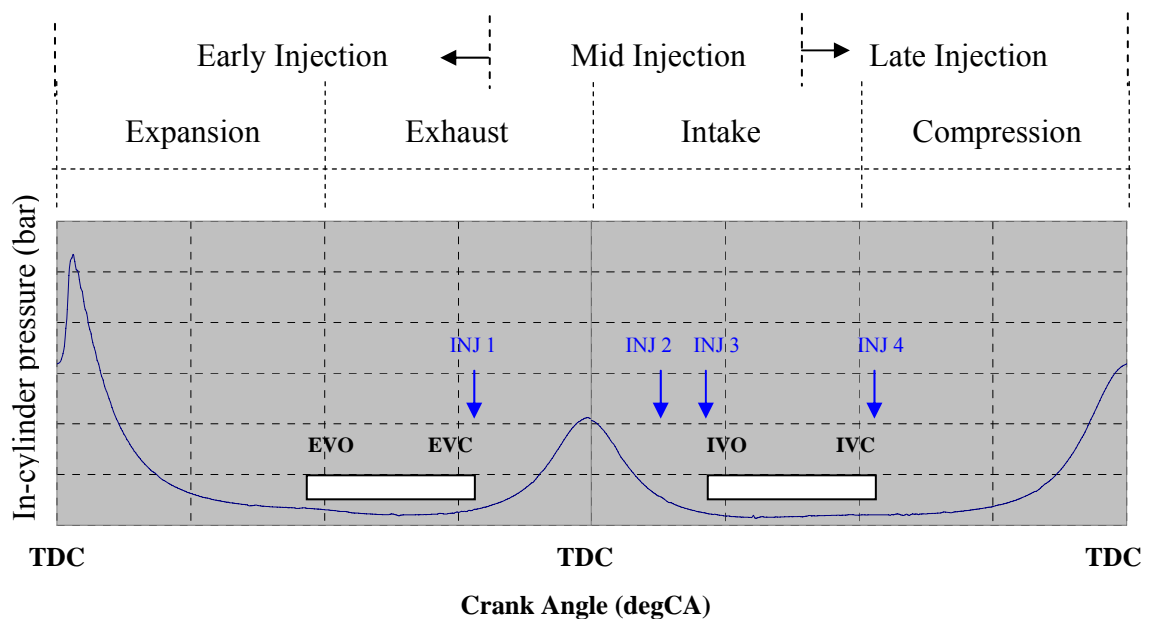


Figure 5.5 Injection Strategy on an Optical Engine at 1600 rpm

	Injection Timing	80 BTDC		40 ATDC		80 ATDC		200 ATDC	
	Spark 320 ATDC	spark	no spark	spark	no spark	spark	no spark	spark	no spark
Lambda 1	OH	▲	▲	o	o	o	o	o	M/F
	CHO	o	o	o	o	o	o	o	M/F
	FULL	o	o	o	o	o	o	o	M/F
Lambda 1.2	OH	x	x	o	o	o	o	M/F	M/F
	CHO	x	x	o	o	o	o	M/F	M/F
	FULL	o	o	o	o	o	o	o	M/F

Spark Timing			310 ATDC	320 ATDC	330 ATDC	340 ATDC	350 ATDC	360 ATDC
Lambda 1	Full	Injection timing at 80 BTDC	o	o	o	o	o	o

(M/F - Misfiring, ▲ - Not clear images, x – No images, o – Test achieved)

Table 5.2 Experimental strategies tested in CAI combustion with NVO at 1600 rpm

Table 5.2 shows the testing matrix for CAI combustion with negative valve overlap. Variable Injection timings in CAI were performed as early injection at the exhaust valve closing timing, mid injection at negative valve overlap period or intake valve opening duration, and late injection at intake valve closing timing. Engine speed was kept constant at 1600 rpm in both cases of with spark and without spark so that the effect of spark could be investigated compared to non-spark assisted CAI. For each injection timings, high speed videos were captured for full chemiluminescence, 310 nm of optical filtered OH chemiluminescence, and 350 nm of optical filtered CHO chemiluminescence. The effect of spark timings was studied for a fixed injection timing of 80 BTDC. The effect of air-fuel ratio on CAI combustion was also studied for each fuel injection timings.

5.3.2 Test procedure

CAI combustion was achieved using gasoline fuel at a compression ratio of 9:1, coolant water temperature of 100 °C and oil temperature of 55 °C. Thus, a warming-up procedure was required before CAI combustion. Once the engine was warmed up and then testing could commence under stable and steady state operation. The optical equipments were switched on and ready for capturing the videos. The DAQ system was also set up to be triggered to start the data acquisition sequence.

The engine was kept motoring to let the grease lubricate the piston and cylinder block for about 10 minutes before increasing the engine speed up to 1600 rpm. The injection and spark system were switched on and adjusted to achieve CAI combustion. Once CAI combustion has been established, the engine and measurement systems were left to stabilize for a few minutes. The DAQ system and high speed camera were then ready to be switched on and triggered. When every experiments setting were ready, the results were captured using the data acquisition system and the high speed camera.

5.4 In-cylinder studies of CAI Combustion with NVO

5.4.1 Effect of injection timing

5.4.4.1 Introduction

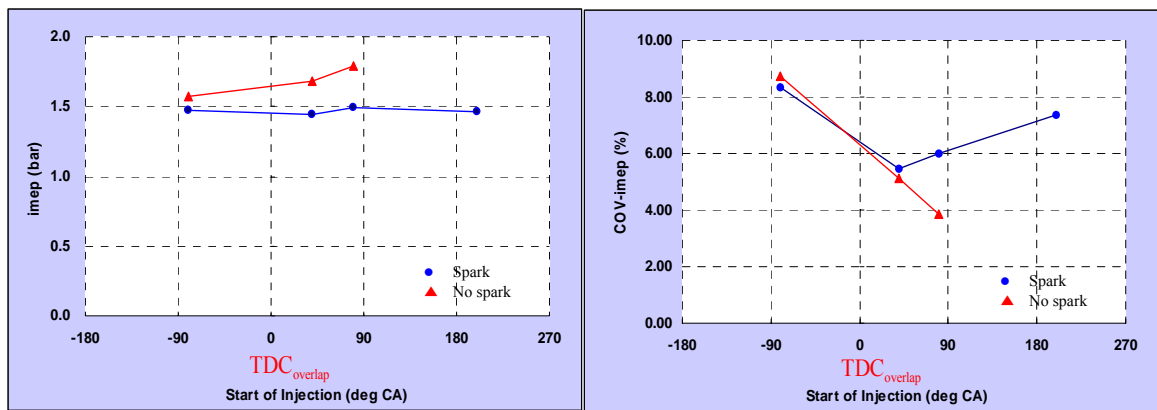
Direct fuel injection into the cylinder for CAI operation has been studied by many other researchers [32, 89, 90, 91] over the decades. Direct fuel injection can be used for effective means of controlling the combustion phasing for optimized engine performance and emissions. When engine speed is increased, combustion phasing is advanced, leading to fast heat release rate and higher peak pressure. When injection timing is advanced, combustion phasing is also advanced, improving the engine performance.

When the fuel is injected directly into the trapped hot residual, direct injection strategy provides a ‘Charge cooling effect’ as the liquid fuel evaporates, which would lower the charge temperature. However, if there is oxygen left in the burned gas, fuel injected into hot residuals can undergo exothermic reactions, causing the charge temperature to rise. Early and mid-injection timings result in more homogenous mixture as vaporized fuel will have more time to be mixed with hot residual gas and fresh air. In comparison, late injection timing causes a stratified mixture due to the lack of mixing time, leading to coexistence of both extremely lean and over rich mixtures. In the following section, the effects of direct injection on CAI combustion will be presented and analyzed for an engine speed of 1600rpm and $\lambda = 1$.

5.4.1.2 Engine performance

Figure 5.6 shows the results of engine performance and cyclic variation in CAI operation under different fuel injection timings. Without spark discharge, as the injection is retarded, the engine output increases and the cyclic variation decreases. But it was not possible to achieve stable CAI combustion with late fuel injection during the compression stroke. Mid-injection timing during the intake valve opening period results in improvement in engine output as more air could be induced into the cylinder when the charge temperature is reduced by the charge cooling effect of the

injected fuel. Mid-injection timing also leads to the most stable combustion, CoVimep is less than 4% which is a noticeable achievement even without spark assistance. It is also noted from Figure 5.6 that as spark is turned on, CAI combustion could be achieved with the late injection. This may be explained by the fact that the late injection tends to produce a stratified fuel distribution [32] that has a fuel rich mixture near the spark plug. The presence of spark discharge can then ignite the stratified fuel rich mixture that in turn will compress the rest of the charge into autoignition combustion. This will be confirmed by the in-cylinder high speed movies to be shown later.



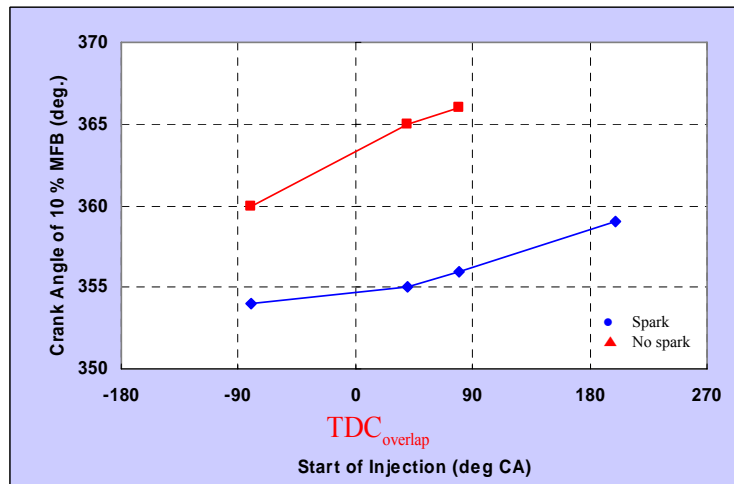
a) Engine loads in CAI

b) Combustion stability in CAI

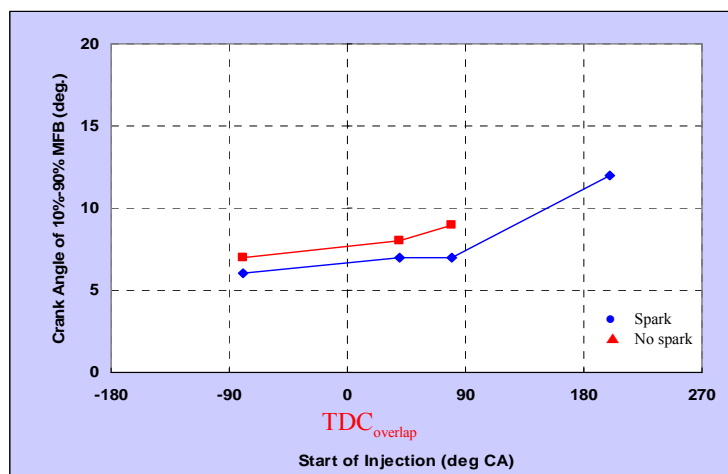
Figure 5.6 Engine loads and CoVimep of CAI combustion with NVO

5.4.1.3 Combustion Characteristics

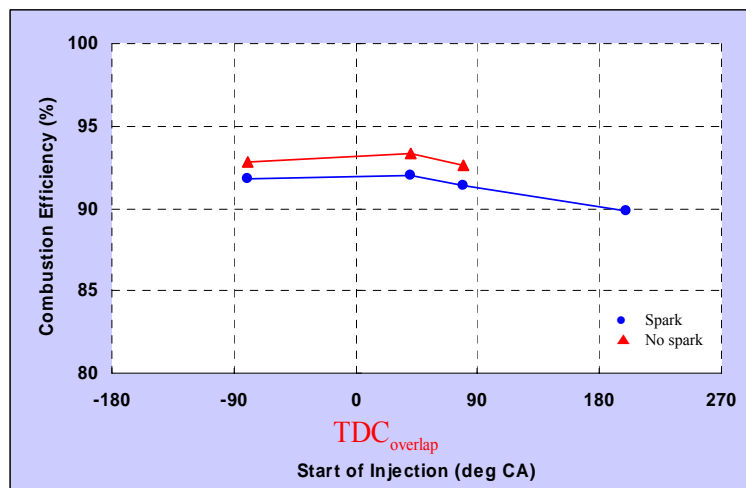
As combustion phasing is one of major means of controlling CAI for optimizing and stable performance, the fuel injection into the cylinder is used for controlling combustion phasing in this study. As the mass fraction burned rate (MFB) is well known as a definition of combustion phasing, as shown in Figure 5.7. The 10 % of MFB (Figure 5.7a) represents a start of combustion since less than 10 % of MFB is extremely low and negligible. Combustion duration is determined from 10 % to 90 % of MFB (Figure 5.7b). Figure 5.7 shows significant effects of direct fuel injection in the start of combustion and combustion duration.



a) Start of CAI combustion



b) CAI combustion duration



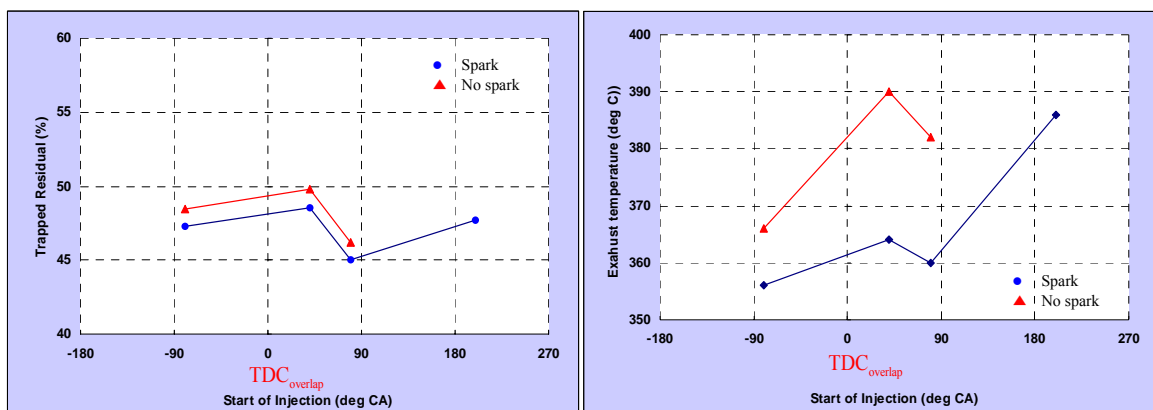
c) Combustion efficiency of CAI

Figure 5.7 10 % of MFB, Combustion duration and Combustion efficiency of CAI with NVO

As shown in Figure 5.7a, when injection timing is advanced, the start of combustion is also advanced. The mid-injection timing shows the best engine performance and stability when combustion starts after TDC. The presence of spark discharge at 40 BTDC results in too advanced combustion and hence less useful work output as more negative work is performed towards the end of the compression stroke.

When injection timing is advanced, the combustion is occurred faster (Figure 5.7b). The presence of spark discharge leads to shorter combustion duration compared to without spark assistance.

Figure 5.7c shows the results of combustion efficiency of CAI operation. The best combustion efficiency of 93% in this study is achieved at mid-injection timings. The lowest combustion efficiency is found for the late injection when fuel rich pockets are more likely to be present in the stratified charge.



a) Residual concentrations

b) Exhaust temperature

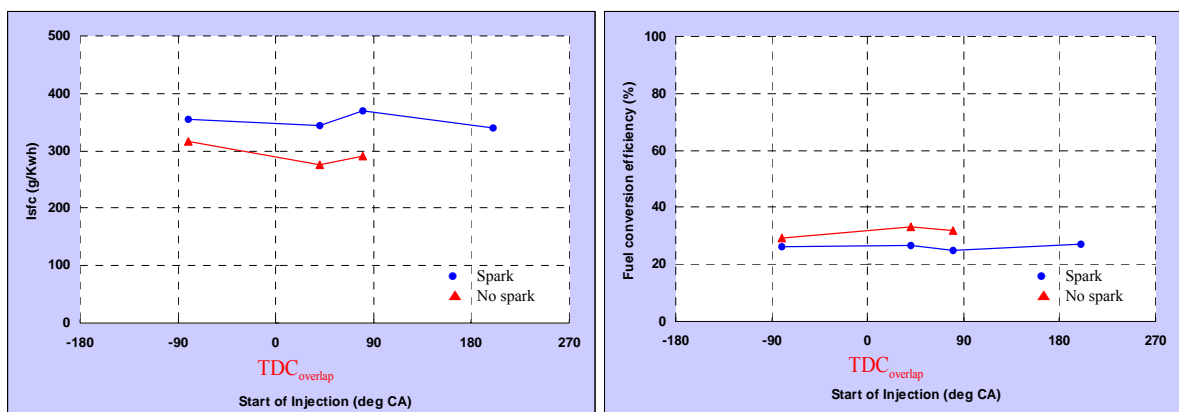
Figure 5.8 Residual concentrations and exhaust temperature

The trapped residual concentration and exhaust gas temperature are shown in Figure 5.8. For the particular valve timings and valve durations used in this study, the residual concentration is about 50%. The dip in the residual concentration at 80 ATDC injection is probably caused by the increased amount of air being inducted into the cylinder as the fresh air is cooled down by the injecting fuel spray during the intake process. The difference between the spark and non spark cases are caused by the exhaust gas temperatures. As the combustion starts and finishes earlier with spark (Figure 5.7b), the resulting burned gases experience longer expansion and hence lower exhaust gas temperature as shown in Figure 5.8b.

The effects of injection timings can be summarized that mid-injection timing shows the most stable CAI operation and higher imep values without spark assistance. Although early injection timing advances the combustion phasing which leads to higher peak pressure and higher heat release rate, early injection timing shows lower imep values as over advanced combustion phasing. Since the charge mixture was cooled down by the fresh fuel injected into the residual, injection timing at intake valve opening timing leads to slightly higher engine load range than at negative valve overlap period.

5.4.1.4 Fuel Consumption and Emissions

Figure 5.9 shows the results of fuel consumption and fuel conversion efficiency. As expected, the advanced combustion phasing is responsible for the higher fuel consumption and lower fuel conversion efficiency associated with spark assisted CAI operation and very early fuel injection.

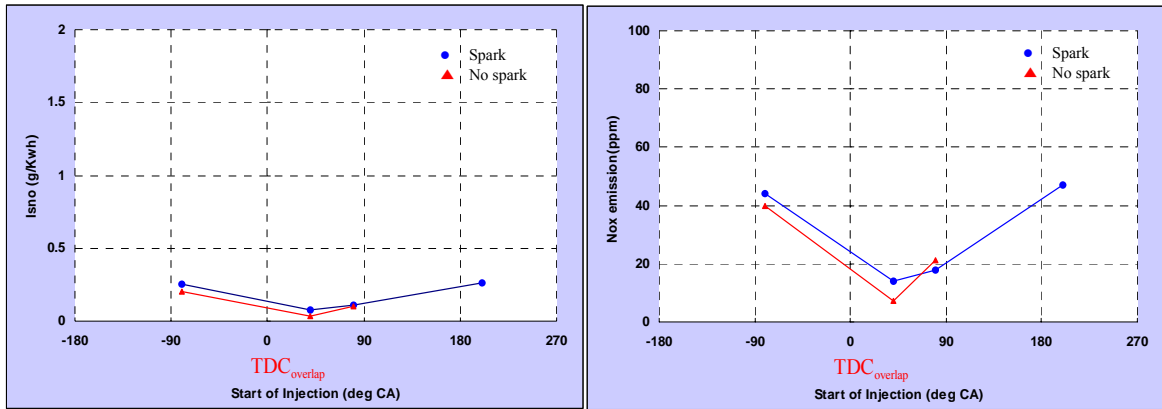


a) ISFC

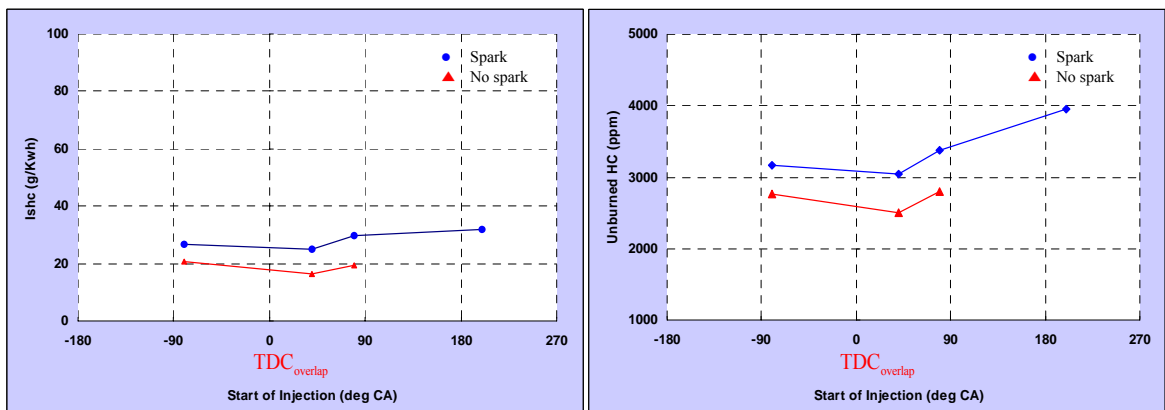
b) Fuel conversion efficiency

Figure 5.9 Fuel Consumption of CAI with NVO

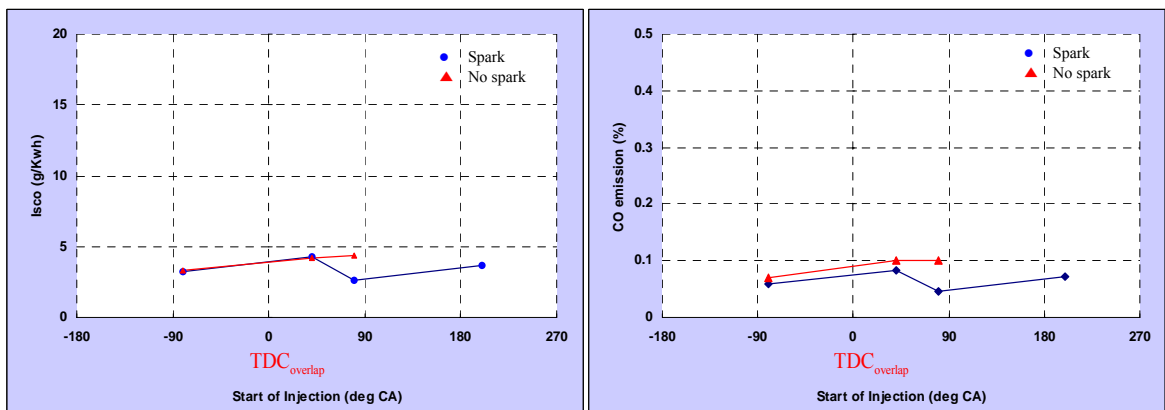
The level of emissions of CAI combustion is shown in Figure 10. Lower level of NO_x emissions is achieved at mid-injection timings compared to early and late injection timings. Advanced combustion phasing associated with very early fuel injection causes higher heat release rate and peak pressure and higher temperature, hence higher NO_x emissions. As the injection takes place at or after 80 deg ATDC, the NO_x emission rises again as the residual concentration starts to drop and more fuel and mixture is burned. The higher NO_x emission with very late injection in the spark assisted CAI operation is more likely a result of stratified charge, as more NO will be formed in the higher combustion temperature region near the spark plug.



a) NOx emissions



b) HC emissions



c) CO emissions

Figure 5.10 Emissions in CAI by direct injection timings

Two clear trends can be observed on uHC emission results shown in Figure 5.10b. Higher uHC emissions from the spark assisted CAI operation is consistent with the lower combustion efficiency shown previously. Late injection causes a significant increase in uHC emissions as the combustion becomes less complete. CO emissions (Figure 5.10c) are very similar to the trend of trapped residual. The variation is in general fairly small and much less than that of uHC and NOx emissions.

5.4.1.5 Simultaneous In-cylinder Heat release and Chemiluminescence Measurements

5.4.1.5.1 Introduction

In order to study the effect of direct fuel injection on CAI, direct visualization is performed with a high speed camera and a high repetition intensifier. Full chemiluminescence, emissions of OH (by an optical filter of 310 nm) and CHO (by an optical filter of 350 nm) were recorded and used to study the in-cylinder autoignition and combustion process. After each experiment, the high-speed video stored in the camera's memory was selectively downloaded to a PC computer. A sequence of individual images was then selected to be shown in the thesis.

During the CAI experiments with direct injection with spark, spark timing was kept at 40 deg BTDC and the video sequence to be shown starts with the spark ignition. In the absence of spark ignition, the first image is chosen to coincide with the first appearance of visible combustion. The last images are determined by the last visible combustion sites or soot. The yellow lines on the first images show the geometry of valves, spark plug and injector. The timing of each image is to be presented in crank angles relative to TDC of the recompression stroke in most cases unless it is stated otherwise.

5.4.1.5.2 Full chemiluminescence of direct visualization

Figures 5.11 and 12 show the results of in-cylinder pressure, temperature and heat release rate of CAI with spark and without spark respectively. The engine speed was kept at 1600rpm and the relative air and fuel ratio was 1.0. The EVC and IVO were set to 80 deg BTDC and 80 deg ATDC. The pressure, temperature and heat release rate are calculated from the average over 100 cycles.

As shown in Figure 5.11, injection at the beginning of the negative valve overlap period (80°CA BTDC) leads to the most advanced combustion and highest temperature and pressure. As the injection is retarded to 40 °CA ATDC the start of combustion is significantly delayed, resulting in lower peak pressure and temperature. Previous modeling study by Cao and Zhao [93] has shown that injection of fuel into

hot residual gas during the recompression stroke can produce active species and minor heat release in the region with oxygen. As the injection timing is retarded into the expansion stage after recompression TDC, both fuel reforming effect and minor heat release will be reduced, resulting in the delayed combustion. This will be confirmed by the in-cylinder visualization results to be shown later. As start of injection is further retarded to the beginning of the intake process (80 °CA ATDC), combustion is advanced and peak pressure and temperature become higher than the previous case with injection at 40 °CA ATDC. Finally, when the injection takes place during the start of the compression stroke, the cylinder pressure is significantly reduced as the combustion is now taking place after TDC. . The late injection timing case is characterized with a peak pressure of 23 bar, temperature of 1630 K and very low heat release rate of 8 J/deg. It leads to extremely unstable and incomplete combustion. It should be noted that in all cases, the peak in-cylinder temperature is less than 1900K and hence the NO emission is rather low.

Results in Figure 12 shows that the start of combustion is delayed as the injection is retarded. The peak cylinder pressure and temperature drops with the retarded combustion. Comparison of results shown in Figure 11 and Figure 12 demonstrates that the presence of spark ignition at 40 °CA BTDC results in earlier combustion, more complete combustion and higher engine output.

Figures 13 ~ 19 show the results of full chemiluminescence at lambda 1 at different injection timings. The combustion sequence was recorded simultaneously with in-cylinder pressure, from which combustion temperature is calculated. The simultaneous pressure, temperature, heat release rate and video footage of combustion sequence are shown for a specific cycle chosen for its best intensity of videos.

The combustion sequences with and without spark ignition are shown in Figure 5.13 and Figure 5.14 respectively for the start of injection at EVC. Images in Figure 5.13 shows that despite the spark discharge the first detectable emission does not appear until 350 °CA ATDC, which is close to the crank angle of 10 % of MFB calculated from the in-cylinder pressure. Examination of the video images shows clearly the presence of flame propagation, during 350 deg CA ATDC to TDC, starts from the spark plug and then expands towards the rest of the combustion chamber.

Independent autoignition site first appears near the bottom right hand corner at TDC and then rapidly expands into larger regions 1 deg CA later. As a result, the heat release rate increases rapidly and reaches a peak at 362 °CA.

On the other hand as shown in Figure 5.14, combustion without spark occurs randomly in the area of local auto-ignition characteristics of CAI combustion. Although combustion duration is normally determined by 10 - 90 % of MFB, the combustion sequence can also be used to demonstrate the significant difference in the combustion duration between the two cases of with and without spark ignition. The video images in Figure 5.13 shows that combustion duration is about 8 ~ 10 crank angles of duration from TDC to 368 CA or even 372 CA with spark and about 4 crank angles of duration from 364 CA to 367 CA without spark as shown in Figure 5.14. CAI combustion without spark assistance shows faster and slightly higher heat release rate and hence shorter combustion duration in the footage sequence. In either case, some soot or after burning of residual gases appears at the end of combustion.

The results with mid-injection timings are presented in Figure 5.15 to Figure 5.18. In the presence of spark ignition (Figure 5.15 and Figure 5.17), the first emission site always appear around the spark plug and expands as a flame. As the flame reaches its halfway, local auto-ignition occurs at 359 deg CA. The first combustion emission without spark appears locally at 362 deg CA and 366 deg CA for the injection before IVO and after IVO, respectively. In most cases during the combustion process with mid-injection timings, surprisingly bright pockets appear in the middle of the combustion chamber and remain for longer period after the main combustion. Bright pockets first appear while the combustion develops, especially when local auto-ignition occurred around the spark plug. They are seen firstly at 369 deg CA in Figure 5.16 and at 357 deg CA in Figure 5.17. It seems that after burn may have taken place near the spark plug that is at a higher temperature and could act as a heating source for surface ignition to take place.

The late injection timing near intake valve closing timing at lambda 1 is shown in Figure 5.19. CAI combustion by late injection timing was extremely difficult to obtain due to misfire. It is noted that this misfire by late injection timing can be overcome by spark assistance since the spark assistance has more pronounced effect

in the partial burned or misfiring region of CAI, detailed in section 5.4.2. The first combustion emission is captured at 347 deg CA and its area expands fairly quickly until TDC. Independent local auto-ignition appears at 357 deg CA. This late injection also shows a very hot pocket in the middle of the combustion process. This hot pocket appears firstly at 352 deg CA and remains until 417 deg CA.

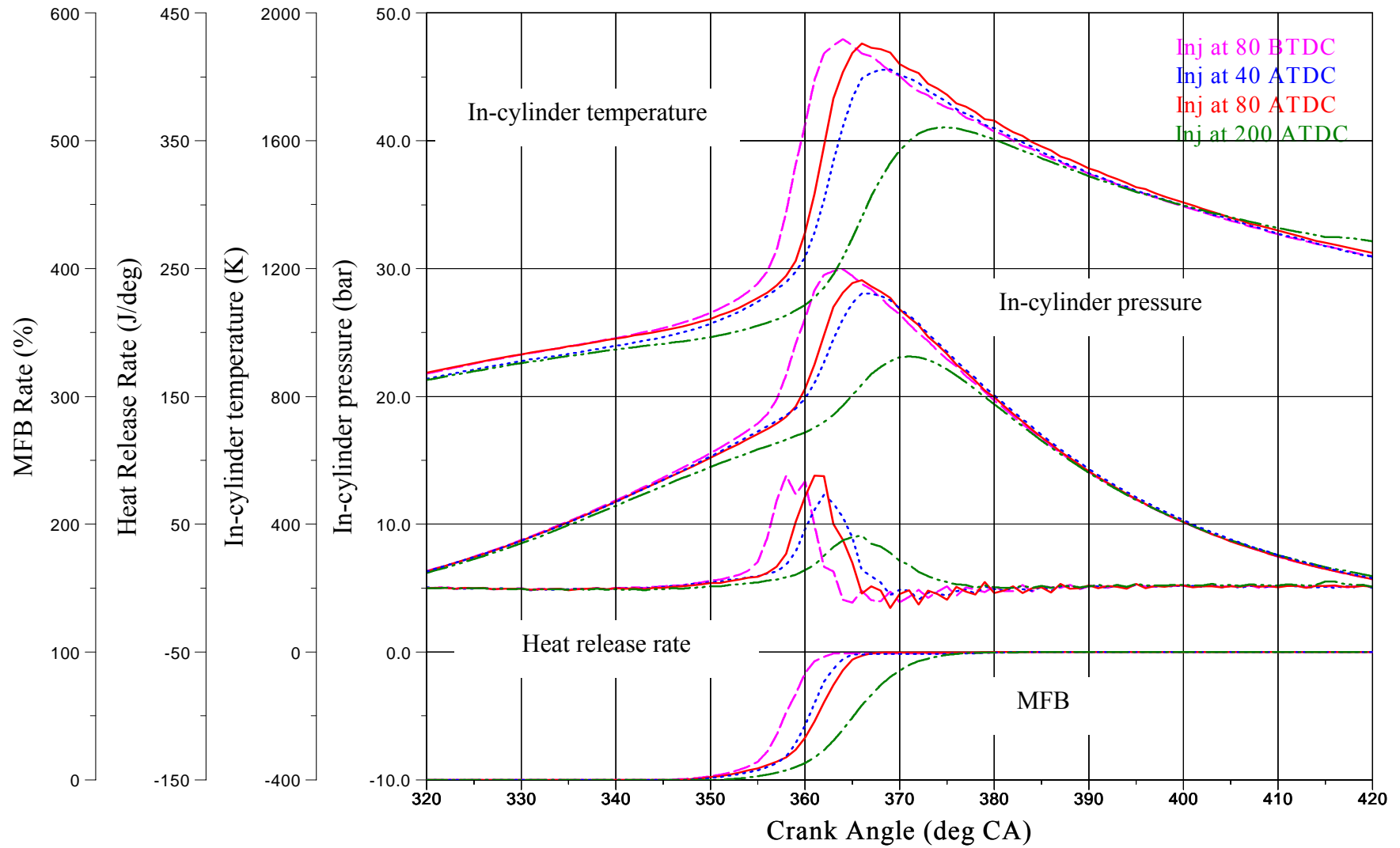


Figure.5.11 In-cylinder pressure, temperature, heat release rate and MFB rate at lambda 1, 1600rpm and with spark assistance.

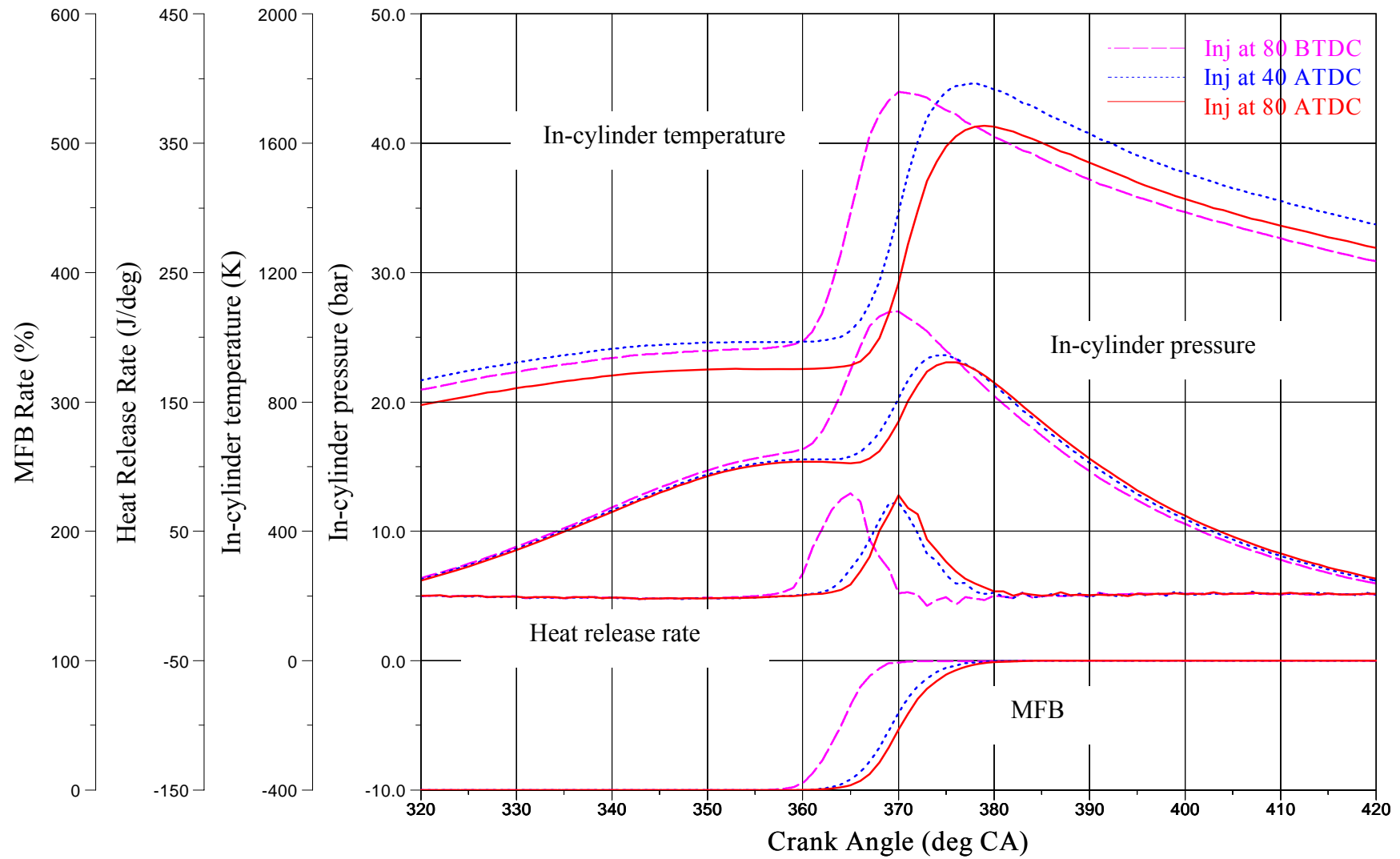


Figure 5.12 In-cylinder pressure, temperature, heat release rate and MFB rate at lambda 1, 1600rpm and No spark assistance.

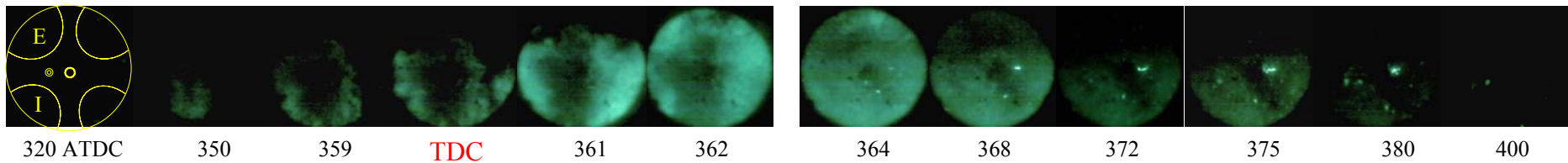
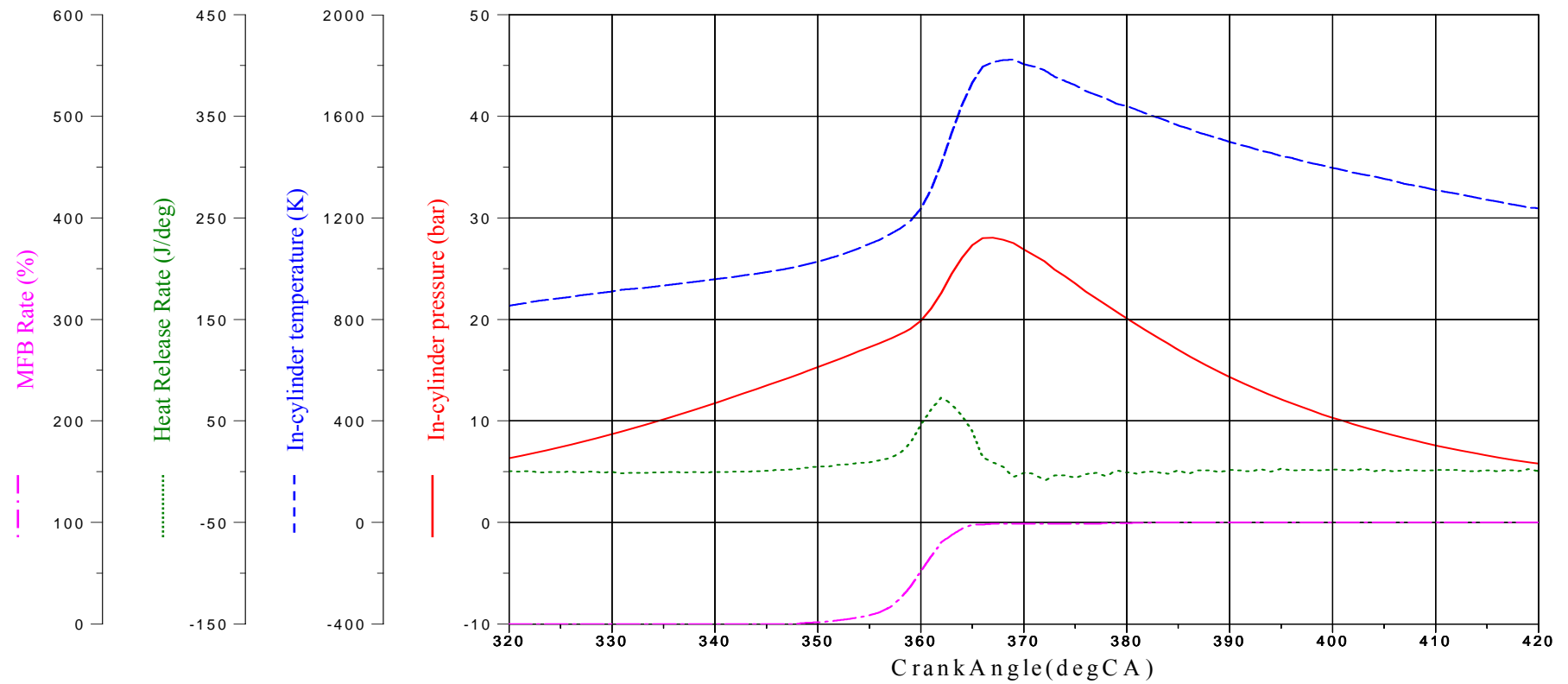


Figure 5.13 Simultaneous In-cylinder pressure, temperature, heat release rate, MFB rate and Full Chemiluminescence images at lambda 1, 1600rpm, Gain 60%, SOI=80 °CA BTDC and with spark assistance.

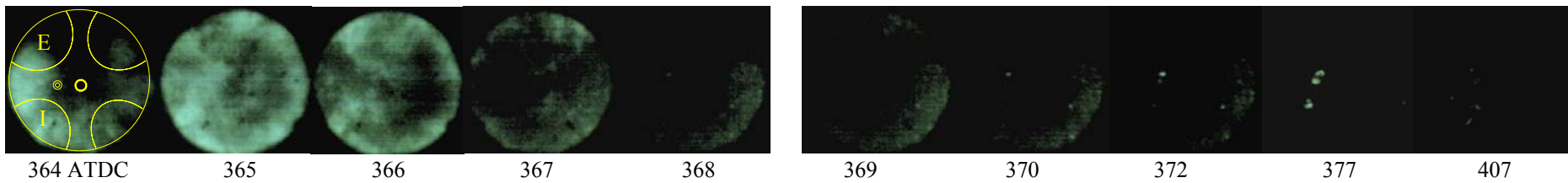
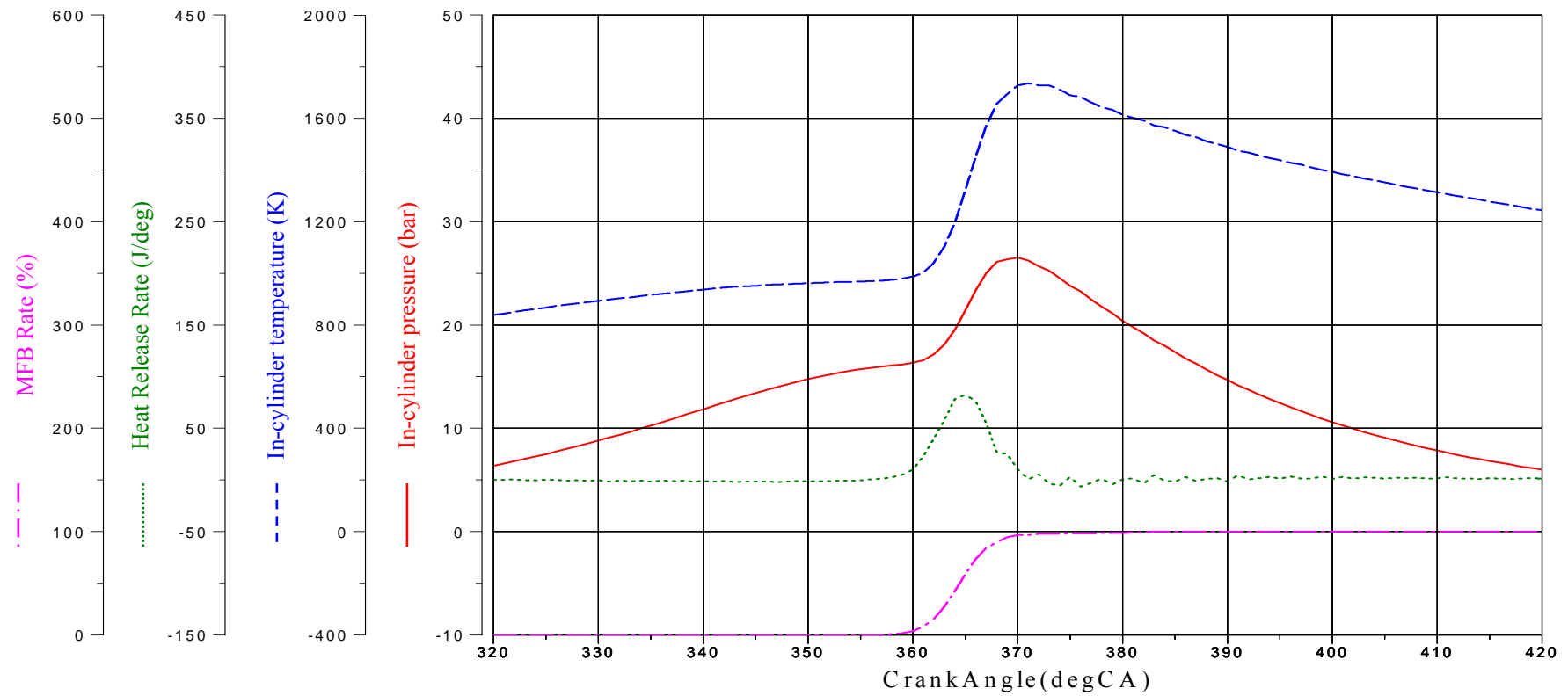


Figure 5.14 Simultaneous In-cylinder pressure, temperature, heat release rate, MFB rate and Full Chemiluminescence images at lambda 1, 1600rpm, Gain 60%, SOI=80 °CA BTDC and with No spark assistance.

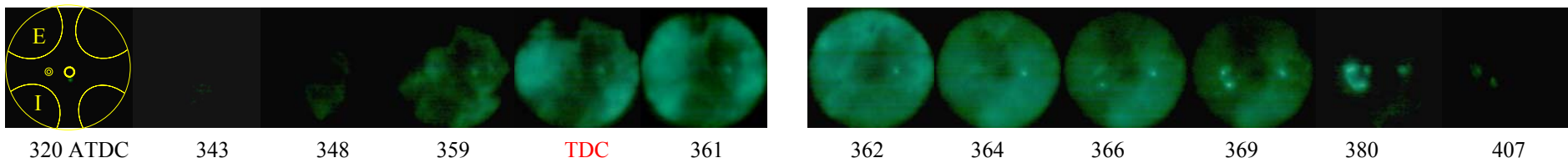
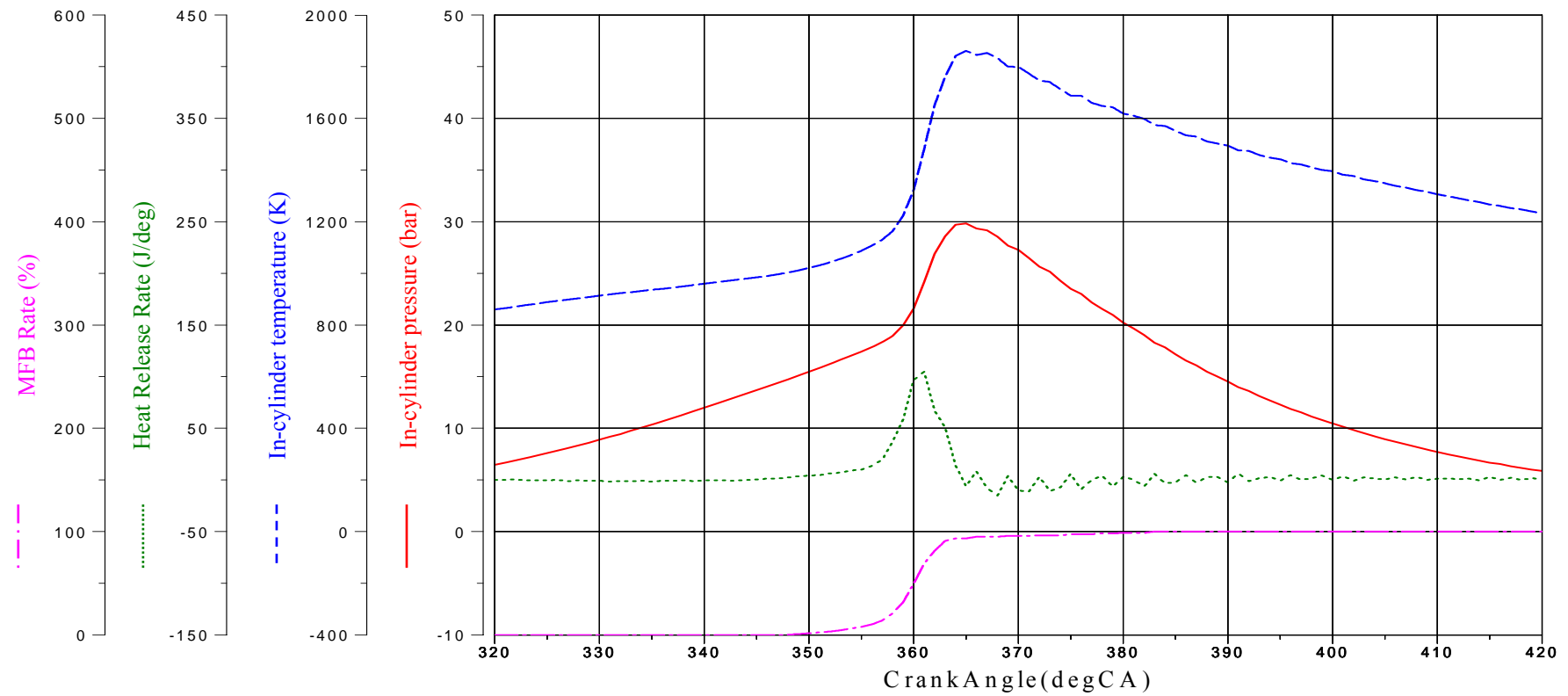


Figure 5.15 Simultaneous In-cylinder pressure, temperature, heat release rate, MFB rate and Full Chemiluminescence images at lambda 1, 1600rpm, Gain 60% , SOI=40 °CA ATDC and with spark assistance.

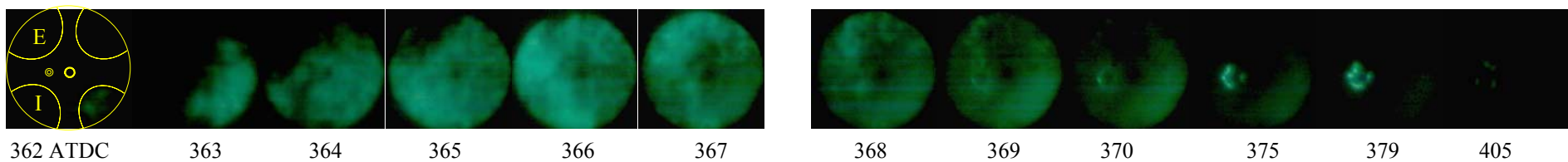
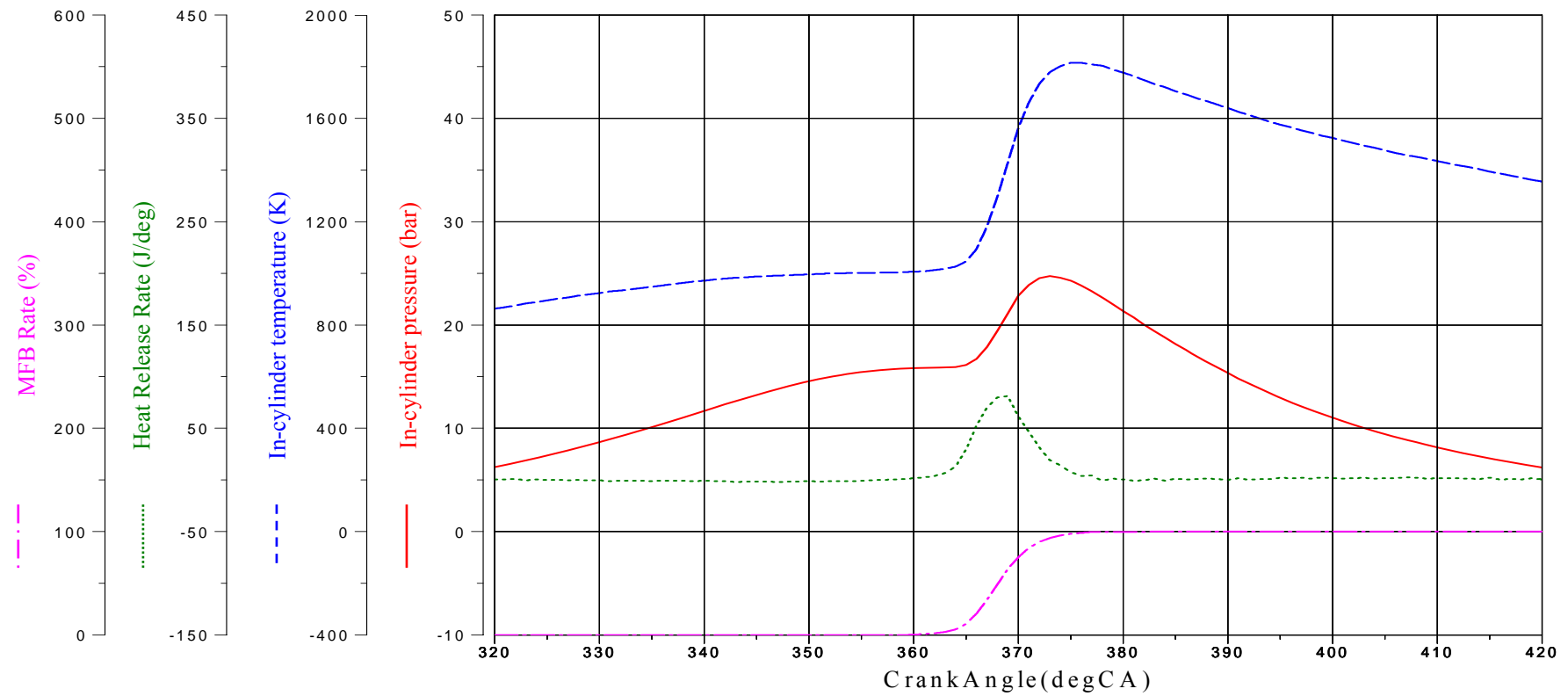


Figure 5.16 Simultaneous In-cylinder pressure, temperature, heat release rate, MFB rate and Full Chemiluminescence images at lambda 1, 1600rpm, Gain 60%, SOI=40 °CA ATDC and with No spark assistance.

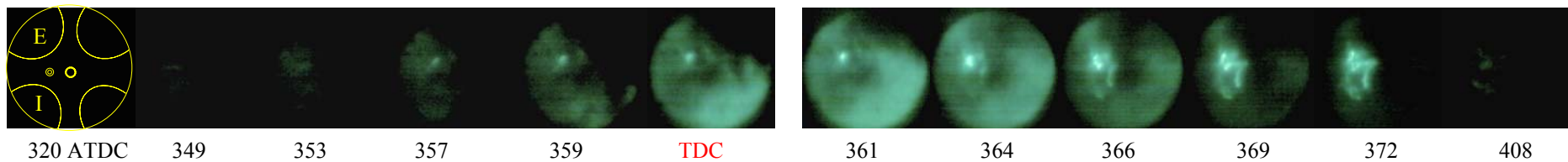
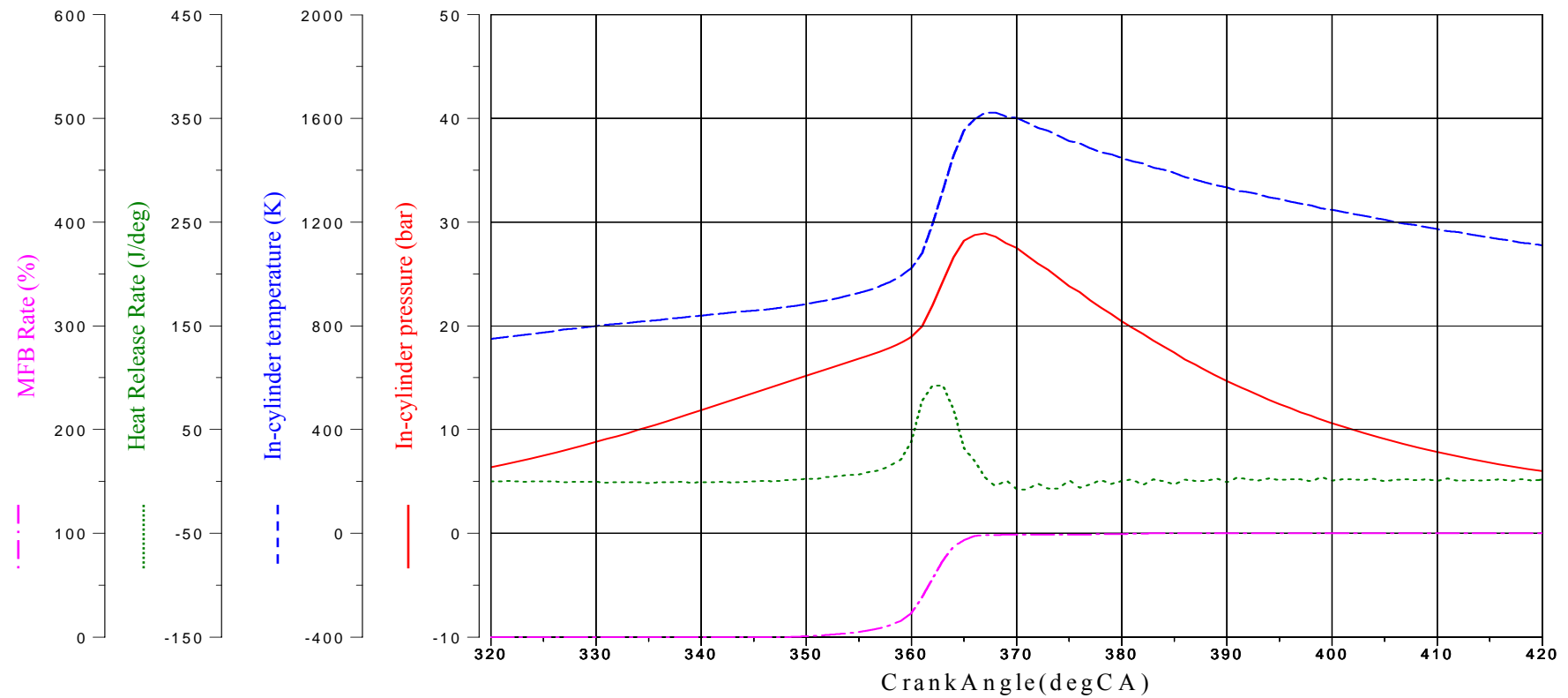


Figure 5.17 Simultaneous In-cylinder pressure, temperature, heat release rate, MFB rate and Full Chemiluminescence images at lambda 1, 1600rpm, Gain 60%, SOI=80 °CA ATDC and with spark assistance.

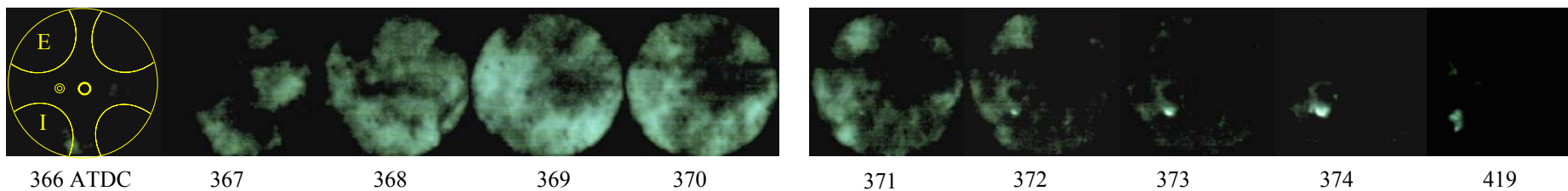
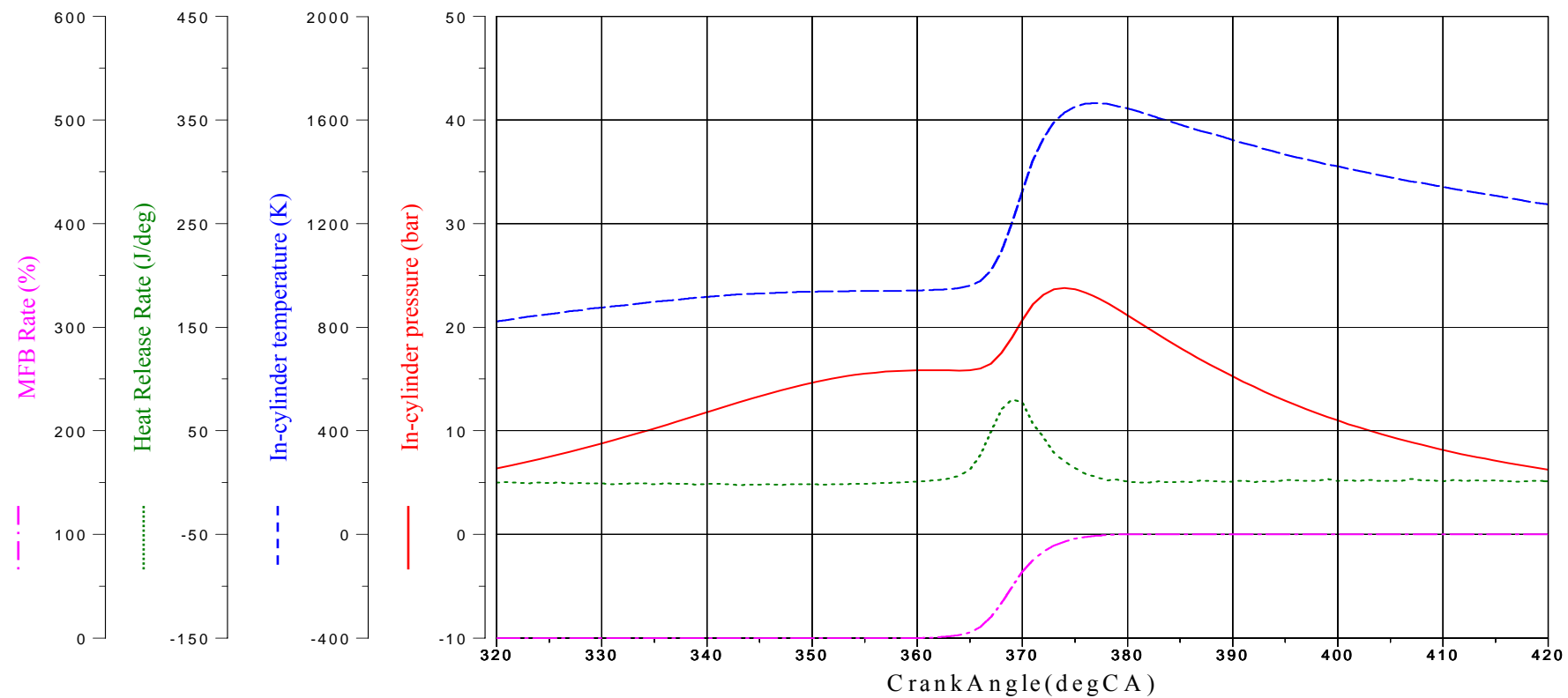


Figure 5.18 Simultaneous In-cylinder pressure, temperature, heat release rate, MFB rate and Full Chemiluminescence images at lambda 1, 1600rpm, Gain 60%, SOI=80 °CA ATDC and with No spark assistance.

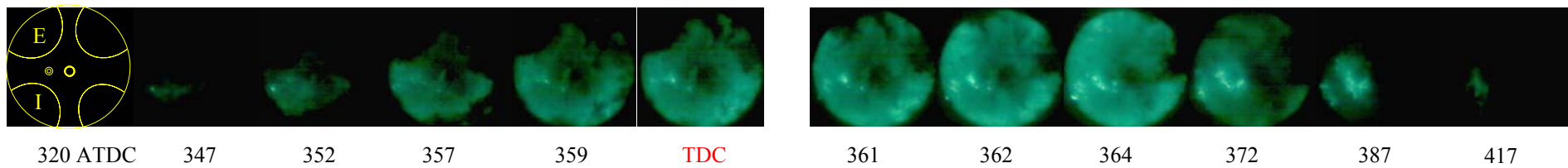
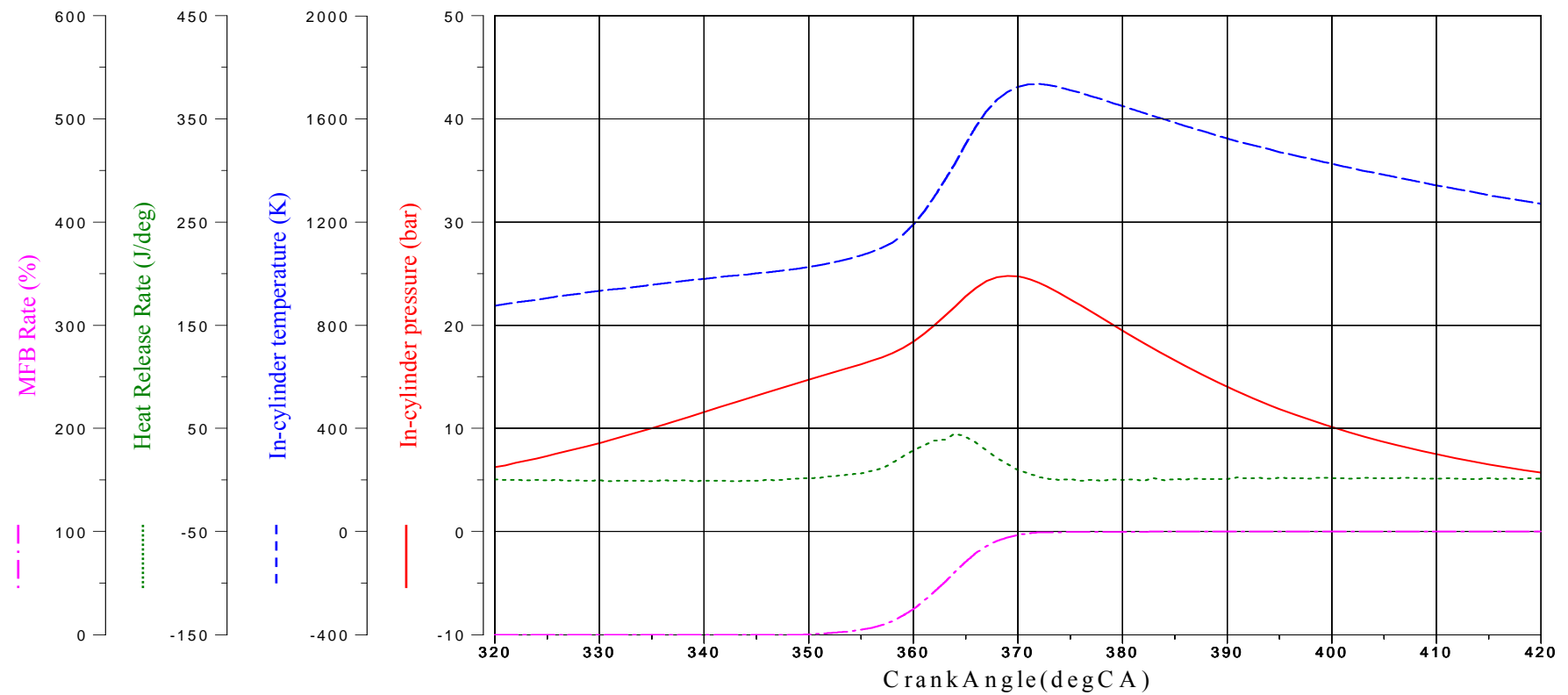


Figure 5.19 Simultaneous In-cylinder pressure, temperature, heat release rate, MFB rate and Full Chemiluminescence images at lambda 1, 1600rpm, Gain 60%, SOI=200 °CA ATDC and with spark assistance.

5.4.1.5.3 OH Chemiluminescence

Chemiluminescence of OH radical with simultaneous in-cylinder studies of CAI combustion is investigated on different injection timings in this section. The OH radical is known as a chemical intermediate during the combustion process, present in the premixed combustion region. In this study, the first OH radicals have been found to appear at in-cylinder temperature of more than 1200 K. However, the intensity of the OH emission is very low and the high speed camera with an intensifier was able to capture their presence in some of the cycles recorded and stored in the in-camera memory. The corresponding in-cylinder pressure of the same cycle is then selected for in-cylinder temperature and heat release rate analysis.

Figures 5.20 – 5.24 show the results of OH chemiluminescence from CAI combustion at lambda 1 at different injection timings. The combustion with early injection at exhaust valve closing timing does not provide enough OH radical intensity in either case with spark and without spark. Therefore, this section shows the results of mid-injection and late injection for CAI combustion. Mid-injection timing strategy results in more intensity and clearer images than late injection timing. In the previous section, it has shown that the mid-injection timing provides the best environment for the charge mixture combusted and stable combustion as the results of the best combustion efficiency, fuel conversion efficiency and lowest NOx emissions

In Figure 5.20, the first OH radical with injection timing at 40deg CA ATDC with spark is detected at 359 deg CA at an averaged in-cylinder temperature of 1300 K. This injection timing develops very fast combustion process for about 2 crank angles from 359 deg CA to 361 deg CA. The OH radical stays in the chamber for about 3 crank angles from 361 deg CA to 363 deg CA and then the area of OH presence shrinks and lasts for another 13 crank angles from 363 deg CA to 376 deg CA after peak heat release rate.

In Figure 5.21, the first OH radical with injection timing at 40 ATDC without spark shows significant local auto-ignition and appears at in-cylinder temperature of about 1250 K. The development of OH radical is extremely fast for 1 crank angle from 368 deg CA. The OH radical remains in the entire chamber for about 4 crank angles from 368 deg CA to 372 deg

CA. The level of OH radicals decreases for about 8 crank angles from 372 deg CA to 379 deg CA.

In figure 5.22 and Figure 5.23, the OH radical distributions at injection timing 80 ATDC with spark and without spark assistance are shown. The first OH radicals in each case are shown at in-cylinder temperatures of about 1150 K and 1250 K respectively. In comparison with the results of injection timing at 40 ATDC, the first OH radical with spark assistance appears at 359 deg CA, develops until 362 deg CA and consumed completely at 374 deg CA. The development of OH radical without spark assistance is shown from 373 deg CA to 376 deg CA and consumed at 390 deg CA.

Figure 5.24 shows the OH radical in CAI at injection timing 200 deg CA ATDC with spark assistance. The combustion is very unstable and misfiring occurs in some cycles, hence it was extremely difficult to capture the data without spark assistance. The results with spark assistance show lower intensity or quantity of OH radicals than those of the other injection timings. A couple of images are obtained in this figure, but it is clear that OH radical appears at in-cylinder temperature more than 1200 K and shows a similar trend of combustion development. Compared with the previous OH images, OH images are only detected in the peripheral region of the combustion chamber, where relative leaner mixture is expected due to the charge stratification effect associated with later injection [94]. In addition, all the results show that OH is more uniformly distributed in pure CAI combustion than that with spark assisted CAI combustion.

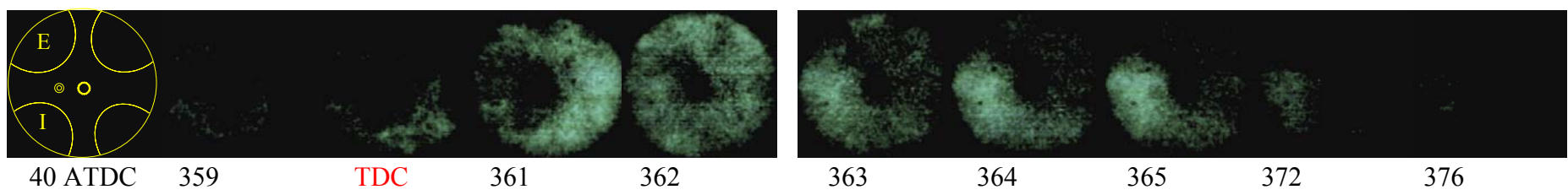
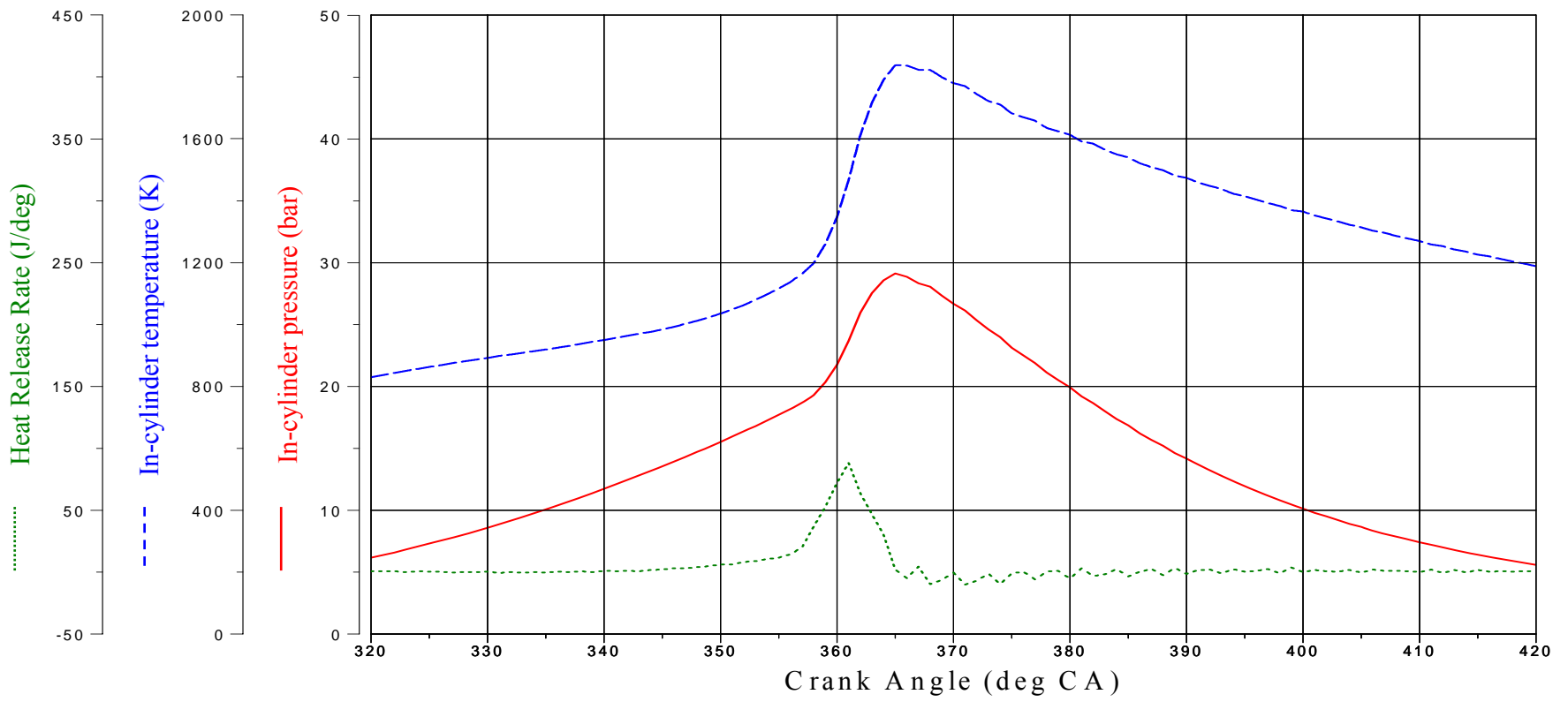


Figure 5.20 Simultaneous In-cylinder pressure, temperature, heat release rate and Chemiluminescence images of OH at lambda 1, 1600rpm, Gain 60%, SOI=40 °CA ATDC and with spark assistance.

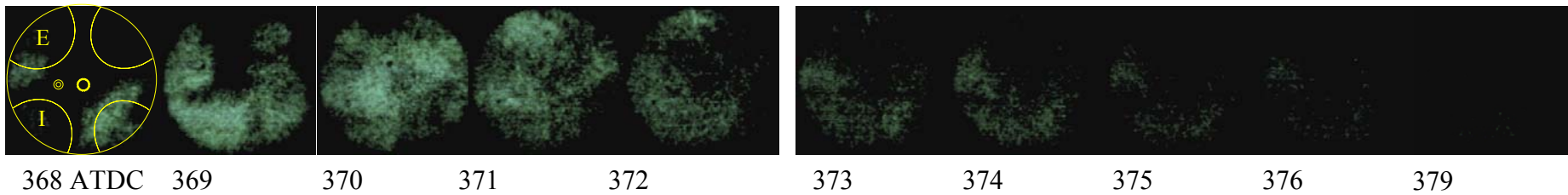
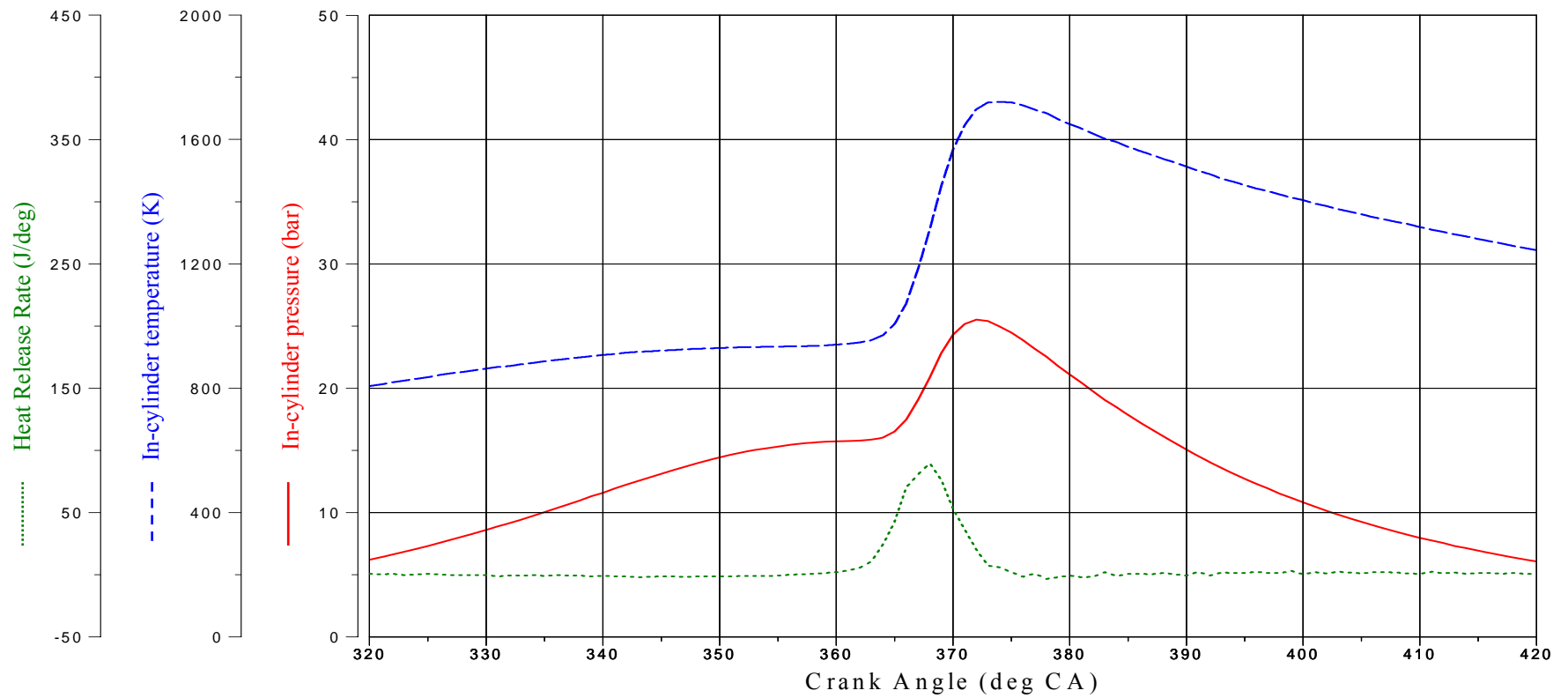


Figure 5.21 Simultaneous In-cylinder pressure, temperature, heat release rate and Chemiluminescence images of OH at lambda 1, 1600rpm, Gain 60%, SOI=40 °CA ATDC and with No spark assistance.

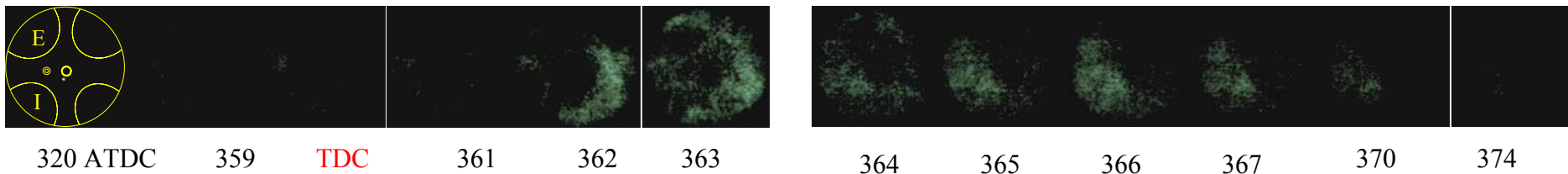
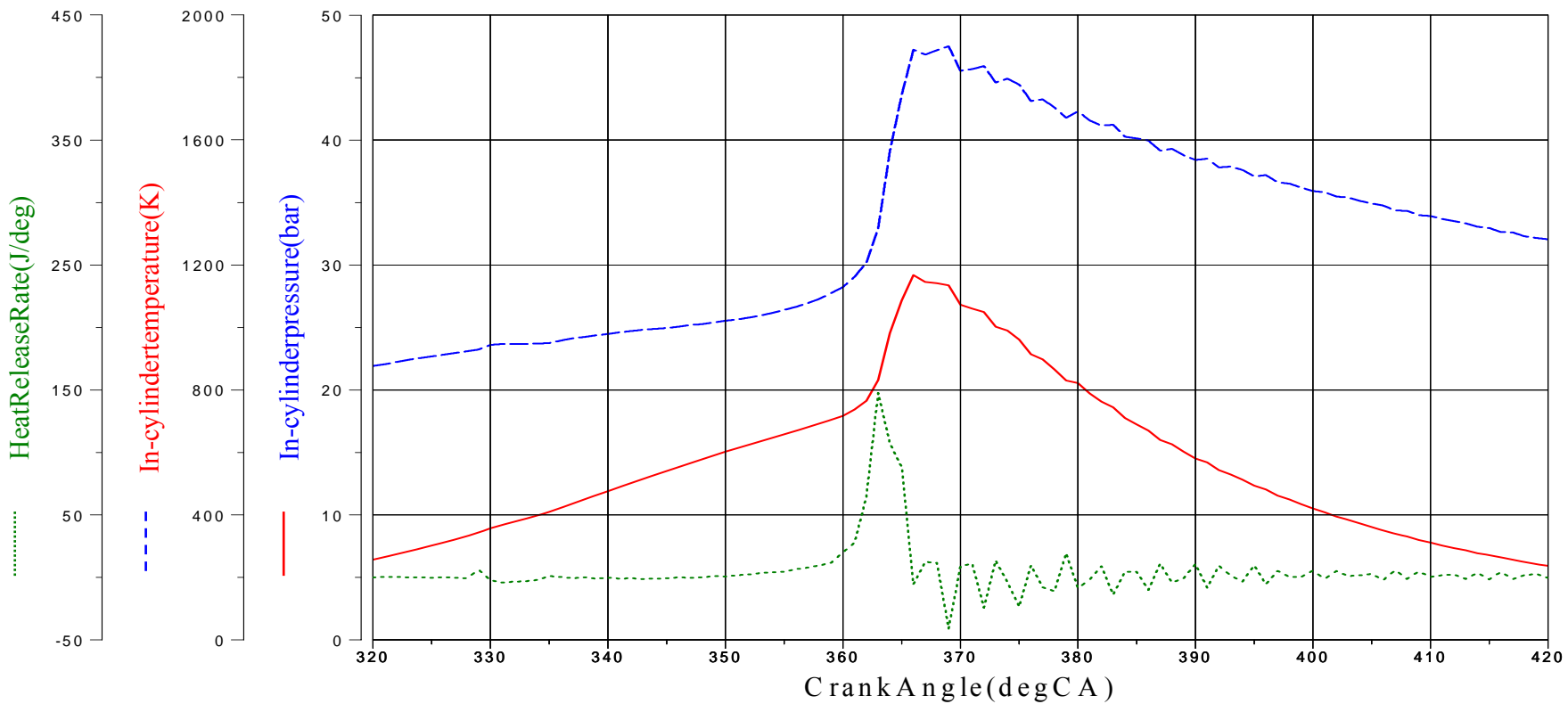


Figure 5.22 Simultaneous In-cylinder pressure, temperature, heat release rate and Chemiluminescence images of OH at lambda 1, 1600rpm, Gain 60%, SOI=80 °CA ATDC and with spark assistance.

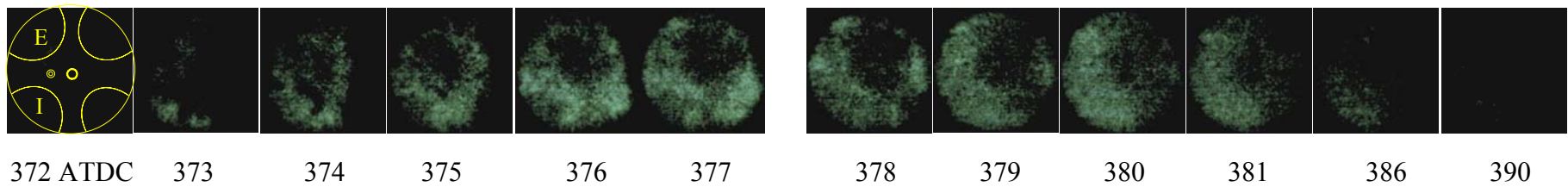
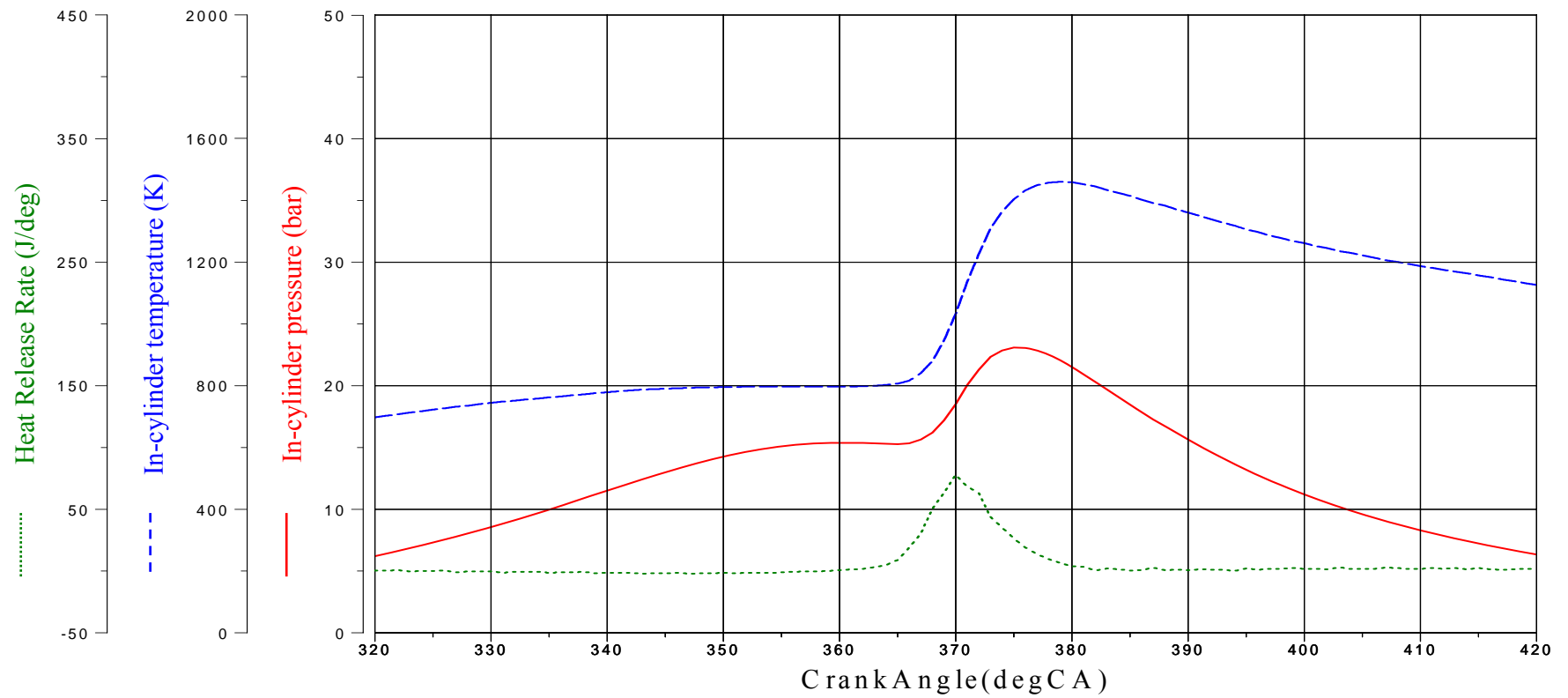


Figure 5.23 Simultaneous In-cylinder pressure, temperature, heat release rate and Chemiluminescence images of OH at lambda 1, 1600rpm, Gain 60%, SOI=80 °CA ATDC and with No spark assistance.

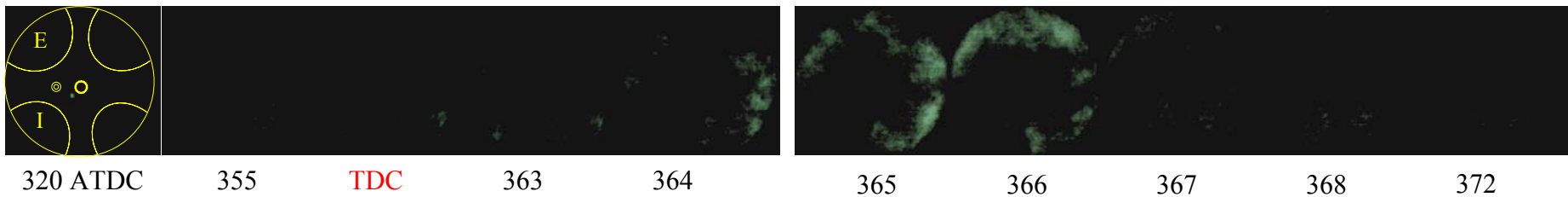
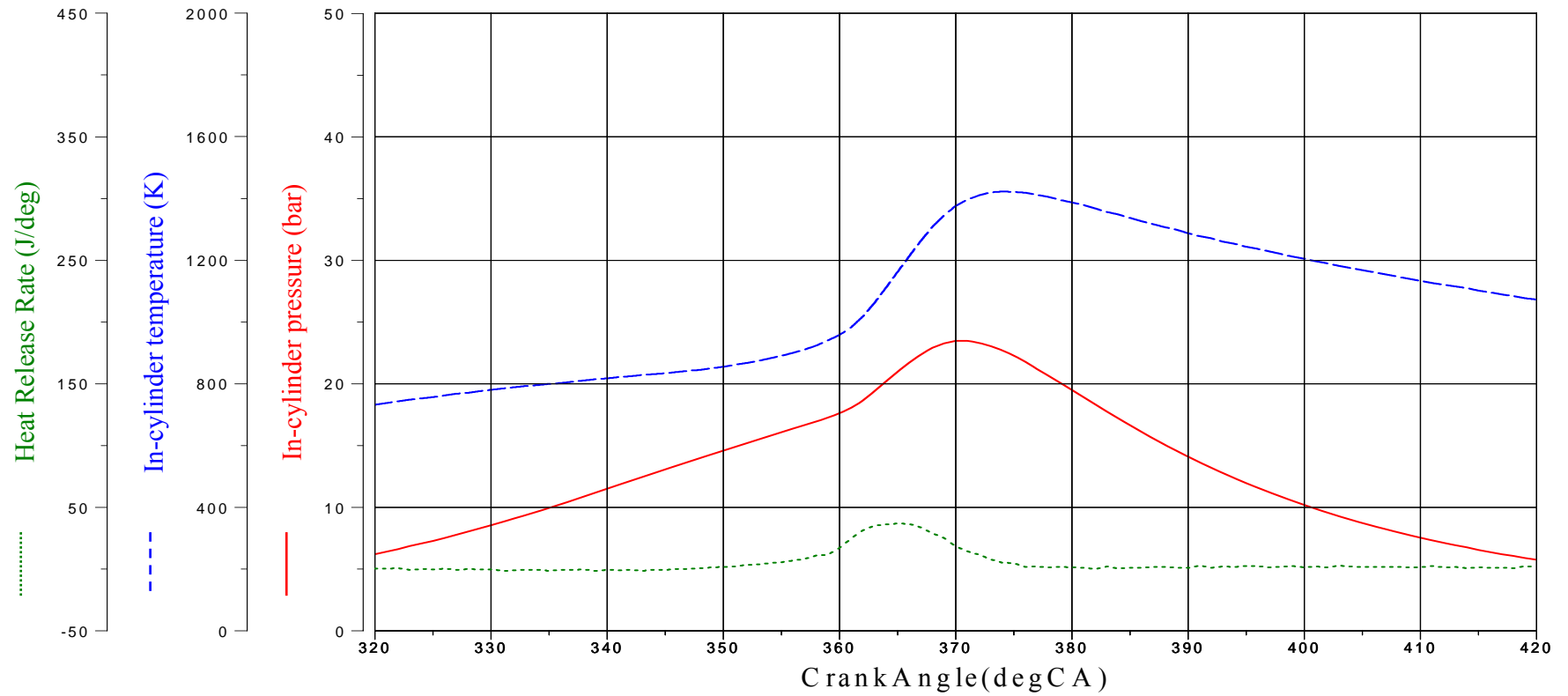


Figure 5.24 Simultaneous In-cylinder pressure, temperature, heat release rate and Chemiluminescence images of OH at lambda 1, 1600rpm, Gain 60%, SOI=200 °CA ATDC and with spark assistance.

5.4.1.5.4 CHO Chemiluminescence

Chemiluminescence of CHO radical of CAI at lambda 1 with injection timings is achieved simultaneously with in-cylinder studies. CHO radical is one of chemical intermediate species produced with formaldehyde in low temperature combustion. This radical is often considered as an indicator of the first stage combustion. Although it indicates the low temperature pre-combustion, the existence of OH radical is overlapped with this CHO radical. However, these results are available to compare the results of OH radicals due to the cyclic variation.

Figure 5.25 ~ 5.31 show the results of chemiluminescence images of CHO radical of CAI by injection timing at 80 deg BTDC, 40 deg ATDC, 80 deg ATDC, and 200 deg ATDC. The first images in the sequences are captured as a first flame of CHO radical and develop through the combustion to the end. As low intensity from the visualization of OH radical in the previous section, this visualization also shows the loss of intensity in the beginning and end of video footage.

In Figure 5.25 and figure 5.26, the first CHO radical of CAI with spark and without spark assistance are captured at 356 °CA and 362 °CA respectively. In practice, the existence of CHO radical in either case is earlier than these crank angles. They represent the low temperature oxidation at those crank angles or /and cool flame zone and appear in the chamber for about 2 crank angles and consumed later. Despite of low intensity in these images, the existence of CHO radical of CAI without spark assistance shows much faster formation and consumption compared to without spark assistance.

Figure 5.27 ~ 5.30 show the chemiluminescence images of CHO radical of CAI with mid-injection timings at negative valve overlap period and intake valve opening timing respectively. The first formation of CHO radical was captured at lower in-cylinder temperature of about 850 ~ 900 K and apparently formed faster without spark assistance. The formations appear for about 2 crank angles without spark assistance, as shown in figure 5.28 and 5.30 and the formation with spark assistance for about 15 crank angles. These CHO radicals are formed locally in the entire chamber without spark assistance. Some soot appeared at the after burned zone as

experienced with the images of OH radicals, but no hot burned pockets appear by these injection timings.

Figure 5.31 shows the result of CHO chemiluminescence of CAI with late injection timing with spark. The first formation is shown at in-cylinder temperature of about 1100 K, 362 °CA and formed for 4 crank angles to 365 °CA. thereafter, the appearance of CHO radical is overlapped with OH radicals. In spite of difficulties of different intensity problems, the quantity of CHO radical in this late injection timing appears less than by mid-injection timings and definitely much less than early injection timing. Consequently, earlier injection timing offers more time for CHO radical to be formed compared to by late injection timing and less complete mixture leads to incomplete combustion as a result.

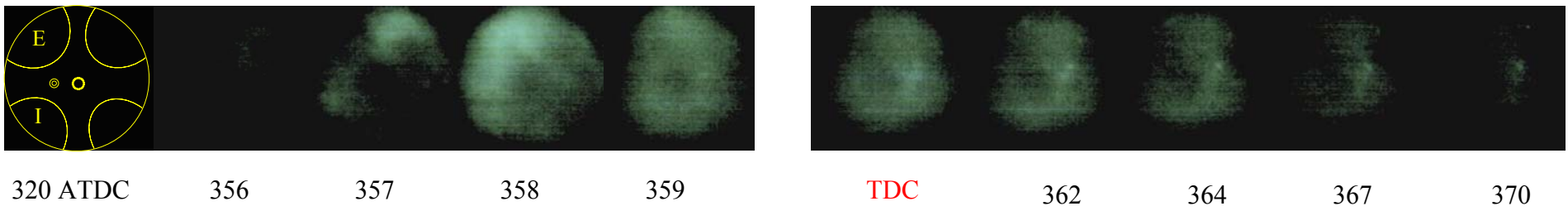
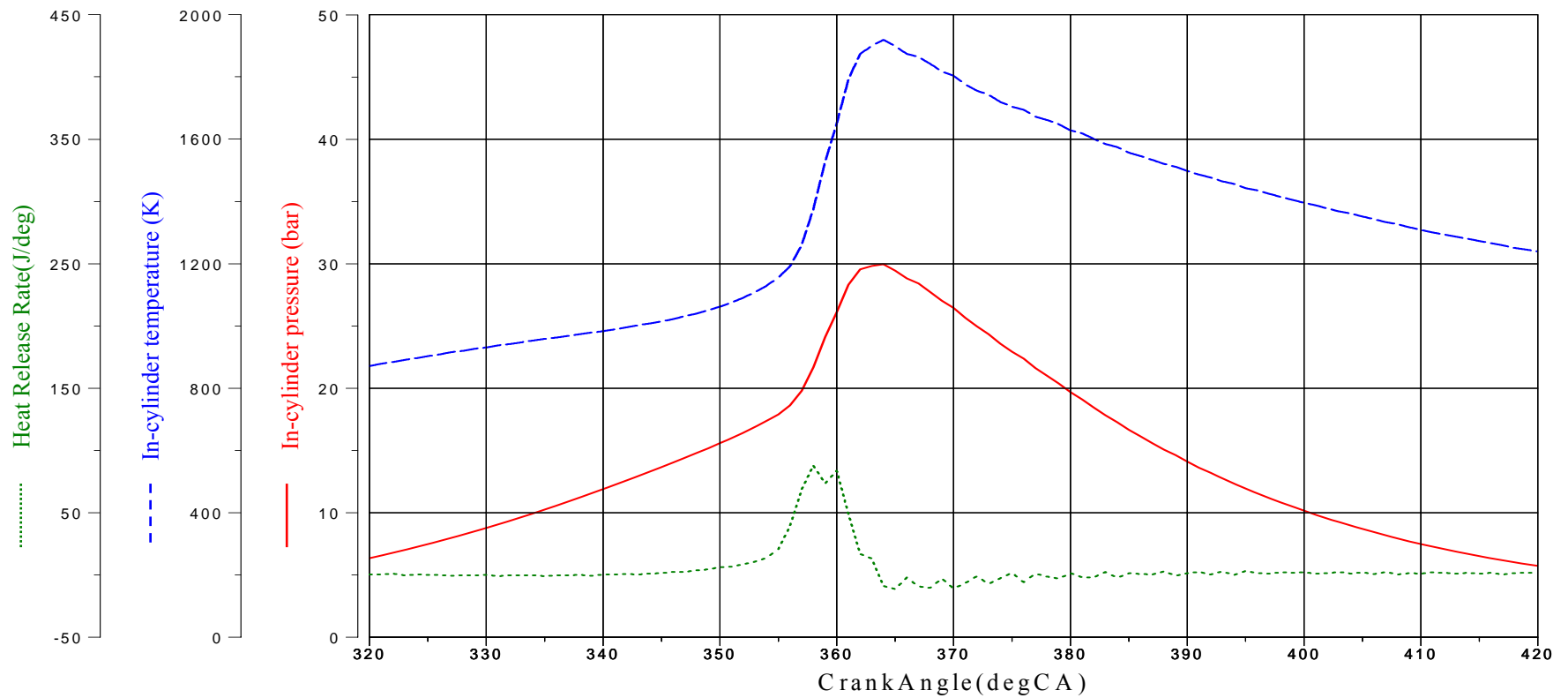


Figure 5.25 Simultaneous In-cylinder pressure, temperature, heat release rate and Chemiluminescence images of CHO at lambda 1, 1600rpm, Gain 60%, SOI=80 °CA BTDC and with spark assistance.

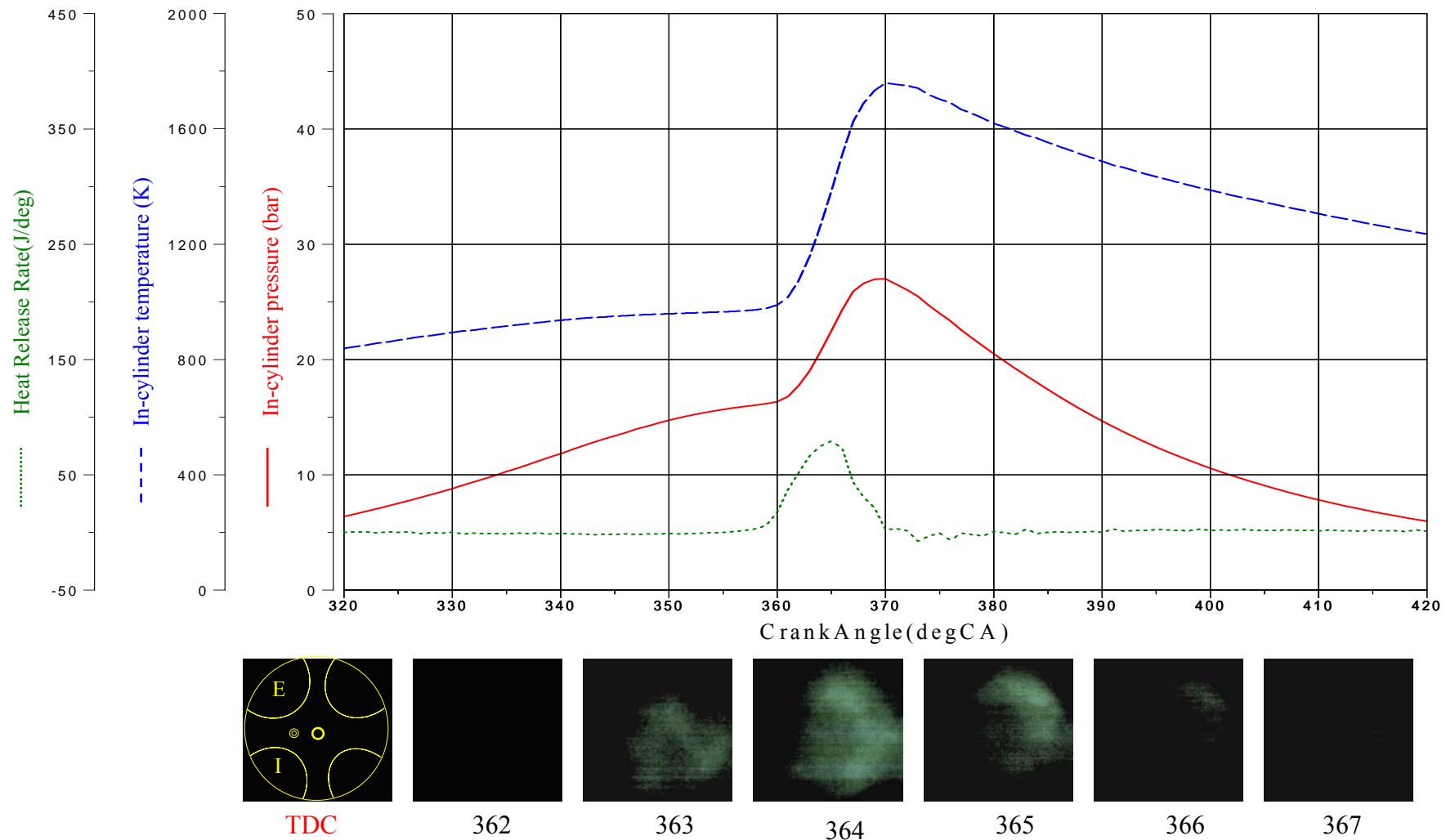


Figure 5.26 Simultaneous In-cylinder pressure, temperature, heat release rate and Chemiluminescence images of CHO at lambda 1, 1600rpm, Gain 60%, SOI=80 °CA BTDC and with No spark assistance.

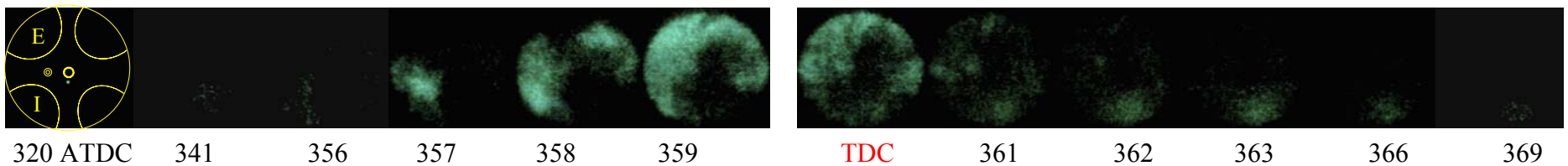
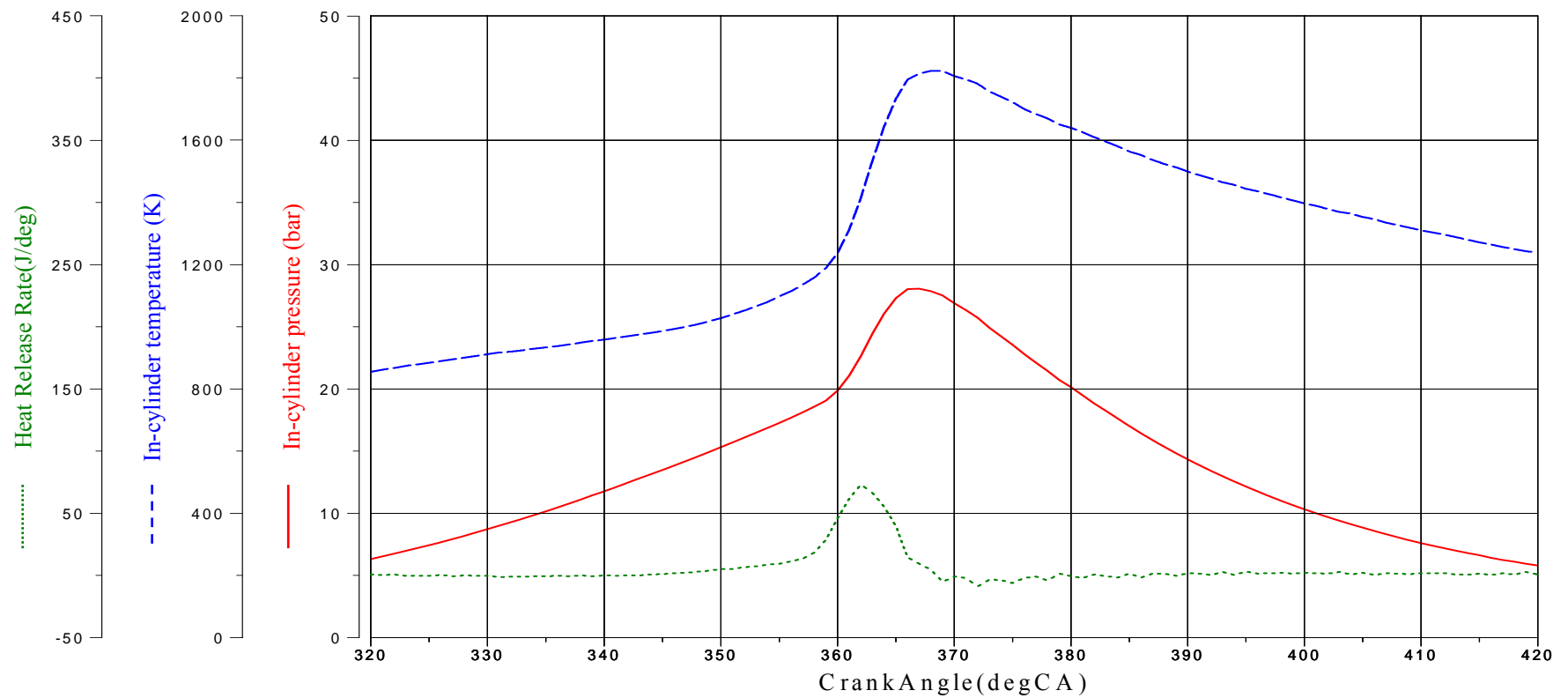


Figure 5.27 Simultaneous In-cylinder pressure, temperature, heat release rate and Chemiluminescence images of CHO at lambda 1, 1600rpm, Gain 60%, SOI=40 °CA ATDC and with spark assistance.

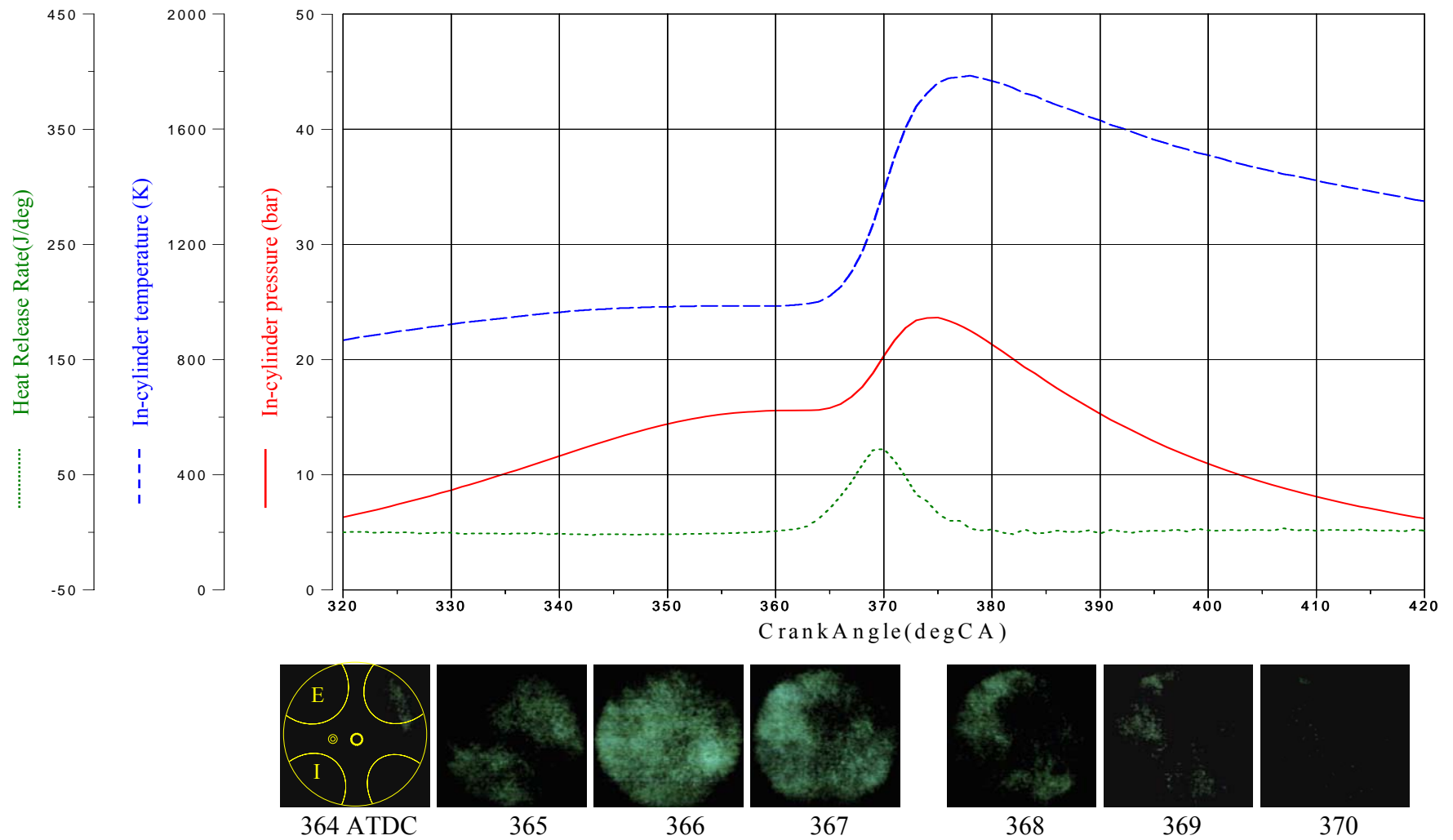


Figure 5.28 Simultaneous In-cylinder pressure, temperature, heat release rate and Chemiluminescence images of CHO at $\lambda = 1$, 1600rpm, Gain 60%, SOI=40 °CA ATDC and with No spark assistance.

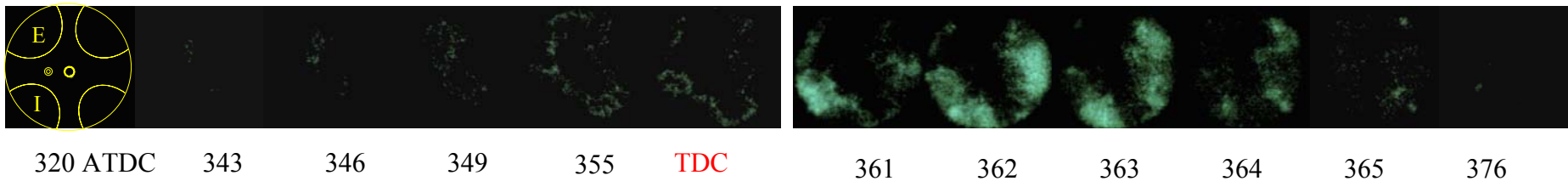
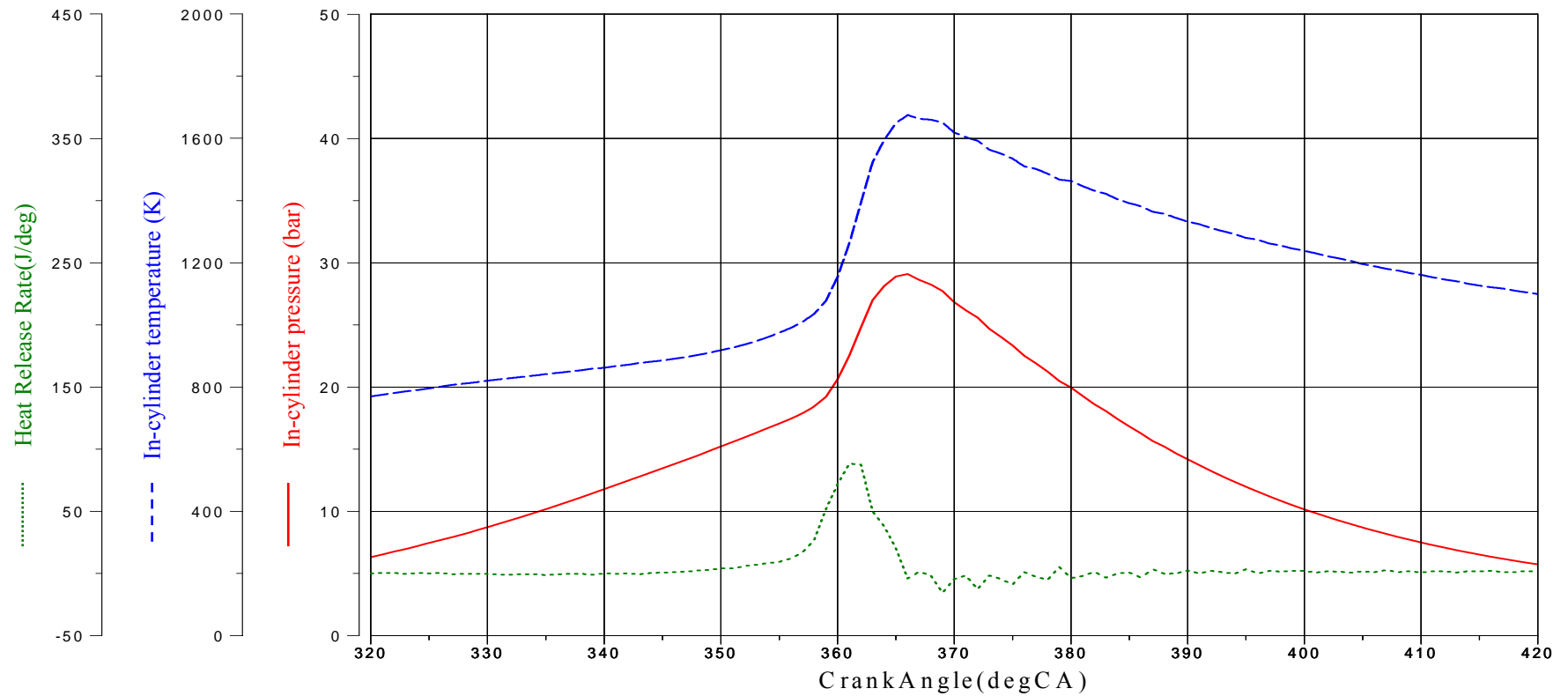


Figure 5.29 Simultaneous In-cylinder pressure, temperature, heat release rate and Chemiluminescence images of CHO at lambda 1, 1600rpm, Gain 60%, SOI=80 °CA ATDC and with spark assistance.

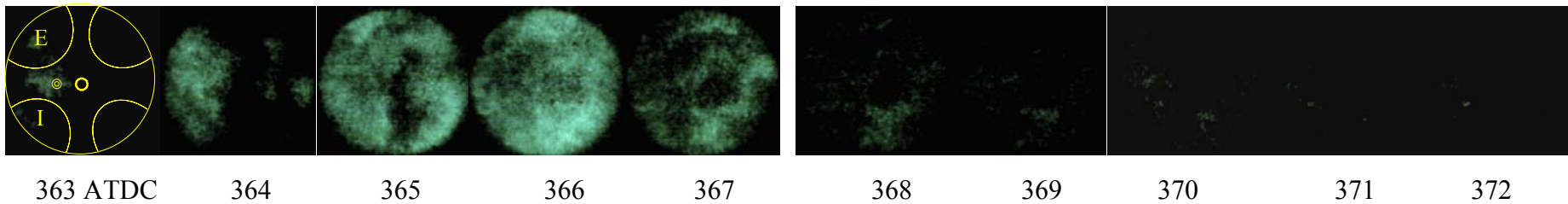
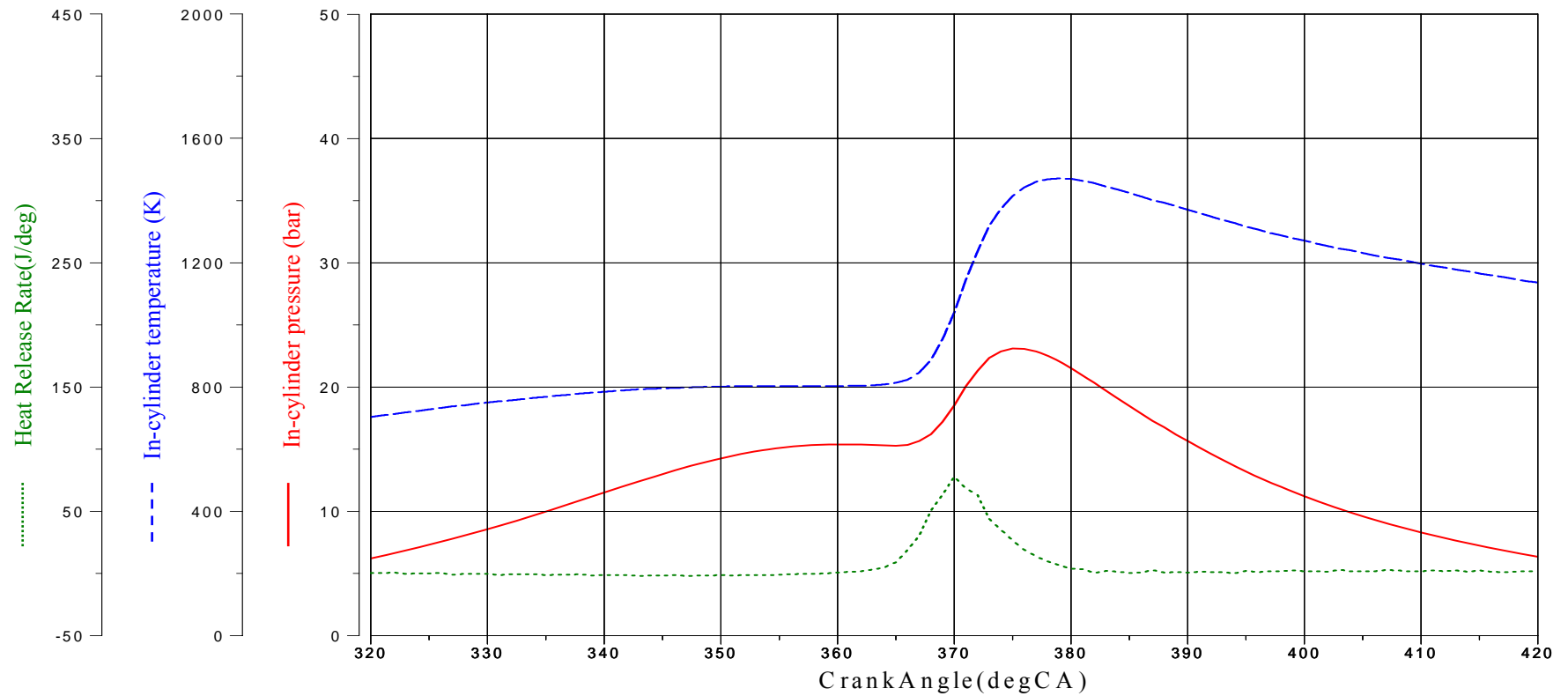
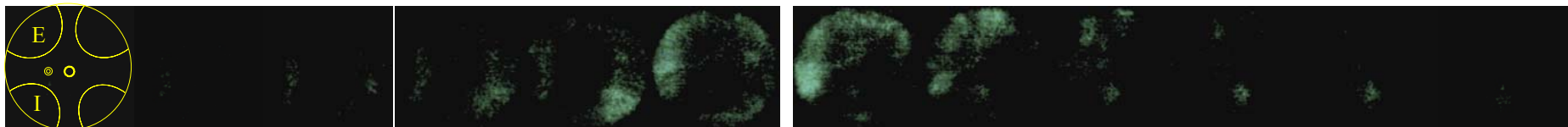
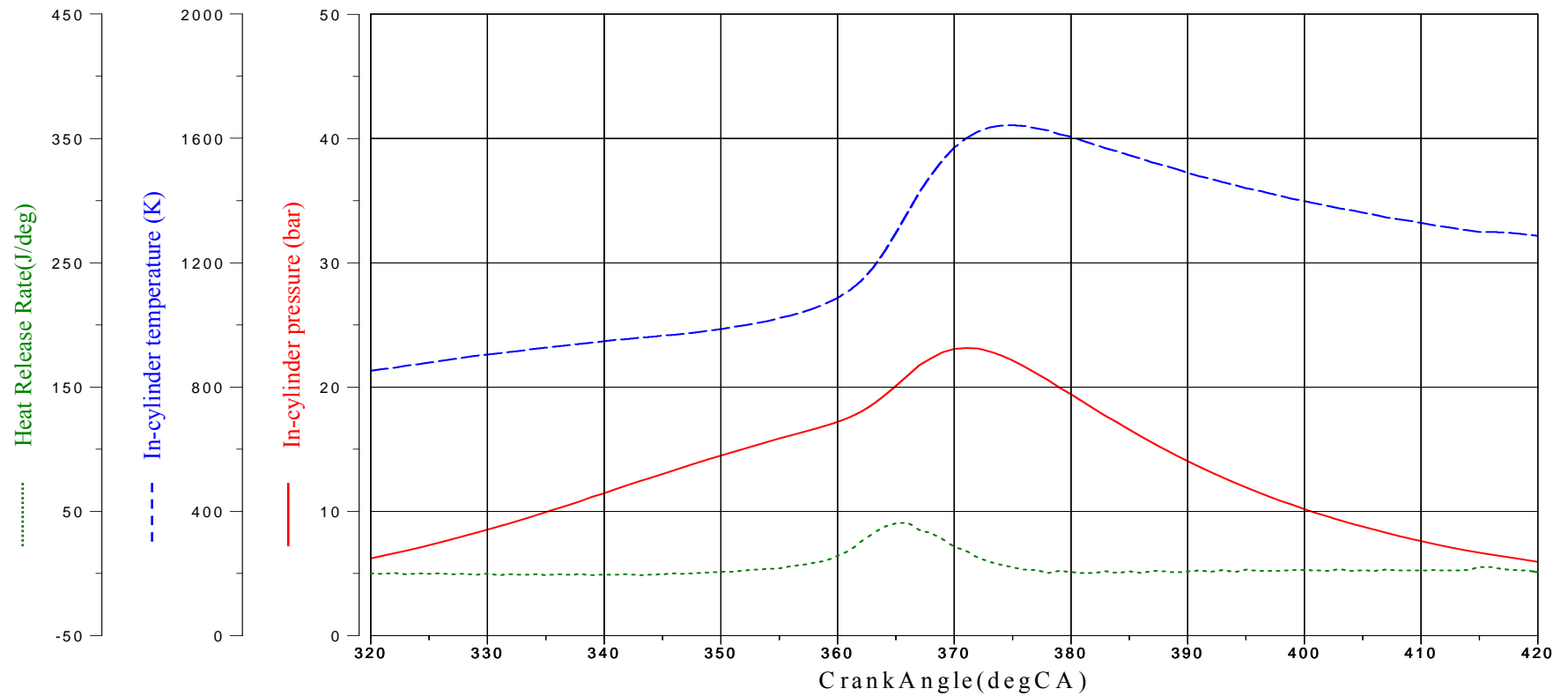


Figure 5.30 Simultaneous In-cylinder pressure, temperature, heat release rate and Chemiluminescence images of CHO at lambda 1, 1600rpm, Gain 60%, SOI=80 °CA ATDC and with No spark assistance.



320 ATDC 362 363 364 365 366 367 368 369 370 371 382

Figure 5.31 Simultaneous In-cylinder pressure, temperature, heat release rate and Chemiluminescence images of CHO at lambda 1, 1600rpm, Gain 60%, SOI=200 °CA ATDC and with spark assistance.

5.4.2 Effect of Spark Timing

5.4.2.1 Introduction

CAI combustion has been investigated with negative valve overlap that it was operated stably without spark assistance in most of the CAI operational region. However, some engine operation requires spark assistance to achieve stable combustion with large amount of residual gas. Two aspects of spark ignition were investigated, the presence and absence of spark and the effects of spark timings

5.4.2.2 Engine performance

The presence of spark causes significant changes of engine performance and combustion stability, especially for the low loads and late injection timings, as shown in Figure 5.32. The results were obtained at 1600 rpm, lambda 1, and EVC/IVC at 280 °CA ATDC/440 CA deg ATDC, injection timing of 80 BTDC. Under such operating conditions, the presence of spark results in lower engine outputs than that without sparks, as shown in Figure 5.32a. As the spark timings is advanced from TDC, the output initially increases and reaches its peak at 340 deg CA ATDC, Further advancement of spark discharge causes reduction of engine's output. On the other hand, the cyclic variation of engine operation is improved with spark ignition as shown in Figure 5.32b.

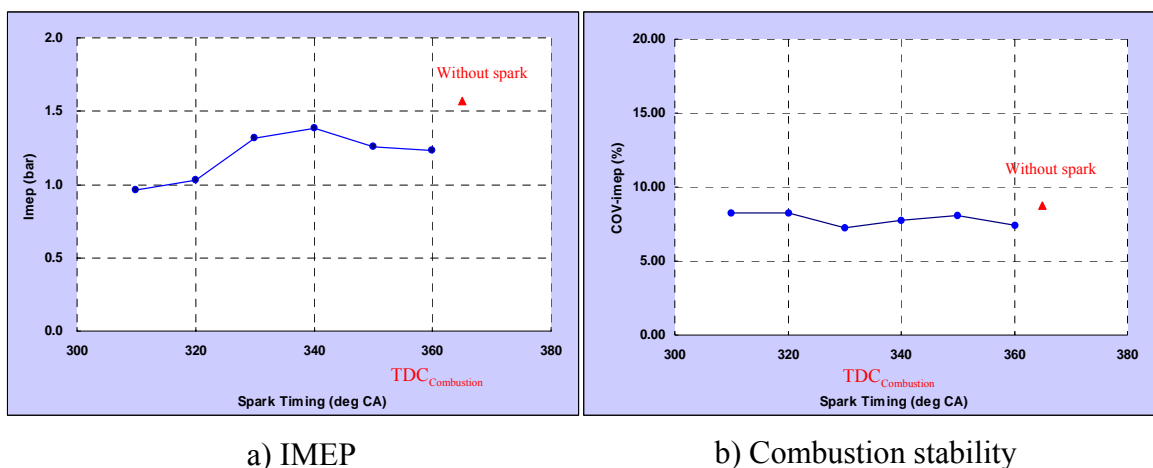


Figure 5.32 Engine loads and CoVimep as a function of spark timings

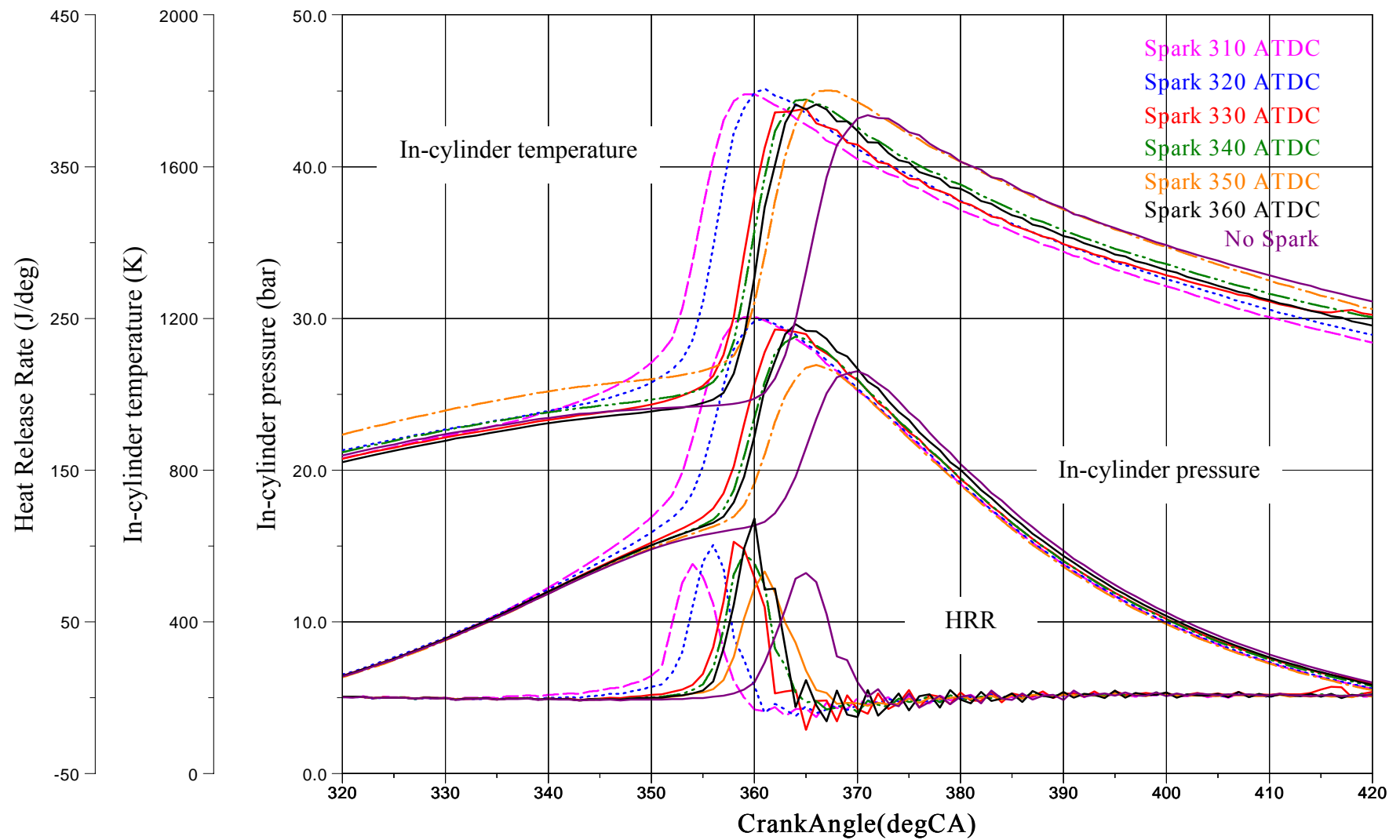
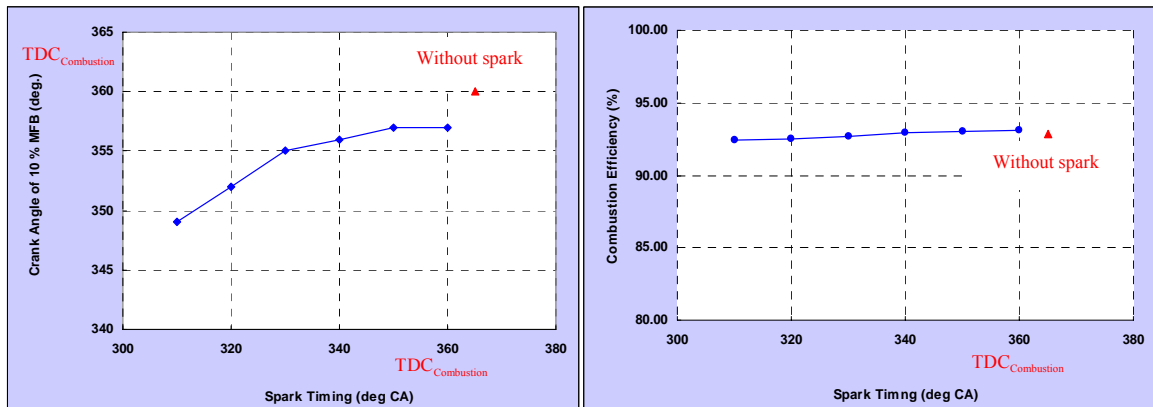


Figure 5.33 Simultaneous In-cylinder pressure, temperature, heat release rate at lambda 1, 1600rpm and with different spark timing

5.4.2.3 Combustion Characteristics

In order to understand better of the spark ignition, the start of combustion and combustion efficiency are analyzed. As shown in Figures 5.33 and 5.34, advanced spark timings start the combustion earlier and spark results in much earlier combustion. Too early combustion caused by spark ignition is responsible for the reduced engine output due to increased negative work done by the piston before top dead centre. As combustion is stable and complete under such operating conditions, combustion efficiency is almost constant irrespective the presence and changes of spark timings.

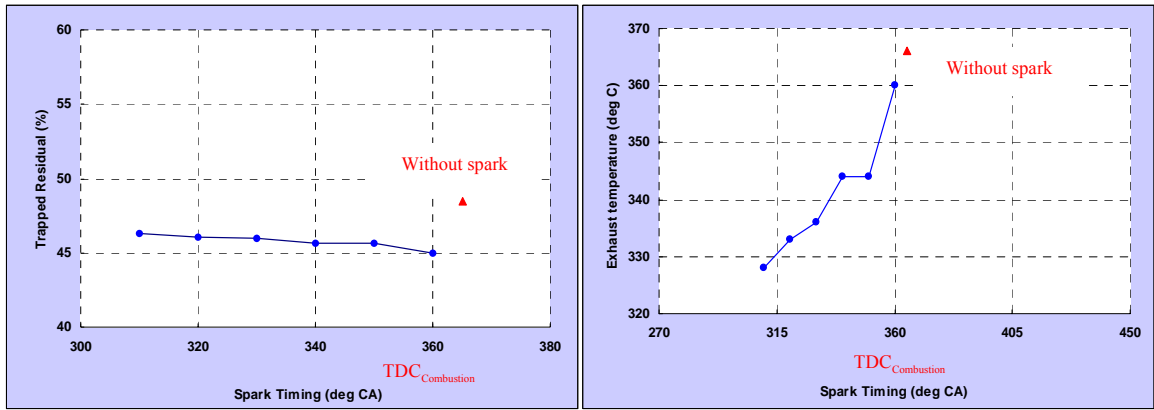


a) Start of combustion

b) Combustion efficiency

Figure 5.34 10 % of MFB and Combustion efficiency in CAI with spark timings

Figure 5.35 show the results of trapped residuals on various spark timings. The combustion without spark assistance in this study shows more trapped residual than with spark assistance. The rate of trapped residual is little affected by the spark timing. As shown in Figure 5.36, the presence of spark lowers the exhaust temperature and the earlier spark timing results in more trapped residuals and results in lower exhaust temperature. The results in Figure 5.35 and Figure 5.36 can be explained by the effect of spark on combustion phasing. As the combustion starts earlier with spark ignition, the burned gas experiences greater expansion and hence lower exhaust temperature. The lower residual concentration seen with spark ignition indicates more burned gases are exhausted during the exhaust process.



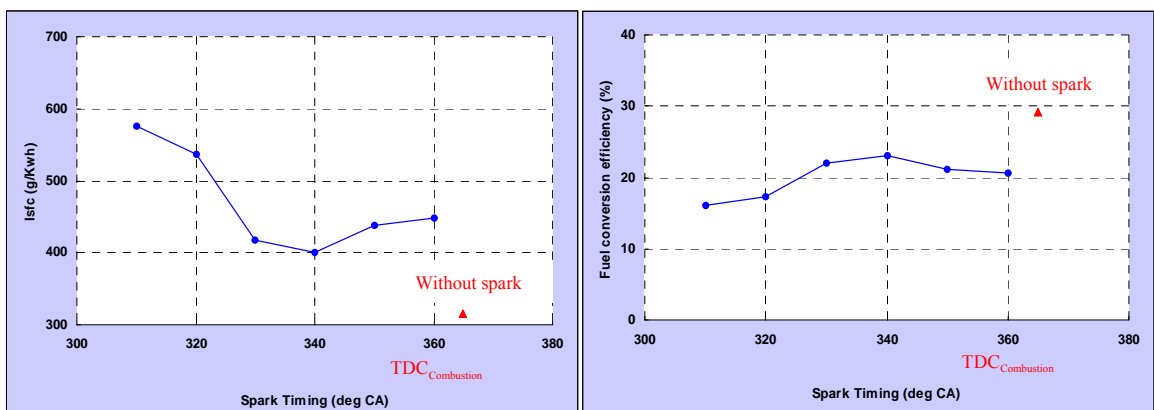
a) Residual concentration

b) Exhaust temperature

Figure 5.35 Trapped residual and exhaust temperature in CAI with spark timings

5.4.2.4 Fuel consumption and emissions

Figure 5.36 shows the results of fuel consumption in CAI with spark timings and without spark assistance. As expected lowest fuel consumption occurs at the maximum imep point at which combustion phasing is optimized. Earliest spark timing leads to higher specific fuel consumption to 570 g/KWh. The optimized combustion at spark timing, 330 and 340 deg CA ATDC results in the lower fuel consumption of 400 g/KWh. CAI operation without spark assistance results in lowest fuel consumption, slightly more than 300 g/KWh and fuel conversion efficiency of 30 %.

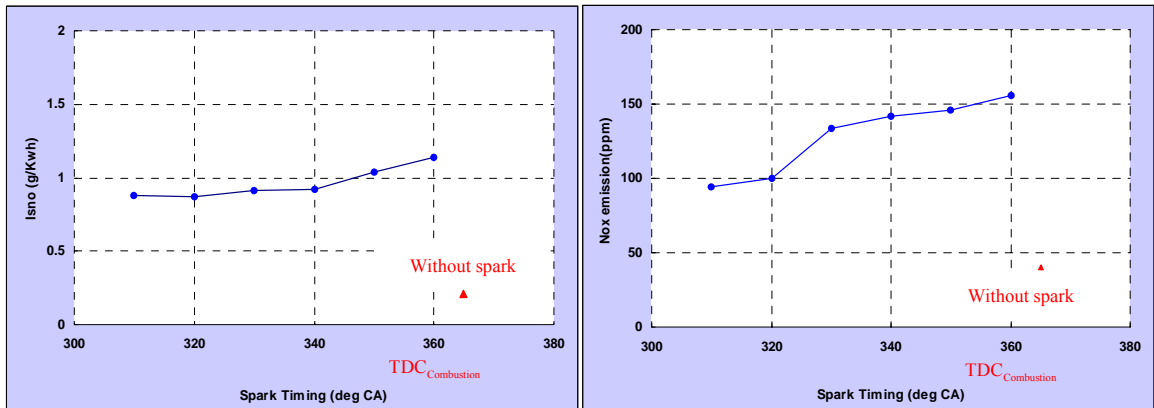


a) ISFC

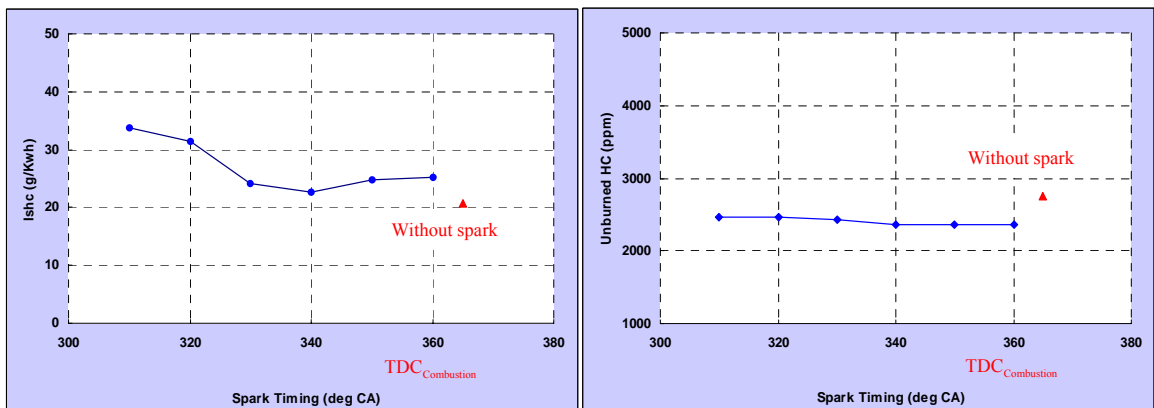
b) Fuel conversion efficiency

Figure 5.36 Fuel consumption in CAI with spark timings

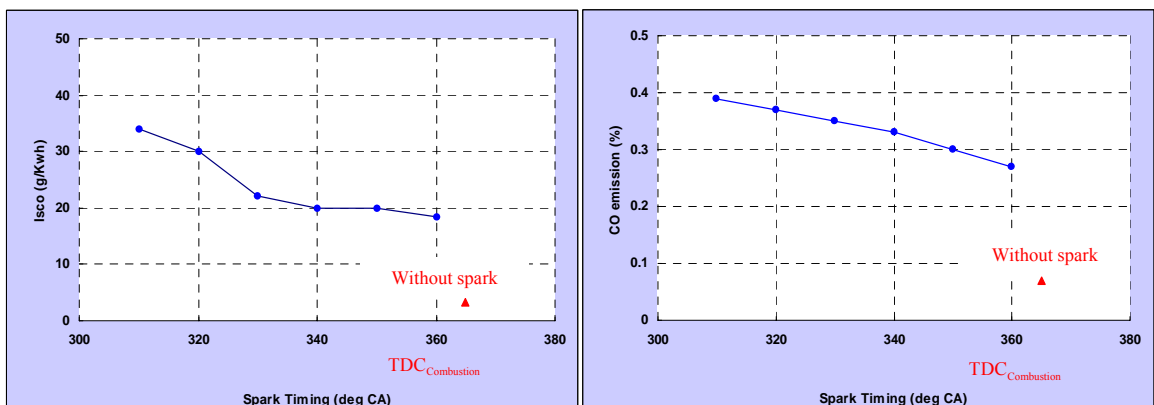
Figure 5.37 shows the results of emissions of CAI with spark timings at lambda 1. As spark assisted CAI advances combustion phasing, the level of NOx emissions shown in Figure 5.37a are higher than that of pure CAI as the combustion temperature decreases with retarded combustion and higher dilution rate.



a) NOx emissions



b) HC emissions



c) CO emissions

Figure 5.37 Emissions in CAI with spark timings

It is interesting to note that although the presence of ignition lowers the absolute level of uHC emissions, the specific uHC emissions are actually higher due to lower engine output. However, both absolute and specific CO emissions are lower without spark ignition. As the combustion temperatures are higher with spark assisted CAI, more complete conversion of CO to CO₂ is expected but the combustion efficiency results are similar for both spark assisted and pure CAI combustions. On the other hand, CO is most sensitive to the local air and fuel ratio. It is possible that flame propagation may have taken place preferentially in the fuel rich regions more of which will be present the earlier in the cycle. In the presence of spark ignition, the lowest uHC and CO emissions are obtained at about 20 ~ 25 g/KWh at spark timings of 330, 340, and 350 deg CA ATDC and the highest levels of both emissions are shown to be about 35 g/KWh at 310 deg CA ATDC. In comparison, uHC and CO emissions are only 20 g/KWh and 4 g/KWh without spark ignition.

5.4.2.5 Simultaneous In-cylinder studies and Full Chemiluminescence

Figures 5.38 to 5.43 show the simultaneous in-cylinder pressure, temperature, heat release rate, MFB rate and full chemiluminescence images in CAI with variable spark timings. The results are the chemiluminescence images and in-cylinder parameters obtained from the same individual cycle.

In general, as spark timing is advanced from TDC, the first flame appears at earlier crank angle. With spark at 310 deg CA ATDC, the first flame is captured at 336 deg CA ATDC and shows the significant propagation to 356 deg CA ATDC, as shown in Figure 5.38. At the spark timings of 330 and 340 deg CA ATDC, show that a short propagation about 3~4 crank angles appears from the first flame obtained at 358 and 357 deg CA ATDC to 361 and 360 deg CA ATDC. In addition, local auto-ignition occurs as shown at 359 and 358 deg CA ATDC in Figure 5.40 and 5.41 respectively. When spark timing is retarded to TDC, the combustion shows more independent auto-ignition. In Figure 5.42 and 5.43, flame propagation appears for about 1~2 crank angles at spark timings 350 and 360 deg CA ATDC respectively. The spark timing at 360 deg CA ATDC is dominated by the typical characteristic of CAI

combustion. The first flame is obtained at 359 deg CA ATDC and local auto-ignition takes place simultaneously in the entire chamber, shown in Figure 5.43.

Figure 5.38 to 5.43 and Figure 5.14 show also mass fraction burn rate with spark and without spark so that the relative contribution of the flame propagation and auto-ignition can be analyzed. The combustion process starts from around spark plug by spark timing 310 °CA to 340 °CA, but locally starts by 350 °CA and TDC. The MFB curves are gradually increased in the beginning of combustion which indicates the flame propagation and then show steeper gradient, the point of change in the gradient will coincide with the start of autoignition combustion. Table 5.3 shows the comparison with the start combustion (10 % of MFB) and gradient change point of MFB. They indicate clearly that 10 % of MFB or start of combustion are almost same as the each gradient change points of MFB.

Crank Angle (°CA)	10% of MFB	10-90 % of MFB duration	Gradient change point of MFB curves
Spark at 310 °CA BTDC	354	19	355
Spark at 320 °CA BTDC	357	11	357
Spark at 330 °CA BTDC	360	12	360
Spark at 340 °CA BTDC	358	9	358
Spark at 350 °CA BTDC	360	17	359
Spark at 360 °CA BTDC	356	14	356
Without spark	365	8	363

Table 5.3 Start of combustion with 10% of MFB and Gradient change point of MFB

Chemiluminescence images show that the earliest spark timing at 310 ° CA ATDC shows that the first flame appears at 336 ° CA ATDC and ends at 385 ° CA ATDC, duration for about 45 crank angles, whilst the 10-90% of MFB calculated from the in-cylinder pressure measurement is 19 CA. As spark timing takes place at TDC the first flame appears at 359° CA ATDC to the final flame is detected at 377 ° CA ATDC, duration for about 18 crank angles, compared with 14 ° CA of 10-90% of MFB. Operation without spark shows even shorter duration from the first flame at 364 ° CA ATDC to the final flame shown at 372 ° CA ATDC, duration for about 8 crank angles, shown in Figure 5.14, and 10-90% of MFB duration is 7 ° CA.

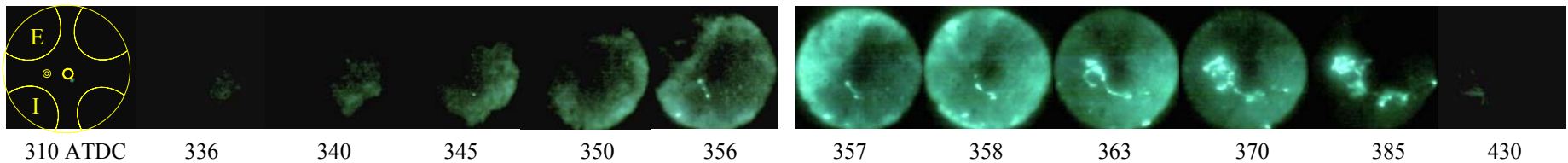
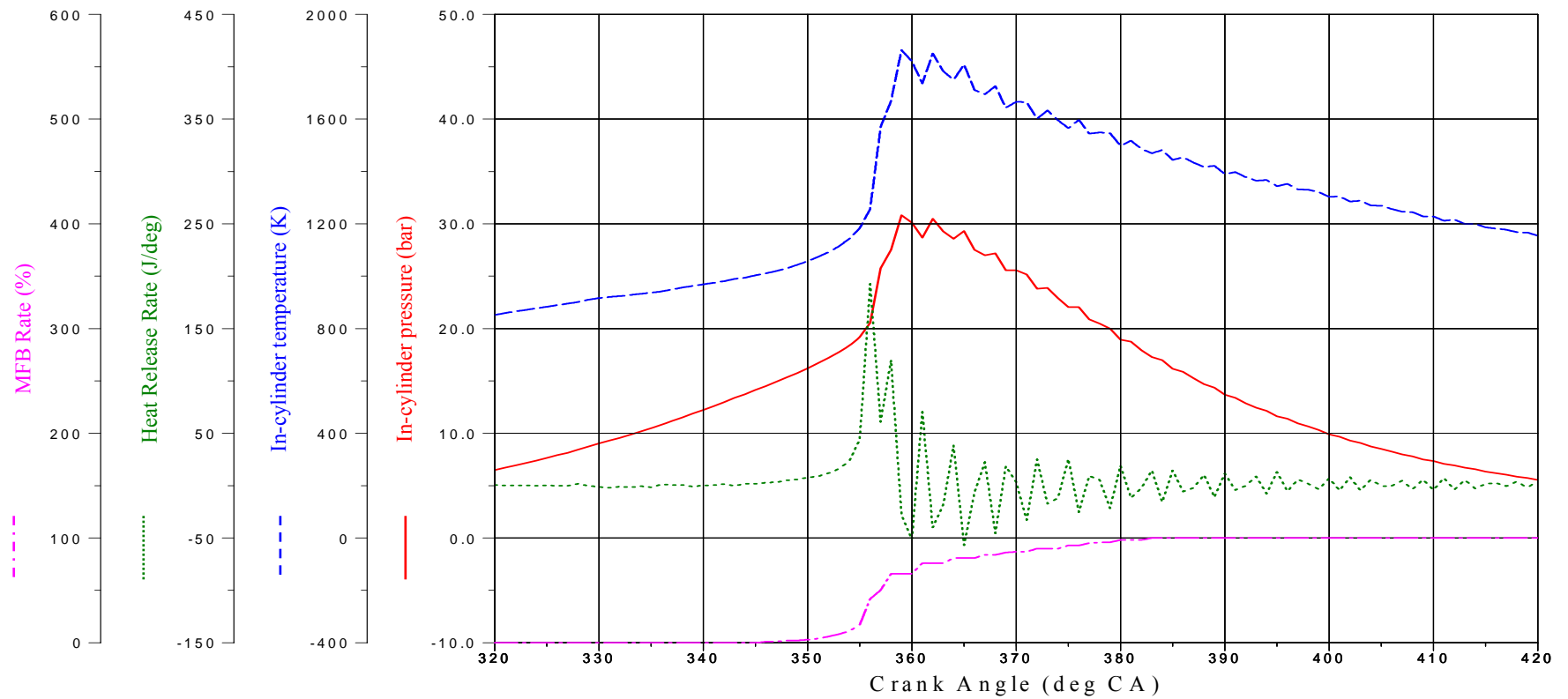


Figure 5.38 In-cylinder pressure, temperature, heat release rate, MFB rate and Full Chemiluminescence images at $\lambda = 1$, 1600rpm, Gain 60%, SOI=80 °CA BTDC and Spark at 310 °CA ATDC.

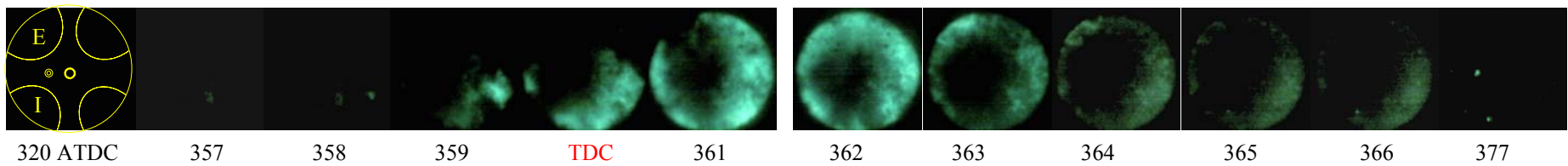
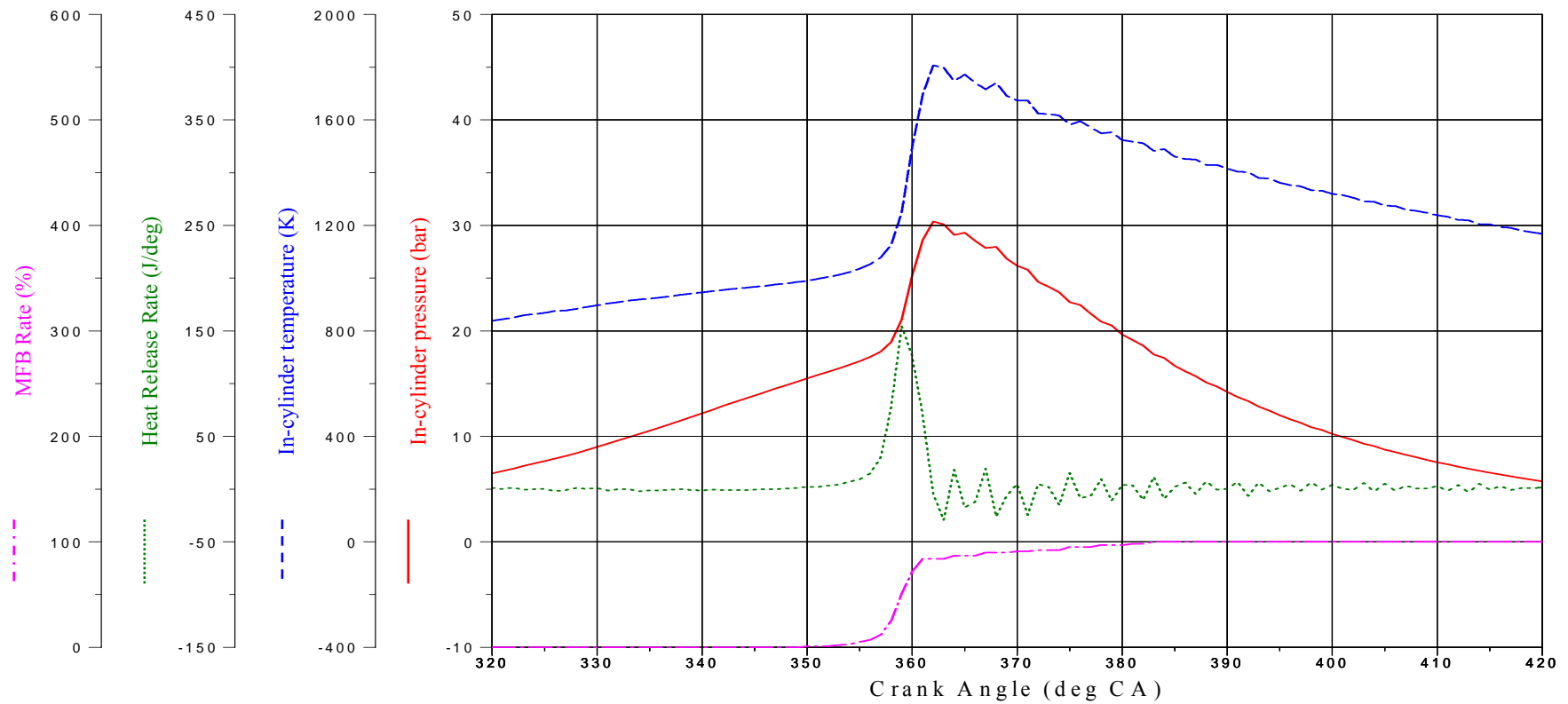


Figure 5.39 In-cylinder pressure, temperature, heat release rate, MFB rate and Full Chemiluminescence images at lambda 1, 1600rpm, Gain 60%, SOI=80 °CA BTDC and Spark at 320 °CA ATDC.

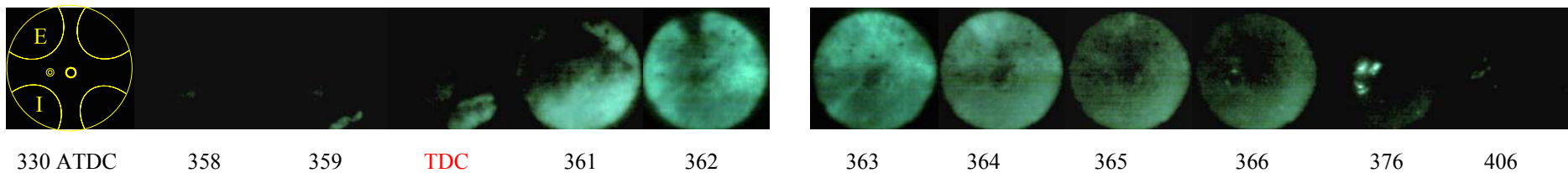
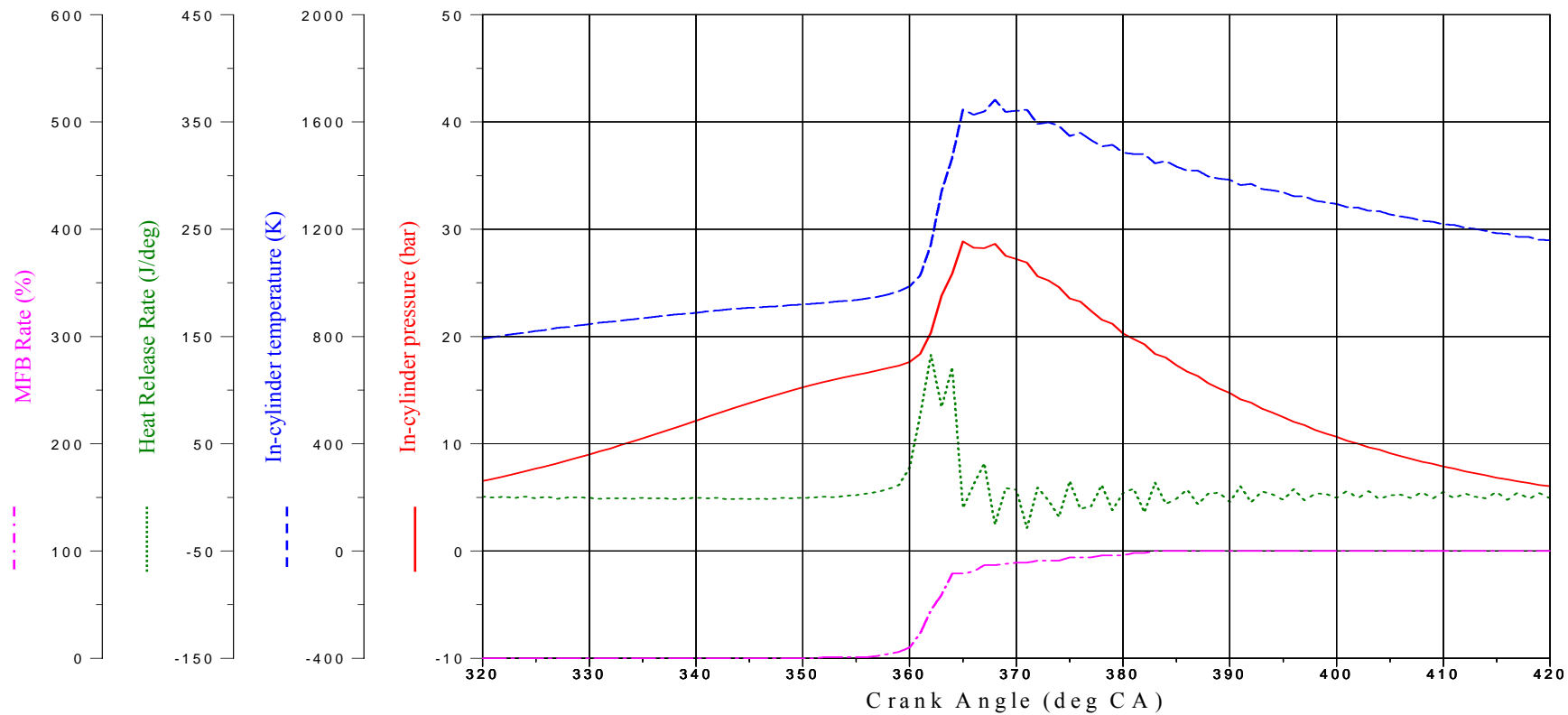


Figure 5.40 In-cylinder pressure, temperature, heat release rate, MFB rate and Full Chemiluminescence images at lambda 1, 1600rpm, Gain 60%, SOI=80 °CA BTDC and Spark at 330 °CA ATDC.

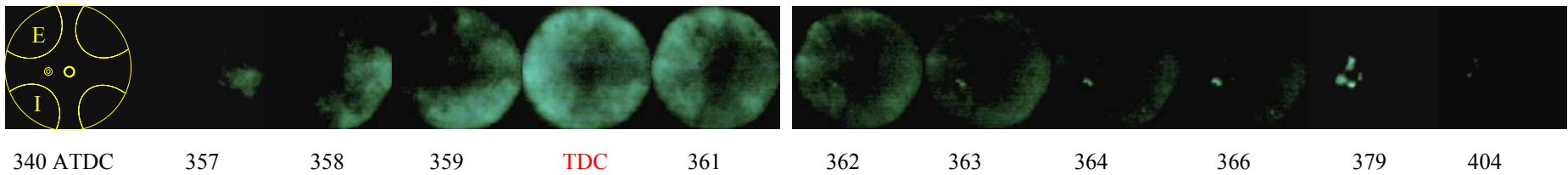
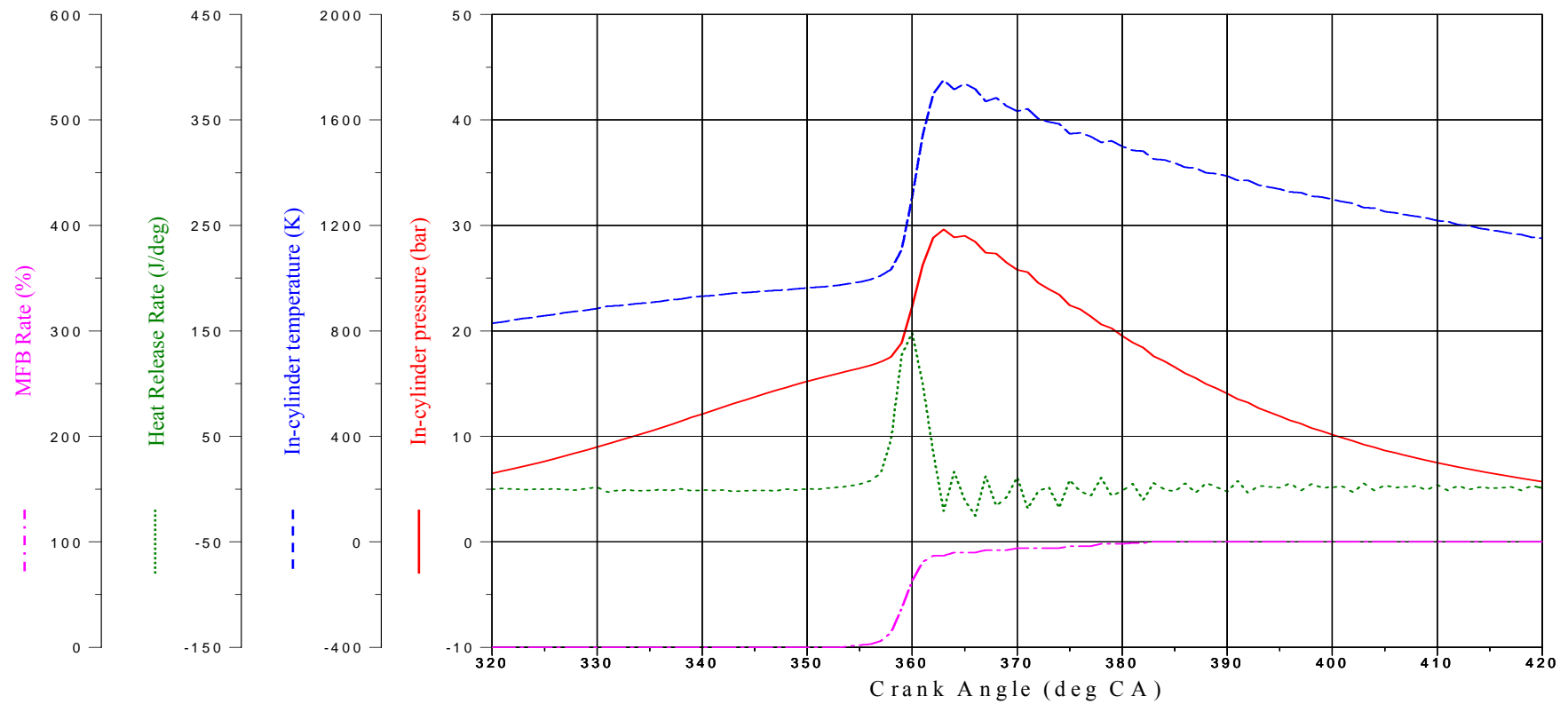


Figure 5.41 In-cylinder pressure, temperature, heat release rate, MFB rate and Full Chemiluminescence images at lambda 1, 1600rpm, Gain 60%, SOI=80 °CA BTDC and Spark at 340 °CA ATDC.

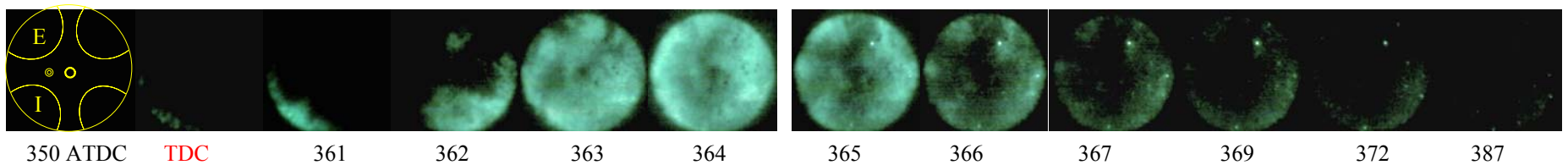
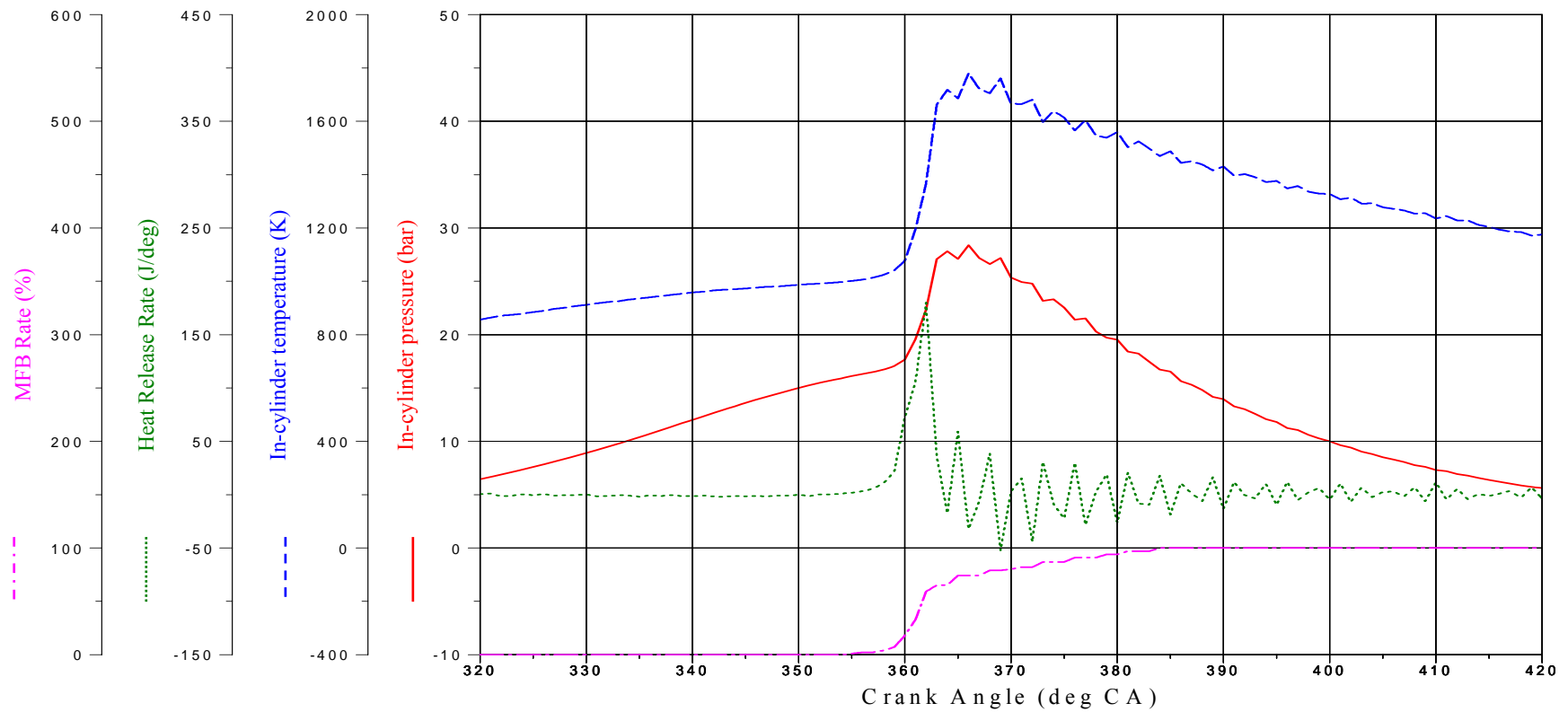


Figure 5.42 In-cylinder pressure, temperature, heat release rate, MFB rate and Full Chemiluminescence images at lambda 1, 1600rpm, Gain 60%, SOI=80 °CA BTDC and Spark at 350 °CA ATDC.

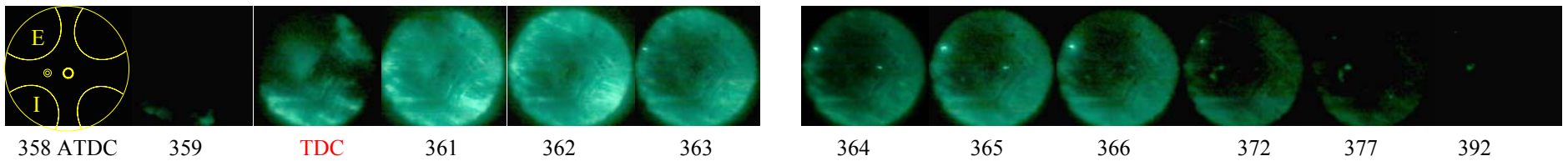
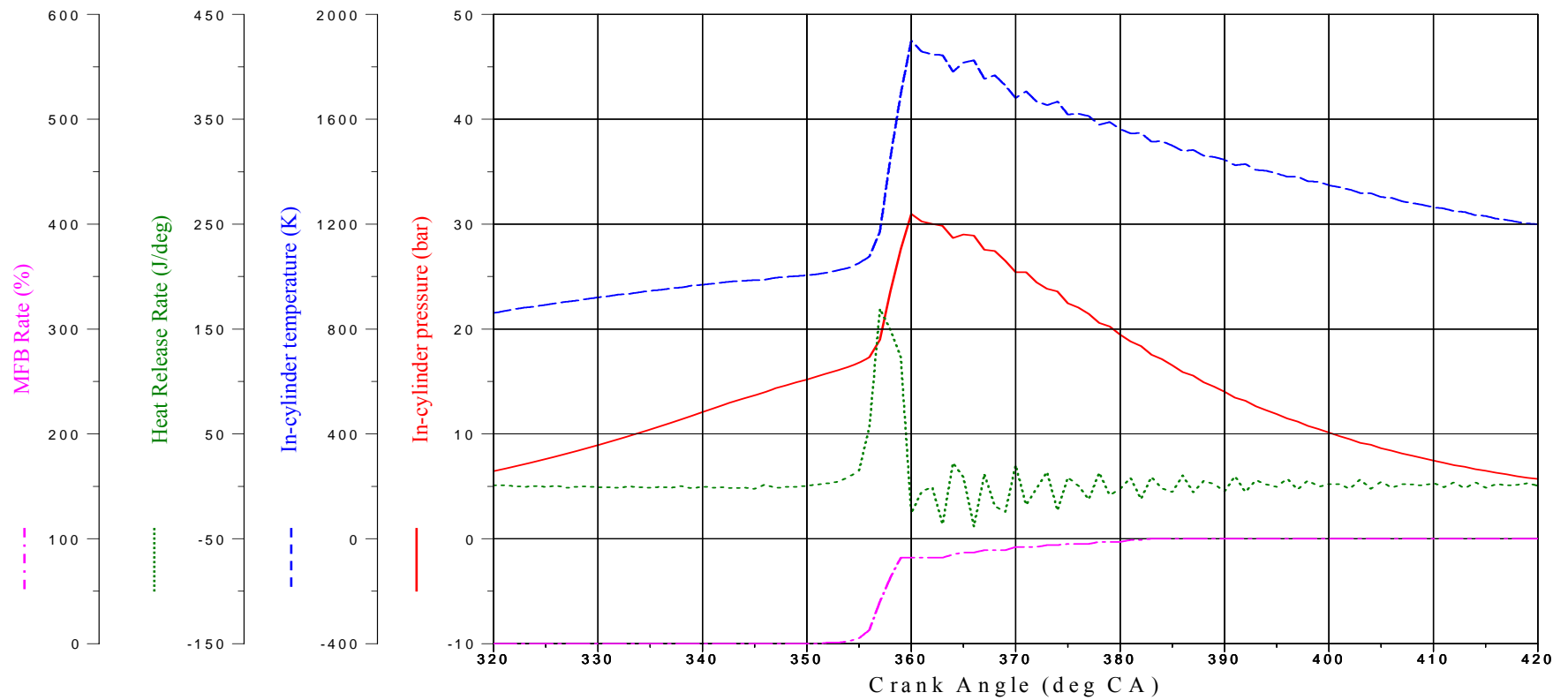


Figure 5.43 In-cylinder pressure, temperature, heat release rate, MFB rate and Full Chemiluminescence images at lambda 1, 1600rpm, Gain 60%, SOI=80 °CA BTDC and Spark at 360 °CA ATDC.

5.4.3 Effect of Air-Fuel Ratio at Lambda 1 and 1.2

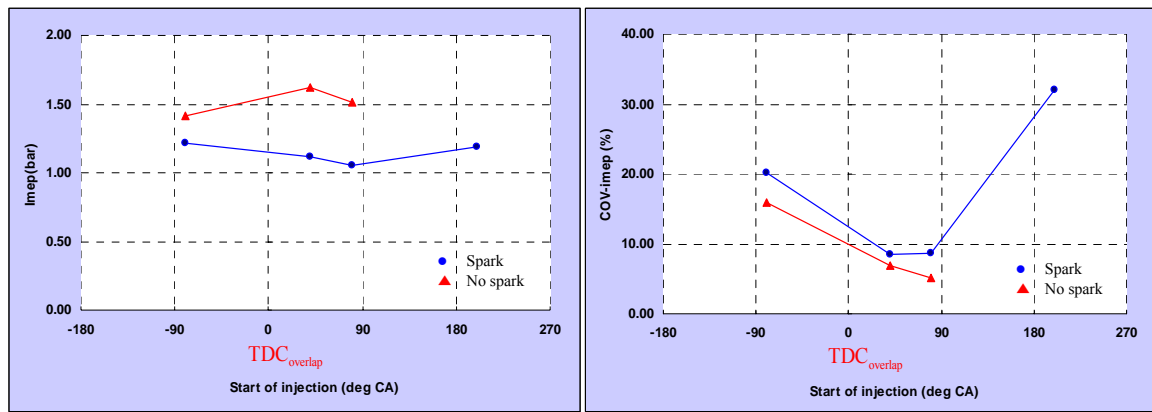
5.4.3.1 Introduction

The CAI operation has been investigated in application of commercial uses compared to SI operation by means of significant reduction of NO_x emissions and fuel consumption. SI operation in production is restricted to stoichiometric conditions in order to reduce emissions since three-way catalysts are only functional at lambda 1. However, whilst CAI combustion introduced extremely lower NO_x emissions and fuel consumption at stoichiometric conditions, it is interesting to further investigate CAI characteristics at lean condition. In particular, the presence of oxygen in the trapped residuals offers the opportunity to promote the heat release reactions when fuel is injected into hot residual gases during the negative valve overlap period

The test procedure and data analysis at lambda 1.2 are performed with different direct injection timings, presence and absence of spark in the same way as at lambda 1, engine speed 1600rpm, EVC/IVO at 280 °CA ATDC/440 CA deg ATDC and spark timing at 320 °CA ATDC.

5.4.3.2 Engine performance at lambda 1.2

Figure 5.44 show the results of engine loads and combustion stability with direct fuel injection timings both with spark and no spark assistance at lambda 1.2. Engine operation is achieved at slightly lower load region, which means that leaner conditions show the potential to enlarge the CAI operational region in the lower load range. The maximum engine load is achieved at about IMEP 1.7 bar without spark assistance at injection timing of 40 deg CA ATDC during the negative valve overlap period. The early injection timing results in the highest IMEP of 1.25 bar with spark assistance, but showing unacceptable cyclic variation. Compared with results at Lambda 1.0 (Figure 5.6), results in Figure 5.44b shows that cyclic variations are higher and more prone to misfire with leaner mixtures.



a) Engine loads in CAI

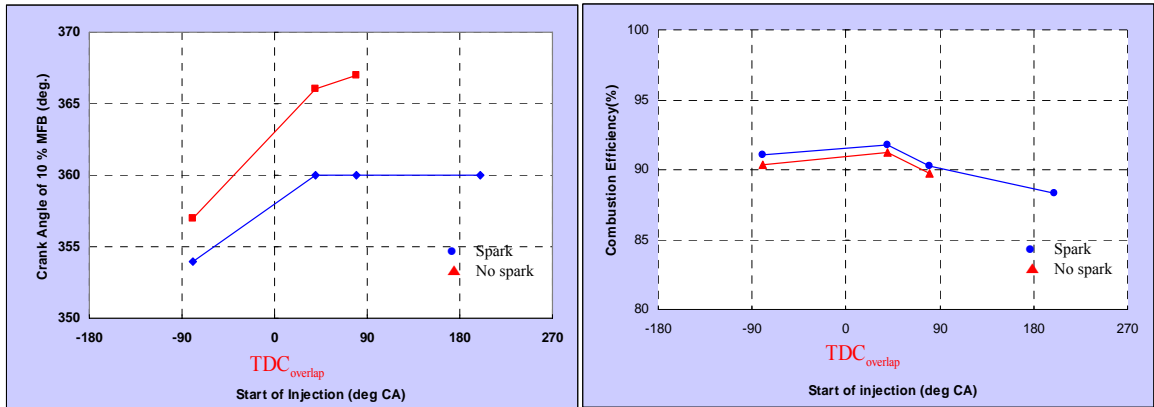
b) Combustion stability in CAI

Figure 5.44 Engine loads and CoVimep at lambda 1.2

Figure 5.44 clearly presents that leaner condition of lambda 1.2 does not provide stable combustion at early and late injection timings due to earlier start of combustion and not enough time for the air-fuel mixture and trapped residual. In spite of reasonable level of engine performance, mid-injection timings are also very high cyclic variations since higher quantity of residual are trapped. As a result, mid-injection timings offer the optimized condition for CAI combustion in terms of engine performance and cyclic variation. The injection timing during the negative valve overlap period shows better engine imep than at intake valve opening timing.

5.4.3.3 Combustion characteristics at lambda 1.2

Figure 5.45 shows the results of start of combustion and combustion efficiency at lambda 1.2. The early injection timing leads to CAI combustion to start earlier than TDC, while CAI with spark assistance at early injection timing is not acceptable due to the high cyclic variation. The results show that the best combustion efficiency appeared at injection timing 40 deg CA ATDC. The spark assisted CAI with mid-injection timings was initiated near by TDC, but results in the lower engine loads than by no spark assistance since more residual is trapped, leading to lower engine loads. Figure 5.45b shows that the spark assisted CAI performs better combustion efficiency in spite of higher cyclic variation and lower engine performance. In comparison with the starts of spark assisted CAI combustion at lambda 1 shown in Figure 5.7a and at lambda 1.2 shown in Figure 5.45a, it appears that spark ignition has more pronounced effects in the stoichiometric mixture than the lean mixture as flame becomes more difficult to develop and propagate in a leaner as well as diluted mixture.



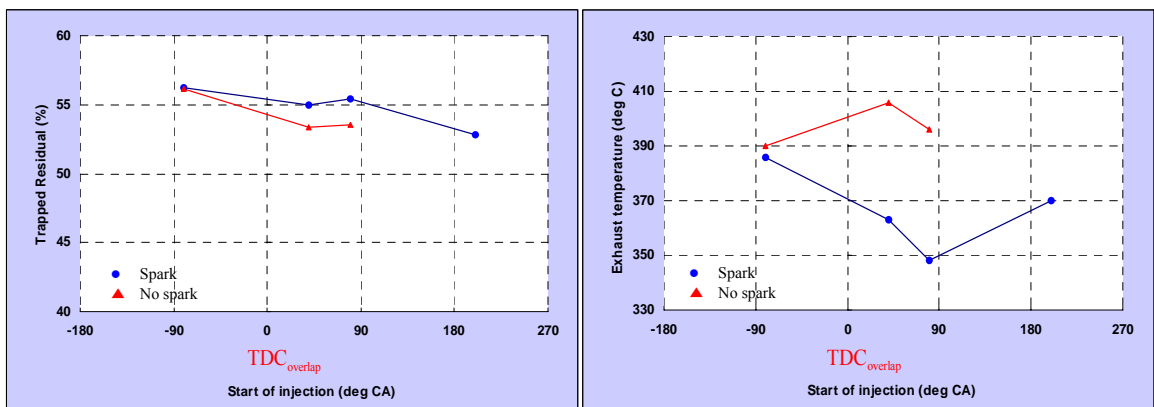
a) Start of combustion

b) Combustion efficiency

Figure 5.45 10 % of MFB and combustion efficiency at lambda 1.2

High engine loads without spark assistance at lambda 1.2 are achieved at mid-injection timings, particularly at 40 °CA ATDC, leading to higher exhaust temperature of about 395 and 405 °C, shown in figure 5.46b. While more residual is trapped in spark assisted CAI at mid-injection timings about 55 %, it provides lower engine loads and lower combustion temperature, but higher level of NOx emissions, shown in figure 5.48a.

Engine operations at early and late injection timings are not acceptable in this study due to high cyclic variations of COVimep of more than 10 %. Figure 5.45 shows the results of residual rate and exhaust temperature at lambda 1.2. The early injection timing in both spark and no spark assistance cause the highest rate of trapped residual as those injection timings advanced the combustion phasing further than TDC. The higher engine output at late injection with spark assistance is achieved at IMEP of 1.2 bar due to lower rate of trapped residual.



a) Trapped residual

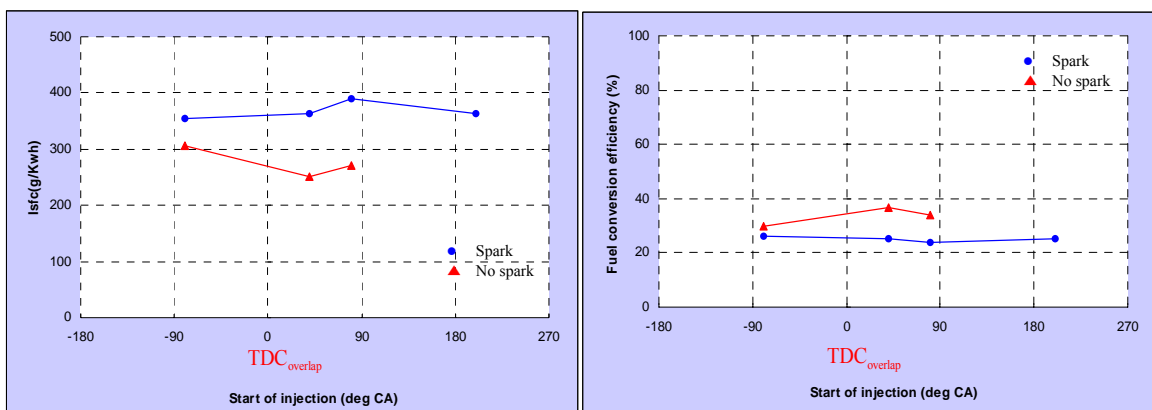
b) Exhaust temperature

Figure 5.46 Residual concentration and Exhaust temperature at lambda 1.2

5.4.3.4 Fuel consumption and emissions at lambda 1.2

Figure 5.47 presents the results of fuel consumption at lambda 1.2. The trends are very similar to the results at lambda 1. Mid injection timings with spark assistance result in higher indicated specific fuel consumption than without spark assistance because more residual is trapped, leading to dilution effect in the mixture shown in Figure 5.47a.

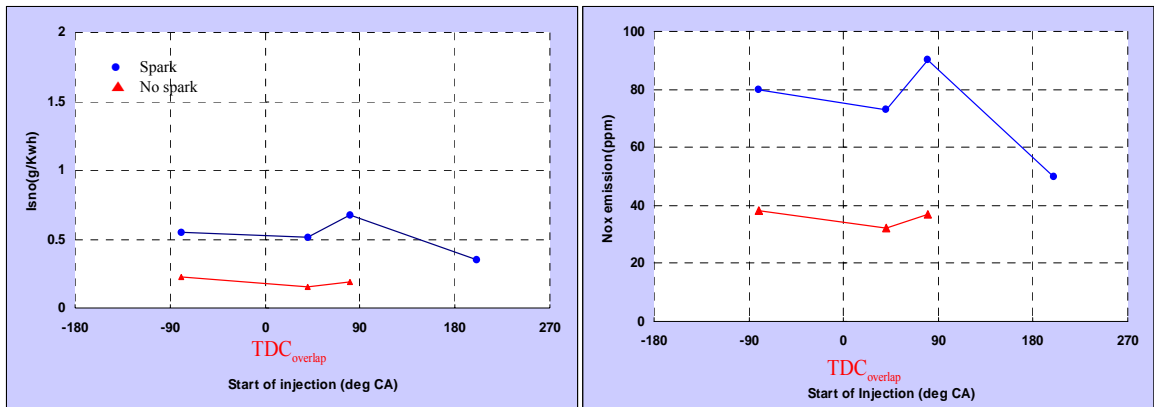
The lowest fuel consumption at lambda 1.2 is accomplished without spark assistance by injection timing at 40 °CA ATDC, during the negative valve overlap period. Figure 5.48 shows the results of emissions at lambda 1.2. As expected, the higher level of NOx emissions are obtained with spark assistance at lambda 1.2 since advanced combustion phasing causes higher heat release rate and higher in-cylinder pressure, temperature, hence resulting in higher NOx emission. Since the level of NOx emissions is dependant on the in-cylinder temperature, higher in-cylinder temperature results in higher level of NOx emissions compared to combustion without spark assistance. In addition, spark assistance initiates combustion earlier and causes the lack of time for the air-fuel mixture and trapped residual, resulting in higher level of emissions. In comparison with injection timings at 40 deg CA ATDC and 80 deg CA ATDC, more residual is trapped by injection timing at 80 deg CA ATDC and lead to higher level of NOx emissions. The level of NOx emissions is very sensitive at the rate of trapped residual with higher EGR rate of around 55 %. The late injection timing at 200 deg CA ATDC at lambda 1.2 shows the lower level of NOx emissions as unacceptable high CoVimep, resulting in incomplete combustion and showing very high level of uHC and CO emissions.



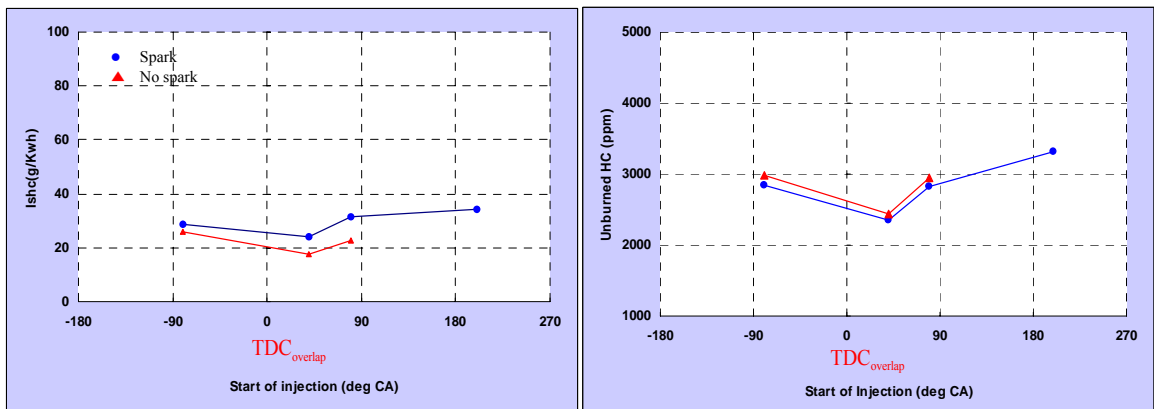
a) ISFC

b) Fuel conversion efficiency

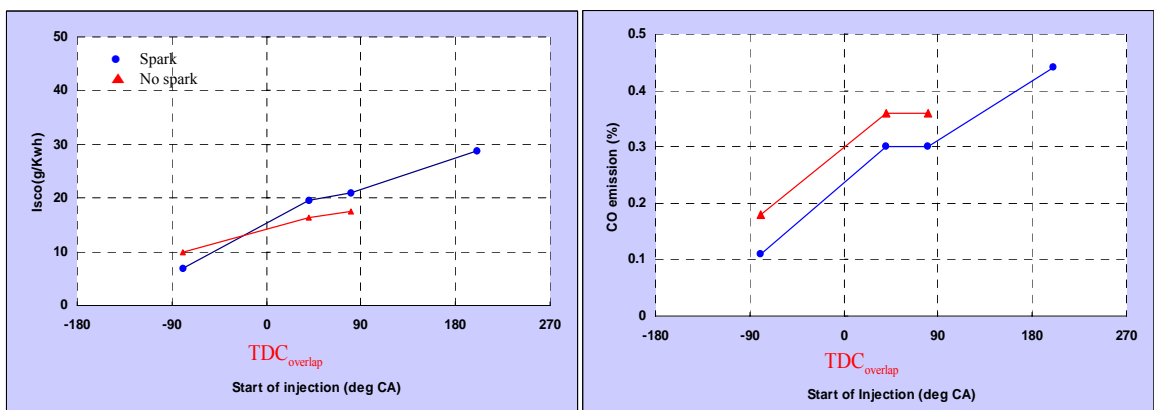
Figure 5.47 Fuel consumption at lambda 1.2



a) NOx emissions at lambda 1.2



b) uHC emissions at lambda 1.2



c) CO emissions at lambda 1.2

Figure 5.48 Emissions in CAI at lambda 1.2

Figure 5.48 shows the results of emissions at lambda 1.2. As expected, the higher level of NOx emissions are obtained with spark assistance at lambda 1.2 since the higher rate of trapped residual provides higher in-cylinder temperature. Since the level of NOx emissions is dependant on the in-cylinder temperature, higher in-

cylinder temperature results IN higher level of NO_x emissions compared to combustion without spark assistance. In addition, spark assistance initiates combustion earlier and causes the lack of time for the air-fuel mixture and trapped residual, resulting in higher level of emissions. In comparison with injection timings at 40 °CA ATDC and 80 °CA ATDC, more residual is trapped by injection timing at 80 °CA ATDC and lead to higher level of NO_x emissions. The level of NO_x emissions is very sensitive at the rate of trapped residual with higher EGR rate of around 55 %. The late injection timing at 200 °CA ATDC at lambda 1.2 shows the lower level of NO_x emissions as unacceptable high CoVimep, resulting in incomplete combustion and showing very high level of uHC and CO emissions.

Figure 5.48b shows the level of uHC emissions at lambda 1.2. The trends of uHC emissions are shown similar to the results in lambda 1. The higher level of uHC emissions in spark assisted CAI is appeared than in spark discharged CAI since the spark provides earlier start of combustion and less time to mixing the mixture with trapped residual, resulting higher level of uHC emissions. The level of CO emissions at lambda 1.2 is much higher than at lambda 1, shown in Figure 5.48c as the leaner condition and more trapped residual leads to incomplete combustion. As a result, higher level of CO emissions obtained.

5.4.3.5 Simultaneous in-cylinder studies and chemiluminescence

5.4.3.5.1 Introduction

The full chemiluminescence, OH and CHO radical are achieved at lambda 1. However, early injection timing in case of both with and without spark assistance does not provide good chemiluminescence intensity due to unstable combustion. The late injection timings cause misfire, which is extremely difficult to capture video footage of chemiluminescence. Therefore, the results obtained mostly by the mid-injection timings and are presented in this section. The results were obtained at 1600 rpm, lambda 1.2, and EVC/IVC at 280 °CA ATDC/440 °CA ATDC, spark timing of 320 °CA ATDC and various injection timings at 80 °CA BTDC, 40 °CA ATDC, 80 °CA ATDC and 200 °CA ATDC .

5.4.3.5.2 Simultaneous In-cylinder studies at lambda 1 and 1.2

Figure 5.50 ~ 5.57 show the simultaneous in-cylinder pressure, temperature and heat release rate at lambda 1.2. The start of combustion in lean CAI combustion is retarded compared to stoichiometric due to the less charge cooling effect. Direct injection is introduced into the hot and more residual gas, causing charge cooling effect. However, less charge cooling effect is occurred at leaner condition since less quantity of fuel is vaporized, leading to the late start of combustion compared to stoichiometric. In addition, in-cylinder pressure, temperature and heat release rate are shown lower than at lambda 1 since lower fuel quantity and retarded start of combustion experienced.

The charge cooling effect is occurred at all injection timing strategy. This charge cooling effect leads to lower pumping work since it reduces compression work during the NVO. Higher pumping work is experienced during the NVO, leading to less minor heat released compared to the early and late injection timings, shown in Table 5.4 and Figure 5.49. As a result, injection at 40 °CA ATDC and during the NVO presents relatively less retarded the start of combustion, resulting in the optimized engine IMEP of 1.62 bar without spark assistance.

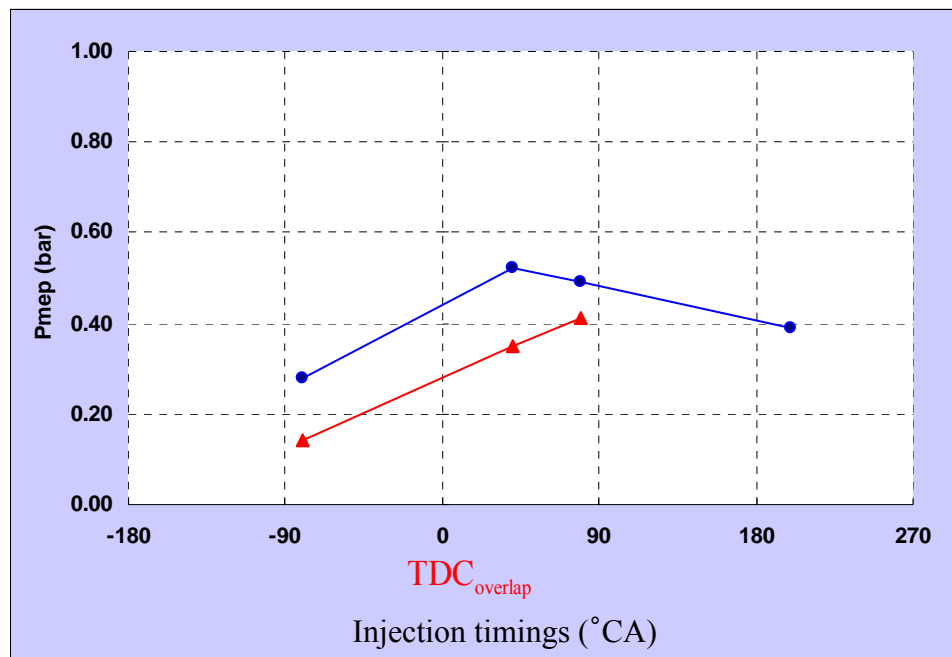


Figure 5.49 PMEP at lambda 1.2

SOI °CA		80	40	80	200
		BTDC	ATDC	ATDC	ATDC
IMEP(bar)	Spark	1.22	1.12	1.05	1.19
	no spark	1.41	1.62	1.51	x
PMEP(bar)	Spark	0.28	0.52	0.49	0.39
	no spark	0.14	0.35	0.41	x

Table 5.4 IMEP and PMEP at lambda 1.2

The minor heat release, ideally mini combustion during the NVO is shown with simultaneous results. The rate of heat released during the NVO does not appear significant difference, but significant pressure and temperature increase by charge cooling effect during the NVO. As the early injection shows the lower pumping work, it presents the most significant increase heat release rate during the NVO in either case with and without spark assistance, shown in figure 5.51.

Although the mid-injection timings are affected by less cooling the charge than the early injection timing, mid-injection timings show the dominant heat release rate, leading to higher in-cylinder pressure and temperature, shown in figure 5.53 and 5.55 respectively. Injection at 40 °CA ATDC during the NVO takes more effect, but it presents similar level of heat release during the NVO due to the higher pumping work. Injection at 80 °CA ATDC, intake valve opening timing provides less pumping work and shows the significant charge cooling effect, leading to higher heat release rate, in-cylinder pressure and temperature. In addition, the start of combustion is advanced not only by the charge cooling effect but also by the spark assistance, showing earlier than stoichiometric with spark assistance.

The late injection at 200 °CA ATDC, exhaust valve closing timing shows no charge cooling effect, but stratification of mixture with locally higher temperature in the richer pocket of fuel in the chamber, leading to earlier start of combustion than stoichiometric. Stratification is caused by less well mixed air/fuel mixture due to less air flow.

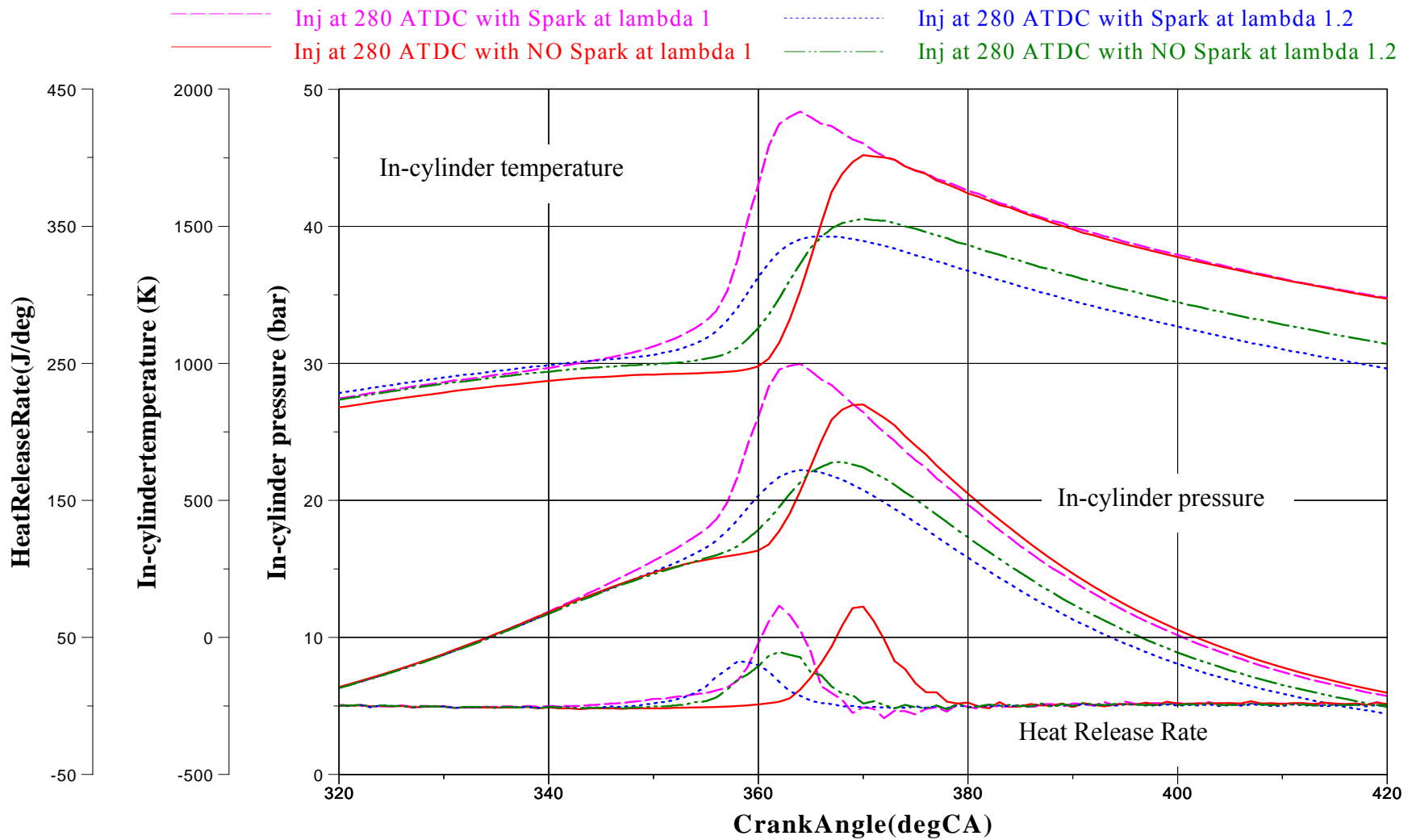


Figure 5.50 Simultaneous In-cylinder pressure, temperature, heat release rate at lambda 1 and 1.2, 1600rpm, SOI=80 °CA BTDC and Spark at 320 ATDC.

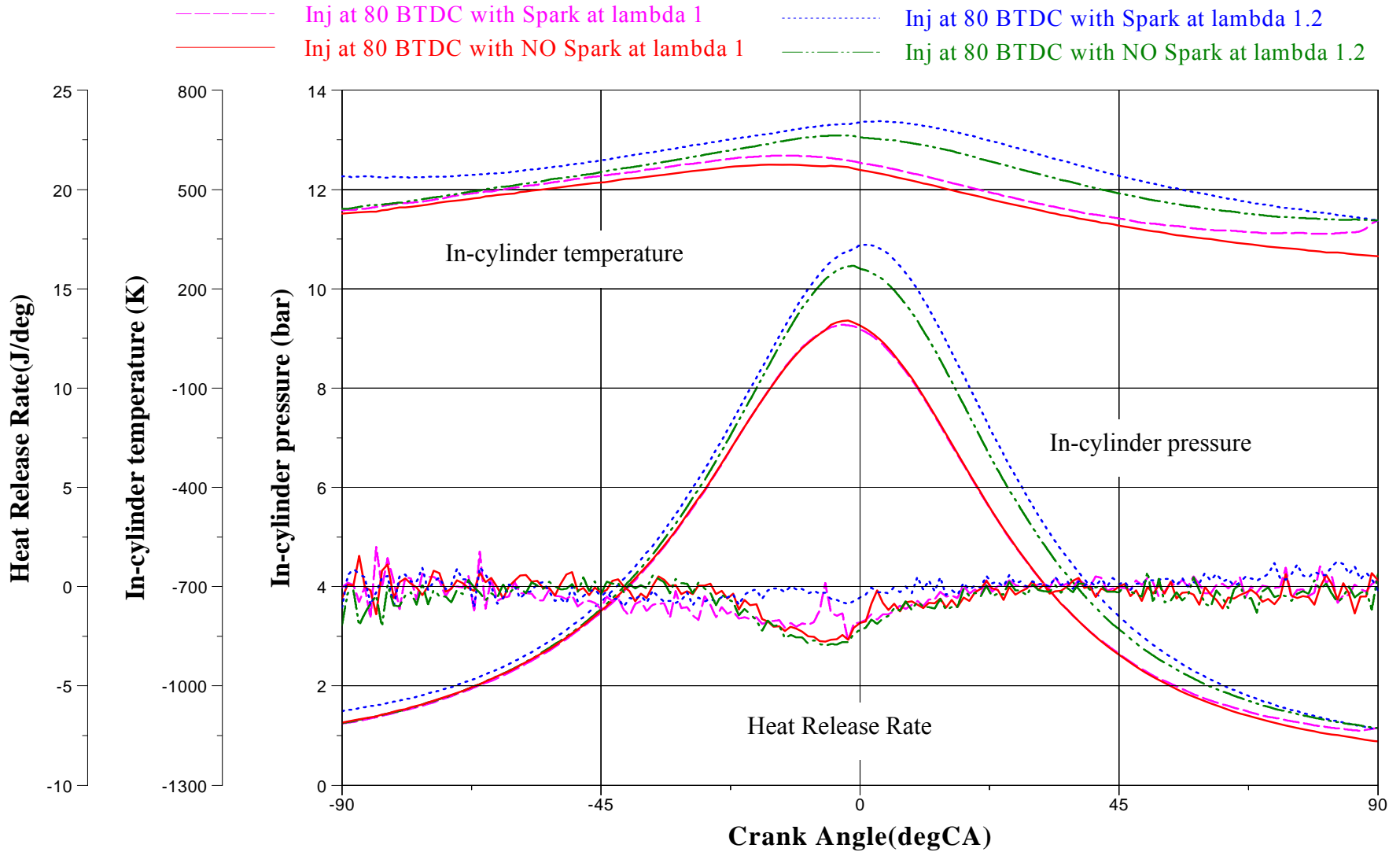


Figure 5.51 Simultaneous In-cylinder pressure, temperature, heat release rate in recompression stroke at lambda 1 and 1.2, 1600rpm, SOI=80 °CA BTDC and Spark at 320 ATDC.

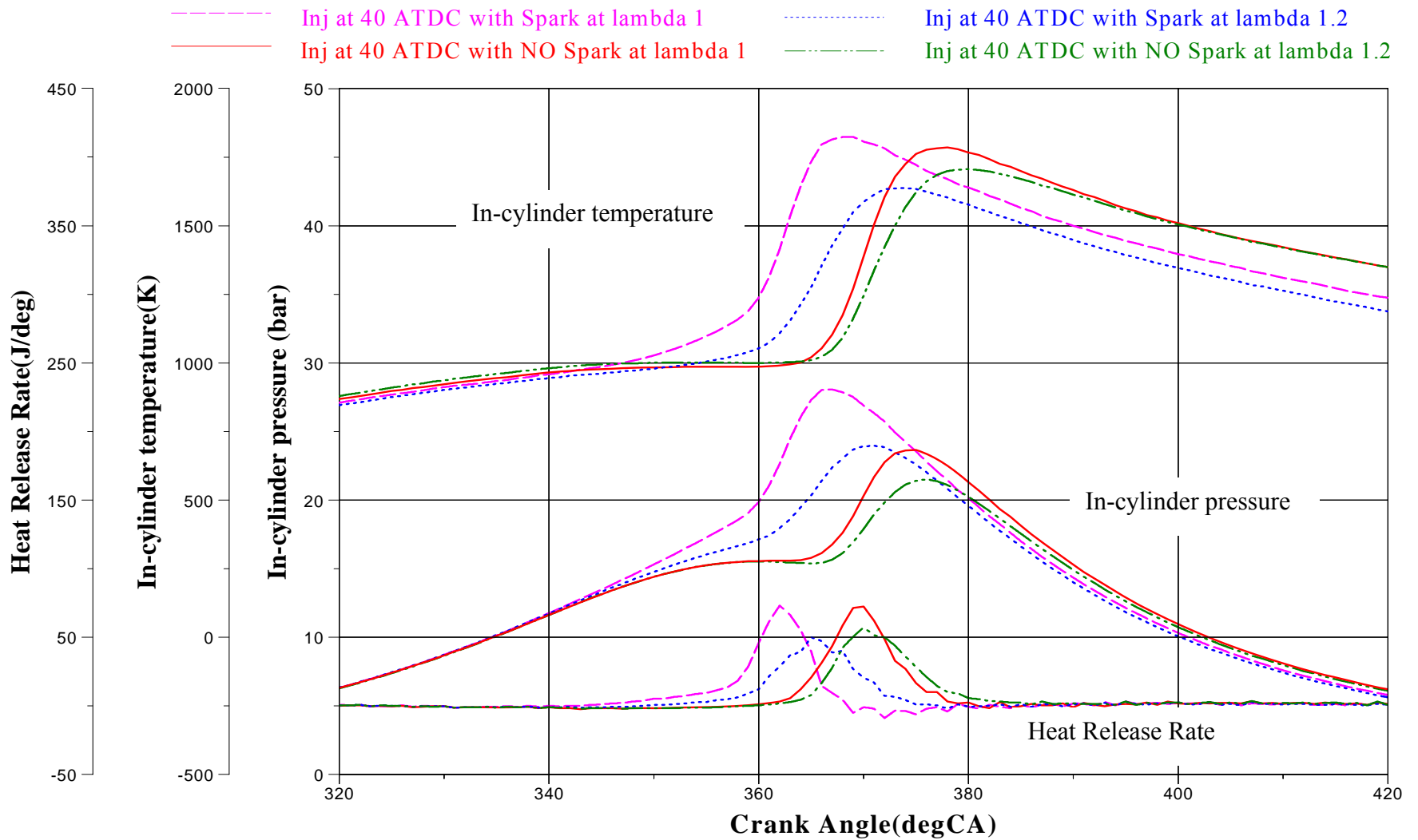


Figure 5.52 Simultaneous In-cylinder pressure, temperature, heat release rate at lambda 1 and 1.2, 1600rpm, SOI=40 °CA BTDC and Spark at 320 ATDC.

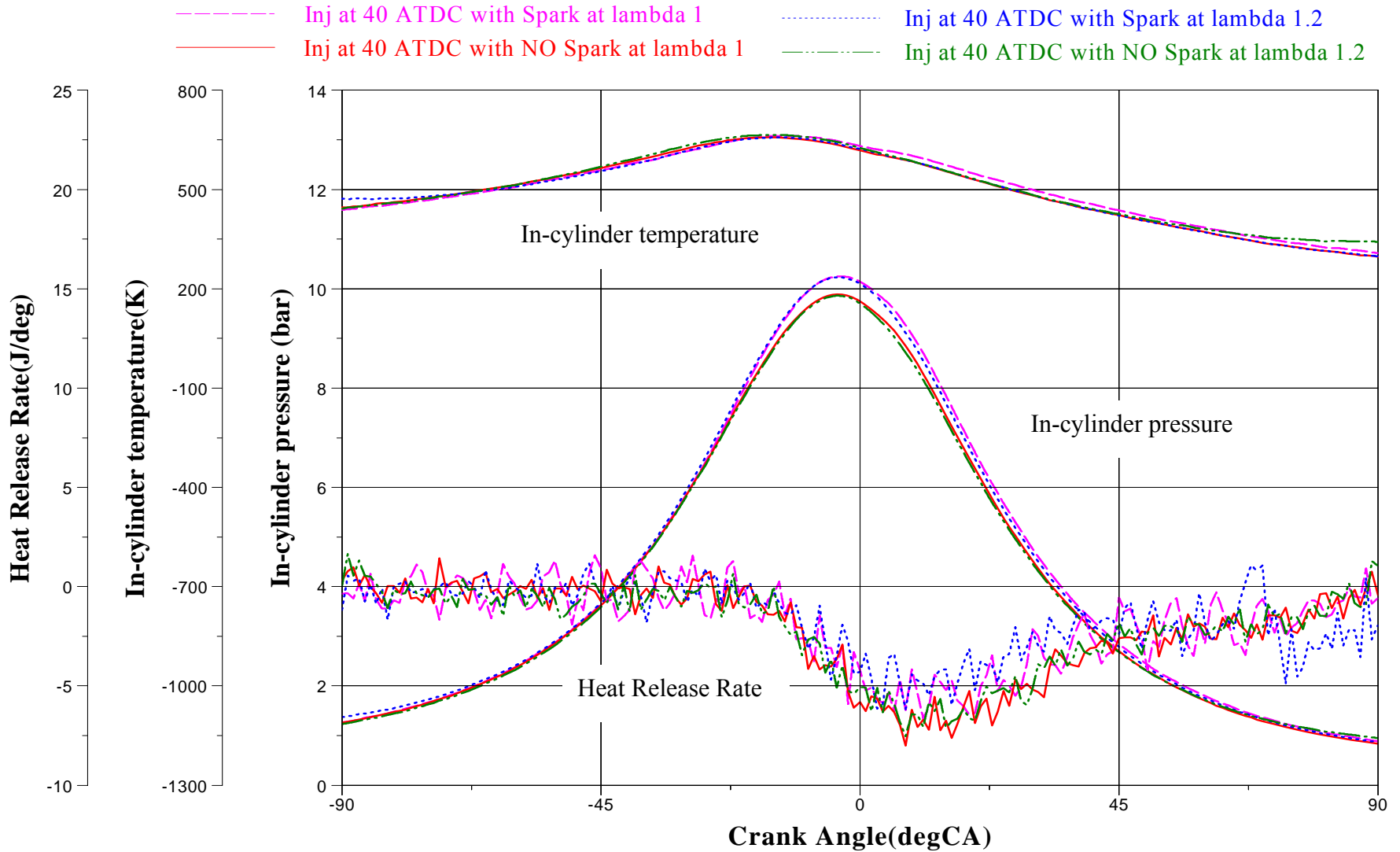


Figure 5.53 Simultaneous In-cylinder pressure, temperature, heat release rate in recompression stroke at lambda 1 and 1.2, 1600rpm, SOI=40 °CA BTDC and Spark at 320 ATDC.

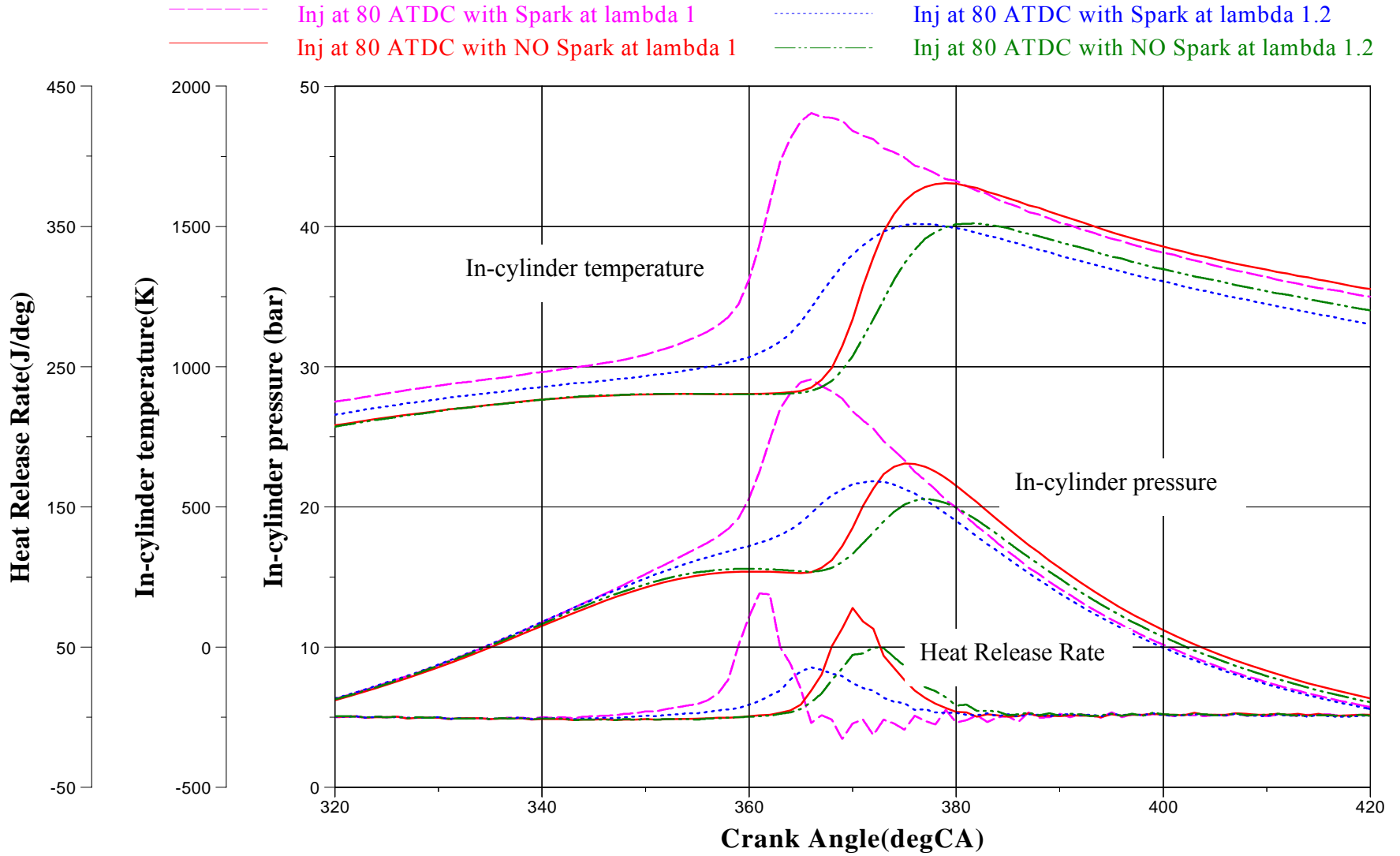


Figure 5.54 Simultaneous In-cylinder pressure, temperature, heat release rate at lambda 1 and 1.2, 1600rpm, SOI=80 °CA ATDC and Spark at 320 ATDC.

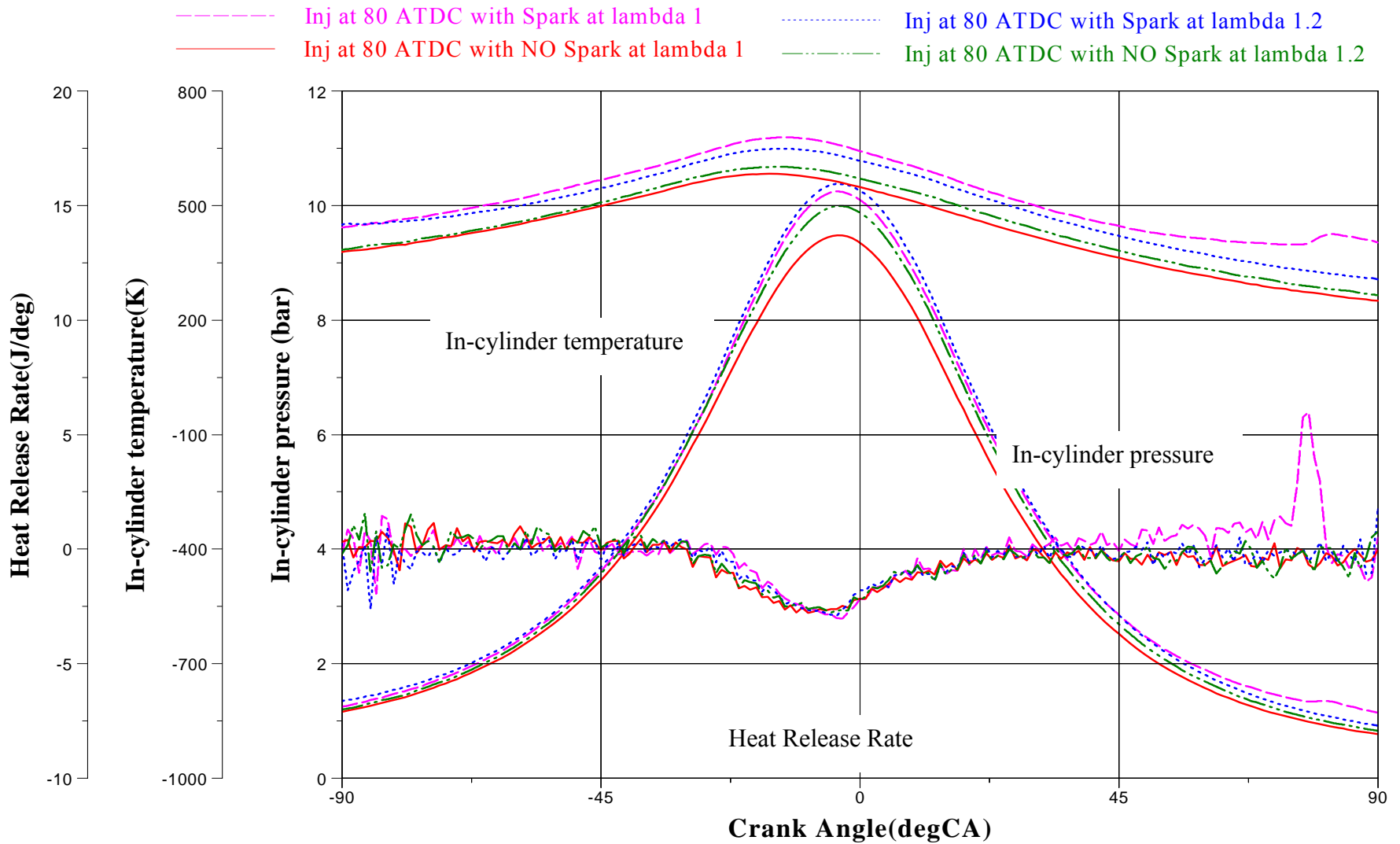


Figure 5.55 Simultaneous In-cylinder pressure, temperature, heat release rate in recompression stroke at lambda 1 and 1.2, 1600rpm, SOI=80 °CA ATDC and Spark at 320 ATDC.

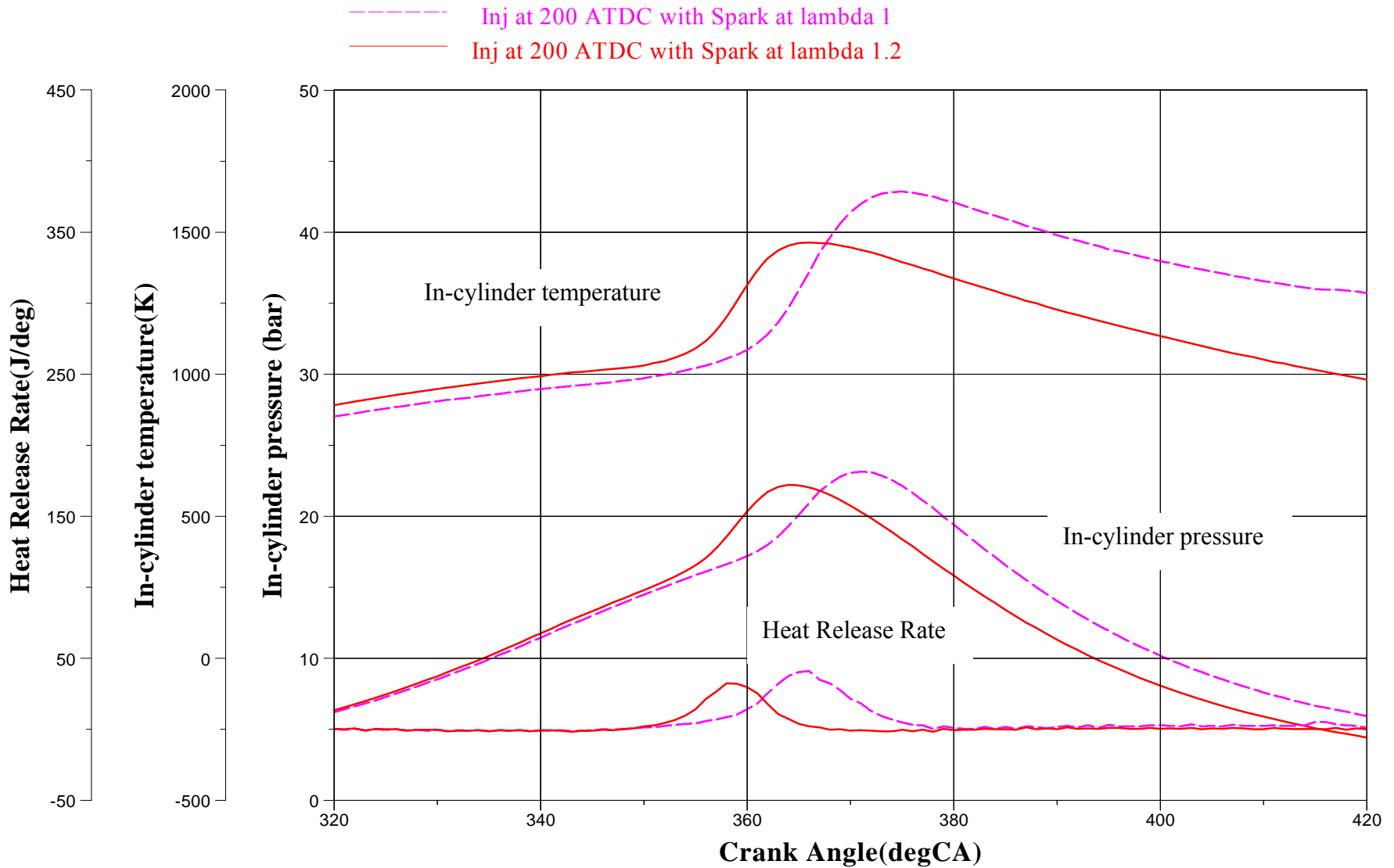


Figure 5.56 Simultaneous In-cylinder pressure, temperature, heat release rate at lambda 1 and 1.2, 1600rpm, SOI=200 °CA BTDC and Spark at 320 ATDC.

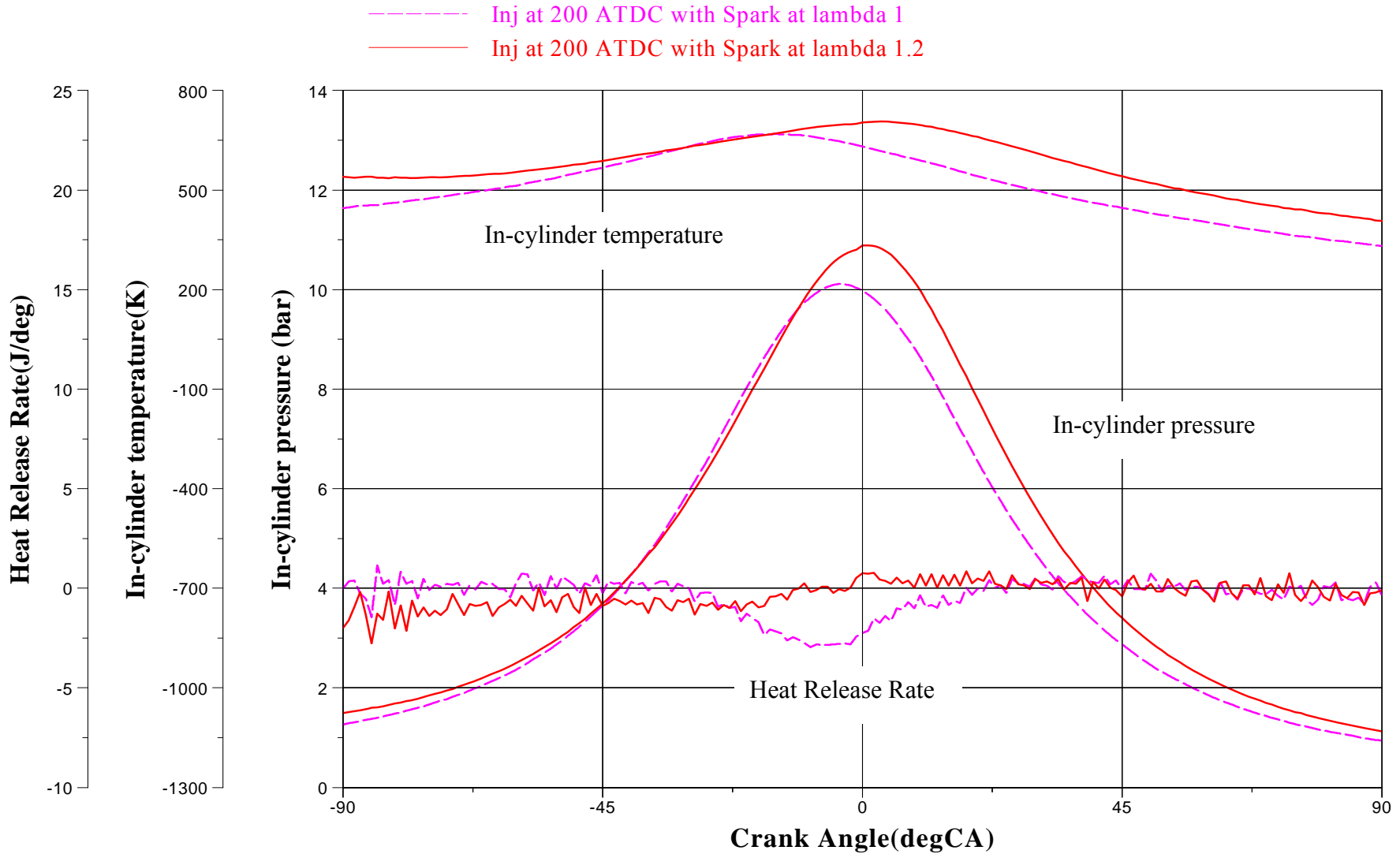


Figure 5.57 Simultaneous In-cylinder pressure, temperature, heat release rate in recompression stroke at lambda 1 and 1.2, 1600rpm, SOI=200 °CA BTDC and Spark at 320 ATDC.

5.4.3.5.3 Full chemiluminescence

In this section, results will be presented for the simultaneous in-cylinder pressure, temperature, heat release rate and full chemiluminescence images from the same engine cycle, which was selected for the best video images. The results were obtained for both with spark and without spark assistance at λ 1.2 at an engine speed of 1600 rpm, EVC=280 °CA ATDC, IVO=440 °CA ATDC at different fuel injection timings. The spark discharge was timed at 320 °CA ATDC and the first video image has been selected to show the first visible combustion.

CASE 1: Early injection during the NVO period (SOI=80 °CA BTDC)— the in-cylinder results during the main combustion period in Figure 5.58 and Figure 5.59 demonstrate that the spark discharge had little effect on the main combustion and heat release process when the relative air and fuel ratio was increased to 1.2. There is no evidence of flame propagation. Combustion started at 359°CA ATDC irrespective of the spark presence. The combustion process was dominated by the multiple autoignited combustion that started and took place mostly away from the spark plug location at the peripheral regions of the combustion chamber.

As shown in Figure 5.51 and discussed previously, higher in-cylinder gas temperature was observed with the leaner mixture than the stoichiometric mixture during the NVO period. It was postulated that the higher temperature was caused by the minor heat release during the NVO period. But this was not evident from the heat release rate curve due to the small amount of heat released. In comparison, the presence of chemiluminescence emission is known to be a more sensitive method to detect endothermic reactions. Figure 5.65 shows the chemiluminescence images together with in-cylinder pressure and temperature histories during the NVO period, the presence of minor heat release can be indirectly identified from the absence of dip in the heat release rate curve near TDC, which is associated with the charge cooling effect of the evaporating fuel spray. The visible chemiluminescence images confirm directly the presence of such process. But perhaps surprisingly, the chemiluminescence emission became visible at the intake valve opening time, which indicates that there was an ignition delay from the end of the fuel injection. The ignition delay could have been caused by not only slow chemical reactions but also

the mixing process. The fuel was injected in the middle of chamber and mixed with hot residual gas. Due to the lack of sufficient oxygen concentration, the heat release reactions would be very slow. As the intake valve opened, air was rushed in and started mixing with fuel and residual gas. As a result, the heat release reactions would take place more quickly in the presence of fresh oxygen at the boundary between the fuel containing hot residual and fresh air. In order to verify such events, simultaneous in-cylinder spatially resolved measurements of residual, air, fuel and temperature would be required.

CASE 2: Mid injection during the end of NVO (SOI=40°CA ATDC) and the start of intake period (SOI=80°CA ATDC) — As shown in Figure 5.60 and Figure 5.62, for both injection timings flames were detected from the spark plug and propagated from 331 to 364 deg CA ATDC for the end of NVO injection and from 338 to 365 deg CA ATDC for SOI= 80 deg CA ATDC. In addition, it is noted that as the SOI timing was delayed from 40 to 80 °CA ATDC, the after-burn event as shown by the brighter areas towards the end of the combustion process becomes more evident, which could have been caused by the fuel rich pockets present.

In the absence of spark discharge, the first visible combustion was delayed and appeared near or after TDC both injection timings, as shown in Figure 5.61 and Figure 5.63. It is noted from Figure 5.61 the combustion started around the spark plug in this particular cycle, probably caused by the hot spark plug. As the injection was delayed into the intake process, bright spots appear in the combustion images, indicating the burning of fuel rich pocket or soot particles.

CASE 3: Late injection during the compression (SOI=200oCA ATDC) — In this case, the engine could not operate stably without spark ignition. Figure 6.64 shows the in-cylinder temperature, pressure, heat release rate curves and the chemiluminescence images with spark ignition at 320 °CA ATDC. The first combustion emission was detected at 356 °CA ATDC. Despite the presence of spark ignition, the combustion appears to be dominated by autoignited combustion at several locations. Compared to other cases, the combustion images seem to indicate more localized and isolated combustion sites, probably due to the inhomogeneity in the fuel distribution.

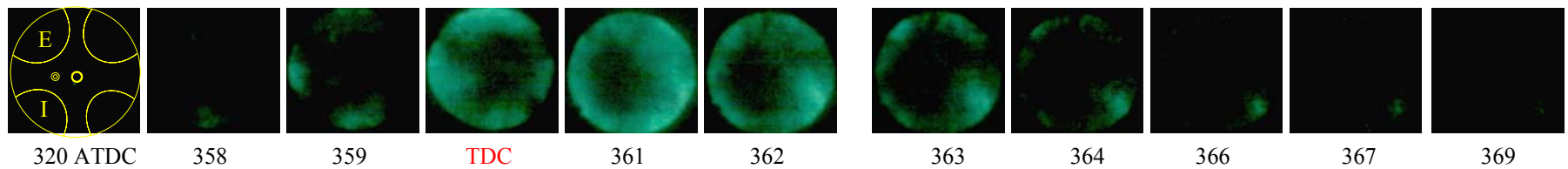
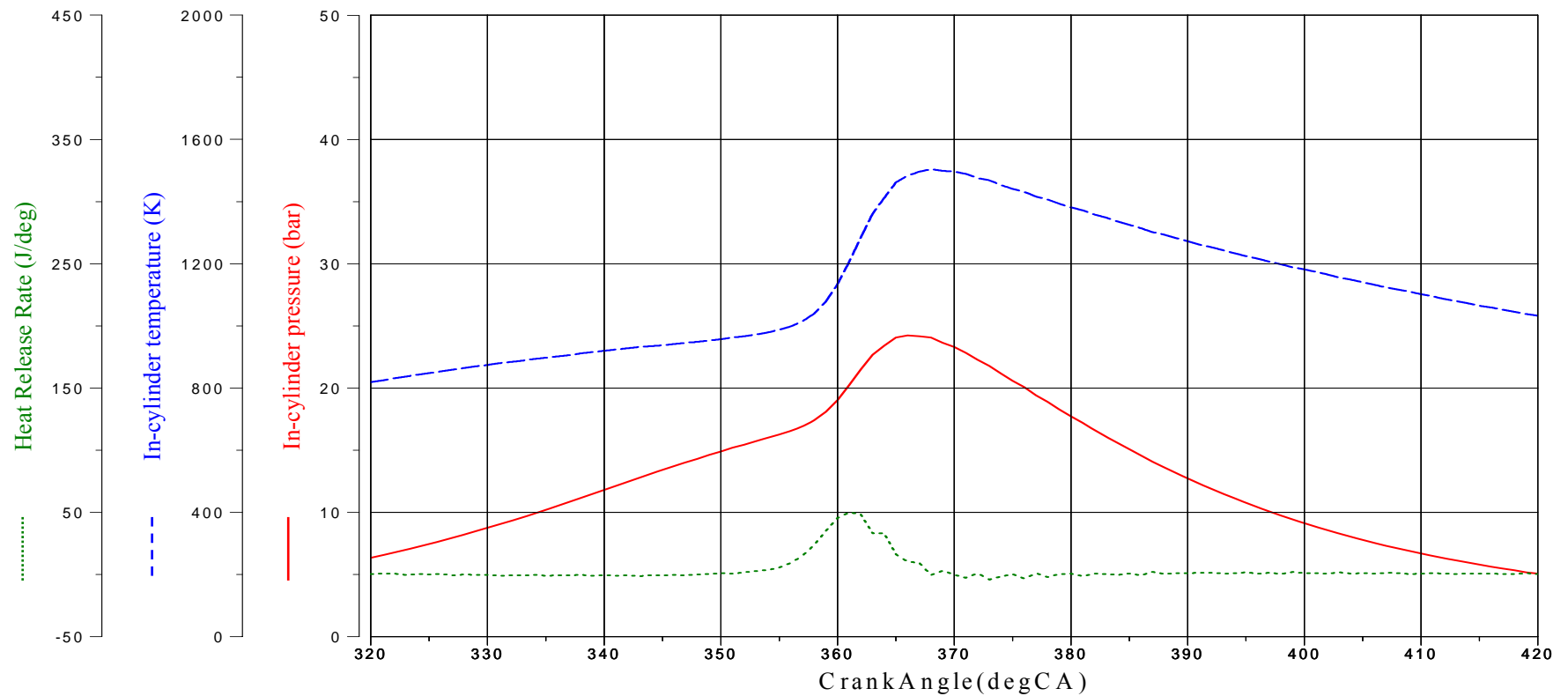


Figure5.58 Simultaneous In-cylinder pressure, temperature, heat release rate and Full Chemiluminescence images at lambda 1.2, 1600rpm, Gain 40%, SOI=80 °CA BTDC and with spark assistance.

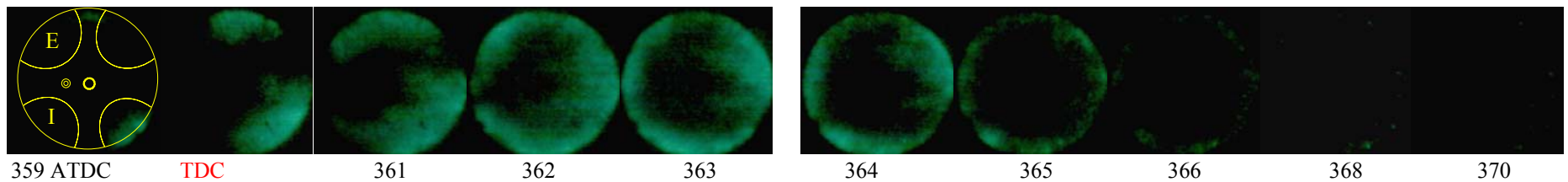
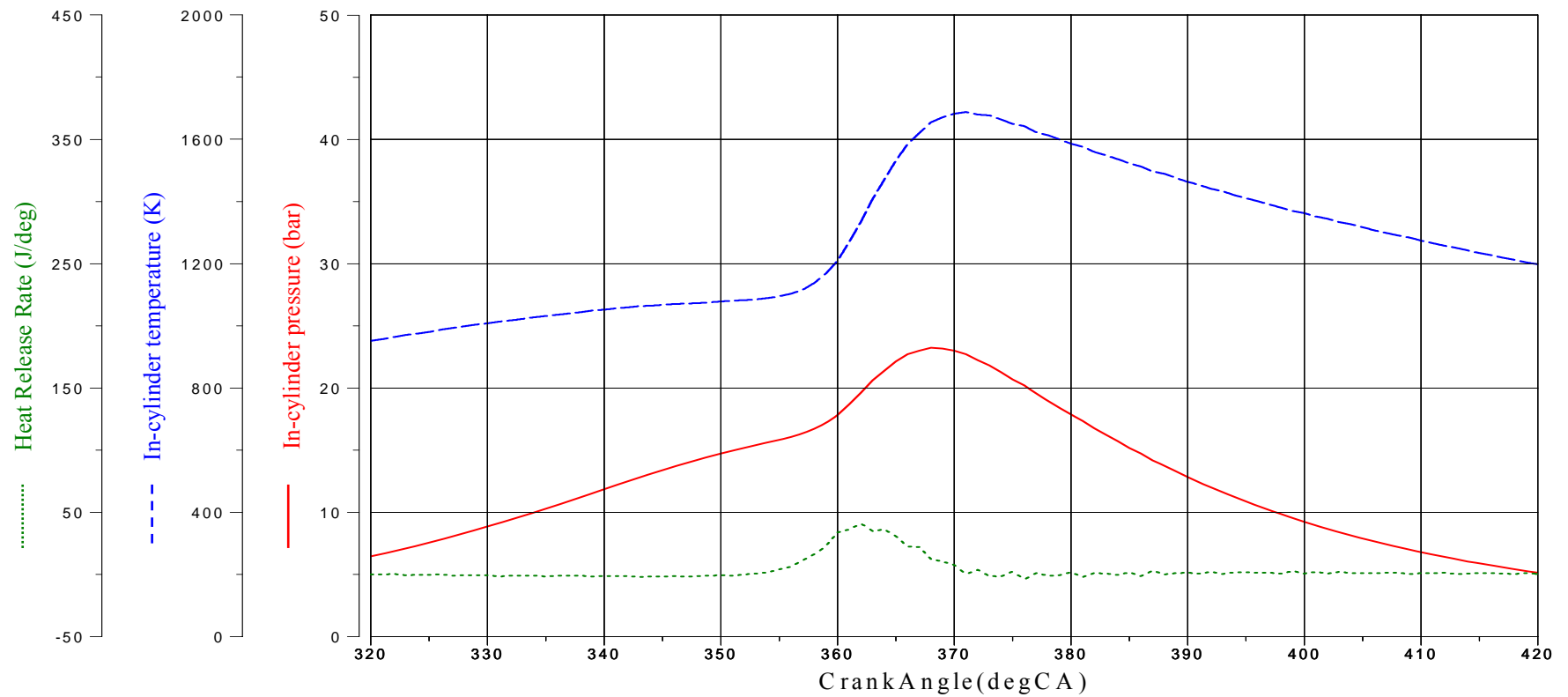


Figure 5.59 Simultaneous In-cylinder pressure, temperature, heat release rate and Full Chemiluminescence images at $\lambda = 1.2$, 1600rpm, Gain 40%, SOI=80 °CA BTDC and without spark assistance.

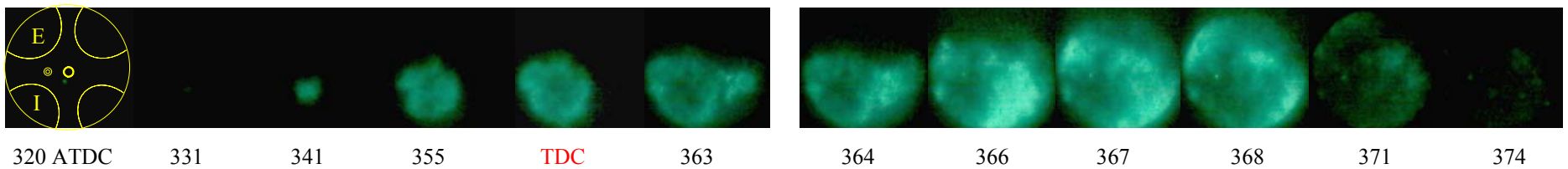
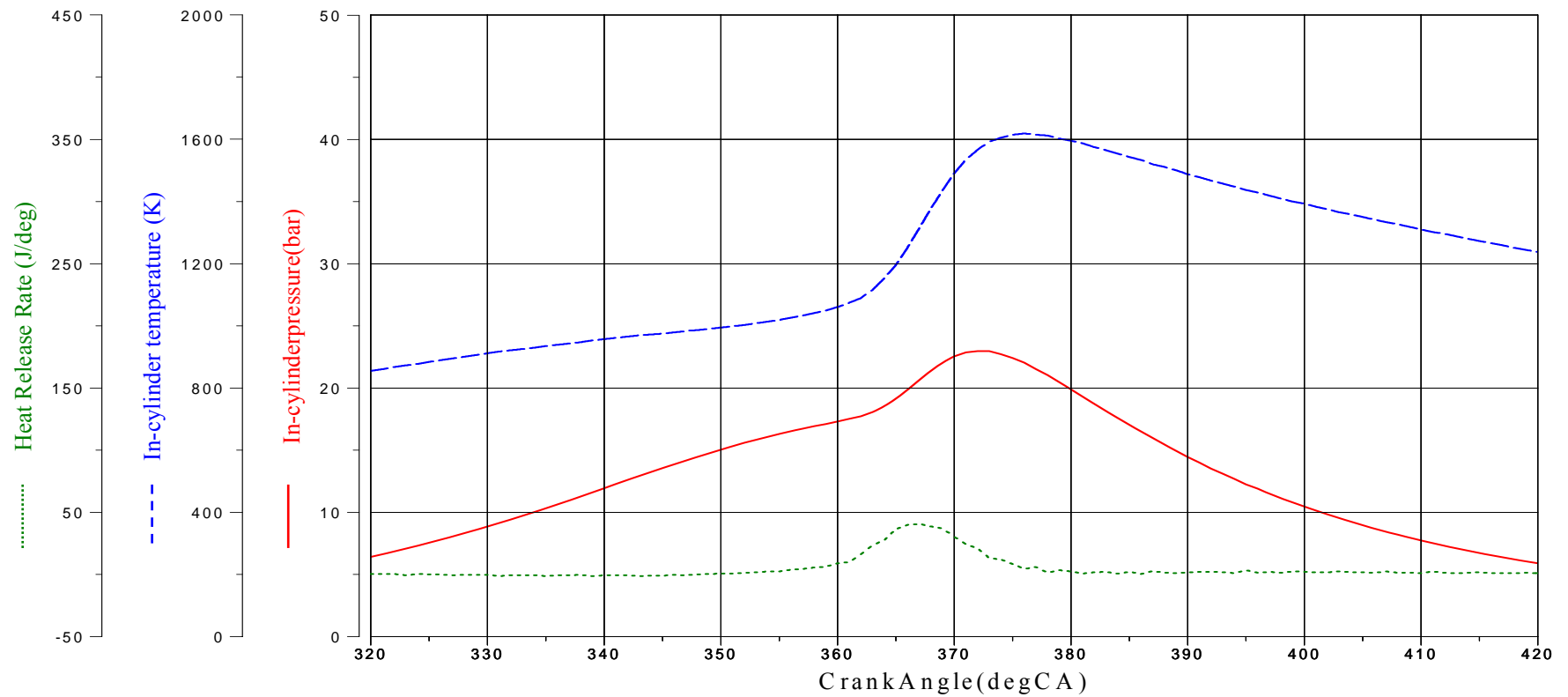


Figure 5.60 Simultaneous In-cylinder pressure, temperature, heat release rate and Full Chemiluminescence images at lambda 1.2, 1600rpm, Gain 40%, SOI=40 °CA ATDC and with spark assistance.

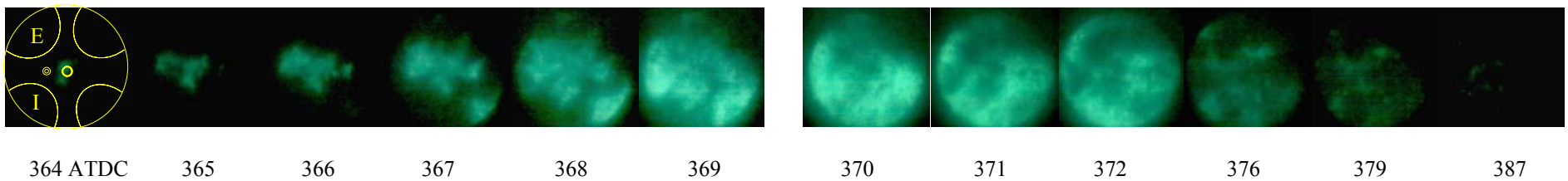
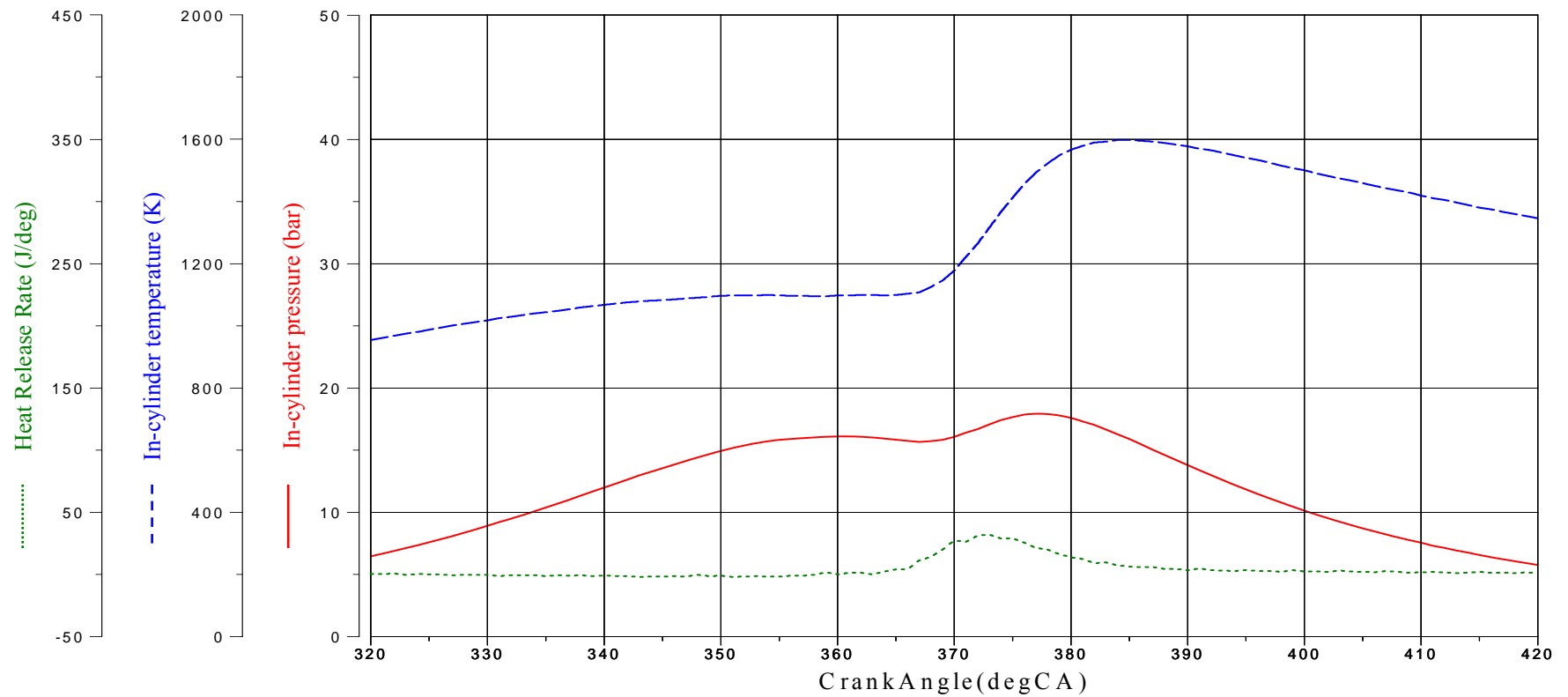


Figure 5.61 Simultaneous In-cylinder pressure, temperature, heat release rate and Full Chemiluminescence images at lambda 1.2, 1600rpm, Gain 40%, SOI=40 °CA ATDC and without spark assistance.

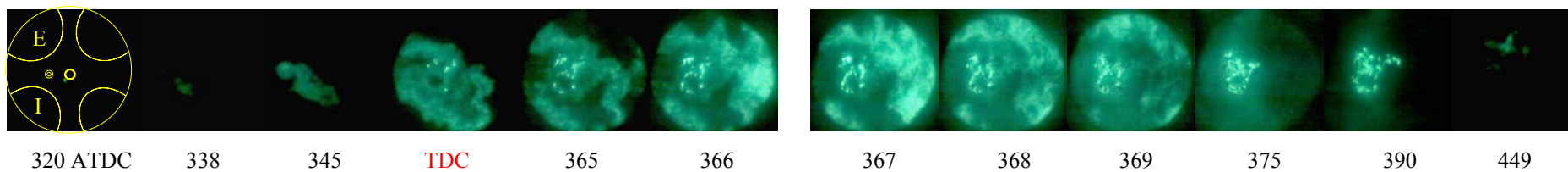
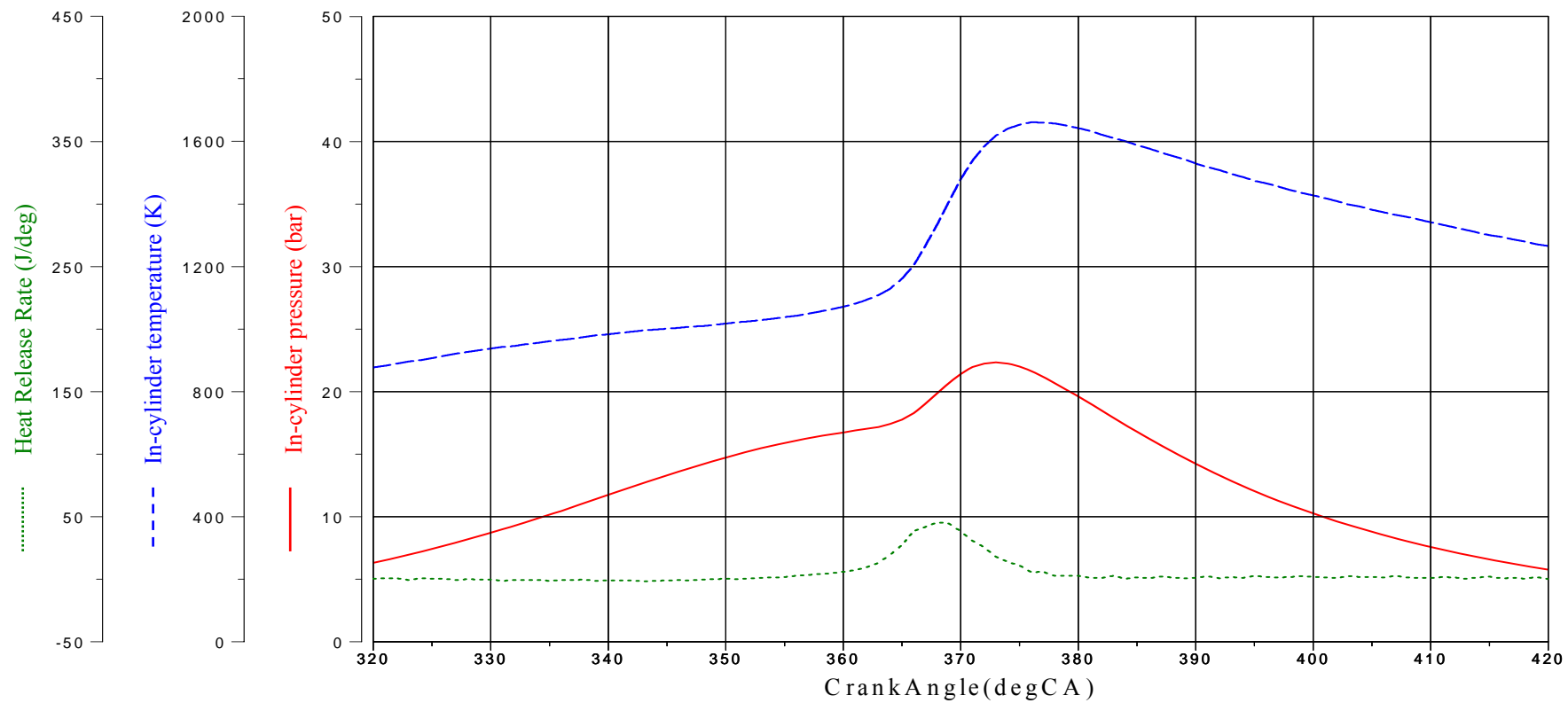


Figure 5.62 Simultaneous In-cylinder pressure, temperature, heat release rate and Full Chemiluminescence images at lambda 1.2, 1600rpm, Gain 40%, SOI=80 °CA ATDC and with spark assistance.

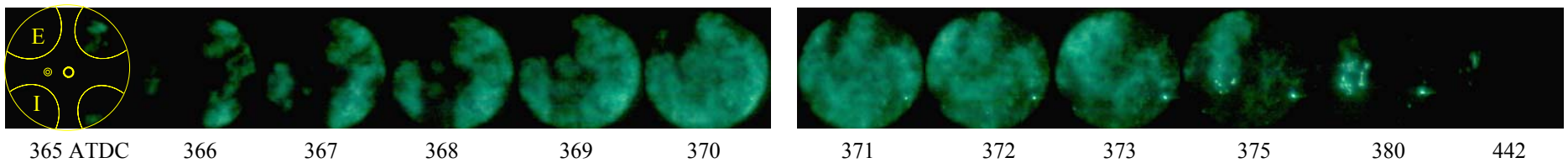
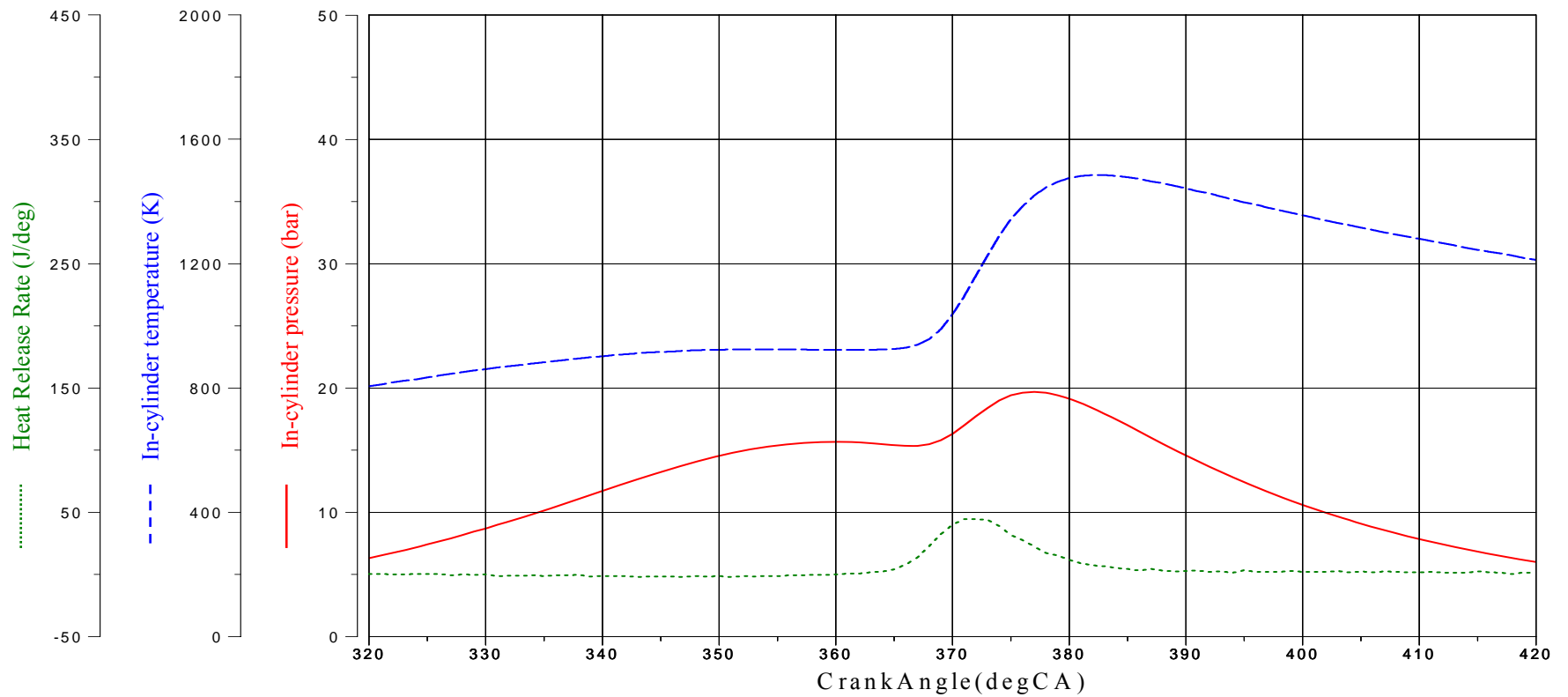


Figure 5.63 Simultaneous In-cylinder pressure, temperature, heat release rate and Full Chemiluminescence images at lambda 1.2, 1600rpm, Gain 40%, SOI=80 °CA ATDC and without spark assistance.

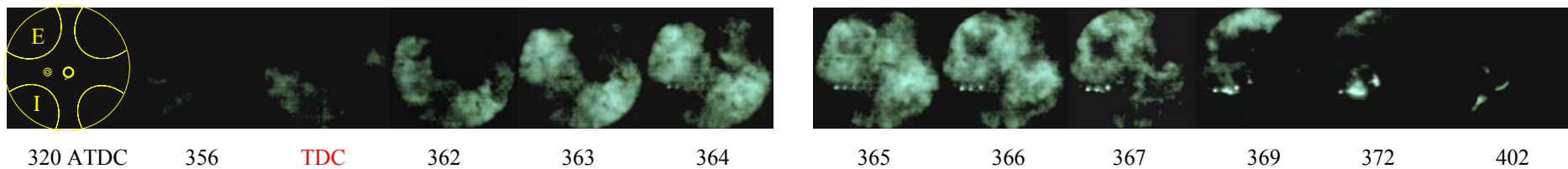
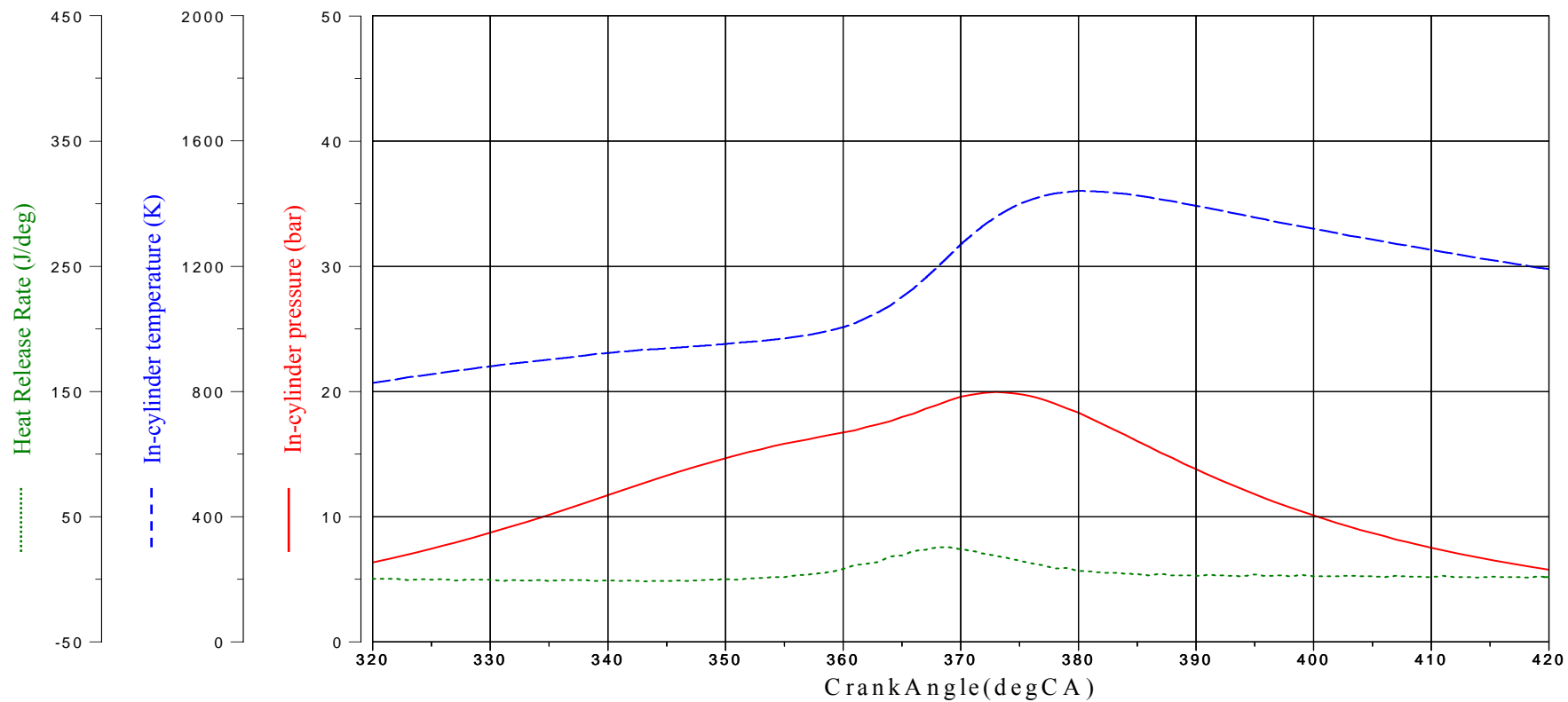


Figure 5.64 Simultaneous In-cylinder pressure, temperature, heat release rate and Full Chemiluminescence images at lambda 1.2, 1600rpm, Gain 60%, SOI=200 °CA ATDC and with spark assistance.

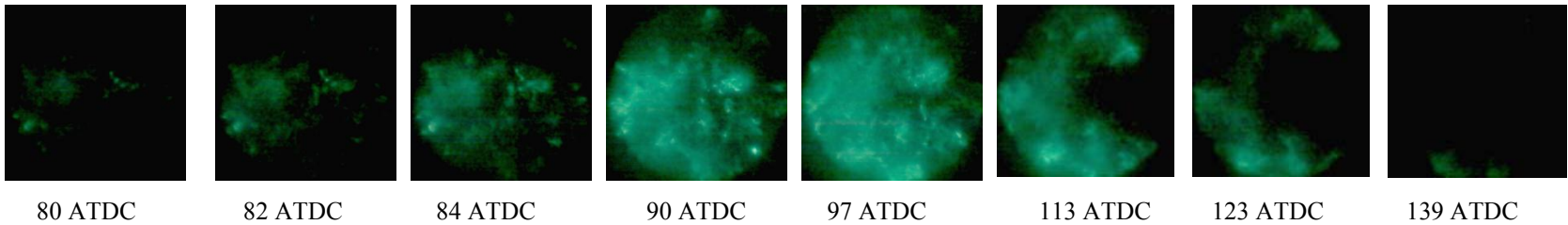
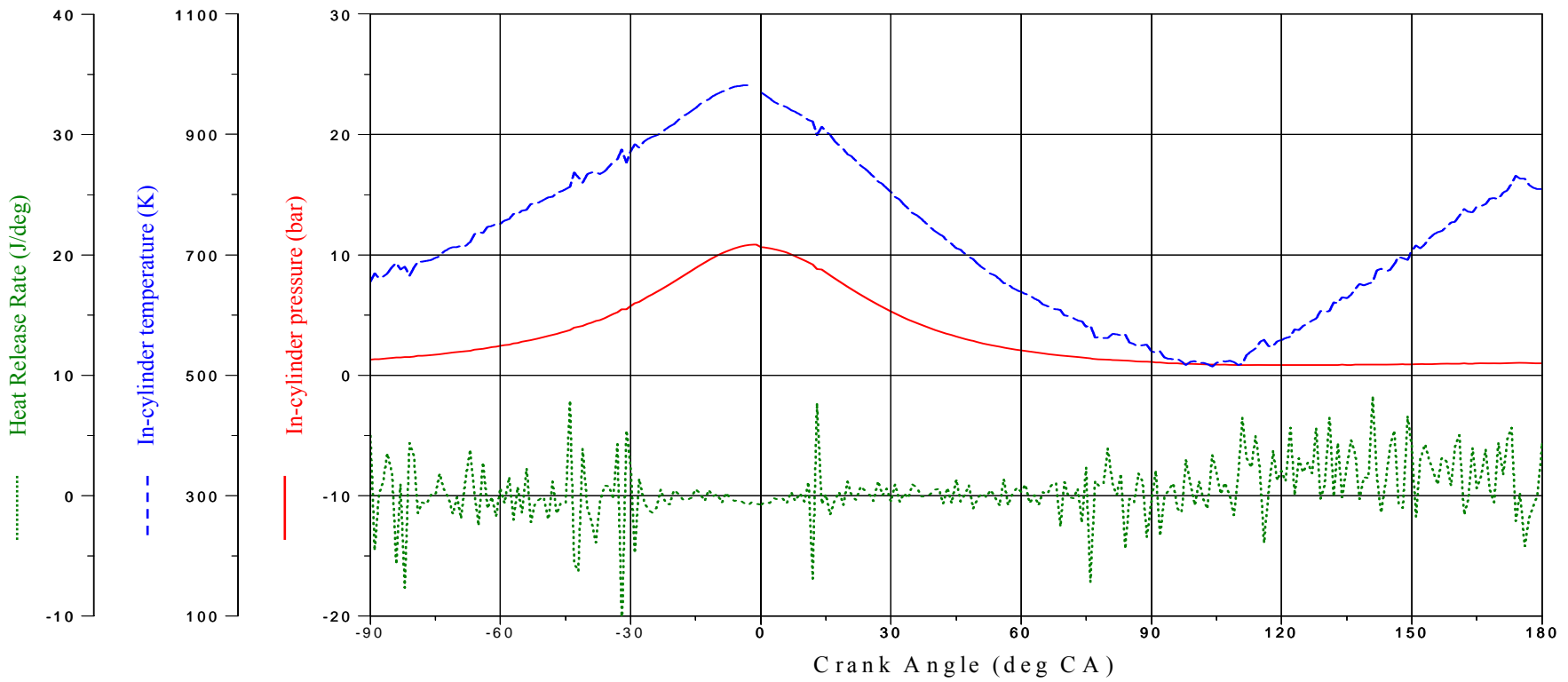


Figure 5.65 Simultaneous In-cylinder pressure, temperature, heat release rate and Full Chemiluminescence images of the mini combustion in the NVO at λ 1.2, 1600rpm, Gain 40%, SOI=80 °CA BTDC and with spark assistance.

5.4.3.5.4 OH chemiluminescence

Chemiluminescence of OH radical was investigated at lambda 1.2 as an intermediate species and representing high temperature regions in the combustion process. The results are shown in Figure 5.66 to 5.69. Due to the nature of highly diluted combustion, the amount of OH radicals would be low and hence the intensity of OH chemiluminescence will be less. Early and late injections did not provide any good images of OH radical. In this study, OH radical was detected in the images from in-cylinder temperature 1200 K up to a maximum of 1650 K that was reached with injection timing of 40 °CA ATDC.

In general, the OH distributions show that the high temperature combustion was mostly located near the peripheral region, similar to that of full chemiluminescence images. However, OH radicals were detected at a much late phase than the full chemiluminescence emission. The first image of OH radicals with spark assistance appeared at 368 °CA ATDC at an averaged in-cylinder gas temperature of 1500 K for SOI=40 °CA ATDC (Figure 5.66) and at 371 °CA ATDC at about 1400 K for 80 °CA ATDC (Figure 5.68), respectively.

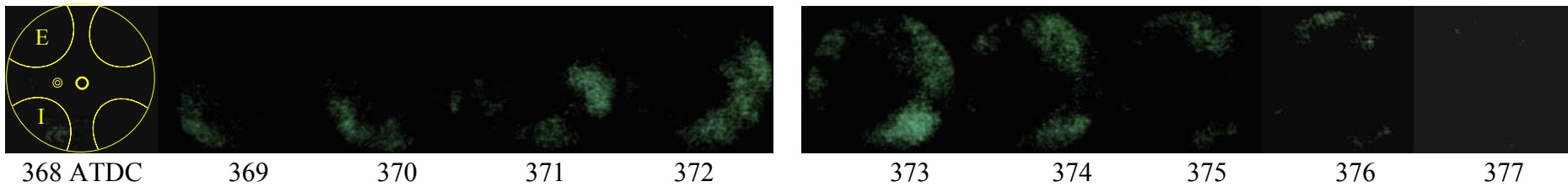
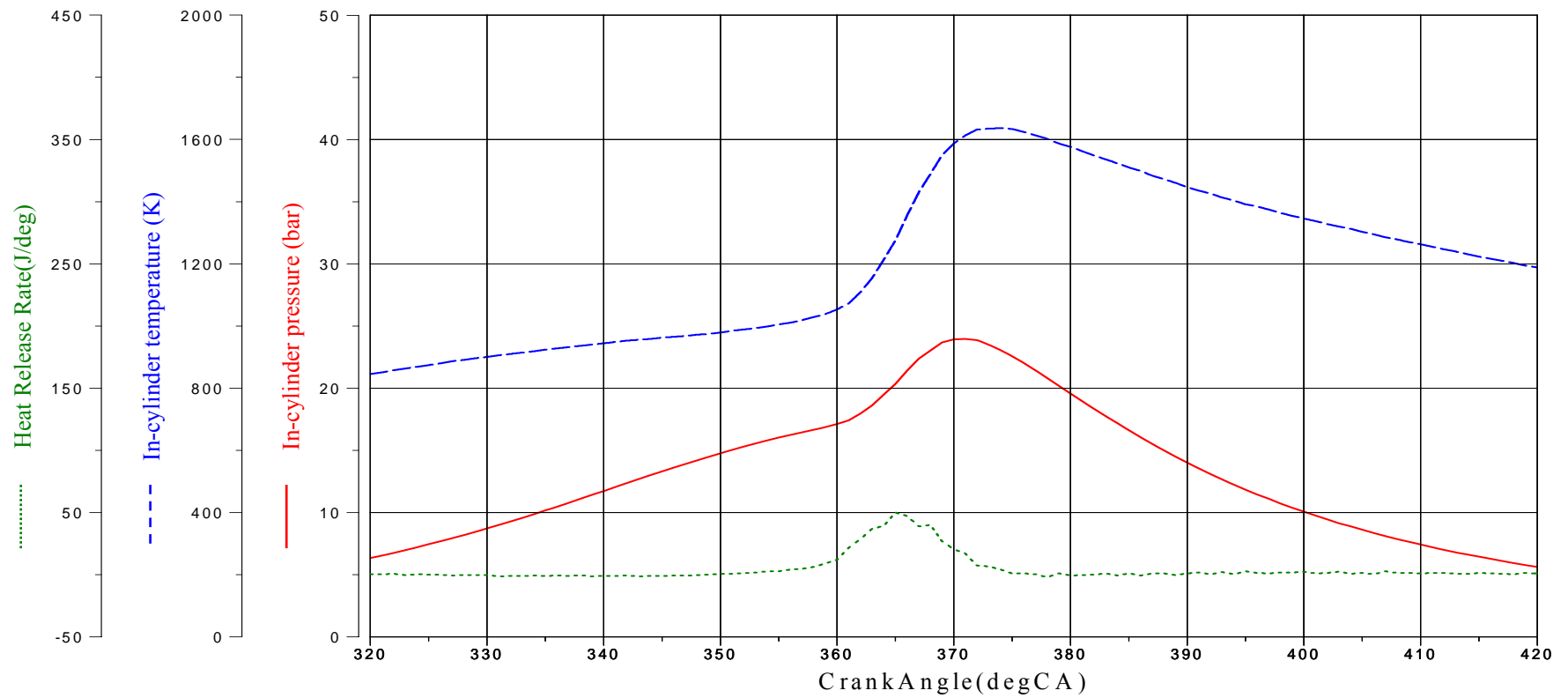


Figure 5.66 Simultaneous In-cylinder pressure, temperature, heat release rate and Chemiluminescence images of OH at lambda 1.2, 1600rpm, Gain 40%, SOI=40 °CA ATDC and with spark assistance.

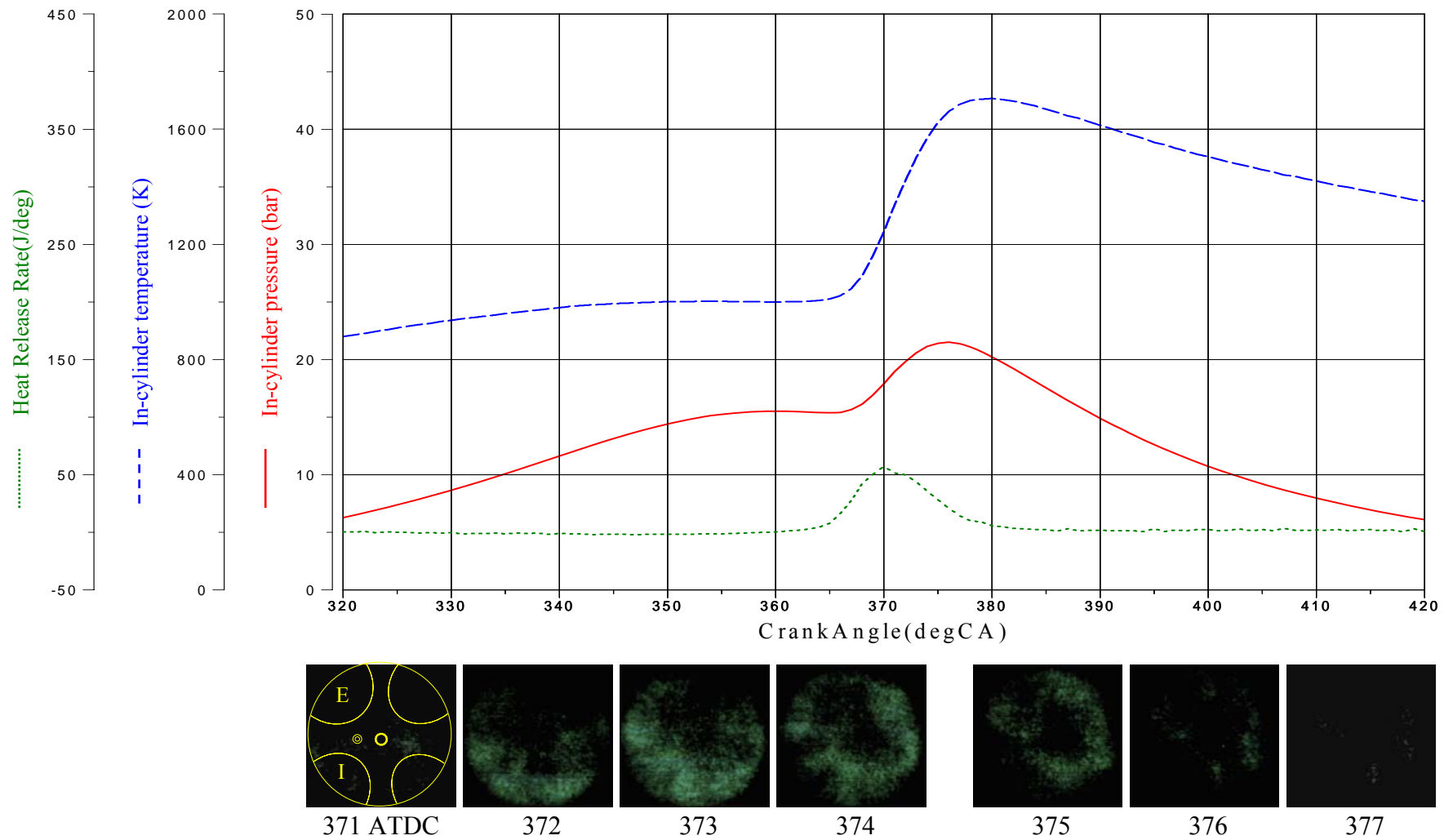


Figure 5.67 Simultaneous In-cylinder pressure, temperature, heat release rate and Chemiluminescence images of OH at lambda 1.2, 1600rpm, Gain 40%, SOI=40 °CA ATDC and without spark assistance.

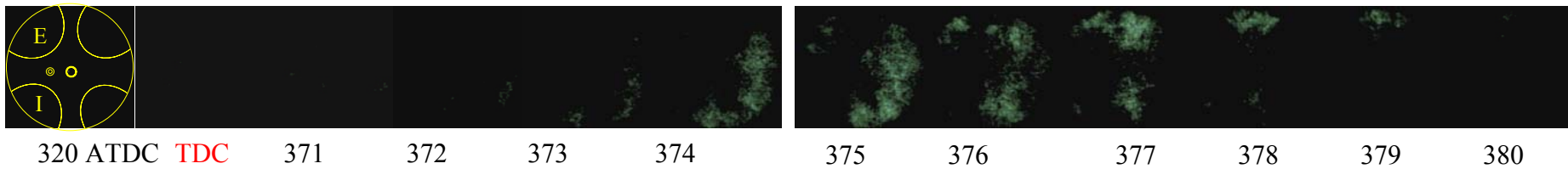
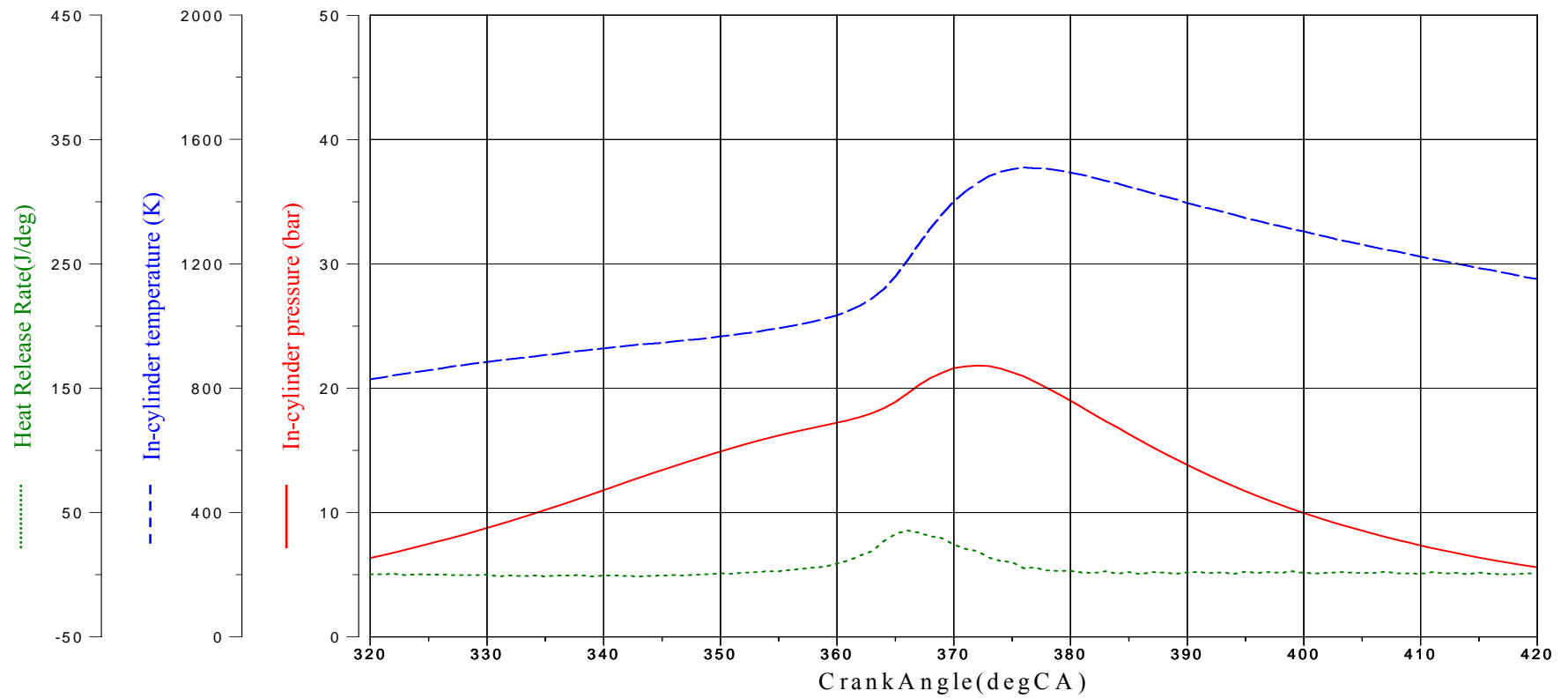


Figure 5.68 Simultaneous In-cylinder pressure, temperature, heat release rate and Chemiluminescence images of OH at lambda 1.2, 1600rpm, Gain 40%, SOI=80 °CA ATDC and with spark assistance.

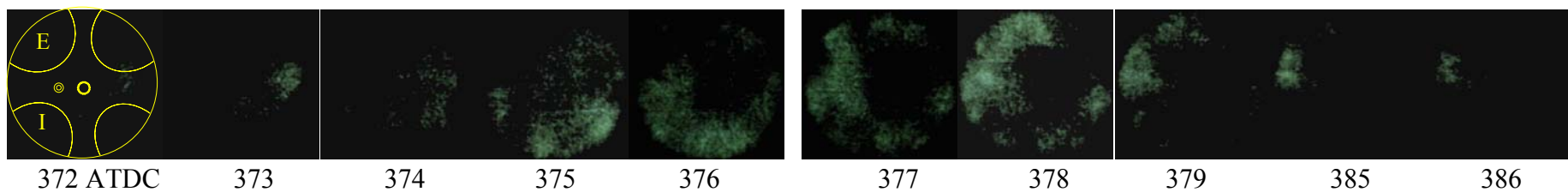
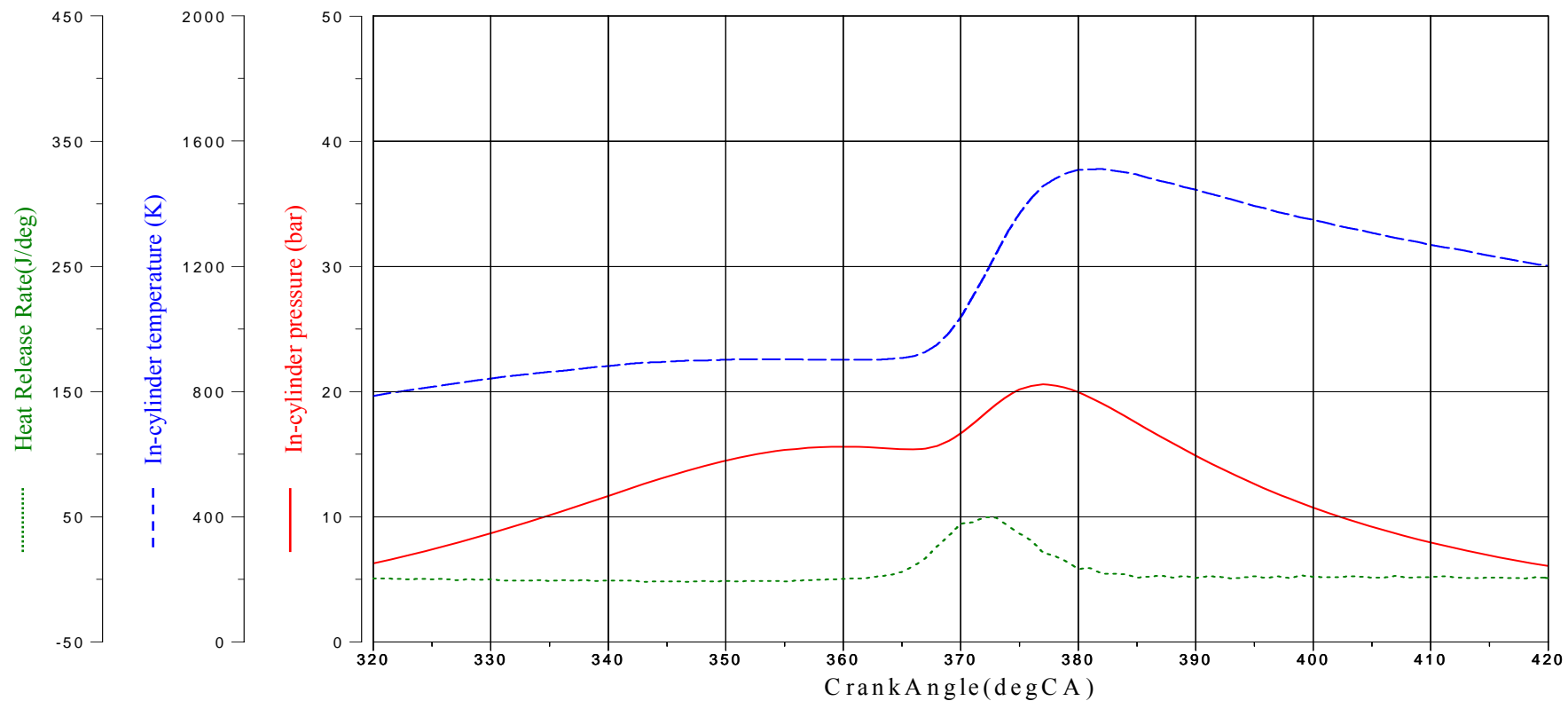


Figure 5.69 Simultaneous In-cylinder pressure, temperature, heat release rate and Chemiluminescence images of OH at lambda 1.2, 1600rpm, Gain 40%, SOI=80 °CA ATDC and without spark assistance.

5.4.3.5.5 CHO chemiluminescence

CHO radical is known as one of chemical intermediates formed during the low temperature autoignition combustion and hence CHO radicals would expect to be present before the main combustion process. Again due to the presence of high percentage of diluents, CHO emissions were low. The early and late injection even did not display any chemical formation in this case.

Results in Figure 5.70 to Figure 5.73 show that CHO radicals were detected at in-cylinder temperature of 1000 ~ 1400 K. For injection timing at 80 °CA (Figure 5.73) the CHO emission was first detected at lower temperature with spark assistance at 900 K at 368 °CA ATDC

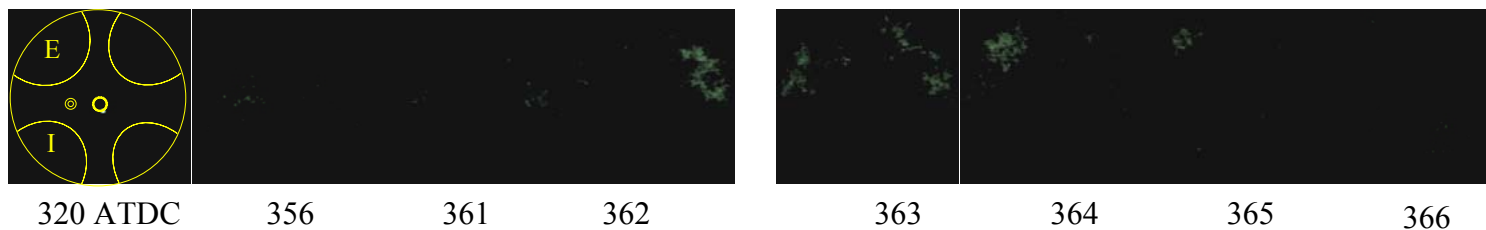
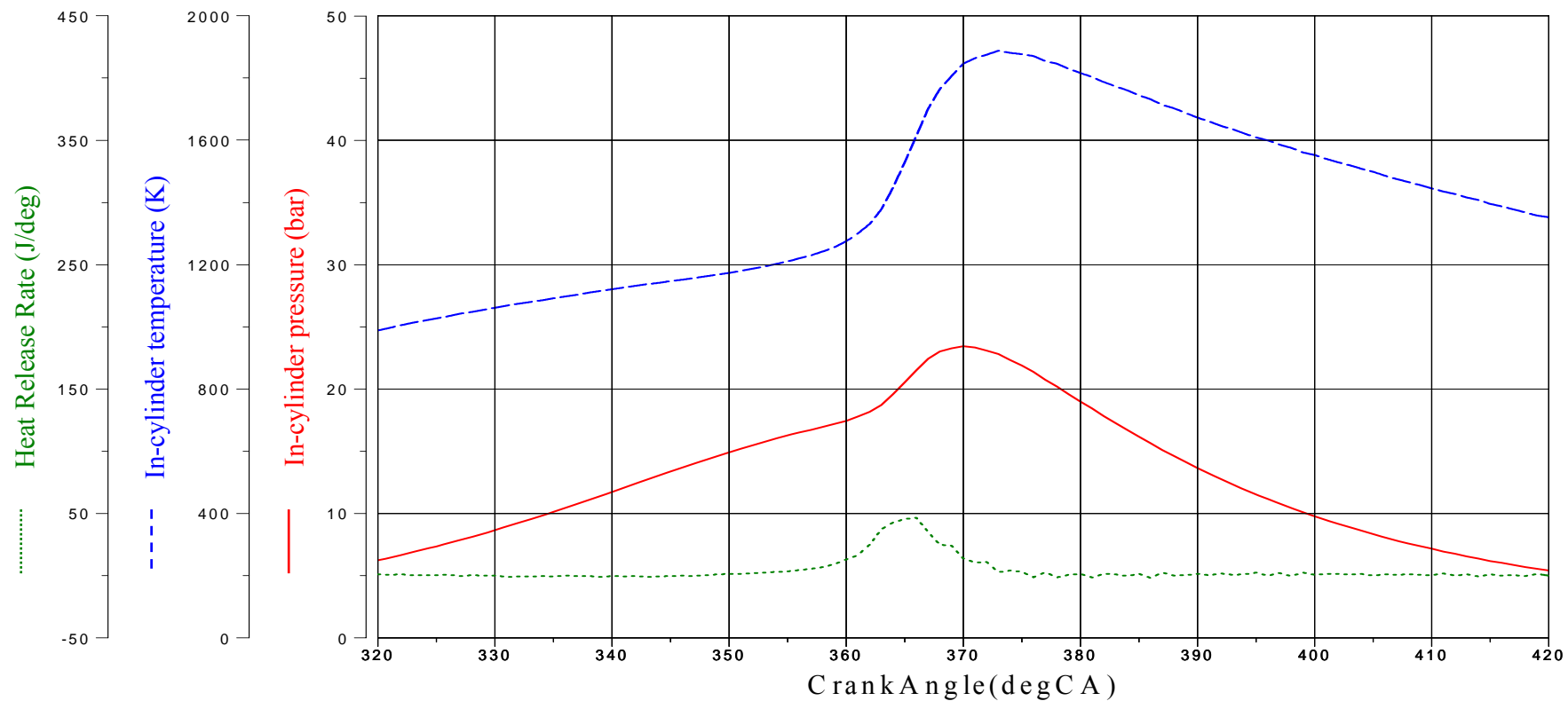


Figure 5.70 Simultaneous In-cylinder pressure, temperature, heat release rate and Chemiluminescence images of CHO at lambda 1.2, 1600rpm, Gain 40%, SOI=40 °CA ATDC and with spark assistance.

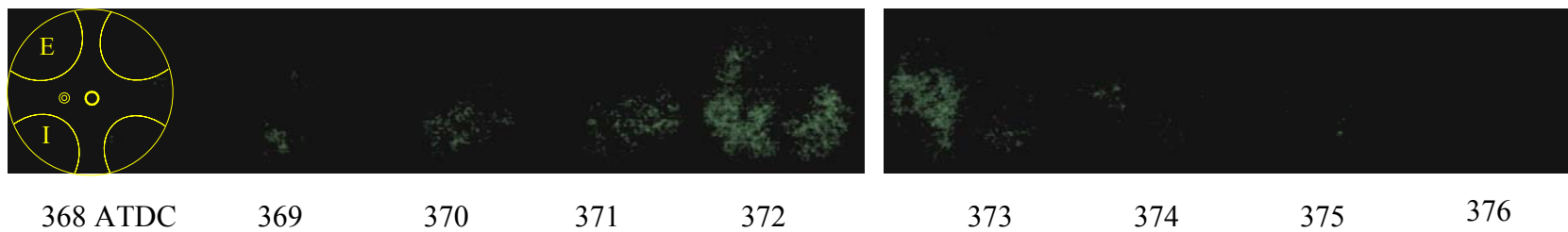
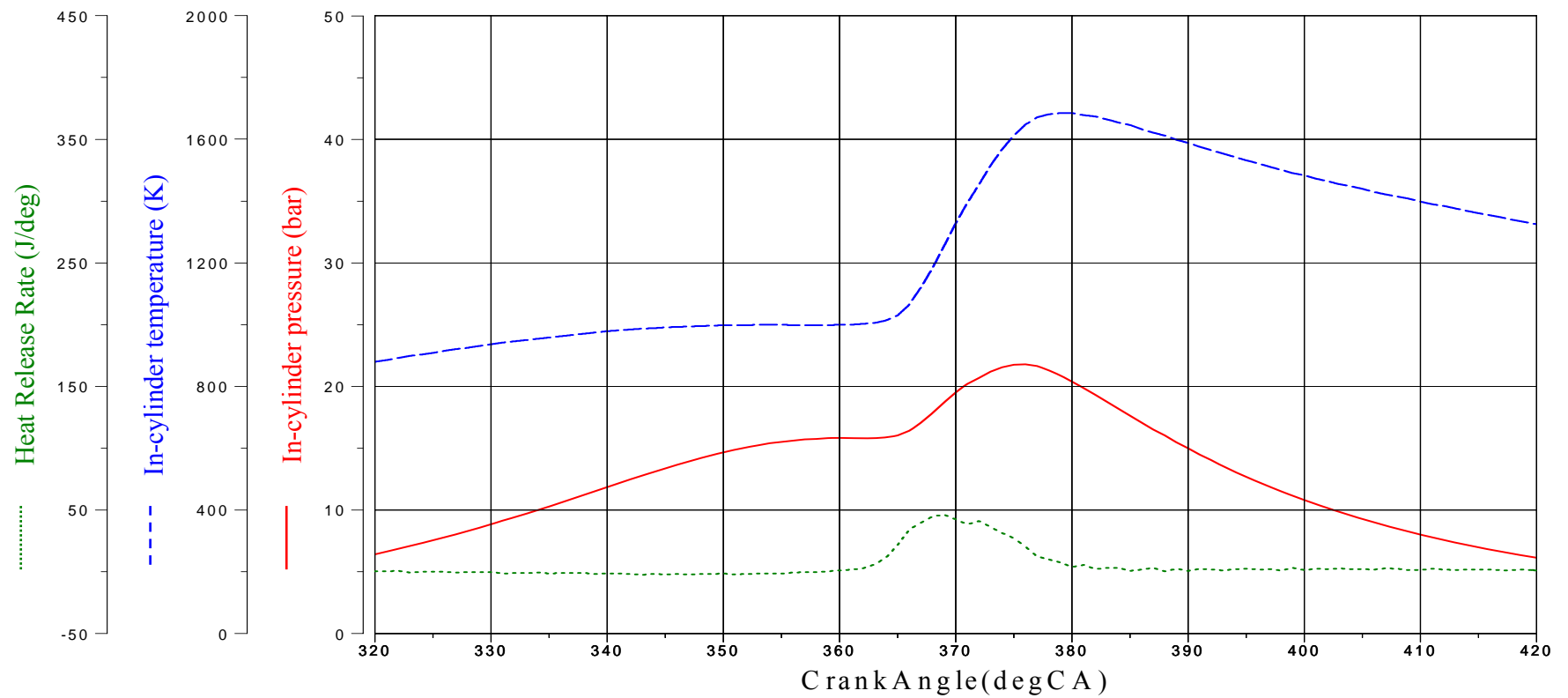


Figure 5.71 Simultaneous In-cylinder pressure, temperature, heat release rate and Chemiluminescence images of CHO at lambda 1.2, 1600rpm, Gain 40%, SOI=40 °CA ATDC and without spark assistance.

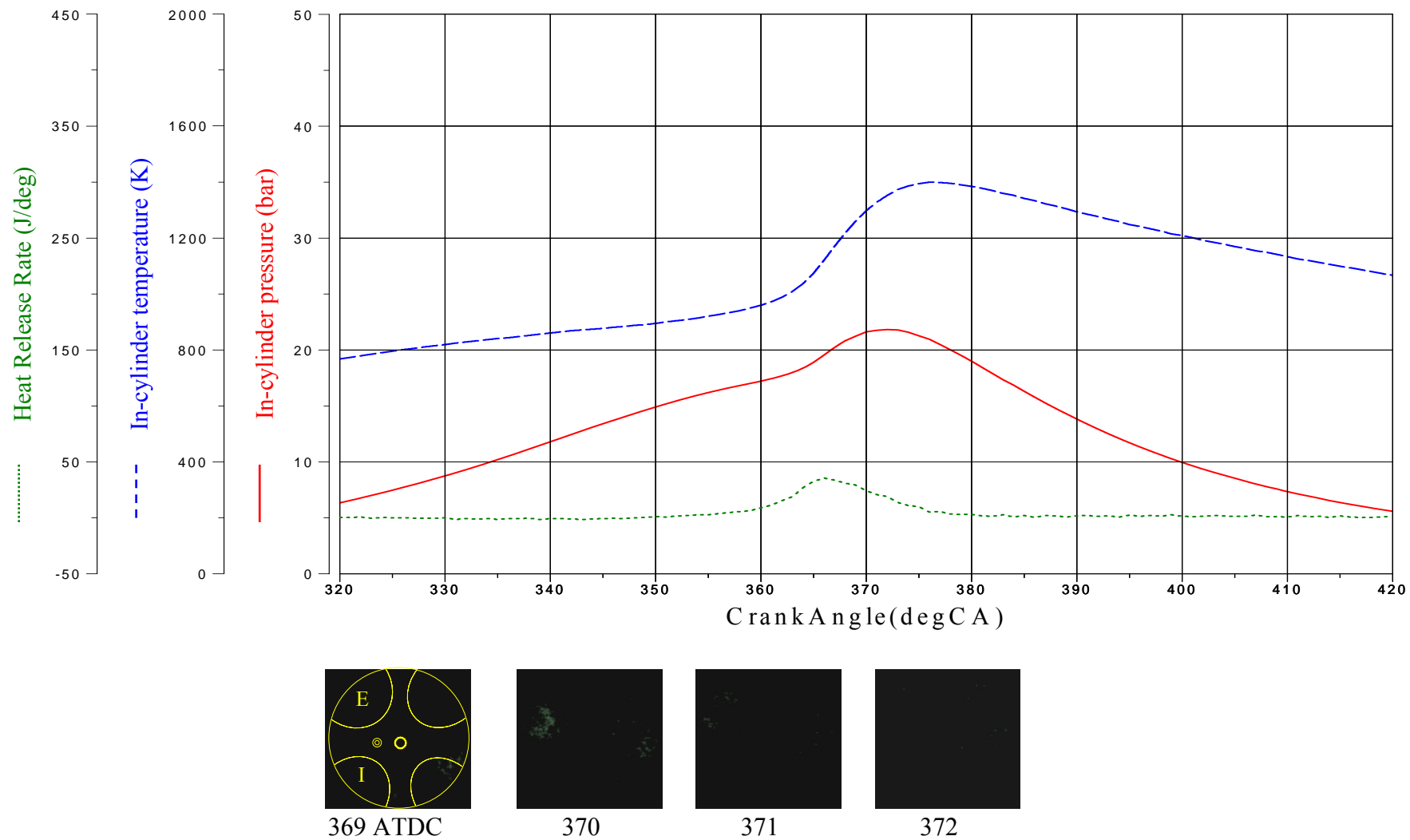


Figure 5.72 Simultaneous In-cylinder pressure, temperature, heat release rate and Chemiluminescence images of CHO at lambda 1.2, 1600rpm, Gain 40%, SOI=80 °CA ATDC and with spark assistance.

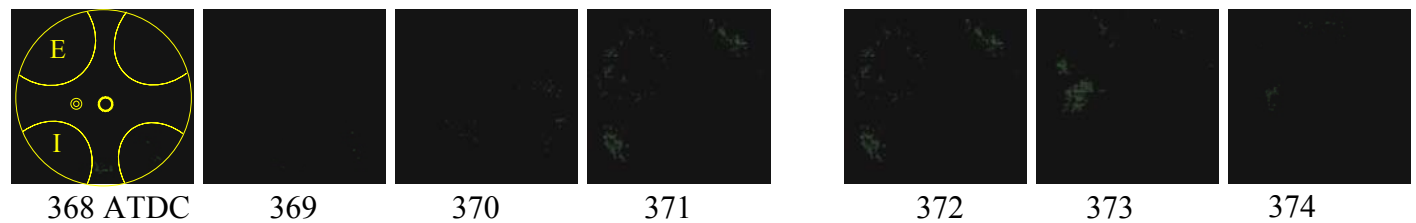
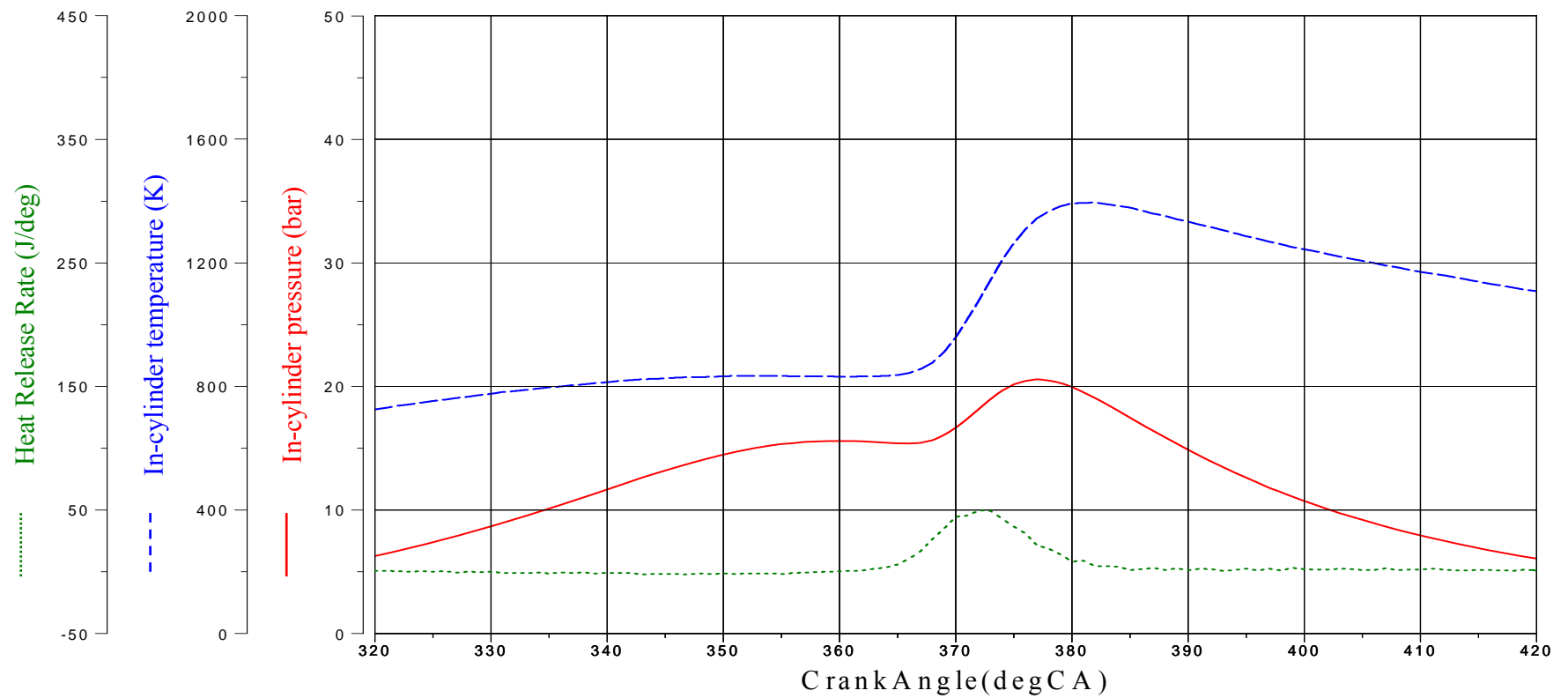


Figure 5.73 Simultaneous In-cylinder pressure, temperature, heat release rate and Chemiluminescence images of CHO at lambda 1.2, 1600rpm, Gain 40%, SOI=80 °CA ATDC and without spark assistance.

5.4.4 Effect of air injection on low temperature combustion

5.4.4.1 Combustion characteristics and performance

As discussed previously, direct fuel injection in the NVO results in the minor heat release or mini combustion and leads to more complete mixture prepared for the next cycle. Direct fuel injection is sprayed into the trapped hot residual and evaporated by the high temperature. In order for the minor heat release to take place, oxygen is required. In addition to operating with leaner fuel and air mixtures, the oxygen concentration during the minor heat release process can also be increased by the additional air included in the mixture of fuel and air to be injected by the assisted injector. In such cases, the relative air and fuel ratio can be kept to one so that a three-way catalyst can be used for further exhaust gas abatement.

The early injection timing at exhaust valve closing timing maximizes the time for minor heat release to take place while the fuelling rate is constant at $\lambda = 1$ and the experiment set up was kept the same as the previous section (Engine speed 1600 rpm, EVC=280 °CA ATDC, IVO=440 °CA ATDC). The quantity of air injection was varied from 10.8 mg/cycle used in the test in the previous section up to 25.43 mg/cycle. The air quantity was adjusted by the injection control unit and monitored by the pulse width of injection signal. The injection pulse width was increased by 1.5, 2, and 2.5 times than 10.8 mg/cycle. The results are shown with the measurement of emissions and simultaneous in-cylinder studies and full chemiluminescence.

Table 5.3 shows the combustion characteristics and engine performance as a function of quantity of air injected with spark assistance at 320 °CA ATDC. .

Quantity of Air Injection	10.8 (mg/cycle)	15.78 (mg/cycle)	20.35 (mg/cycle)	25.43 (mg/cycle)
10% of MFB (° CA ATDC)	355	353	353	353
50% of MFB (° CA ATDC)	359	356	356	356
90% of MFB (° CA ATDC)	363	359	358	358
10~50% of MFB (° CA)	4	3	3	3
50~90% of MFB (° CA)	4	3	2	2
10~90% of MFB (° CA)	8	6	5	5
IMEP (bar)	1.2	1.11	1.09	1.1
Peak pressure (bar)	27.8	29.6	29.8	30.1
Peak temperature (K)	1593.72	1677.19	1689.71	1703.04
ISFC (g/KWh)	433.33	468.47	477.06	472.73
ISNOx (g/KWh)	0.34	0.40	0.60	0.83
Comb Efficiency (%)	91.65	92.22	92.61	92.41
PMEP (bar)	0.48	0.47	0.47	0.48
CoVimep (%)	8.05	7.76	8.5	7.97
Trapped residual (%)	46.31	46.19	46.12	45.93

Table 5.3 Combustion characteristics and engine performance for different quantity of direct air injection in spark assisted CAI

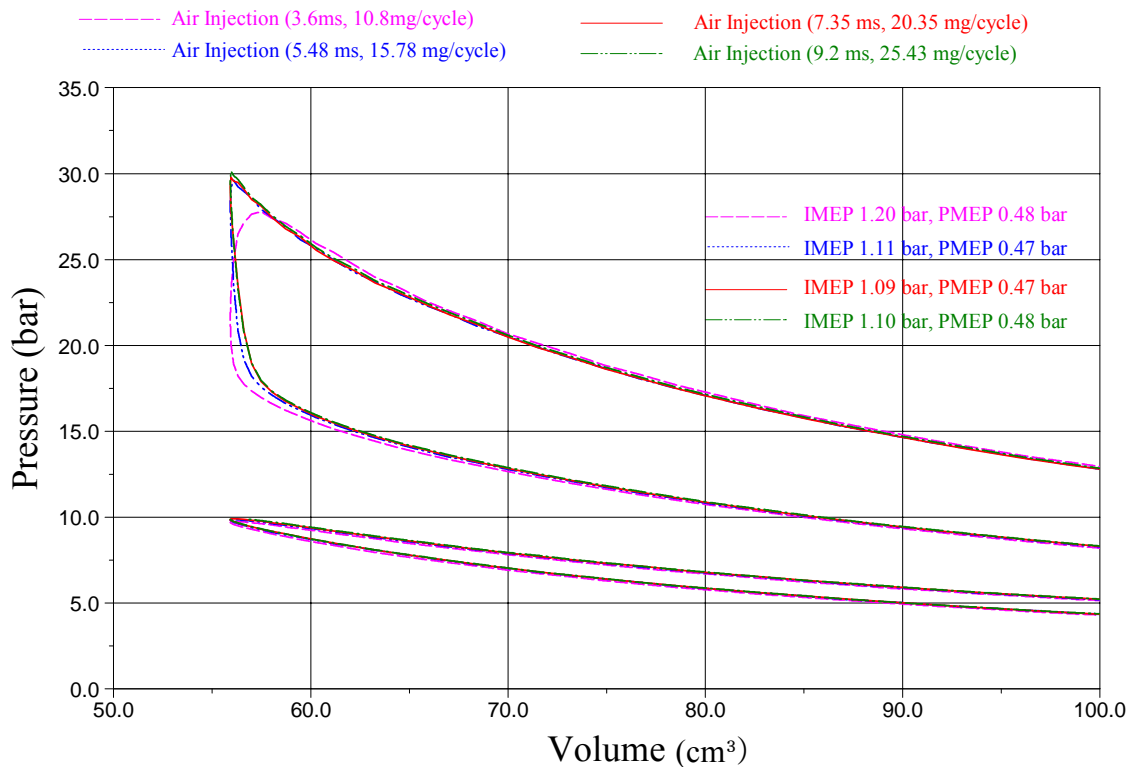


Figure 5.74 Effect of air injection on in-cylinder pressure

However, advanced start of combustion by more air quantity leads to lower engine loads. Figure 5.74 shows the P-V diagrams for different quantities of air injected, illustrating the larger area of positive work done by the minimum air injection. As a result of faster combustion and higher combustion temperature, the NO_x emission increased with increased air injection.

More air injection quantity does not affect the cyclic variation in spite of the effect of combustion phasing, showing similar level of CoVimep. Combustion efficiency is improved marginally.

Figure 5.75 shows that as the quantity of air was increased from 10.8 mg/cycle to 15.78mg/cycle, combustion started earlier and combustion duration was shortened. Further increase in the amount of air injected had less effect on combustion phasing and combustion duration. The results indicate that the amount of air injected can be a parameter to be used to alter the combustion phasing for optimized engine operation.

Figure 5.76 indicates that in-cylinder pressure and temperature during the NVO period was raised by the increased air injected, though the heat release rate does not show any obvious changes.

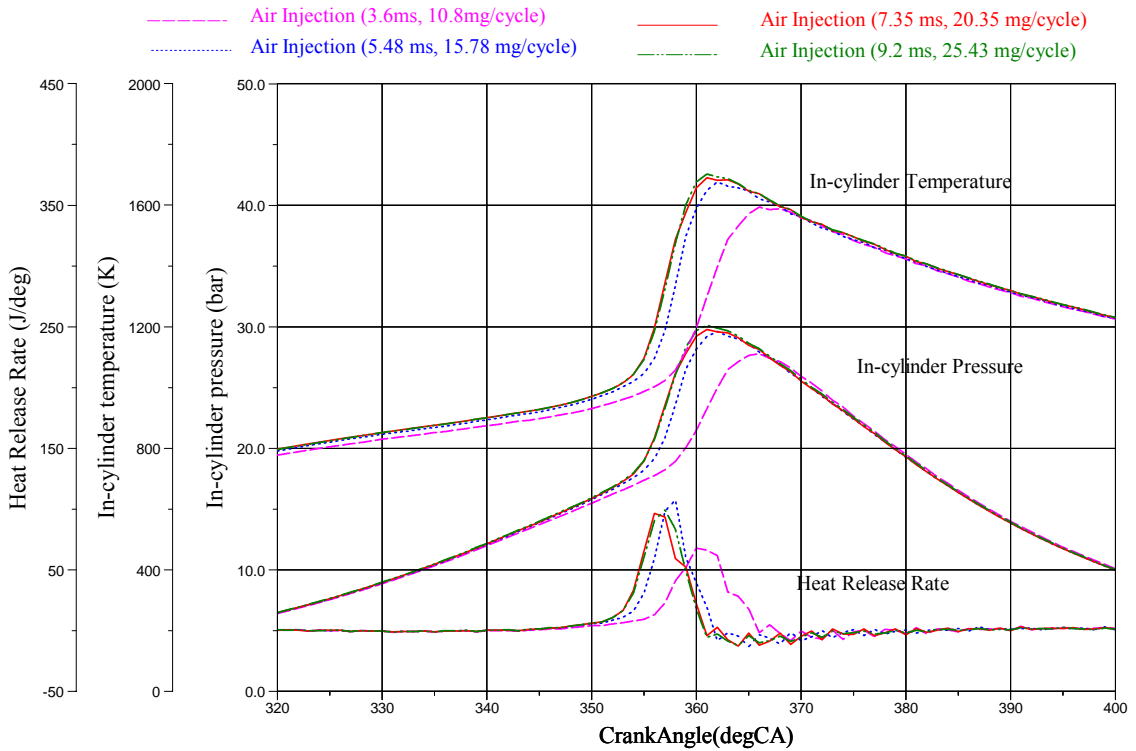


Figure 5.75 Main combustion with simultaneous in-cylinder pressure, temperature, heat release rate at lambda 1, 1600rpm, SOI=80 °CA BTDC with spark assisted at 320 °CA BTDC by Air Injection

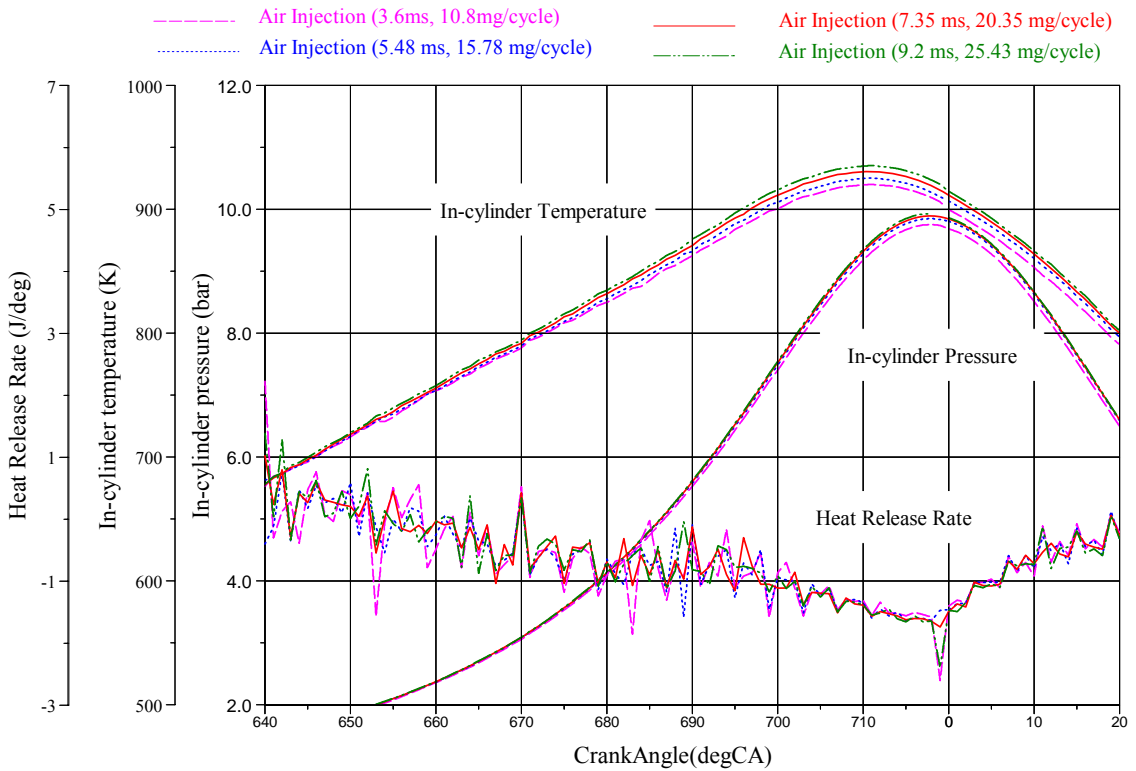


Figure 5.76 Mini combustion with simultaneous in-cylinder pressure, temperature, heat release rate at lambda 1, 1600rpm, SOI=80 °CA BTDC with spark assisted at 320 °CA BTDC by Air Injection

5.4.4.2 Simultaneous in-cylinder studies and full chemiluminescence

Simultaneous in-cylinder pressure, temperature, heat release rate and chemiluminescence with spark assistance are achieved at lambda 1 by different quantity of direct air injection, shown in from Figure 5.77 to 5.92. The combustion sequences were captured in consecutive cycles in order to investigate the first minor combustion during NVO period, the main combustion in the same cycle, and the, minor combustion in the NVO period afterwards. This would allow the interactions between the minor heat release process and main combustion to be analyzed. Therefore, after the in-cylinder pressure and heat release rate curves are presented, the first minor combustion is presented, followed by the main combustion and then 2nd minor combustion. Some of results are different from the results presented in the previous section since these results are recorded from the individual cycles rather than 100 cycles recorded.

Significant emission from the minor combustion process is shown in spite of negligible heat release rate results obtained from the in-cylinder pressure measurements in the NVO period. For all the cases examined, it is noted that if the first minor heat release process prior to the main combustion was characterized with visible emissions, the 2nd minor heat release process during the NVO after the main combustion was often characterized with lower and shorter duration of chemiluminescence emission (e.g, Figure 5.78 vs Figure 5.80, Figure 5.82 vs Figure 5.84) or vice versa (Figure 5.86 vs Figure 5.88). It is probable that if the initial minor combustion generates more active species as well as higher temperature, it would advance the ensuing main combustion leading to lower residual gas temperature for the minor combustion to take place in the following cycle. This in turn will delay the start of main combustion in the next cycle, causing the burned gas temperature to rise and hence higher minor combustion activities in the next NVO period. Therefore, a repeatable cyclic variation is present in the combustion phasing and heat release process as shown in Figure 5.93 to 5.97. The figures are captured at lambda 1, 1600rpm, SOI=80 °CA BTDC with spark assisted at 320 °CA BTDC by Air Injection. They show four recorded consecutive cycles which include in-cylinder pressure, heat release data and MFB rate. The first cycle is shown faster combustion and indeed the second cycle is slower and followed by a faster combustion in the third cycle.

In accordance with the heat release analysis results shown in Table 5.3, the chemiluminescence images show that more quantity of air injection caused shorter or faster combustion duration. As shown in Figure 5.79 and 5.91, the main combustion with 10.8 mg/cycle of air injection was detected from 335 deg CA ATDC up to TDC for 25 crank angles and it was from 338 deg CA ATDC up to 356 deg CA ATDC for 18 crank angles for 25.43 mg/cycle of air injection. However, the rest of combustion sequences are not comparable to the heat release data due to the presence of soot emissions that lasted long after the main combustion event. Figure 5.78 and 5.80 show the results to monitor with 10.8 mg/cycle of air injection.

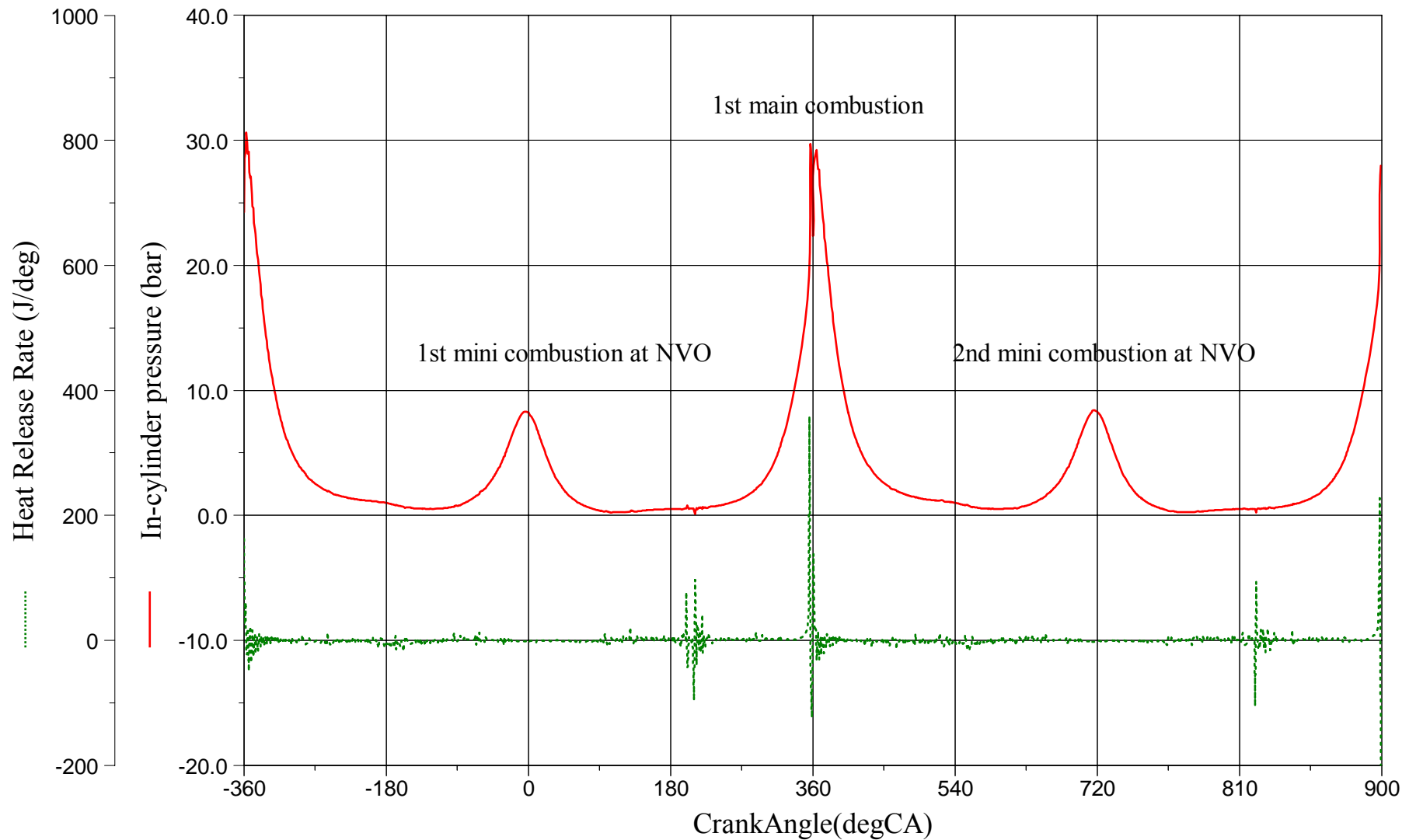


Figure 5.77 Simultaneous In-cylinder pressure, heat release rate at lambda 1, 1600rpm, SOI=80 °CA BTDC with spark assistance at 320 °CA BTDC, Air Injection 10.8 mg/cycle.

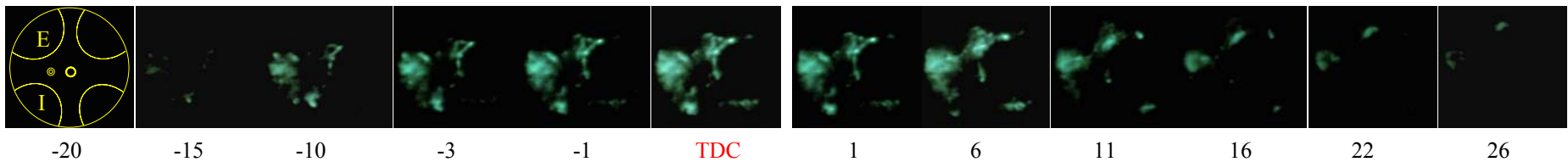
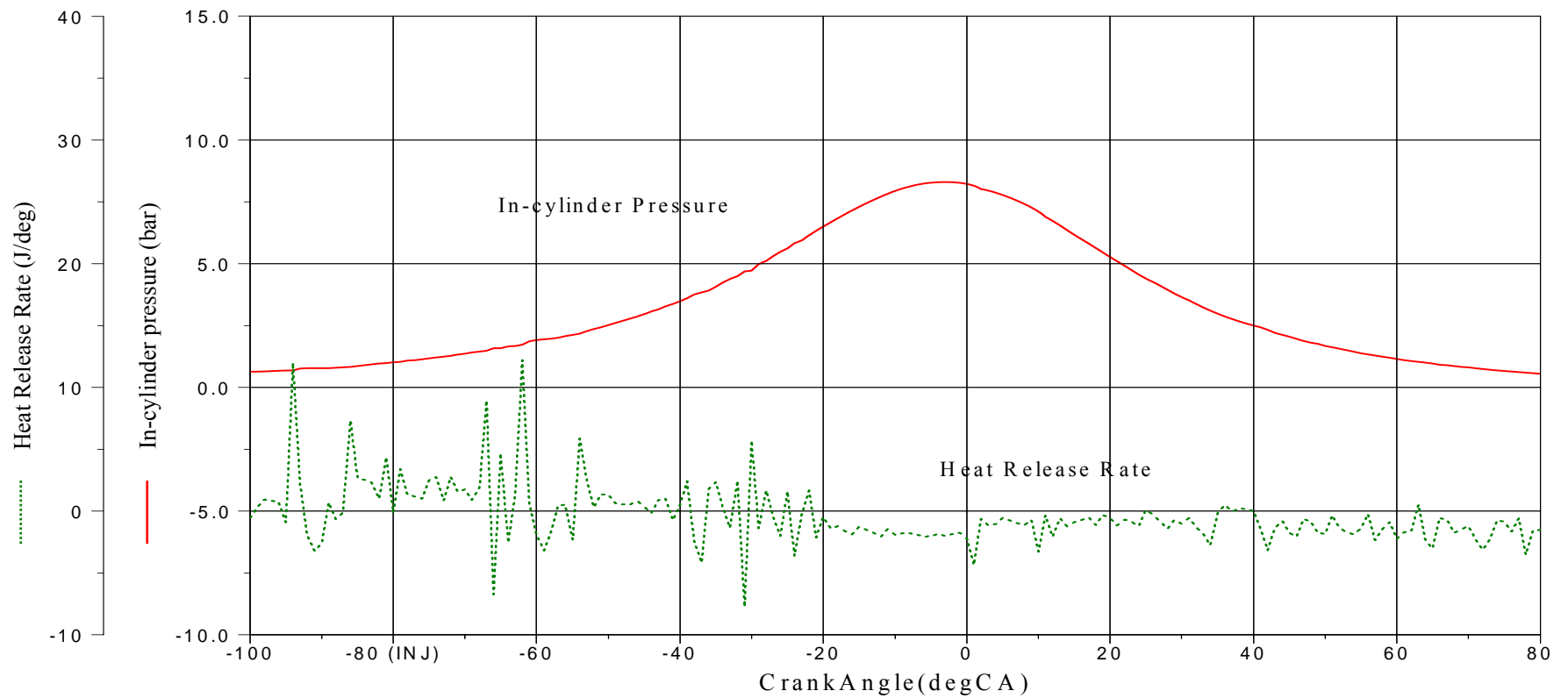


Figure 5.78 Mini combustion with simultaneous In-cylinder pressure, heat release rate and Full Chemiluminescence images at lambda 1, 1600rpm, Gain 50 %, SOI=80 °CA BTDC with spark assistance at 320 °CA BTDC, Air Injection 10.8 mg/cycle

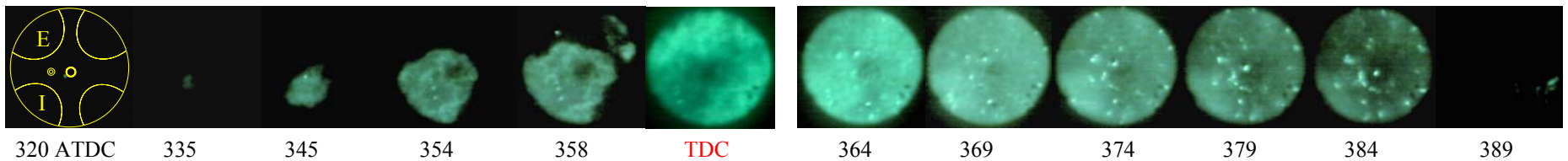
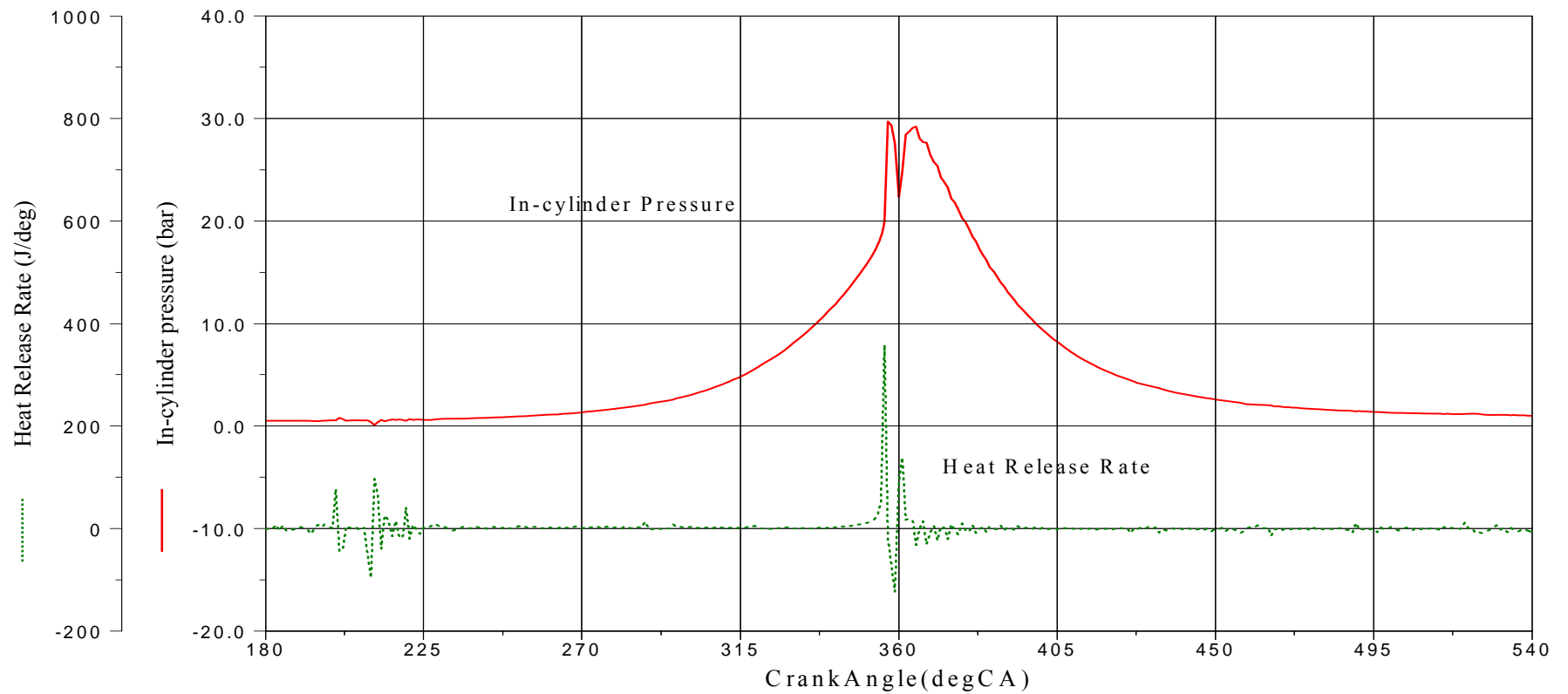


Figure 5.79 Main combustion with simultaneous In-cylinder pressure, heat release rate and Full Chemiluminescence images at lambda 1, 1600rpm, Gain 50 %, SOI=80 °CA BTDC with spark assistance at 320 °CA BTDC, Air Injection 10.8 mg/cycle

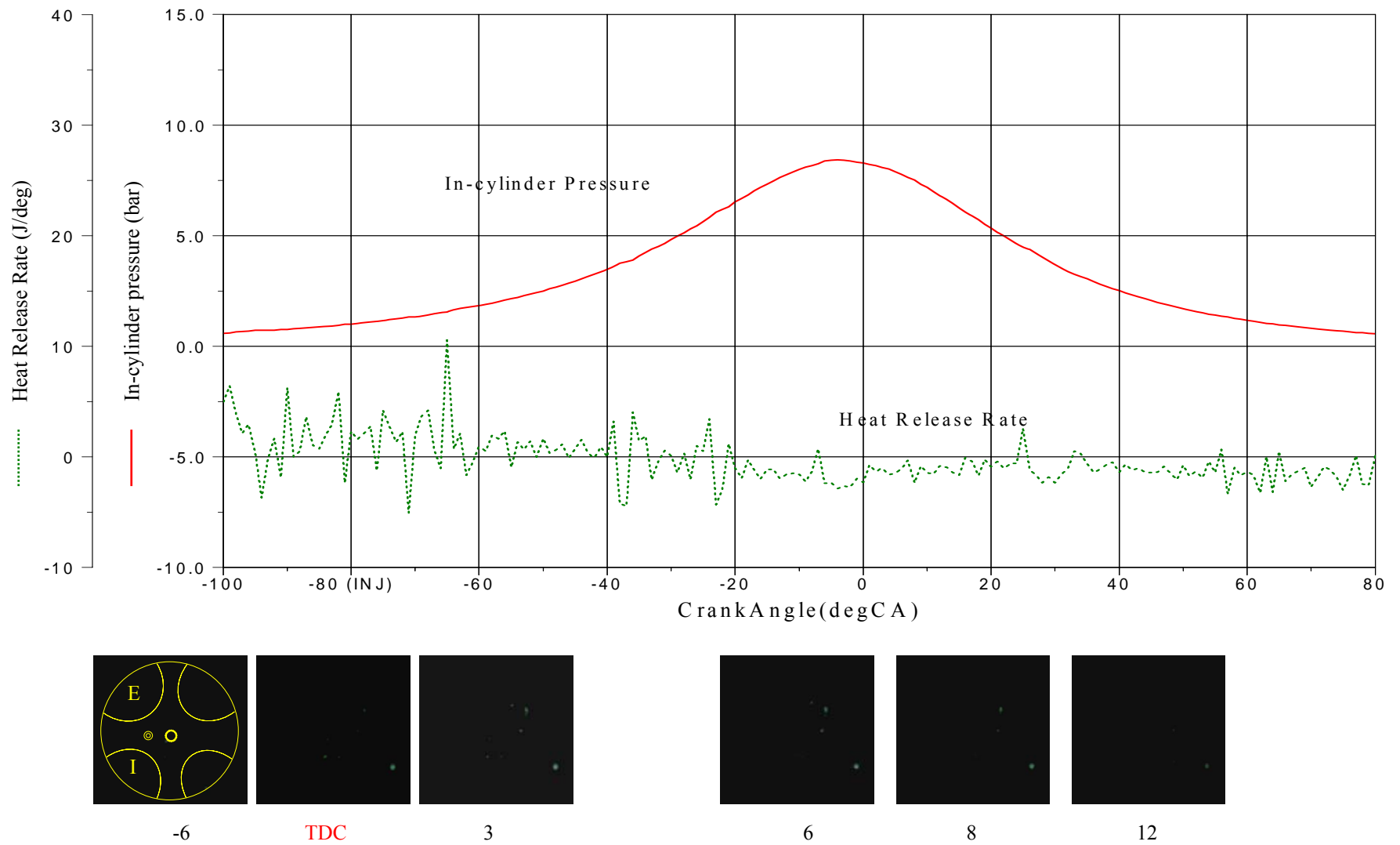


Figure 5.80 Mini combustion with simultaneous In-cylinder pressure, heat release rate and Full Chemiluminescence images at lambda 1, 1600rpm, Gain 50 % , SOI=80 °CA BTDC with spark assistance at 320 °CA BTDC, Air Injection 10.8 mg/cycle

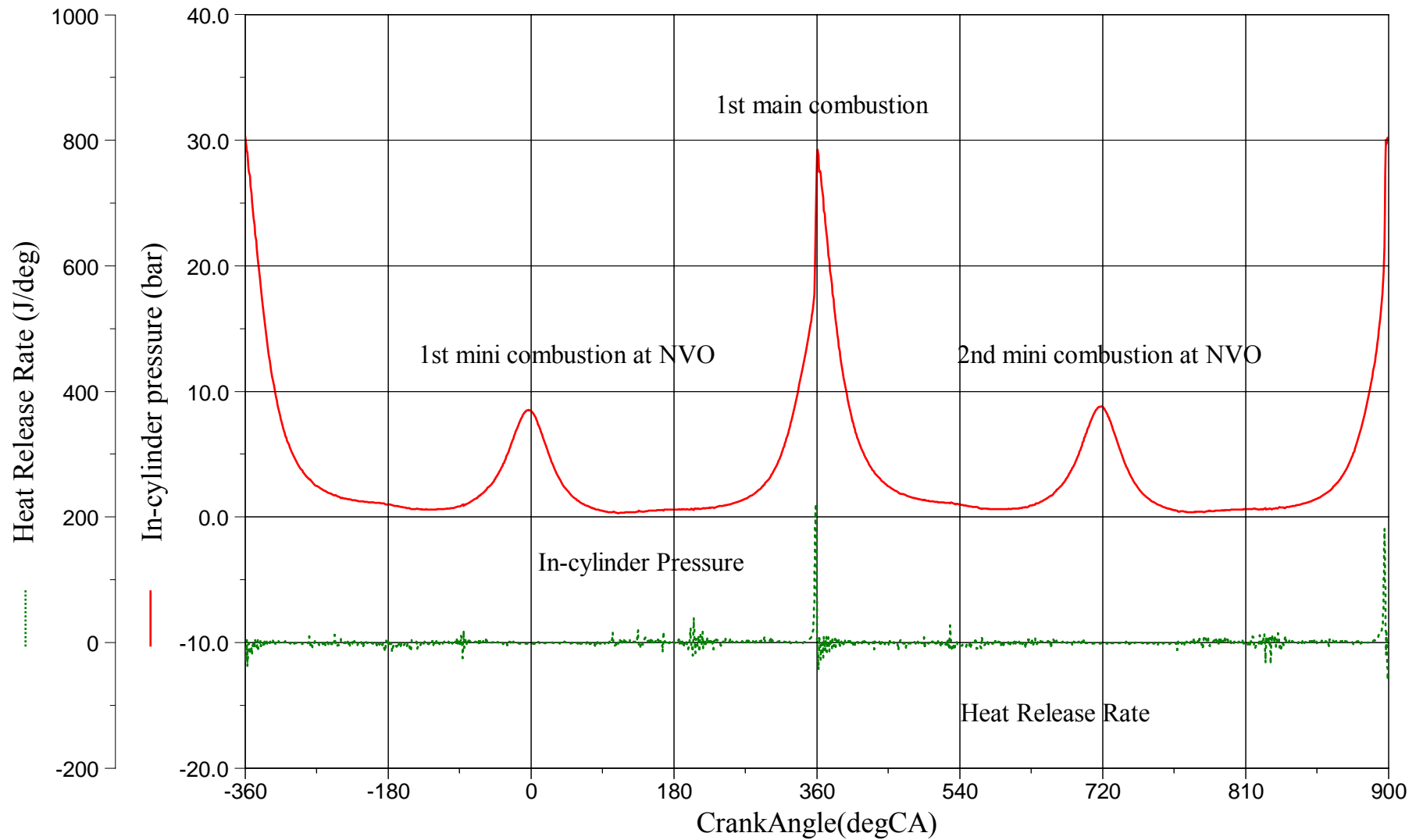


Figure 5.81 Simultaneous In-cylinder pressure, heat release rate and Full Chemiluminescence images at lambda 1, 1600rpm, Gain 50 % , SOI=80 °CA BTDC with spark assistance at 320 °CA BTDC, Air Injection 15.78 mg/cycle .

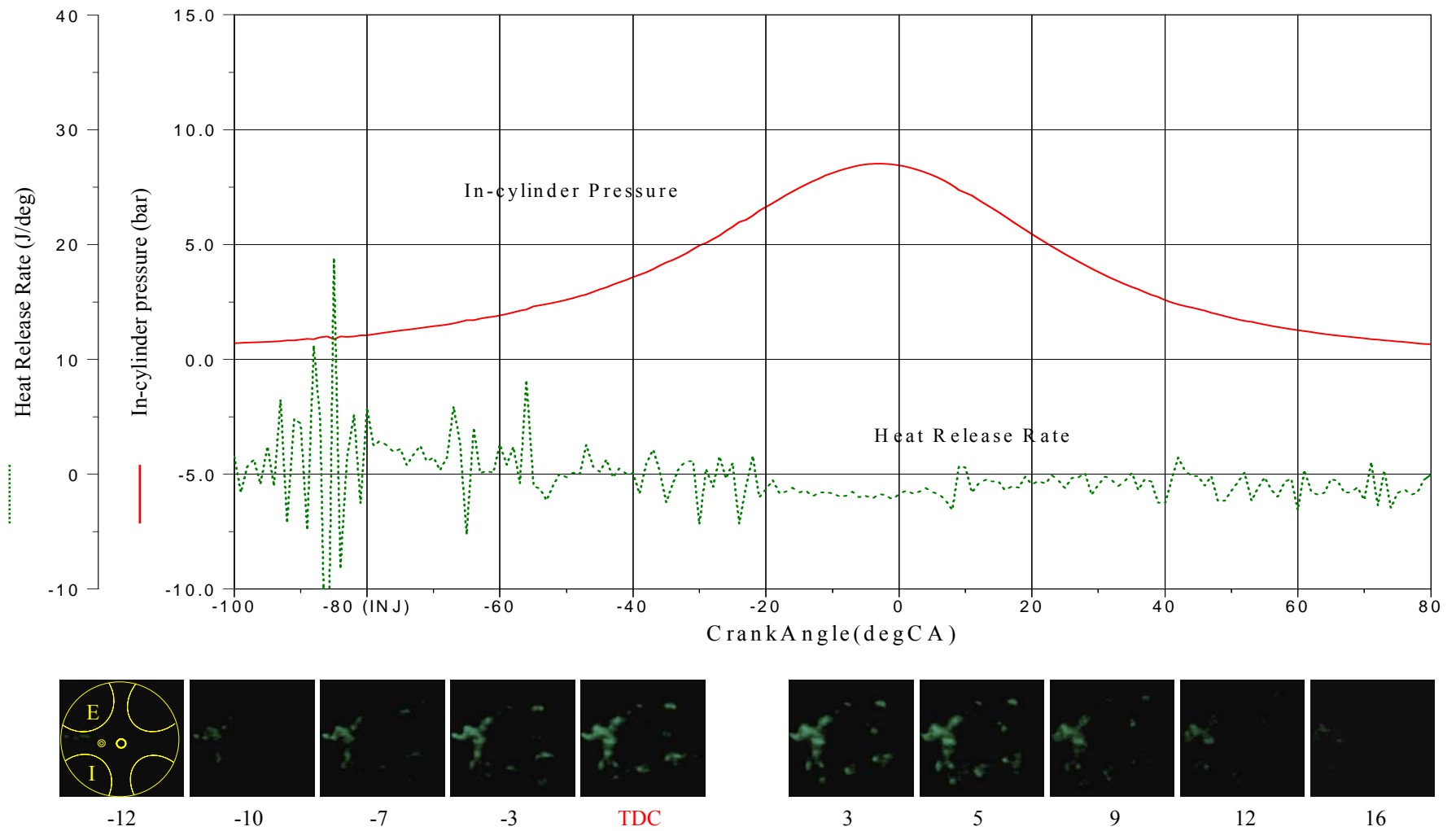


Figure 5.82 Mini combustion with simultaneous In-cylinder pressure, heat release rate and Full Chemiluminescence images at lambda 1, 1600rpm, Gain 50 %, SOI=80 °CA BTDC with spark assistance at 320 °CA BTDC, Air Injection 15.78 mg/cycle

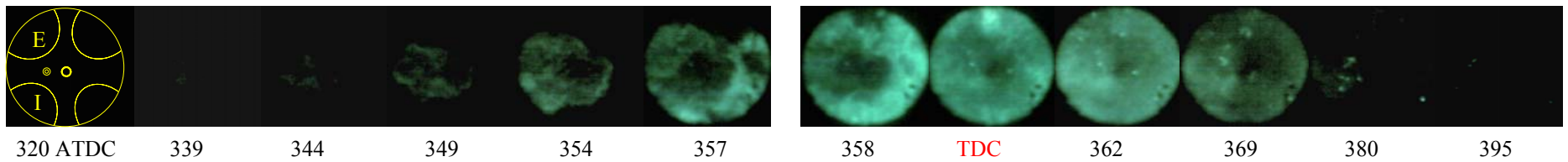
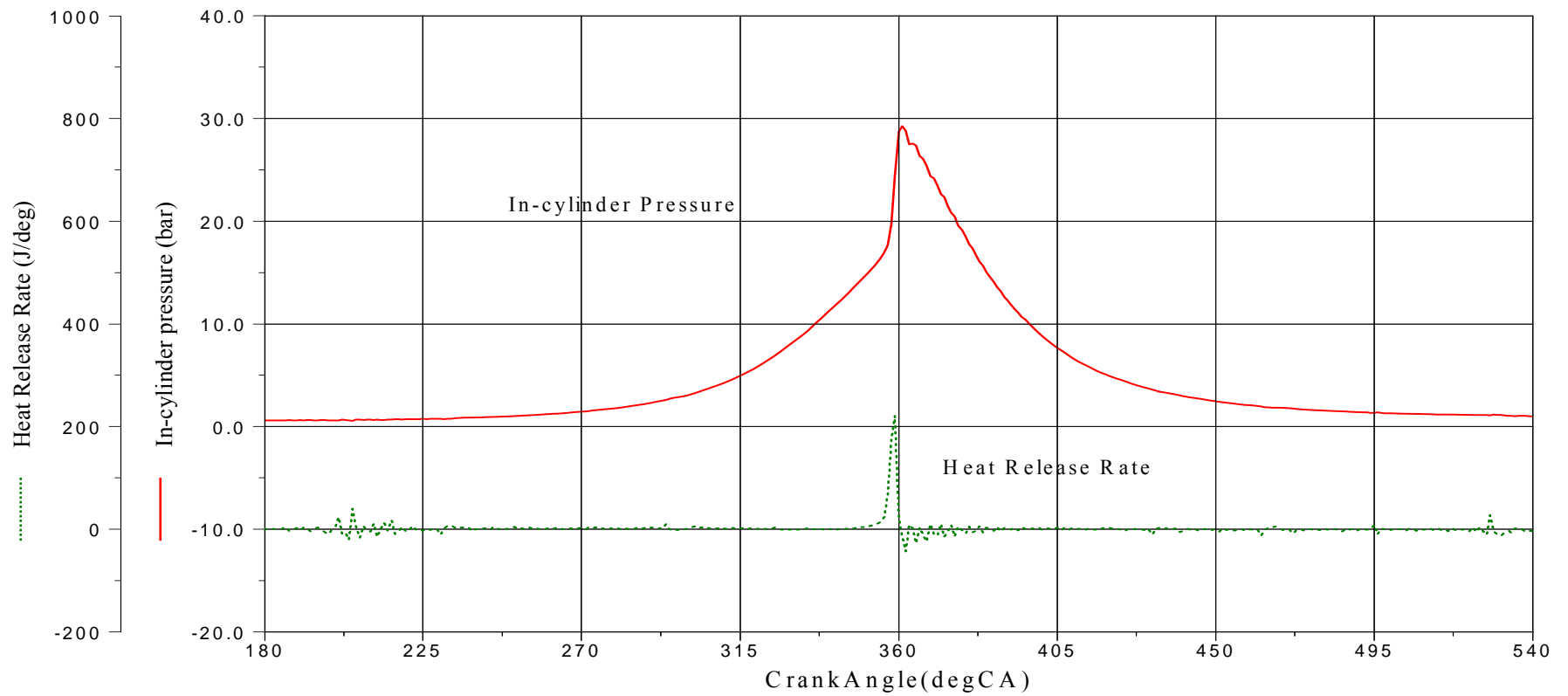


Figure 5.83 Main combustion with simultaneous In-cylinder pressure, heat release rate and Full Chemiluminescence images at lambda 1, 1600rpm, Gain 50 %, SOI=80 °CA BTDC with spark assistance at 320 °CA BTDC, Air Injection 15.78 mg/cycle

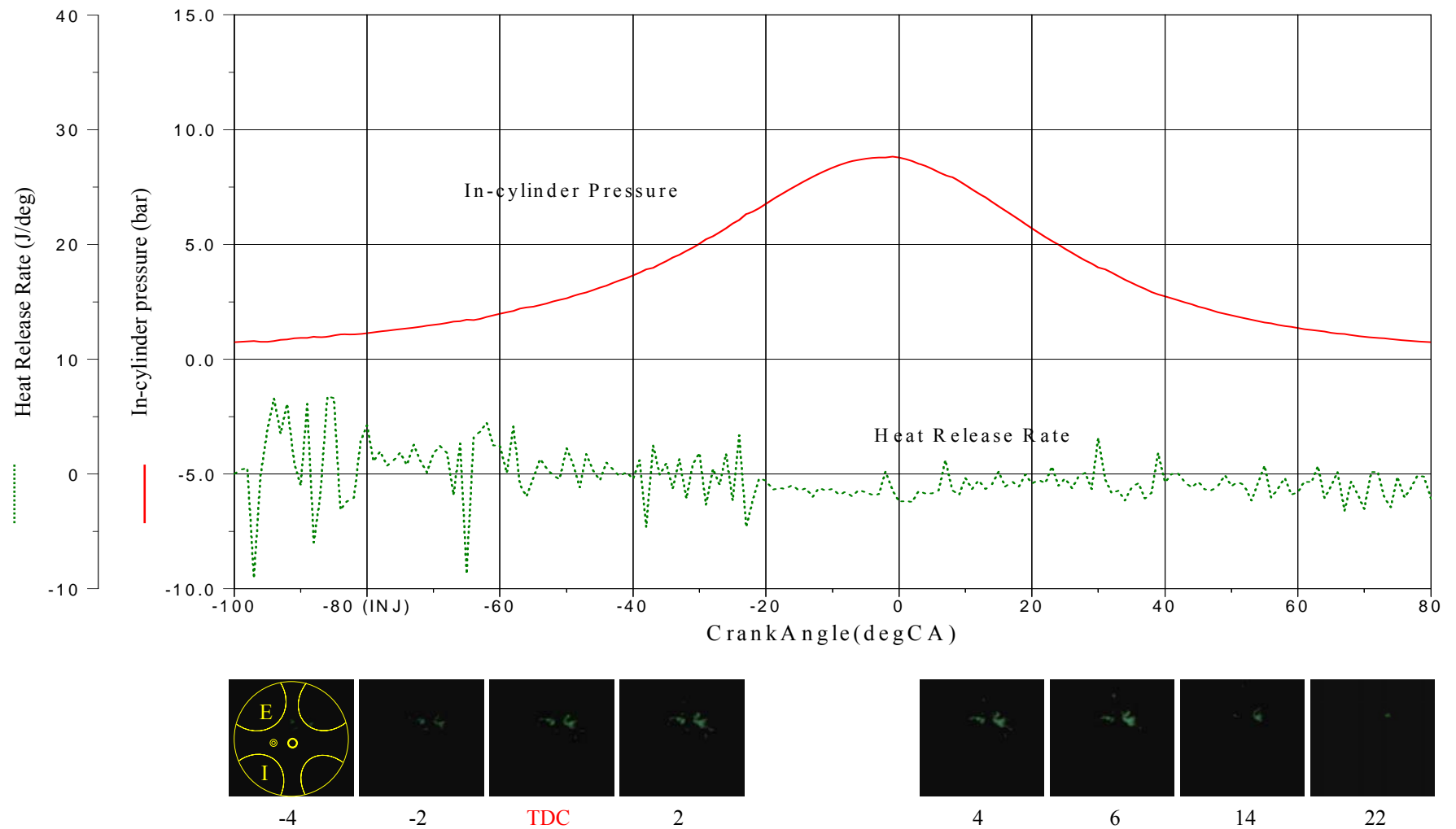


Figure 5.84 Mini combustion with simultaneous In-cylinder pressure, heat release rate and Full Chemiluminescence images at lambda 1, 1600rpm, Gain 50 %, SOI=80 °CA BTDC with spark assistance at 320 °CA BTDC, Air Injection 15.78 mg/cycle

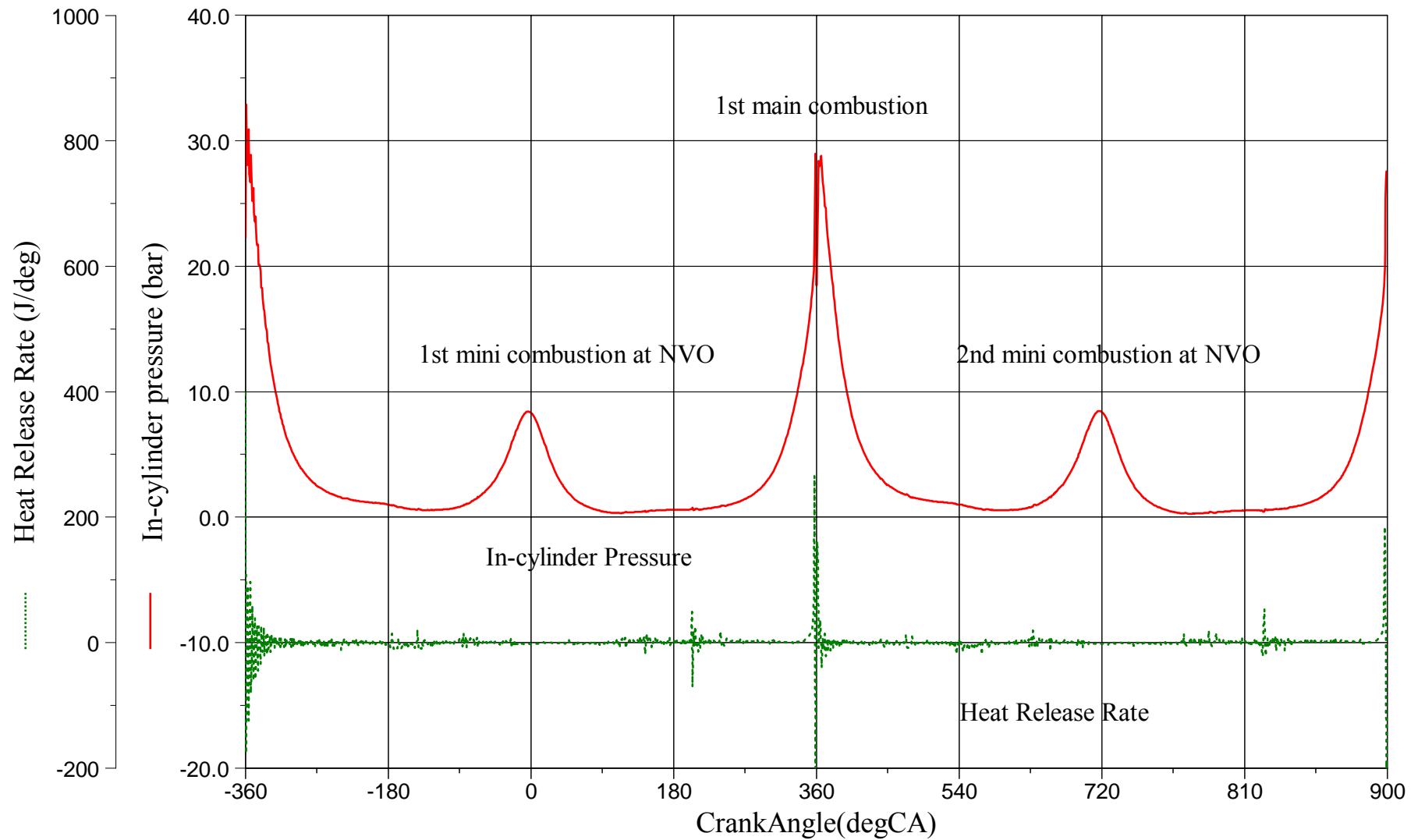


Figure 5.85 Simultaneous In-cylinder pressure, heat release rate and Full Chemiluminescence images at lambda 1, 1600rpm, Gain 50 %, SOI=80 °CA BTDC with spark assistance at 320 °CA BTDC, Air Injection 20.35 mg/cycle .

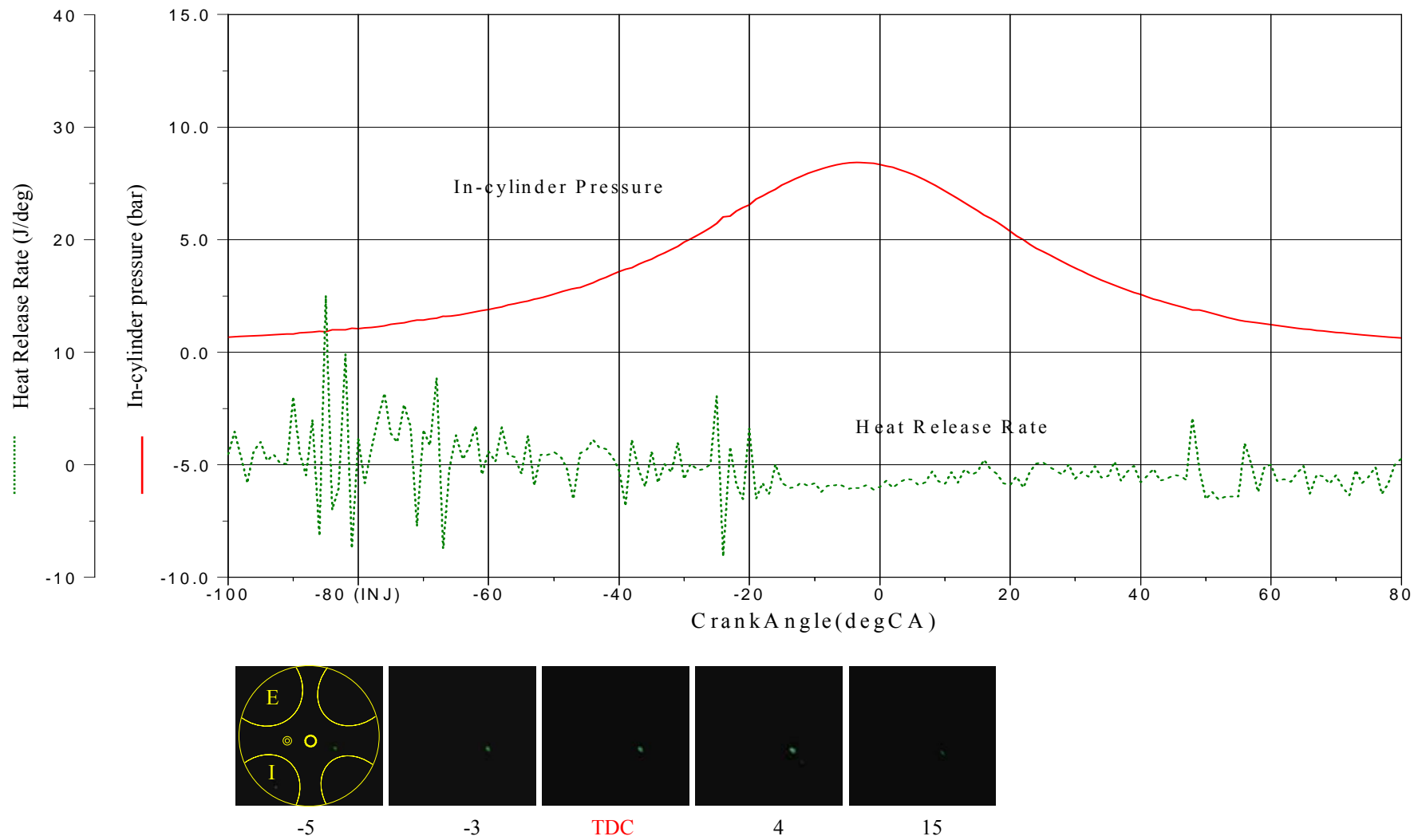


Figure 5.86 Mini combustion with simultaneous In-cylinder pressure, heat release rate and Full Chemiluminescence images at lambda 1, 1600rpm, Gain 50 %, SOI=80 °CA BTDC with spark assistance at 320 °CA BTDC, Air Injection 20.35 mg/cycle

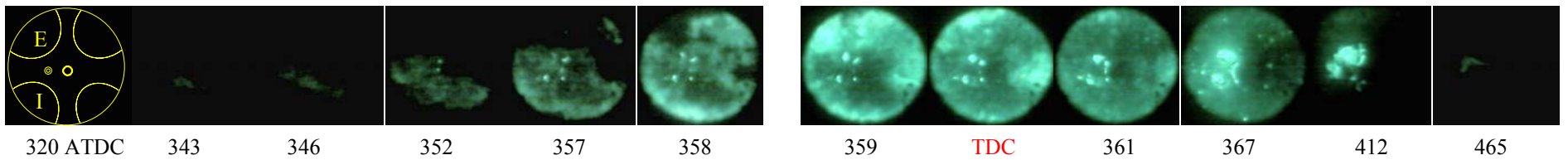
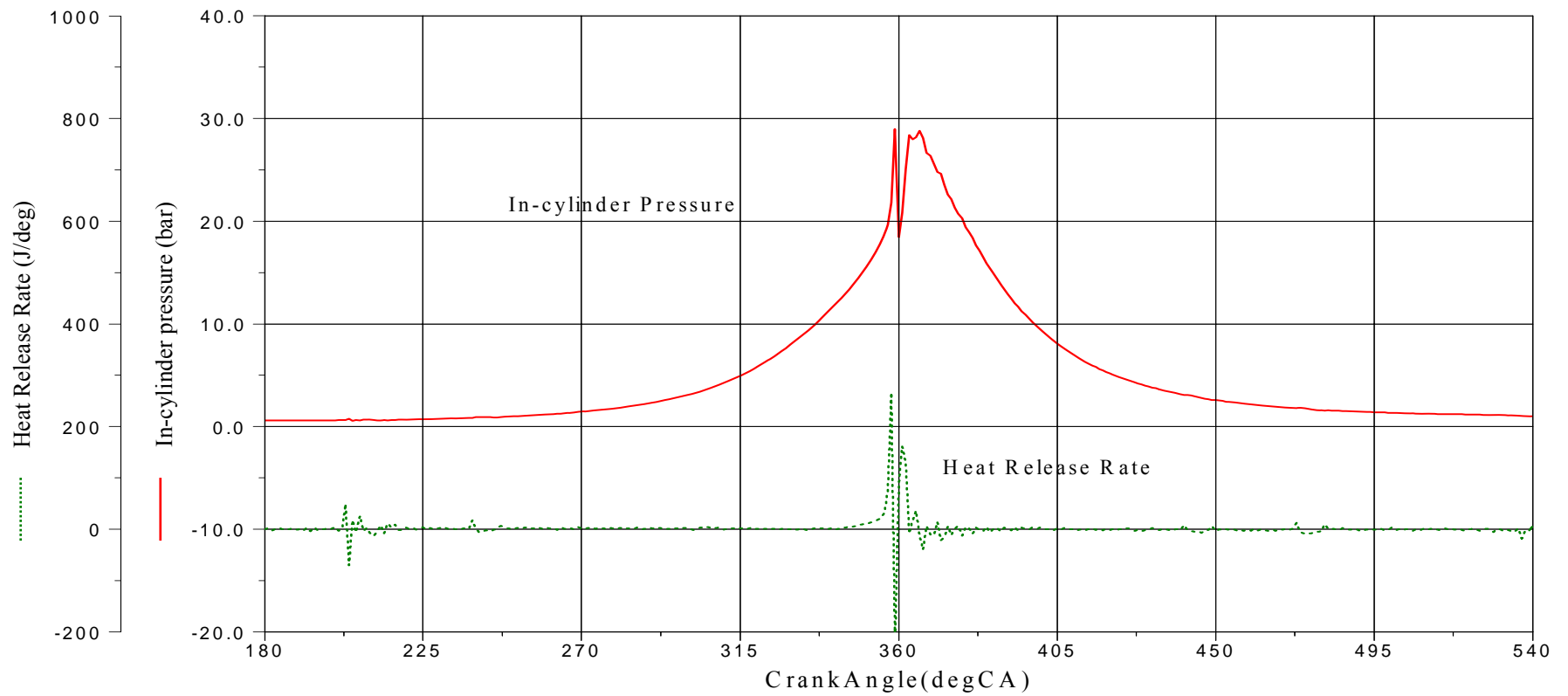


Figure 5.87 Main combustion with simultaneous In-cylinder pressure, heat release rate and Full Chemiluminescence images at $\lambda = 1$, 1600rpm, Gain 50 %, SOI=80 °CA BTDC with spark assistance at 320 °CA BTDC, Air Injection 20.35 mg/cycle

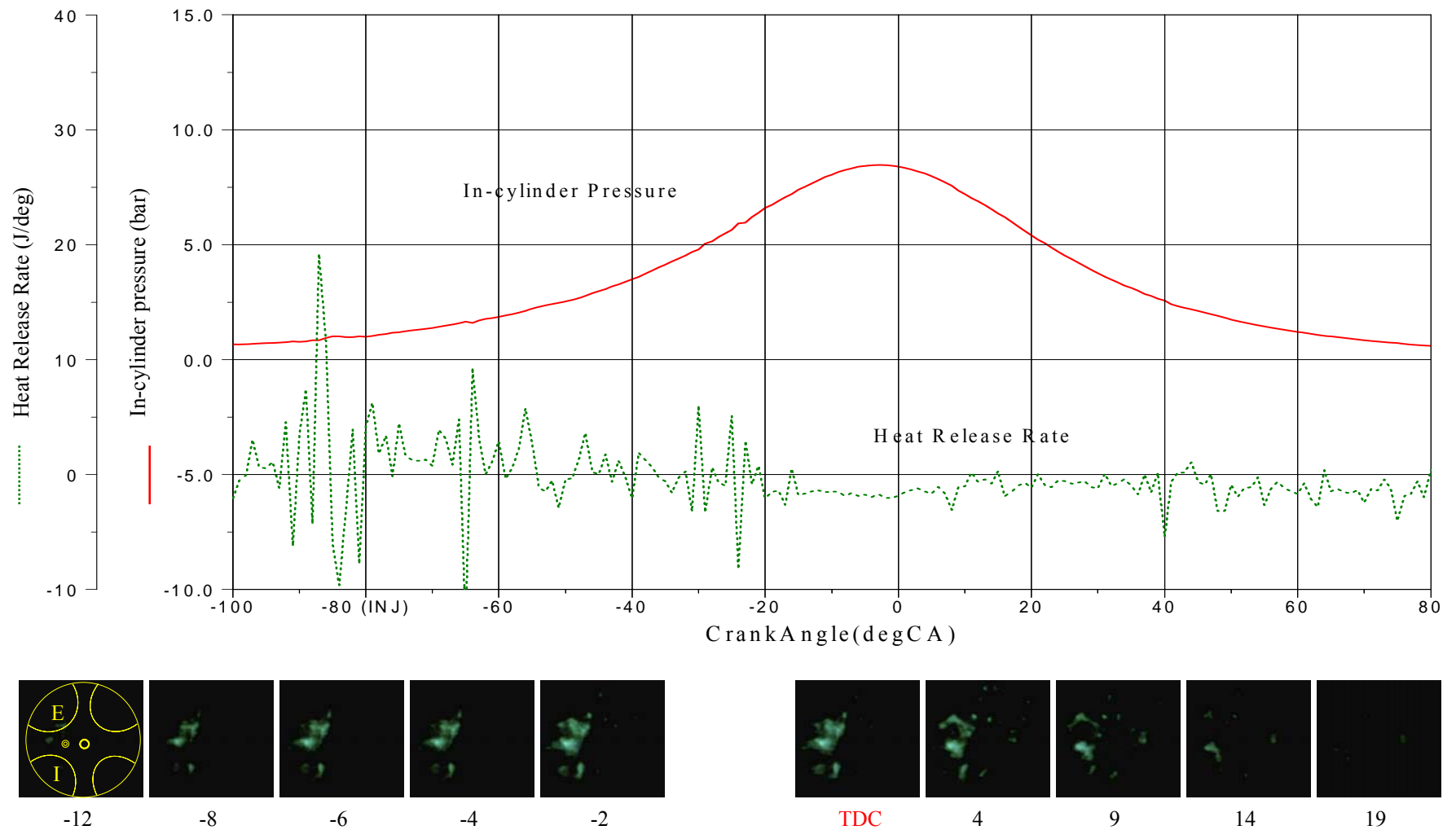


Figure 5.88 Mini combustion with simultaneous In-cylinder pressure, heat release rate and Full Chemiluminescence images at lambda 1, 1600rpm, Gain 50 %, SOI=80 °CA BTDC with spark assistance at 320 °CA BTDC, Air Injection 20.35 mg/cycle

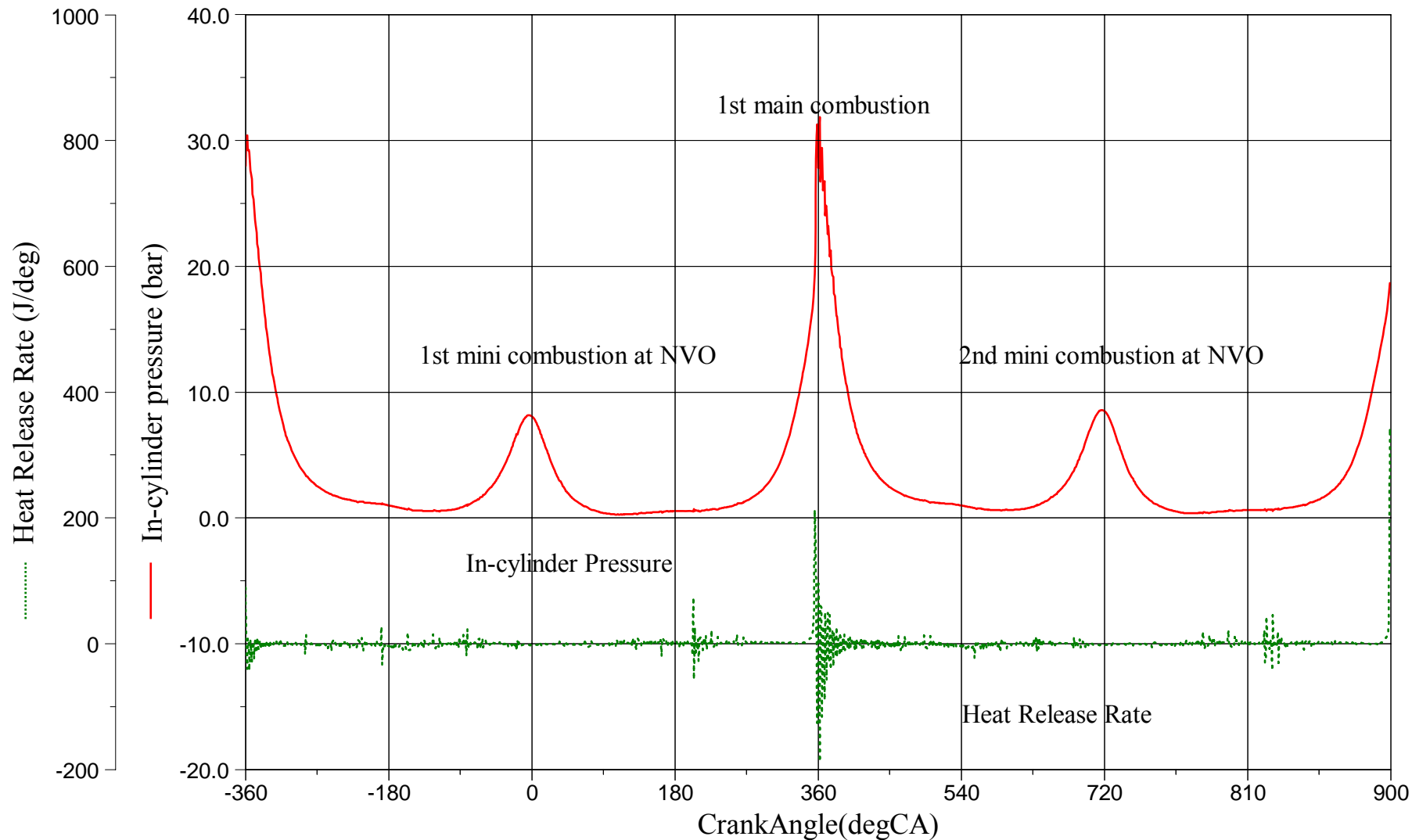


Figure 5.89 Simultaneous In-cylinder pressure, heat release rate at lambda 1, 1600rpm, SOI=80 °CA BTDC with spark assistance at 320 °CA BTDC, Air Injection 25.43 mg/cycle

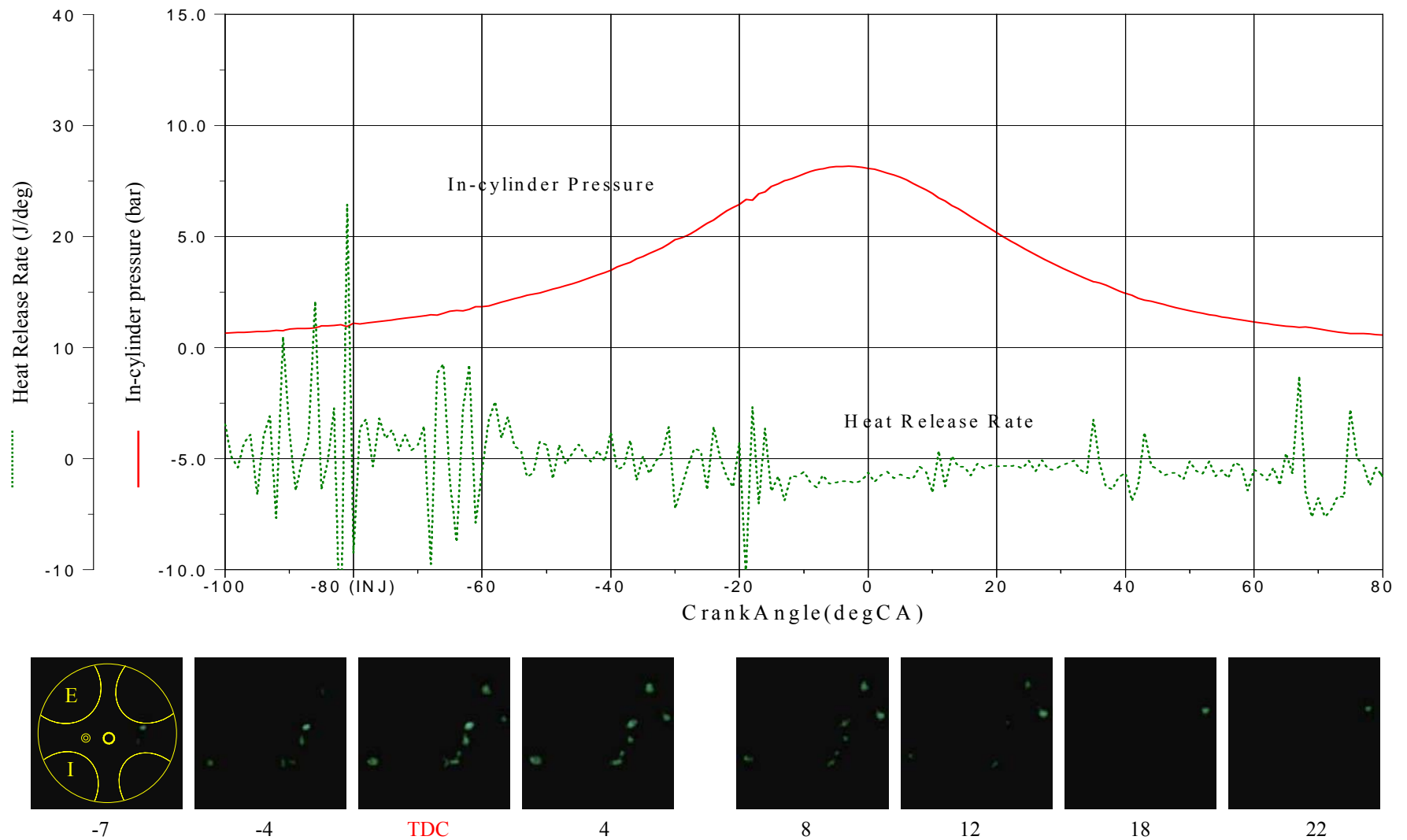


Figure 5.90 Mini combustion with simultaneous In-cylinder pressure, heat release rate and Full Chemiluminescence images at lambda 1, 1600rpm, Gain 50 %, SOI=80 °CA BTDC with spark assistance at 320 °CA BTDC, Air Injection 25.43 mg/cycle

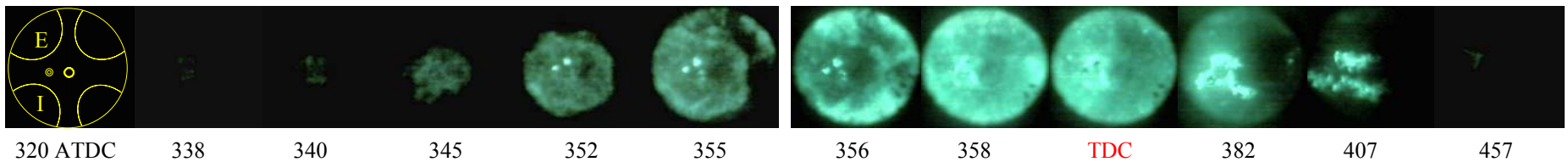
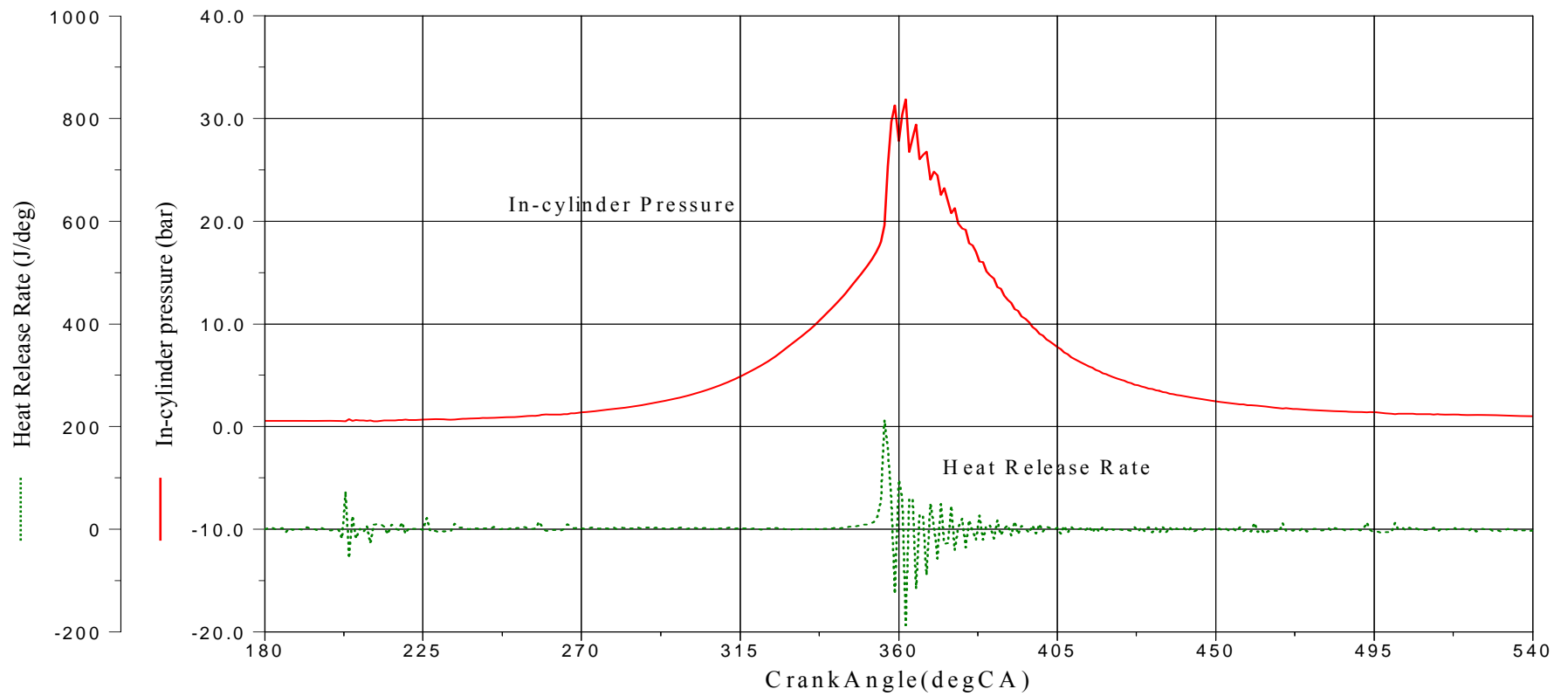


Figure 5.91 Main combustion with simultaneous In-cylinder pressure, heat release rate and Full Chemiluminescence images at $\lambda = 1$, 1600rpm, Gain 50 %, SOI=80 °CA BTDC with spark assistance at 320 °CA BTDC, Air Injection 25.43 mg/cycle

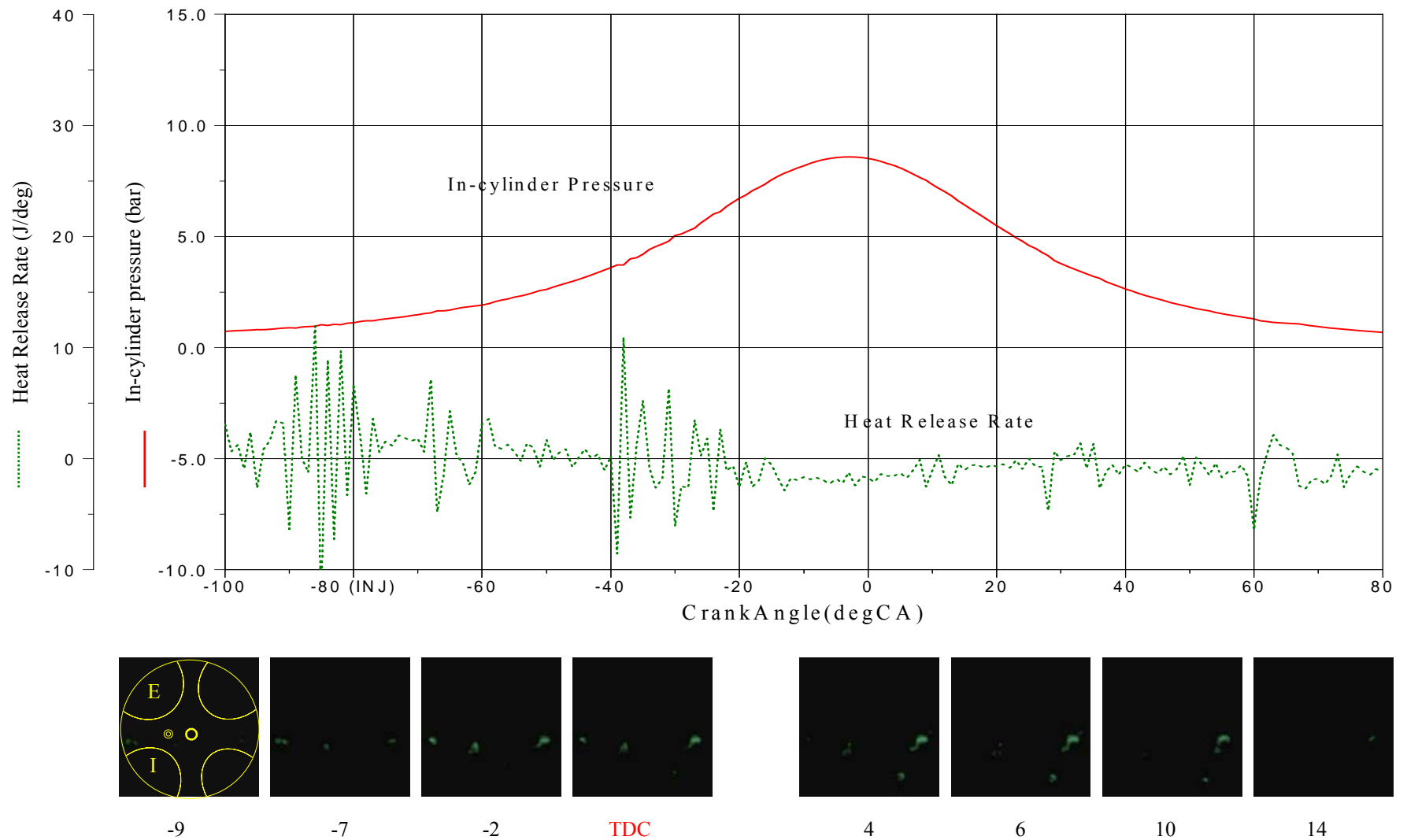


Figure 5.92 Mini combustion with simultaneous In-cylinder pressure, heat release rate and Full Chemiluminescence images at lambda 1, 1600rpm, Gain 50 %, SOI=80 °CA BTDC with spark assistance at 320 °CA BTDC, Air Injection 25.43 mg/cycle

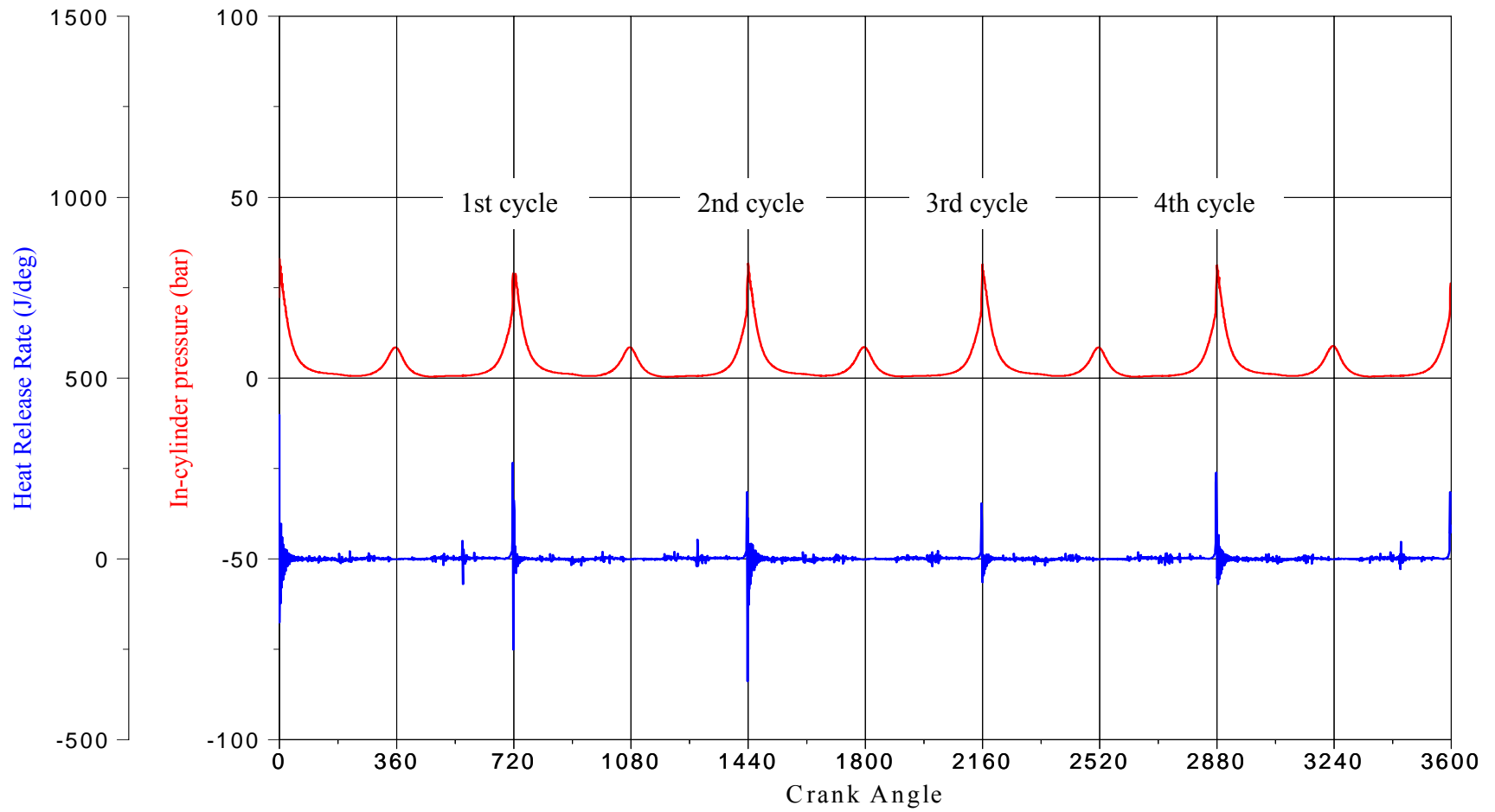


Figure 5.93 Consecutive four cycles with in-cylinder pressure and heat release data at lambda 1, 1600rpm, SOI=80 °CA BTDC with spark assistance at 320 °CA BTDC

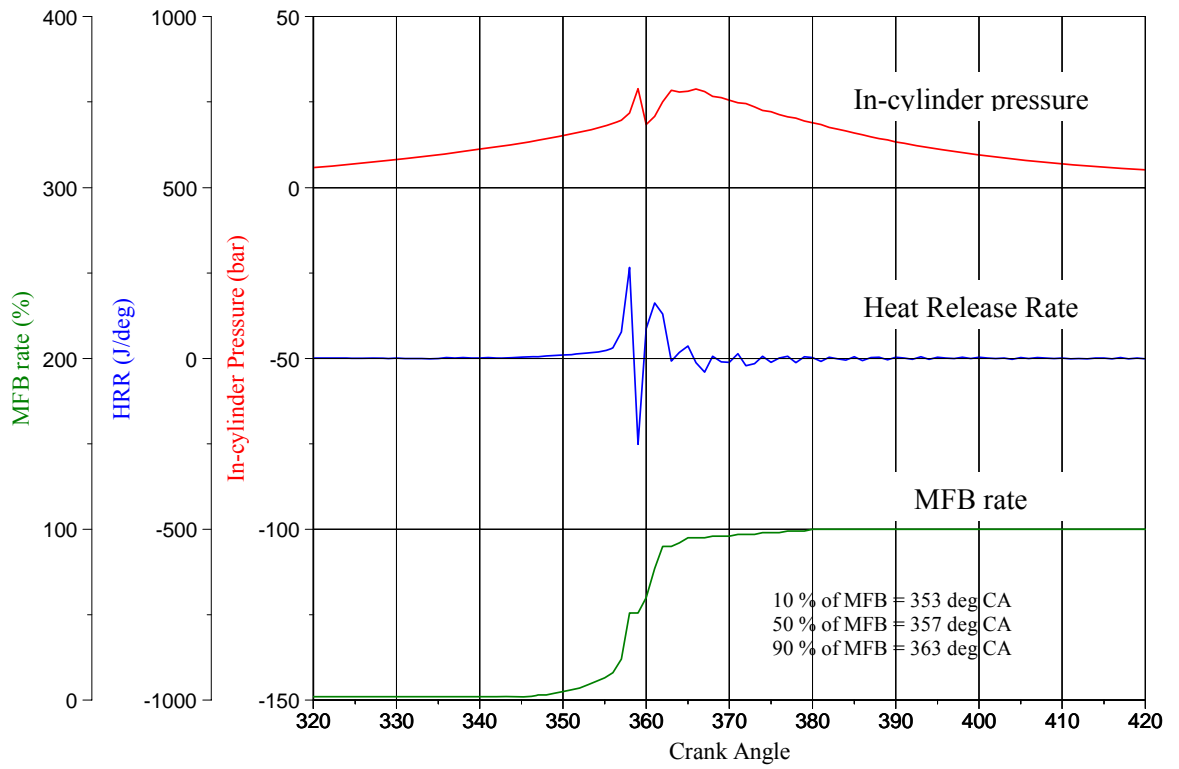


Figure 5.94 1st cycle with in-cylinder pressure, HRR and MFB rate

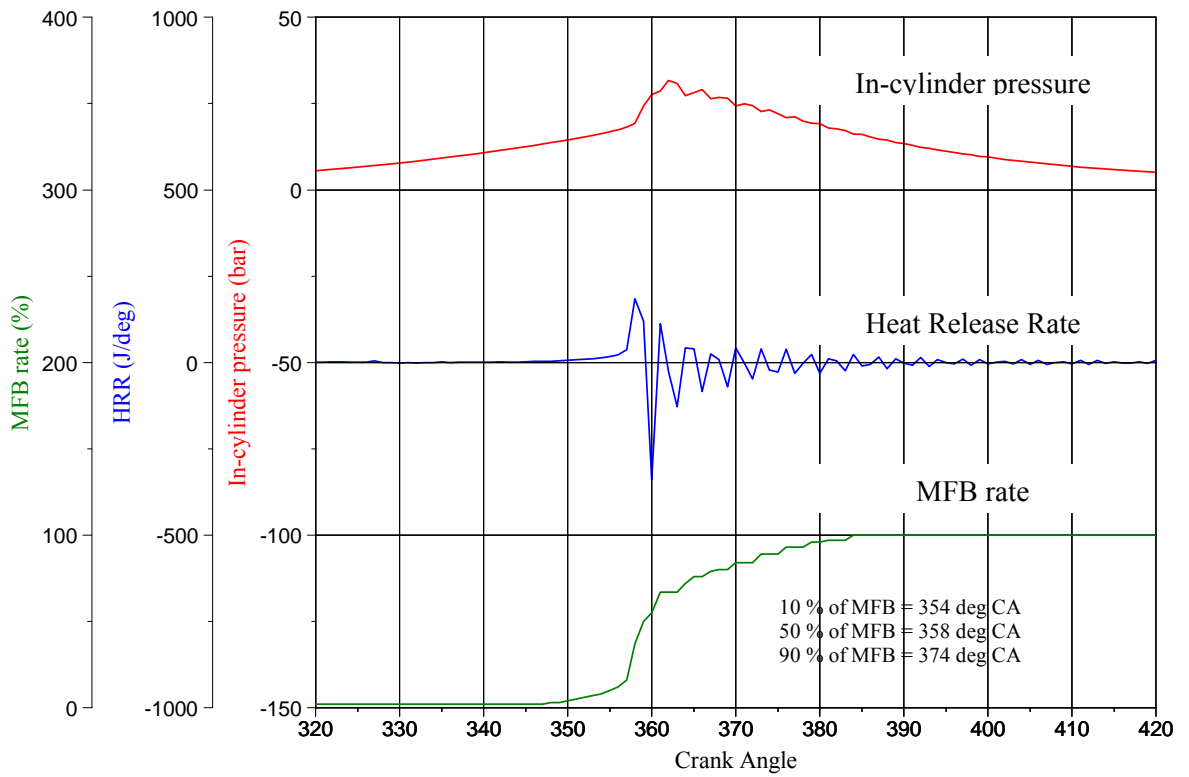


Figure 5.95 2nd cycle with in-cylinder pressure, HRR and MFB rate

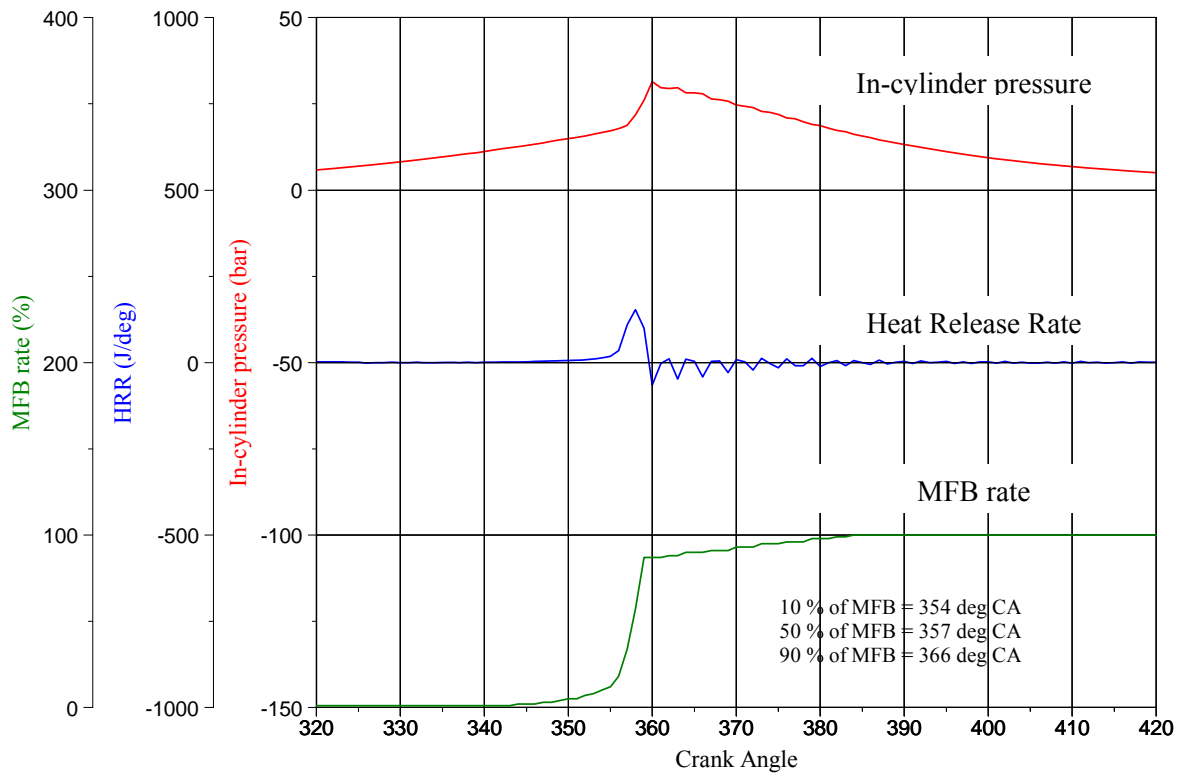


Figure 5.96 3rd cycle with in-cylinder pressure, HRR and MFB rate

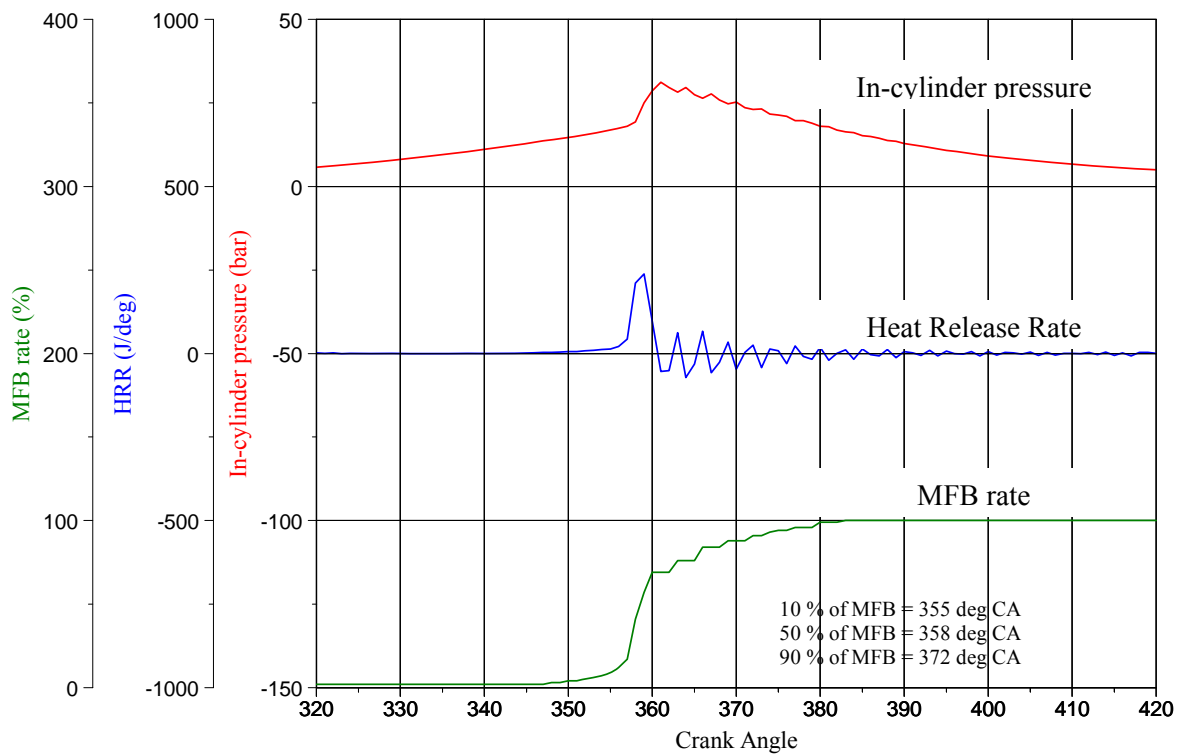


Figure 5.97 4th cycle with in-cylinder pressure, HRR and MFB rate

5.5 Summary

This chapter has described the experimental investigation on a Ricardo Hydra single cylinder optical engine in CAI combustion to investigate simultaneously in-cylinder heat release process and combustion characteristics. The experimental facilities and set up are also presented in this chapter.

The investigation is based on extensive in-cylinder studies on four key engine operation parameters. They are direct fuel injection timings, spark timing, air-fuel ratio, and direct air injection. Their effects on combustion characteristics, engine performance, emissions were analyzed through detailed heat release analysis and high-speed images of chemiluminescence emissions. Each of the parameters or a combination of these parameters can be used to alter the autoignition and combustion process for optimized engine operations.

Chapter 6

Summary and Conclusion

Chapter 6 – Summary and Conclusions

6.1 Introduction

Comprehensive studies have been carried out on CAI combustion operation in a Ricardo E6 single cylinder with positive valve overlap and a Ricardo hydra optical single cylinder engine with negative valve overlap. The CAI combustion operation was achieved on the Ricardo E6 engine by using variable compression ratio and intake air heater as well positive valve overlap to obtain internal EGR. Investigation was conducted to determine the operational range of CAI combustion, the combustion characteristics, performance and emissions as functions of air/fuel ratios and engine speeds. Thereafter, the enlargement of CAI operational range was performed on the same engine by intake air boosting. The boosting pressures varied from 0.5 bar to 1 bar gauge pressure by adjusting a gate valve at the exhaust end. Furthermore, external EGR was implemented to fill the load region between N/A CAI to boosted CAI.

The second part of the work was carried out on a Ricardo hydra optical engine equipped with low lift camshafts to operate with negative valve overlap. Simultaneous in-cylinder studies and chemiluminescence analysis were performed. The strategies to initiate CAI combustion are introduced by the negative valve overlap, heating intake air and air assisted direct fuel injection system. The results show the effects on CAI combustion of varying direct fuel injection timings, spark timings and air/fuel ratio. A high speed camera and intensifier system synchronized with the in-cylinder pressure measurements from a piezo-electric pressure transducer has been used to obtain simultaneous combustion visualization and heat release analysis of different combustion phenomena.

6.2 CAI Operation with Positive Valve Overlap

The positive valve strategy has been shown insufficient to initiate CAI combustion due to lower temperature of the recycled burned gas. It is also limited in its ability to recycle high quantity of burned gases. Up to about 40 % internal EGR was achieved with the current valve set up (IVO/IVC=440 CA deg ATDC/560 CA deg ATDC, EVO/EVC190= CA deg ATDC/280 CA deg ATDC). The CAI operation was successfully achieved by combining variable compression ratio from 12 to 16 with variable intake temperature, as well as internal EGR through positive valve overlap. CAI combustion was achieved with the use of intake charge heating through an intake charge heater in this study to simplify the experimental control, in practice, the employment of a heat exchanger has been shown to be capable of providing the required thermal energy through the heat exchange process with hot exhaust gases. It was found that a higher compression ratio allowed CAI combustion to operate at lower intake temperature with the highest percentage of internal EGR. While engine speed is increased from 1000 to 2000 rpm, the percentage of trapped residual decreased to 15 % at a higher compression ratio and lower intake temperature.

The CAI operational range was determined in terms of engine loads between 1000 to 2500rpm. Minimum IMEP 1.2 bar was obtained at intake temperature 220 °C to IMEP 2.5 bar at intake temperature 190 °C at compression ratio 16, due to misfire limit. It was also limited at the higher engine load region by knocking combustion due to the higher intake temperature.

As one of the advantages of CAI combustion, fuel consumption has been shown to be at lower levels from about 160 g/KWh to 290 g/KWh through the entire operational region, other than at compression ratio 16, compared to SI combustion. Due to the high dilution combustion in CAI operation, the level of NO_x emissions was extremely low from about 0.15 g/KWh to 1 g/KWh, almost negligible compared to SI combustion. On the other hand, the levels of uHC and CO emissions were slightly higher than SI combustion. The uHC emissions are shown to range from about 13 g/KWh to 45 g/KWh and about 3.2 g/KWh to 37 g/KWh for CO emissions. However, it is noted that CO emissions are shown to be lower at the low loads to middle loads range in the operational range.

6.3 Enlargement of CAI operational range

Intake air boosting was employed to increase the upper load limit of CAI operation. Boosting pressure at 0.5 bar and 1 bar were used. Due to the high pressure in the intake system, the percentage of internal EGR was reduced significantly. The thermal energy was mostly provided by the intake heating.

The boosting intake air has led to a significant improvement of CAI upper limit from IMEP 4.5 bar up to IMEP 8 bar at boosting pressure 1 bar, CR=12 at intake temperature between 150 ~ 180 °C.

Detailed experiments were undertaken at CR 12 and intake temperature 180 °C at boosting pressure 1 bar as well as 0.5 bar. The results show that the operational region was limited by the leanest air/fuel ratio at IMEP 2.5 bar and stoichiometric operation at 4 bar at boosting pressure 0.5 bar. As the boosting pressure was set to 1 bar, the load limit was shifted to a region between IMEP 3.3 bar at lean burn limit to 4.5 bar with stoichiometric mixture. However, it was also limited partly at higher engine speed, especially at 1 bar boosting pressure due to knocking combustion. External EGR was implemented to introduce recycled burned gases into the mixture with boosted fresh air by means of adjusting a gate valve at the end of exhaust and external EGR pipe. The pressure in the external EGR pipe was adjusted from 0.7 bar and 1.2 bar at boosting pressure 0.5 bar and 1 bar respectively. The CAI operation with external EGR was successfully between the load region of N/A and boosted CAI at 1 bar boost pressure.

The boosting pressure strategy shows that it has to compromise to meet emissions and fuel consumption targets compared to the results of naturally aspirated CAI, including NO_x emissions. Since the boosting air offers higher engine loads range in CAI, fuel conversion efficiency is monitored and shown from about 42 % to 70 %, which would be reduced when the turbocharger/supercharger efficiency is taken into account. The level of NO_x emissions have been shown to be again extremely low at less than about 6.5 g/KWh in the entire operational region by boosting air and external EGR. The uHC and CO emissions were at a similar level of results in N/A CAI, from about 6 g/KWh to 23 g/KWh at uHC emissions and from about 3 g/KWh

to 27 g/KWh at CO emissions. It is noted that the level of uHC emissions has been shown even lower than in N/A CAI in condition of 0.5 bar and external EGR implemented from about 6 g/KWh to 10 g/KWh.

This experiment shows that the boosting intake air is beneficial to enlarge the CAI operational range and external EGR can be used in the load region between N/A CAI and boosted CAI. As one of the major advantages in CAI, extremely low level of NO_x emissions has been successfully achieved in CAI.

6.4 In-cylinder Studies of CAI Combustion with Negative Valve Overlap

A Ricardo hydra engine was used to investigate the characteristics of CAI combustion in conjunction with simultaneous direct visualization. In order to investigate CAI combustion process, simultaneous chemiluminescence study was performed with CAI control strategies such as direct fuel injection timings, spark timings and air/fuel ratio. The high speed images of total chemiluminescence and that of OH radical and CHO species were simultaneously recorded and analyzed with heat release characteristics determined from the in-cylinder pressure measurements.

Direct fuel injection timings were varied from early (exhaust valve closing timing) and mid (NVO and intake valve opening timing) to late (intake valve closing timing) injections. The results have shown that early and late injection timings caused high cyclic variations for the valve timings investigated and earlier injection timings often resulted in advanced combustion phasing. Compared to mid-injection timings, injection during the NVO period results in slightly lower engine output than injection at intake valve opening timing. The early injections lead to slightly lower NO_x and uHC emissions, but higher CO emissions.

Spark timings are shown to affect the combustion phasing and engine output. The results from the current study shows that the presence of spark did not necessarily advance the combustion phasing as previous works had shown. It was found that the presence of spark helped to improve the stability of CAI in partial and misfiring region.. The best spark timings for the given valve timings and engine speeds were found between 20 and 30 deg BTDC for optimum engine output. Earlier and late

spark timings resulted in higher fuel consumption at about 580 g/KWh and 360 g/KWh respectively. The in-cylinder visualization results show that as the spark timing was retarded, the percentage of spark ignited flame propagation towards the total heat release process was reduced. The effect of spark ignition became almost negligible when spark timing was retarded beyond TDC.

When leaner air and fuel mixture was used, the autoignited combustion was retarded due to lower burned gas temperature. The results shows that higher levels of emissions were present at lambda 1.2 than those at lambda 1, which is not again a typical trend of CAI. The chemiluminescence images from lean-burn CAI combustion show that full chemiluminescence, OH and CHO radical appeared in lower intensity due to the lack of chemical reaction from hydro carbon fuel. When fuel injection took place during the recompression phase of the NVO period, there was a small heat release in the NVO, even minor combustion, as visualized in full chemiluminescence video footage.

The minor combustion during the NVO period was found to be affected by the quantity of air supplied to the air assisted injector. As the amount of air injection was increased, the minor combustion and the amount of heat released were increased, as more oxygen was available for heat release reactions to take place. This resulted in advanced combustion phasing and increases in the peak pressure, leading to a more complete combustion. The early injection leads to earlier combustion, showing locally rich pockets of fuel and large size of soot from the middle of combustion to the end. The late injection allowed more time for the mixture mixing, leading to a more homogeneous mixture distribution in the chamber, shown as a number of small spots in the chamber. It is also noted that there was a limit to air injection at the maximum air quantity of 25.43 mg/cycle, beyond which it did not affect performance and combustion characteristics. Furthermore, the heat released histories demonstrate very clear the 'Charge cooling effect' after the fuel injection with chemiluminescence images.

6.5 Recommendations for future work

This study has shown for the first time the high-speed images of full chemiluminescence emission, OH and CHO radicals during the NVO period as well as the main combustion phase in a CAI engine, though separately. Therefore, simultaneous full, OH radical and CHO or CH₂O species with combustion characteristics would identify the CAI combustion further, possibly by a couple of high speed cameras and combination of optical lenses. A beam splitter was used to capture simultaneous OH and CHO images, but it was not feasible to achieve due to the lower intensity of species in CAI combustion.

In addition, a sampling valve could be one other solution to investigate chemical reaction or mechanism by capturing the in-cylinder species at a certain crank angle and analyze the captured chemical species by GC-MS analysis. Such information will not only provide better understanding of the effect mixture composition but also the information for developing more accurate chemical kinetics for autoignition and combustion under highly diluted conditions.

References

1. 'The Kyoto Protocol to the United Nations Framework Convention on Climate Change', UNFCCC Document NO. FCCC/CP/1997/Add.1, March 1998.
2. Hua Zhao., Jian Li., Tom Ma., and Nicos Ladommatos., 'Performance and Analysis of A 4-Stroke Multi-Cylinder Gasoline Engine With CAI', SAE 2002-01-0420, 2002
3. Onishi, S., Hong Jo, S., Shoda, K., Do Jo, P., and Kato, S., 'Active Thermo-Atmosphere Combustion (ATAC) – A new Combustion Process for Internal Combustion Engines', SAE paper 790501, 1979.
4. Noguchi, M., Tanaka, Y., Tanaka, T., and Takeuchi, Y. 'A Study on Gasoline Engine Combustion by Observation of Intermediate Reactive Products during Combustion', SAE paper 790840, 1979
5. Euro III-V legislated emission levels, Vehicle Certification Agency (VCA), obtained from <http://www.carfueldata.org.uk/June> 2004
6. 'California Exhaust Emissions Standards and Test Procedures for 2004 and Subsequent Model Passenger Cars. Light Duty Trucks and Medium Duty Vehicles, California Environmental Protection Agency Air Resources Board' (CARB), June 2004.
7. Johnson, T. V., 'Mobile Emissions Control Technologies in review, International conference on 21st Century Emissions technology', IMechE Conference Transactions 2002-2, ISBN 186058 322 9, 2000.
8. Heywood, J. B., 'Internal Combustion Engine Fundamentals', pp 601, 413, McGraw-Hill, ISBN 0-07-100499-8, 1988
9. Stone, R., 'Introduction to internal combustion engines', 3rd edition, p.171, Macmillian Press, ISBN 0-333-86058 322 9. 2000.
10. 'Honda readies activated radical combustion 2-stroke engine for production motorcycle', Automotive Engineer, pp. 90-92, SAE publications, January 1997.
11. Najt, P. M., and Foster, D. E., 'Compression-ignited homogeneous charge combustion', SAE paper 830264, 1983.
12. Thring, R. H., 'Homogeneous-charge compression ignition engines', SAE paper 892068, 1989.
13. Stockinger, V., Schapertons, H., and Kuhlmann, U., 'Investigations on a gasoline engine working with self-ignition by compression', MTZ vol.53, pp 80-85, 1992.
14. Marriott, C., and Reitz, R., 'Experimental Investigation of direct injection-gasoline for premixed compression ignited combustion phasing control', SAE 2002-01-0418, 2002.
15. Olsson, J., and Johansson, B., 'Closed loop control of an HCCI engine', SAE paper 2001-01-1031, 2001
16. Christensen, M., Hultqvist, A., and Johansson, B., 'Demonstrating the multi fuel capability of a homogeneous charge compression ignition engine with variable compression ratio' SAE paper 1999-01-3679, 1999

17. Lavy, J., Dabadie, J., Angelberger, C., Duret, P. (IFP), Willand, J., Juretzka, A., Schaflien, J. (Daimler Chrysler), Ma, T., Lendress, Y., Satre, A. (PSA Peugeot Citroen), Shultz, C., Kramer, H. (PCI-Heidelberg University), Zhao, H., Damiano, L. (Brunel University), 'Innovative ultra-low NOx controlled auto-ignition combustion process for gasoline engines: the 4-SPACE project', SAE paper 2000-01-1837, 2000.
18. Zhao, H., Li, J., Ma, T., and Ladommatos, N., 'Performance and analysis of a 4-stroke multi-cylinder gasoline engine with CAI combustion', SAE paper 2002-01-0420, 2001.
19. Koopmans, L., and Denbratt, I., 'A four-stroke camless engine, operated in Homogeneous charge compression ignition mode with a commercial gasoline', SAE paper 2001-01-3610, 2001.
20. Law, D., et al., 'controlled combustion in an IC-engine with a fully variable valve train', SAE paper 2000-01-0251, 2000.
21. Lida, N., Ichikura, T., Kase, K., Yoshiteru, E., 'Self-ignition and combustion stability in a methanol fuelled low heat rejection ceramic ATAC engine – analysis of cyclic variation and high wall temperatures and lean burn operation', JSAE paper 0389-4304/97, 1997.
22. Zhao, H., et al., 'HCCI and CAI engines for the automotive industry', p. 12, Woodhead Publishing Limited, ISBN 978-1-84569-128-8, 2007.
23. Fergusen, C., 'Internal combustion engines applied thermosciences', John Wiley and Sons, New York, 1986.
24. Li, J., Zhao, H., and Ladommatos, N., 'Research and development of controlled auto-ignition combustion in a four-stroke multi-cylinder gasoline engine', SAE paper 2001-01-3608, 2001.
25. Oakley, A., Zhao, H., Ma, T., and Ladommatos, N., 'Experimental studies on controlled auto-ignition combustion of gasoline in a 4-stroke engine', SAE paper 2001-01-1030. 2001.
26. Stanglmaier, R., and Roberts, C. E., 'Homogeneous Charge Compression Ignition: Benefits, Compromises, and Future Engine Applications', SAE paper 1999-01-3682, 1999.
27. Aoyama, T., Hattori, Y., Sato, Y., 'An experimental study on premixed-charge compression ignition gasoline engine' SAE paper, 960081, 1996.
28. Aroonsrisopon, T., Foster, D., Morikawa, T., Lida, M., 'Comparison of HCCI Operating ranges for combinations of intake temperature, Engine speed, and Fuel composition', SAE paper 2002-01-1924, 2002.
29. Sjorberg, H., Dec, J., 'An investigation of the relationship between measured intake temperature, BDC temperature, and combustion phasing for premixed and DI HCCI engines', SAE paper 2004-01-1900, 2004.
30. Urushihara, T., Hiraya, K., Kakuhou, A., and Itoh, T., 'Expansion of HCCI operating region by the combination of Direct Fuel Injection, Negative Valve Overlap and Internal Fuel Reformation', SAE paper 2003-01-0749, 2003.

31. Standing, R., Kalian, N., Ma, T., and Zhao, H., 'Effects of Injection Timing and Valve timings on CAI operation in a multi-cylinder DI gasoline engine', SAE paper 2005-01-0132, 2005.
32. Li, Y., Zhao, H., Bruzos, N., Ma, T., and Leach, B., Effect of Injection timing on Mixture and CAI combustion in a GDI engine with an Air-Assisted Injector', SAE paper 2006-01-0206, SAE Special Publication SP-2005, *Homogeneous Charge Compression Ignition (HCCI) Combustion 2006* ISBN No:0-7680-1740-8, 2006.
33. Christensen, M., Johansson, B., Amneus, P., and Mauss, F., 'Supercharged homogeneous charge compression ignition' SAE paper 980787. 1998.
34. Christensen, M., Johansson, B., 'Supercharged homogeneous charge compression ignition with Exhaust gas recirculation and pilot fuel' SAE paper 2000-01-1835. 2000.
35. Olsson, J., Tunestal, P., Haraldsson, G., Johansson, B., 'A turbocharged dual fuel HCCI engine', SAE paper 2001-01-1896, 2001.
36. Yab, D., Wyszynski, M., Megaritis, A., Xu, H., 'Applying boosting to gasoline HCCI operation with residual gas trapping' SAE paper 2005-01-2121, 2005.
37. Yab, D., Wyszynski, M., Megaritis, A., 'Effect of Inlet Valve timing on Boosted Gasoline HCCI with Residual Gas Trapping', SAE paper 2005-01-2136, 2005.
38. Wilhelmsson, C., Tunestal, P., Johansson, B., 'Operation strategy of a dual fuel HCCI engine with VGT', SAE paper 2007-01-1855, 2007.
39. Kalian, N., Standing, R., and Zhao, H., 'Effects of Ignition Timing on CAI Combustion in a multi-cylinder DI Gasoline Engine', SAE paper 2005-01-3720, SAE 2005 Powertrain and Fluid Systems Conference, 2005.
40. Hyvonen, J., (Fiat-GM Powertrain Sweden) Haraldson, G., and Johansson, B., (Division of Combustion Engines, Lund Institute of Technology) 'Operating conditions Using Spark Assisted HCCI Combustion during Combustion Mode Transfer to SI in a Multi-cylinder VCR-HCCI Engine' SAE paper 2005-01-0109, 2005
41. Fuerhapter, A., Piock, W.F., and Fraidl, G.K., 'CSI - Controlled Auto Ignition – the best solution for the fuel consumption – Versus Emission Trade-Off?' SAE paper 2003-01-0754, 2003.
42. Osbourne, R.J., Li, G., Sapsford, S.M., Stokes, J., Lake, T.H., and Heikal, M.R., 'Evaluation of HCCI for future Gasoline Powertrains', SAE paper 2003-01-0750, 2003.
43. Kalian, N., 'Investigation of CAI and SI combustion in a 4-cylinder Direct Injection Gasoline engine', PhD thesis, Sept., 2006.
44. Urushihara, T., Yamaguchi, K., Yoshizawa, K., and Itoh, T., 'A study of a gasoline-fuelled Compression Ignition Engine-Expansion of HCCI operating range Using SI combustion as a Trigger of Compression Ignition' SAE 2005-01-0180, 2005.
45. Milovanovic, M., Blundell, D., Pearson, R., Turner, J., (Lotus engineers), Chen, R., (Department of Aeronautical and Automotive engineering, Loughborough

- University), 'Enlarging the Operational range of a Gasoline HCCI Engine by Controlling the Coolant Temperature' SAE paper, 2005-01-0157, 2005.
46. Aroonsrisopon, T., Werner, P., Waldman, J.O., Sohm, V., Foster, D.E, Morikawa, T., and Lida, M., 'Expanding the HCCI Operation with the Charge Stratification', SAE paper 2004-01-1756, 2004.
 47. Koopman, L., Strom, H., Lundgren, S., Backland, O., (Volvo Car Corporation) Denbratt, I., (Chalmers University of Technology) 'Demonstrating a SI-HCCI-SI mode change on a Volvo 5-cylinder Electronic Valve Control Engine' SAE paper 2003-01-0753, 2003.
 48. Milovanovic, N., Blundell, D., Gedge, S., and Turner, J., 'SI-HCCI-SI Mode Transition at Different Engine Operating Conditions' SAE paper 2005-01-0156, 2005.
 49. Glyde, H. S., 'Experiments to determine Velocities of Flame propagation in a Slide Valve Petrol Engine', J. Inst, Petroleum Technologists, Vol. 16, 756-776, 1930
 50. Marvin, C. F., and Best, R. D., 'Flame Movement and pressure Development in an Engine Cylinder', NACA Report 399, 1931
 51. Withrow, L., Rassweiler, G. M., 'Slow Motion Shows Knocking and non-Knocking Expositions', SAE Trans., Vol. 39, pp. 297-303, 1936
 52. Withrow, L., Rassweiler, G. M., 'Motion Pictures of Engine Flames Correlated with Pressure Cards', SAE Trans., Vol. 39, pp. 185-204, 1938
 53. Nakanishi, K., Hirano, T., Inoue, T., and Ohihashi, S., 'The Effects of Charge Dilution on Combustion and Its Improvement-Flame Photograph Study', SAE paper 750054, 1975
 54. Bates, S., 'Flame Imaging Studies of Cycle-by-Cycle Variation in a SI Four-stroke Engine', SAE paper 892086, 1989
 55. Ask, T. O., Almas, T., Valland, H., and Paulsen, H., 'Study of the Initial Flame Growth in a Spark Ignition Engine', COMMODIA 94, Japan, 69-83, 1994
 56. Miller, C. D., 'Roles of Detonation Waves and Autoignition in Spark Ignition Engine-Knock as Shown by Photographs Taken at 40,000 and 200,000 Frames per sec' SAE Trans. Vol. 1, 98-143, 1947
 57. Smith, J.R., Green, R.M., Westbrook, C.K., and Pitz, W.J., 'An Experimental and Modeling Study of Engine Knock', Proc. Of 20th Symposium (International) on Combustion, pp. 91-100, 1984
 58. Konig, G., Sheppard, C.G.W., 'End Gas Autoignition and Knock in a Spark Ignition Engine', SAE paper 902135, 1990
 59. Baritaud, T.A., and Green, R., 'A 2-D Flame Visualization Technique Applied to the IC Engine', SAE paper 860025, 1986
 60. Zur Loye, A.O., and Bracco, F.V., 'Two-Dimensional Visualization of Premixed-Charge Flame Structure in an IC Engine', SAE paper 870454, 1987
 61. Ziegler, G.F.W., Zettlitz, A., Meinhardt, P., Herweg, R., Maly, R., and Pfister, W., 'Cycle-Resolved Two-Dimensional Flame Visualization in a Spark-Ignition Engine', SAE paper 881634, 1988

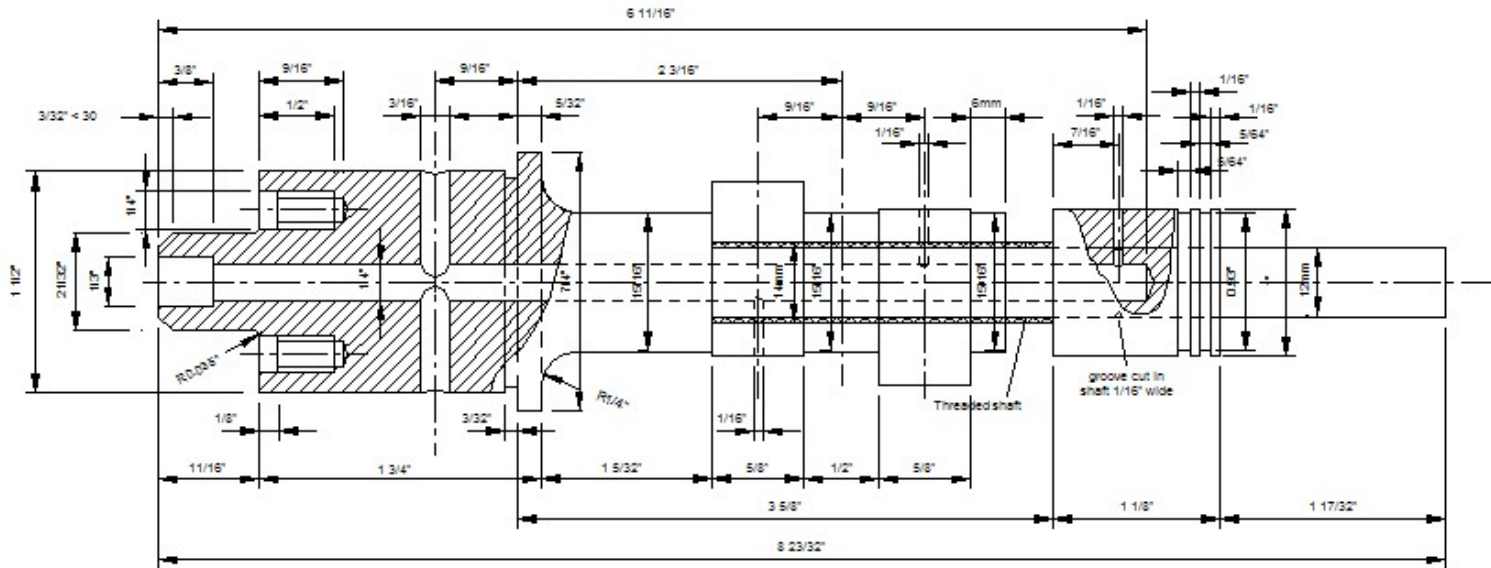
62. Mantzaras, J., Felton, P.G., and Bracco, F.V., '3-D Visualization of Premixed Charge Engine Flames:Islands of Reactants and Products; and Homogeneity', SAE paper 881635, 1988
63. Hicks, R.A., Lawes, M., Sheppard, C.G.W., and Whitacker, B.J., 'Multiple laser sheet Imaging Investigation of Turbulent Flame Structure in a Spark Ignition Engine', SAE paper 941992, 1994
64. Withrow, L., and Rassweiler, G.M., "Spectroscopic Studies of Engine Combustion', *Ind. Eng. Chem.* Vol. 23, pp. 769-776, 1931.
65. Rassweiler G.M., Withrow, L., 'Emission Spectral of Engine Flames' *Ind. Eng. Chem.*, Vol., 24, pp. 528-538, 1932
66. Withrow, L., and Rassweiler, G.M., 'Absorption Spectra of Gaseous Charges in a Gasoline Engine', *Ind. Eng. Chem.* Vol. 25, pp. 923-931, 1933.
67. Rassweiler G.M., Withrow, L., 'Spectrographic Detection of Formaldehyde in an Engine prior to Knock', *Ind. Eng. Chem.* Vol. 25, pp. 1359-1366, 1933.
68. Downs, D., Street, J.C., and Wheeler, R.W., 'Cool-Flames in a Motored Engine', *Fuel*, Vol. 32, p. 279, 1953.
69. Shoji, H., Tosaka, Y., Yoshida, K., and Saima, A., 'Radical Behaviour in Pre-flame Reactions Under Knocking Operating in a Spark Ignition Engine', SAE paper 942061, 1994.
70. Shoji, H., Shimizu, T., Nishzawa, T., Yoshida, K., and Saima, A., 'Spectroscopic Measurement of Radical Behaviour Under Knocking Operation', SAE paper 962104, 1996.
71. Eckbreth, A.C., 'Laser Diagnostic for Temperature and Species', Amsterdam, Overseas Publisher Association, ISBN 90-5699-532-4, 1996.
72. Dec, J.E., Espey, C., 'Chemiluminescence imaging of autoignition in a DI diesel engine', SAE paper 982685, 1998.
73. Hultqvist, A., Christensen, M., Johansson, B., Franke, A., Richter, M., and Alden, M., 'A Study of the Homogeneous Charge Compression Ignition Combustion Process by Chemiluminescence Imaging', SAE paper 1999-01-3680, 1999.
74. Zhao, H., Ladammatos, N., 'Engine Combustion Instrumentation and Diagnostics', SAE, Inc. Warrendale, Pa., ISBN 0-7680-0665-1, 2001.
75. Felton, P., Mantzaras, J., Bomse, D., and Woodin, R., 'Initial Two-Dimensional Laser Induced Fluorescence Measurements of OH radicals in an Internal Combustion Engine', SAE paper 881633, 1988.
76. Schipperijn, F., Nagasaka, R., Sawyer, R., and Green, R., 'Imaging of Engine Flow and Combustion Processes', SAE paper 881631, 1988.
77. Tanaka, T., Tabata, M., 'Planar Measurements of OH radicals in an SI Engine Based on Laser Induced Fluorescence', SAE paper 940477, 1994.
78. Serpenguzel, A., Hahn, R., and Acker, W., 'Single Pulse Planar Laser Induced Fluorescence Imaging of Hydroxyl Radicals in a Spark Ignition Engine', SAE paper 932701, 1993.
79. Andresen, P., Meijer, G., Schluter, H., Voges, H., Koch, A., Hentschel, W., Oppermann, W., and Rothe, E., 'Fluorescence Imaging Inside an Internal

- Combustion Engine Using Tunable Excimer Lasers', *Applied Optics*, Vol. 29, No. 16, pp. 2392-2404, 1990.
80. Benson, S.W., 'The Kinetics and Thermochemistry of Chemical Oxidation With Application To Combustion and Flames', *Progr. Energy Combust. Sci.*, Vol. 7, pp. 125-134., 1981.
 81. Bauerle, B., Warnatz, J., and Behrendt, F., 'Time-Resolved Investigation of Hot Spots in the End Gas of an SI engine by Means of 2D Double-Pulse LIF of Formaldehyde', *Proc. 26th Symposium (international) on Combustion*, The Combustion Institute, 1996.
 82. Brackmann, C., Nygren J., Bai X., Li, Z., Bladh, H., Axelsson, B., Denbratt, I., Koopmans, L., Bengtsson, P-E, and Alen, M., 'Laser-induced fluorescence of formaldehyde in combustion using third harmonic Nd:YAG laser excitation', *Spectrochim. Acta A*, 59:3347-3356, 2003
 83. Metz, T., Bai, Ossler, F., and Alden, M., 'Fluorescence lifetimes of formaldehyde (H₂CO) in the $\tilde{A}1A_2 \rightarrow \tilde{X}1A_1$ band system at elevated temperatures and pressures', *Spectrochim. Acta A*, 60:1043-1053, 2004.
 84. Graf, N., Gronki, J., Schulz, C., Baritaud, T., Cherel, J., Duret, P., and Lavy, J., 'In-cylinder Combustion Visualization in an Auto-Ignition Engine Using Fuel Tracer and Formaldehyde-LIF Imaging', SAE paper 2001-01-1924, 2001.
 85. Thirouard, B., Cherel, J., 'Nature of CAI Combustion and Air/Fuel Ratio Stratification Effects', *Oil & Gas Science and Technology - Rev. IFP.*, Vol. 61, No. 1, pp., 95-119, 2006.
 86. Collin, R., Nygren, J., Richter, M., Alden, M., Hildingsson, L., and Johansson, B., 'Simultaneous OH- and Formaldehyde-LIF Measurements in an HCCI Engine', SAE paper 2003-01-3218, 2003.
 87. Hildingsson, L., Persson, H., Johansson, B., Collin, R., Nygren, J., Richter, M., Alden, M., Hasegawa, R., and Yanagihara, H., 'Optical Diagnostics of HCCI and UNIBUS Using 2-D PLIF of OH and Formaldehyde', SAE paper 2005-01-0175, 2005.
 88. Richter, M., Axelsson, B., and Alden, M., 'Engine Diagnostics Using Laser Induced Fluorescence Signals Collected Through an Endoscopic Detection System', SAE paper 982465, 1998.
 89. Leach, B., Zhao, H., Li, Y., Ma, T., 'Control of CAI combustion through injection timing in a GDI engine with an air-assisted injector', SAE paper 2005-01-0134, 2005.
 90. Standing, R., Kalian, N., Ma, T., Zhao, H., 'Effects of injection timing and valve timings on CAI operation in a multi-cylinder DI gasoline engine', SAE paper 2005-01-0132, 2005.
 91. Cao, L., Zhao, H., Jiang, X., Kalian, N., 'Investigation into the effect of injection timing on stoichiometric and lean CAI operations in a 4-stroke GDI engine', SAE paper 2006-01-0417, 2006.
 92. Christensen, M., Johansson, B., "Influence of mixture quality on premixed-charge compression ignition gasoline engine", SAE paper 982454.

93. Cao, L., Zhao, H., Jiang, X., 'Investigation into Controlled Auto-Ignition Combustion in a GDI Engine with Single and Split Fuel Injections', SAE paper 2007-01-0211, 2007.
94. Yufeng Li, Hua Zhao, Nikolaos Brouzos, Tom Ma, '2007-01-0196 : Parametric Study on CAI Combustion in a GDI Engine with an Air-Assisted Injector', SAE Paper 2007-01-0196

Appendix A. Variable valve timing camshaft of Ricardo E6 engine

Adjustable valve timing camshaft for Ricardo E6 engine



Variable valve timing camshaft
Designed by Dr. Kayiu Mann
Modified by Changho Yang
Date: February, 2008
Brunel University

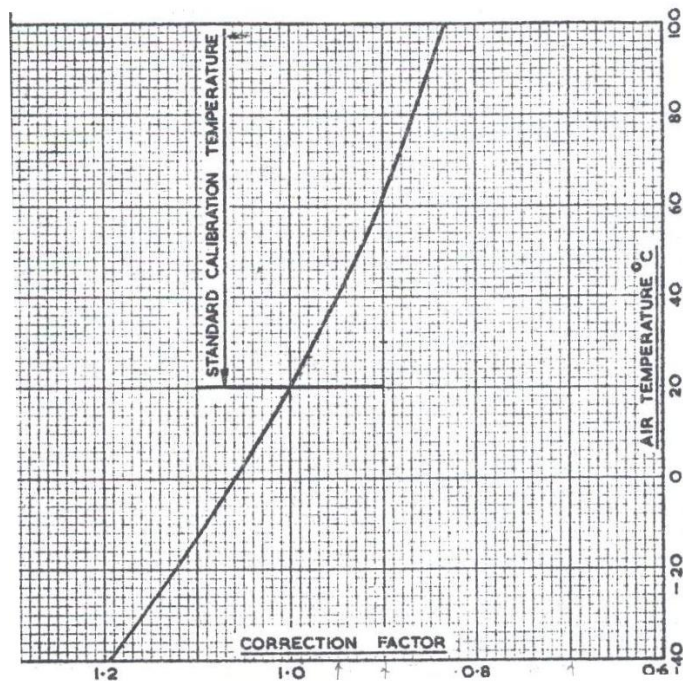
Appendix B. Technical features and pictures of a manometer



Reading meter of a manometer



Orifice measurement part of a manometer



Viscous Flow Air Meter

Temperature Correction for Meters Calibrated at 20 °C

Combined Calibration with Multislope Manometer

Vertical Position volume	=	2.840	×	Manometer reading
Top Inclined	=	1.420	×	Manometer reading
2 nd	=	0.580	×	Manometer reading
3 rd	=	0.284	×	Manometer reading
Bottom	=	0.143	×	Manometer reading